

**Synthesis and Characterization of Novel
Mesogenic Materials**

By

Hari Krishna Bisoyi

Thesis submitted to Jawaharlal Nehru University, New Delhi for the award
of the degree of

Doctor of Philosophy



Raman Research Institute

Bangalore – 560080

June 2009

Dedicated to

My beloved

Parents

Raman Research Institute

CERTIFICATE

This is to certify that the thesis entitled “*Synthesis and Characterization of Novel Mesogenic Materials*” submitted by *Hari Krishna Bisoyi*, for the award of the degree of **DOCTOR OF PHILOSOPHY** of Jawaharlal Nehru University, New Delhi, is his original experimental investigation and conclusions. The subject matter of this thesis has not been previously published or submitted to any other university for the award of any other degree, diploma, associateship, fellowship or any other similar title.

Prof. Ravi Subrahmanyam

Director

Raman Research Institute

Bangalore- 560080

Prof. Sandeep Kumar

(Thesis Supervisor)

Raman Research Institute

DECLARATION

I hereby declare that the entire work embodied in this thesis is the result of the experimental investigation carried out by me independently at Raman Research Institute, Bangalore, under the guidance and supervision of Prof. Sandeep Kumar. The experimental work and conclusions presented in this thesis work has not been previously submitted and no part of this thesis work has formed the basis for the award of any other degree, diploma, fellowship, associateship or any other similar title.

Prof. Sandeep Kumar

Hari Krishna Bisoyi

(Thesis Supervisor)

Raman Research Institute

Bangalore- 560080

ACKNOWLEDGEMENTS

I am very grateful to my thesis supervisor Prof. Sandeep Kumar for his valuable and inspiring guidance throughout my research work. There are no adequate words to explain his keen interest, immense patience, kind advice, sustained encouragement, constant help and thought provoking discussions that I had with him during this time. I am grateful to him for revealing me the richness of some basic synthetic organic chemistry. It was a great experience to work with and learn so many things from him both as a scientist and as a human being. He has always encouraged not only to become a good researcher but also a good human being as well. It has been a great pleasure and I really enjoyed working with him.

I would like to express my gratitude to Prof. V. Lakshminarayanan, for his keen interest in my research work and many valuable discussions that I had with him. I have learnt some basic electrochemistry during some of the electrochemical and conductivity studies of our compounds.

I especially thank Prof. K. A. Suresh and Prof. J. K. Vij for providing some of their facilities to carry out some of our experimental analysis.

I wish to express my gratefulness to Prof. B. K. Sadashiva, Prof. N. V. Madhusudana and Dr. B. Ramesh for their keen interest in this work and for useful discussions and suggestions during the period as advisory committee members.

I take this opportunity to thank Dr. V. A. Raghunathan for his keen interest and valuable help in the interpretation of XRD data. I have learnt the basics of XRD from him, which has been very helpful for interpreting the data described in this thesis.

I am thankful to all other SCM faculty members for their support and valuable suggestions.

I would like to acknowledge NMR Research Centre, Indian Institute of Science, Bangalore for recording NMR spectra of the compounds and Central Electro Chemical Research Institute, Karaikudi for providing some of their facilities.

My sincere thanks to Mr. H. T. Srinivasa, Mr. Rame Gowda for their help in various ways during the period. I appreciate the kind of help, co-operation and encouragement given to me by my colleagues, Santanu Kumar Pal and Satyam Kumar Gupta during the period. I had very useful discussions with them on both academic and non-academic matters and I had enjoyable time.

I sincerely thank Mrs. K. N. Vasudha for recording IR spectra, DSC thermograms, X-ray diffraction and elemental analysis. I also thank Mr. K. Radhakrishnan for his valuable and timely help throughout my research work.

My thanks to Mr. A. Dhason, Mr. Ram, Mr. Mani, and Mr. Shashidhara for their kind help in various ways.

I would like to thank RRI library staff for providing me an excellent, timely and significant help during my research work. The ever smiling staff would oblige for all our

requests including books and journals from various other libraries. This is the first time I have come across such a well maintained library.

I also thank various other departments of RRI and the administration, computer section, accounts, workshop, transport, security, canteen, hostel and clinic for their constant support throughout my Ph. D life.

I was lucky to have Sanat, Sajal, Ganesh, Brindaban, as my seniors, Bharat Kumar, P. Suresh Kumar, Bibhu Ranjan Sarangi, A. V. Radhakrishnan, Tripta Bhatia, Arif Kamal, Antara Pal and Dibyendu Roy as my batchmates and D. H. Nagraju, Rakesh Kumar Pandey, Radhika, as my juniors. I wish to thank all my friends and research colleagues in the institute who made my stay enjoyable.

My deep gratitude to my beloved parents, my sister, my beloved wife *Sanghamitra*, my in-laws, my dear makara Girija and her family for being a constant source of affectionate encouragement and help throughout my research work. I have greatly benefited by their valuable suggestions and thought provoking advices. It is my pleasure to thank my thesis supervisor's wife Navita for her kind suggestions during the period.

CONTENTS

CHAPTER 1: Introduction

1.1 Liquid crystals	1
1.2 Liquid crystals as an intermediate phase (mesophase) of matter	2
1.3 Brief history of thermotropic liquid crystals	4
1.4 Classification of liquid crystals	6
1.4.1 Lyotropic liquid crystals	7
1.4.2 Thermotropic liquid crystals	8
1.4.3 Calamitic liquid crystals	9
1.4.3.1 Nematic Phase	10
1.4.3.2 The chiral nematic phase	11
1.4.3.3 Smectic phases	12
1.4.3.4 Smectic C* phase	14
1.4.3.5 Ferro- antiferro- and ferrielectric chiral smectic C phases	15
1.5 Discotic liquid crystals	16
1.6 Banana liquid crystals	16
1.7 Polymeric liquid crystals	19
1.8 Discotic liquid crystals: the discovery	21
1.9 Structure of the liquid crystalline phases formed by discotic mesogens	23
1.9.1 Nematic Phases of discotic mesogens	23
1.9.2 Smectic phases of discotic mesogens	24

1.9.3 Columnar phases of discotic mesogens	25
1.9.3.1 The hexagonal columnar mesophase (Col _h)	25
1.9.3.2 The rectangular columnar mesophase (Col _r)	26
1.9.3.3 The columnar oblique mesophase (Col _{ob})	28
1.9.3.4 The columnar plastic mesophase (Col _p)	28
1.9.3.5 The columnar helical (H) phase	29
1.9.3.6 The columnar lamellar mesophase	29
1.9.3.7 The columnar square (tetragonal) phase	30
1.10 Cubic phase	31
1.11 Structure of the discotic mesogens	31
1.12 Chemistry of discotic liquid crystals	32
1.13 Characterization of discotic liquid crystal phases	34
1.14 DLCs as materials for a new generation of organic electronics	35
1.15 Why discotics ?	36
1.16 Discotics as semiconductor: molecular concepts, one-dimensional electrical & photoconductivity	37
1.16.1 Size of the discotic core	43
1.16.2 Connecting groups	44
1.16.3 Phase behaviour and transition temperatures	45
1.17 Alignment of discotic liquid crystals	47
1.17.1 Planar alignment of discotics	47

1.17.2 Face-on arrangement (Homeotropic) of discotics	50
1.18 Applications of discotic liquid crystals	51
1.18.1 Discotic liquid crystals in display devices	51
1.18.2 Discotics in Xerographic processes	52
1.18.3 Discotics in holographic optical data storage	54
1.18.4 Discotics in organic light-emitting diodes	55
1.18.5 Discotics in organic field-effect transistors	56
1.18.6 Discotic liquid crystals as photosynthetic light harvesting materials	57
1.18.7 Discotics as gas sensors	60
1.18.8 Discotics as precursors of novel carbonaceous nanostructures	61

**CHAPTER 2: Green chemistry approach to the synthesis of liquid
crystalline materials**

2.1 Part A: Microwave-assisted facile synthesis of alkoxy-cyanobiphenyls and their dimers	72
2.1.1 Introduction	72
2.1.2 Results and discussion	77
2.1.3 Conclusions	85
2.2 Part B: Microwave-assisted synthesis of monohydroxy-functionalised triphenylenes and their novel liquid crystalline derivatives	86
2.2.1 Results and discussion	92
2.2.2 Thermal behavior of unsymmetrical triphenylenes	96

2.2.3 X-ray diffraction studies	99
2.2.4 Conclusions	102
2.3 Experimental	103
2.3.1 General information	103
2.3.2 General procedure for the synthesis of 4'-alkoxy-4-cyanobiphenyls	104
2.3.3 General procedure for the synthesis of α,ω -bis(4'-cyanobiphenyl-4-yloxy)alkanes	105
2.3.4 General procedure for the synthesis of monohydroxy pentaalkoxytriphenylenes	105
2.3.5 General procedure for the synthesis of unsymmetrical triphenylene derivatives	106
 CHAPTER 3: Microwave-assisted facile synthesis of rufigallol and its novel room-temperature liquid crystalline derivatives	
3.1 Introduction	121
3.2 Results and discussion	127
3.2.1 Microwave assisted synthesis of rufigallol	127
3.2.2 Synthesis of hexaethers of rufigallol and their characterization	129
3.2.3 Mesophase behavior of the novel rufigallol derivatives	132
3.2.4 X-ray diffraction study	136
3.3 Conclusions	140
3.4 Experimental	140

3.4.1 General information	140
3.4.2 Synthesis of rufigallol and its liquid crystalline derivatives	141
CHAPTER 4: Synthesis and characterization of novel liquid crystalline oligomers	
4.1 Part A: Molecular double cables: synthesis and mesomorphism	163
4.1.1 Introduction	163
4.1.2 Results and Discussion	167
4.1.2.1 Mesophase behavior of the star-shaped oligomers	172
4.1.2.2 X-ray diffraction studies of the oligomers	174
4.1.3 Conclusions	177
4.2 Part B: Nanophase segregated mesophase morphology in self-organized disc-rod oligomesogens	178
4.2.1 Results and discussion	185
4.2.1.1 Thermal phase behavior of the novel oligomesogens	187
4.2.1.2 X-ray diffraction studies of the novel oligomers	190
4.2.2 Conclusions	193
4.3 Experimental	193
4.3.1 General information	193
4.3.2 Preparation of pentamers 11 and 12	193
4.3.3 Preparartion of heptamer 13	195
4.3.4 Preparation of heptamer 17	196
4.3.5 Preparation of disc-rod oligomers 41	196

**CHAPTER 5: Functionalized Carbon nanotubes in the supramolecular
order of discotic liquid crystals**

5.1 Introduction	217
5.2 Results and discussion	231
5.3 Carbon nanotubes in triphenylene and rufigallol-based room temperature monomeric and polymeric discotic liquid crystals.	237
5.4 Results and discussion	238
5.5 Conclusions	246
5.6 Experimental	247
5.6.1 General information	247
5.6.2 Preparation of hydroxyl functionalized triphenylene 4	247
5.6.3 Functionalization of CNTs	248
5.6.4 Preparation of liquid crystalline nanocomposites 7c	248
5.6.5 Synthesis of 1,5-dihydroxy-2,3,6,7-tetrakis(3,7-dimethyloctyloxy)-9,10-anthraquinone, 10	249
5.6.6 Polymerization of 1,5-dihydroxy-2,3,6,7-tetrakis(3,7-dimethyloctyloxy)-9,10-anthraquinone	249
5.6.7 Synthesis of 2,6-Bis(3,7-dimethyloctyloxy)-3,7,10,11-tetrakis(pentyloxy)-triphenylene, 16	250
5.6.8 Polymerization of 2,6-dihydroxy-3,7,10,11-tetrakis(pentyloxy)-triphenylene	251
5.6.9 Preparation of liquid crystalline nanocomposites with ODA	

CHAPTER 6: SUMMARY

List of abbreviations used in this Thesis

LC	Liquid Crystal	DNA	Deoxyribonucleic Acid
LCD	Liquid Crystal Display	N	Nematic
Sm	Smectic	N _D	Discotic Nematic
Col	Columnar	N*	Chiral Nematic
1D	One Dimensional	TGB	Twist Grain Boundary
P _S	Spontaneous Polarization	N _b	Biaxial Nematic
2D	Two Dimensional	N _D *	Chiral Discotic Nematic
N _{Col}	Columnar Nematic	N _L	Nematic Lateral
Col _h	Columnar Hexagonal	Col _p	Columnar Plastic
Col _r	Columnar Rectangular	Col _{ob}	Columnar Oblique
Col _L	Columnar Lamellar	Col _{tet}	Columnar Tetragonal
H	Helical	UV	Ultraviolet
DLC	Discotic Liquid Crystal	POM	Polarizing Optical Microscopy
XRD	X-ray Diffraction	DSC	Differential Scanning Calorimetry
CT	Charge Transport	FT-IR	Fourier Transform Infrared
LED	Light Emitting Diode	FET	Field Effect Transistor
TOF	Time of Flight	NMR	Nuclear Magnetic Resonance
HBC	Hexabenzocoronene	PAH	Polyaromatic Hydrocarbon
PTFE	Polytetrafluoroethylene	TP	Triphenylene

LB	Langmuir Blodget	Pc	Phthalocyanine
TN	Twisted Nematic	STN	Super Twisted Nematic
TNF	Trinitrofluorenone	ITO	Indium Tin Oxide
AFM	Atomic Force Microscope	STM	Scanning Tunneling Microscope
CNT	Carbon Nanotube	SWNT	Single Walled Carbon nanotube
CVD	Chemical Vapor Deposition	MWNT	Multi Walled Carbon nanotube
DC	Direct Current	DWNT	Double Walled Carbon Nanotube
AC	Alternating Current	IPS	In-Plane Switching
PEG	Polyethylene Glycol	GPC	Gel Permeation Chromatography
Cr	Crystalline	TGA	Thermo Gravimetric Analysis
Cr*	Partially Crystalline	HOPG	Highly Oriented Pyrolytic Graphite
I	Isotropic	ODA	Octadecylamine
MW	Microwave	DMSO	Dimethy Sulphoxide
MEK	Methyl Ethyl Ketone	PDI	Polydispersity Index
ppm	parts per million	TCQ	Tricycloquazoline
Cub	Cubic	NMP	N-Methyl Pyrolidinone
OPV	Organic Photovoltaic	HHA	Hexahydroxyanthraquinone
AR	Analytical Reagent	TLC	Thin Layer Chromatography
TMS	Tetra Methyl Silane	Equi.	Equivalent
Rec.	Recovered	Cat-B-Br	Catechol B-Bromoborane
DMF	Dimethylformamide	AP	As Prepared
CPI	Complementary Polytopic Interaction		
PR-TRMC	Pulse Radiolysis Time Resolved Microwave Conductivity		
ILCC	International Liquid Crystal Conference		
HPLC	High Pressure Liquid Chromatography		

CHAPTER 1

Introduction

1.1 Liquid crystals

Liquid crystals (LCs) are unique functional soft materials which combine both *order* and *mobility* on a molecular, supramolecular and macroscopic level [1]. Liquid crystals are accepted as the fourth state of matter after solid, liquid and gas. Liquid crystals form a state of matter intermediate between the solid and the liquid state. For this reason, they are referred to as intermediate phases or *mesophases*. This is a true thermodynamic stable state of matter. The constituents of the mesophase are called *mesogens*. The mesogens can be organic (forming thermotropic and lyotropic phases), inorganic (metal oxides forming lyotropic phases) [2] or organometallic (metallomesogens) [3] etc. LCs are important in material science as well as in the life science. Important applications of thermotropic LCs are electrooptic displays, temperature sensors and selective reflecting pigments. Lyotropic systems are incorporated in cleaning process, and are important in cosmetic industries. They are used as templates for the preparation of mesoporous materials and serve as model systems for biomembranes. LCs are important in living matter. Most important are the biological membranes, DNA can form lyotropic mesophases etc. Anisotropic fluid states of rigid polymers are used for processing of high strength fibers like Kevlar. LCs can potentially be used as new functional materials for electron, ion, molecular transporting, sensory, catalytic, optical and bio-active materials. LCs are extremely diverse since they range from DNA to high strength synthetic polymers like Kevlar (used for bullet-proof vests, protective clothing, high performance

composites for aircraft and automotive industries) and from small organic molecules like alkyl and alkoxy cyanobiphenyls used in liquid crystal displays (LCDs) to self-assembling amphiphilic soap molecules. Recently their biomedical applications such as in controlled drug delivery, protein binding, phospholipid labeling, and in microbe detection have been demonstrated. Apart from material science and bio-science, LCs are now playing significant role in nanoscience and nanotechnology such as synthesis of nanomaterials using LCs as template, the design of LC nanomaterials, alignment and self assembly of nanomaterials using LC phases and so on. Owing to their dynamic nature, photochemically, thermally or mechanically induced structure changes of liquid crystals can be used for the construction of stimuli-responsive materials. Although LCs have diverse applications such as temperature sensing, solvents in chemical reactions, in chromatography, in spectroscopy, in holography, etc., they are primarily known for their extensive exploitation in electrooptical display devices such as watches, calculators, telephones, personal organizers, laptop computers, flat panel television etc.

1.2 Liquid crystals as an intermediate phase (mesophase) of matter

The molecules comprising a solid generally possess both positional and orientational order, meaning that the centre of mass of the molecules occupy specific locations and the molecular axes point in certain directions. So it possesses anisotropic properties that is various physical properties are direction dependent. When the solid melts to a liquid, both the positional and orientational order vanish. In this state there are no preferred locations for the centre of mass or preferred direction of orientation for the molecular axes. In the liquid state, the molecules diffuse freely throughout the sample and the centers of mass

move in random directions. So it is an isotropic phase. In addition to the solid and liquid phases, there are condensed phases that exhibit intermediate order. The simplest case is one in which the molecules are generally fixed at lattice points but in addition to vibration, may freely rotate. This type of material is referred to as plastic crystals. However, If one axis of a molecule is much longer or shorter than the other two axes, then it is possible for additional phases to form in which there is some positional and orientational order, but much less than is found in solids and plastic crystals. These are liquid crystal phases, in which the *molecules diffuse* throughout the sample while maintaining some *positional and orientational order* albeit short-ranged. The ability of the molecules to move among the various lattice sites imparts fluidity to these structures, but since all directions within the phase are not identical, they are anisotropic rather than isotropic fluids. So liquid crystals combine the anisotropic properties of solids and fluidity of liquids. Since these anisotropic ordered fluids lie in between solids and liquids and possess properties of both, they are called intermediate phases or *mesophases*.

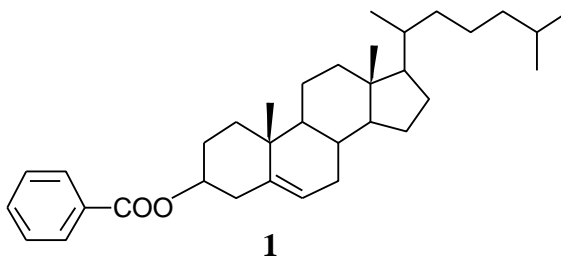
The description given above for the solid state is really appropriate for a crystalline solid. Some substances in the liquid state change into an amorphous solid rather than a crystalline solid when cooled. The molecules in the amorphous solids are fixed in place, but there is no overall pattern to the arrangement of these molecules. The molecules are arranged more or less randomly, but unlike in the liquid and liquid crystal state, they do not diffuse throughout the substance.

Let us mention a fourth state of matter called the plasma phase. It has nothing to do with liquid crystals, but it is a true state of matter just as the solid, liquid and gaseous states are. If a substance is heated to a very high temperature, the random motion

becomes so violent that electrons that are normally bound to the atoms get knocked off. This phase of matter is composed of positively charged ions and negatively charged electrons, which normally attract each other so strongly that the ions and electrons bind together. The temperature is so high, however, that the rate the ions and electrons bind together is equal to the rate the electrons are being knocked off atoms. Thus the substance exists in this state with unbound electrons and ions. It is a new phase of matter that normally exists in and around stars. Scientists presently create plasma in their experiments on nuclear fusion.

1.3 Brief history of thermotropic liquid crystals

The discovery of liquid crystals is usually attributed to an Austrian botanist by the name of Friedrich Reinitzer. In 1888, while determining the melting point of cholesteryl benzoate **1**, he noticed the unusual melting behavior of this compound [4]. It melts at 145.5 °C from solid to form a cloudy liquid and at 178.5 °C it appears to melt again to a clear liquid. He also observed some unusual colour behavior upon cooling. This strange phenomenon of the existence of “double melting” was explained by the German physicist Otto Lehmann [5]. He first referred to them as ‘soft crystals’; later he used the term ‘crystalline fluids’. As he became more convinced that the opaque phase was a uniform phase of matter sharing properties of both liquids and solids, he began to call them “liquid crystals”. The discovery of liquid crystals itself was a multidisciplinary task and so also the present day science and technology of liquid crystals. It should be noted that researchers as early as 1850s actually dealt with liquid crystals but did not realize the uniqueness of the phenomena [6].



Over the next decade about 15 Liquid crystals became known. All these materials were discovered by chance only, as no relationship between the molecular shape and liquid crystalline state was known. During the first half of the twentieth century, progress was mostly made by chemists, who discovered new types of liquid crystal molecules. Daniel Vorländer, a professor of chemistry at the University of Halle, started systematic synthetic work in order to find out structure-mesophase relationship in the beginning of twentieth century and by 1935 about 1100 liquid crystalline compounds were prepared in his laboratory alone [7]. He remarked that all the compounds exhibiting mesophases had elongated (rod-like) molecules, now called *calamitic* molecules. In 1965 at the International Liquid Crystal Conference (ILCC), the application of cholesteric liquid crystals in thermography was presented, but in 1968 ILCC, Heilmeyer's group gave the first indication for an application of liquid crystals in electrooptical display technology. This report increased the interest in liquid crystal research exponentially which continues even today. By 1992 the number of liquid crystalline materials increased to about 50,000. To date more than hundred thousand liquid crystalline compounds are known in the literature.

In 1977, Chandrasekhar and his colleagues reported that not only rod-like i.e. calamitic molecules, but also compounds with disc-like molecular shape are able to form

mesophases [8]. Currently more than 3000 discotic liquid crystals are known in the literature.

The latest addition in the liquid crystal family is banana-shaped molecules in 1996 [9]. Typically their molecular structure can be regarded as being composed of three units; an angular central unit, two linear rigid cores and terminal chains. The discovery of ferroelectricity in non-chiral banana shaped molecules has led to a very intense research activity in the field. Several hundred bent molecular shape compounds have been synthesized so far. Bent shaped molecules provide access to mesophases with polar order and supramolecular chirality.

1.4 Classification of liquid crystals

There are various ways of classifying liquid crystals such as: depending on the molar mass of the constituent molecules; low molar mass (monomeric and oligomeric), and high molar mass (polymeric) liquid crystals; depending on how the liquid crystalline phase has been obtained whether by adding solvent (*lyotropic*) or by varying the temperature (*thermotropic*); depending the nature of the constituent molecules (organic, inorganic and organometallic); depending on the geometrical shape of the molecules (rod- like , disc-like, bent core); depending on the arrangement of the molecules in the liquid crystalline phase (nematic, smectic, columnar, helical, B phases etc). The classification of liquid crystals is shown in Figure 1.

However, the most widely used classification of liquid crystals is into two major categories; (a) Thermotropic liquid crystals (Mesophase formation is temperature dependent), and (b) Lyotropic liquid crystals (Mesophase formation is solvent and

concentration dependent). If a compound displays both thermotropic and lyotropic liquid crystalline phases then it is called *amphotropic* liquid crystal.

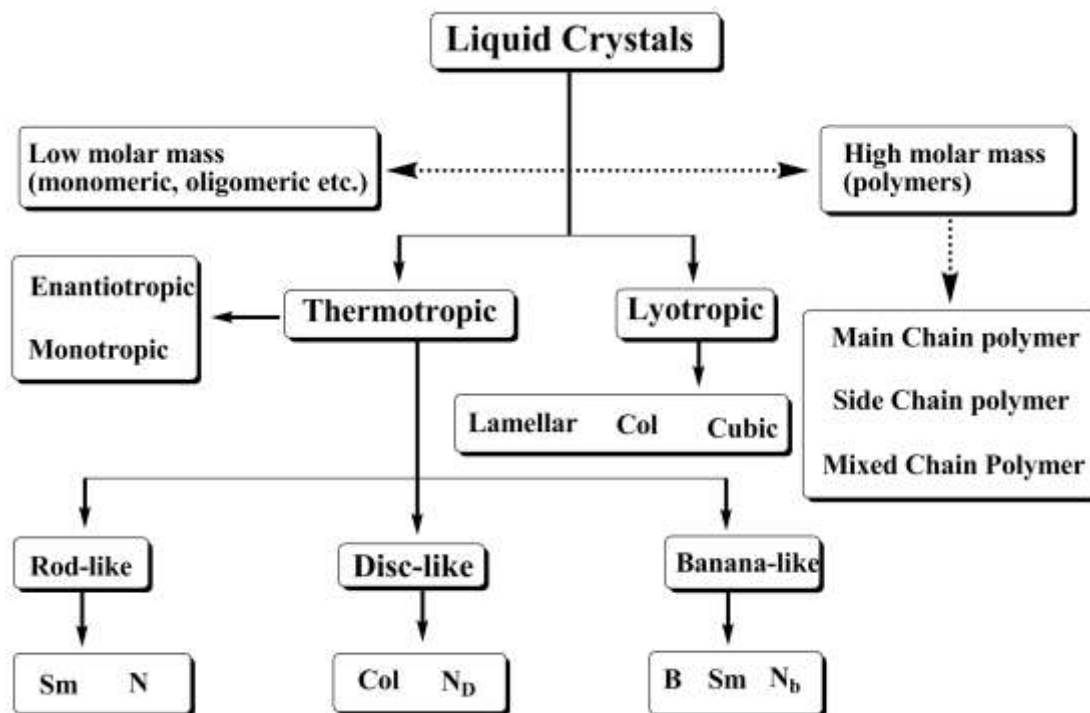


Figure 1. Classification of liquid crystals.

Since this thesis deals with **thermotropic liquid crystals**, a very brief introduction of the lyotropic liquid crystals has been given below owing to their biological significance and they play an important role in living systems [10].

1.4.1 Lyotropic liquid crystals

Lyotropic liquid crystals are composed of molecules with amphiphilic properties dissolved in a solvent. The amphiphilic compounds are characterized by two distinct parts of contrasting character, a hydrophilic polar “head” and a hydrophobic nonpolar “tail”. Mesophase formation in lyotropic liquid crystals is controlled by concentration

and/or temperature. Typical examples of lyotropic liquid crystals are soaps in water and various phospholipids. Just as there are many different types of structural modifications for thermotropic liquid crystals, there are several different types of lyotropic liquid crystal phase structures. Each of these different types has a different extent of molecular ordering within the solvent matrix. Three different classes of lyotropic liquid crystal phase structures are widely recognized. These are the lamellar, the hexagonal columnar and the cubic phases (Figure 2), and their structures have each been classified by X-ray diffraction techniques.

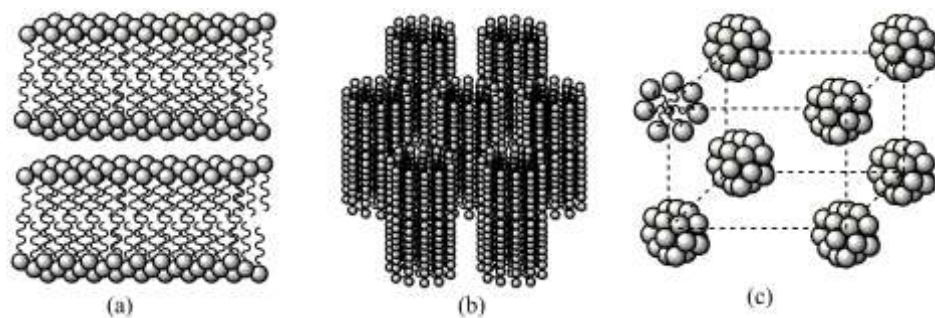


Figure 2. Lyotropic liquid crystalline phases.

1.4.2 Thermotropic liquid crystals

When the liquid crystalline phases are obtained by varying the temperature of the compounds then they are called thermotropic liquid crystals. The mesophase can be obtained by heating a solid or by cooling an isotropic liquid. The transition temperature from the crystal to the mesophase is called the *melting point*, while the transition temperature from the mesophase to the isotropic liquid is named as *clearing point*. When thermodynamically stable mesophases are obtained both heating and cooling then the phases are called *enantiotropic*. If the mesophase is obtained only while cooling the

isotropic liquid then it is called *monotropic* phase and is a metastable mesophase, and the mesophase transition occurs below the melting point. The essential requirement for a molecule to be a thermotropic liquid crystal is a structure consisting of a central core (often aromatic) and a flexible peripheral moiety (generally aliphatic chains). Moreover, along with the geometric anisotropy, interaction anisotropy and microsegregation are the driving parameters for mesophase formation. Based on the shape of the mesogenic molecules, thermotropic liquid crystals are classified into three main groups: (a) calamitic (rod-like); (b) discotic (disc-like), and (c) bent core (banana-like).

1.4.3 Calamitic liquid crystals

The most common type of molecules that form mesophase is rod-like molecules. These molecules possess an elongated shape i.e. the molecular length (l) is significantly greater than the molecular breadth (b) as depicted in Figure 3.

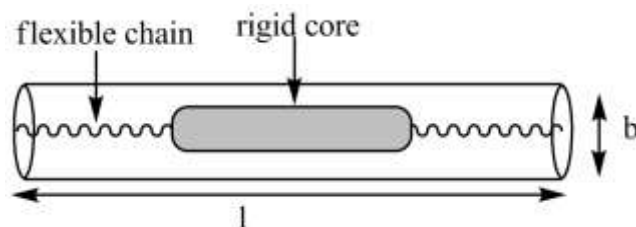


Figure 3. Representation of a calamitic liquid crystal where $l \gg b$.

The shape anisotropy in combination with interaction anisotropy and microsegregation of incompatible parts in calamitic liquid crystals leads to a number of mesophase morphologies. Most of the calamitic liquid crystalline compounds consist of two or more ring structures, bonded together directly or via linking groups. They usually have terminal hydrocarbon chains and some time lateral substituents as well. The typical chemical structure of these molecules can be represented by the general template as

shown in Figure 4, where A and B are core units (benzene, naphthalene, biphenyl etc.), R and R' are flexible moieties such as normal and/or branched alkyl groups, M and N are generally small lateral substituents (-X, -NO₂, -CH₃, -OCH₃, -CN etc.). Y is a linking group to the core units and X & Z are linking groups of terminal chains and core units.

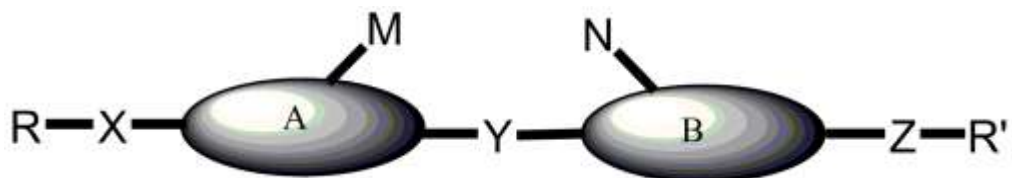


Figure 4. General template of calamitic liquid crystals.

Lateral substituents M and N are responsible to modify the mesophase morphology and physical properties of calamitic liquid crystals. Calamitic liquid crystals can be further classified into (a) Nematic (from Greek word *nematos* meaning “thread”), and (b) Smectic (from the Greek word *smectos* meaning “soap”) etc. depending on the arrangement of the mesogens in different mesophases.

1.4.3.1 Nematic Phase

The nematic phase has a high degree of long-range orientational order of the molecules, but no long range positional order. This is the least ordered mesophase (closest to the isotropic liquid state). It differs from the isotropic liquid in that the molecules are spontaneously oriented with their long axes approximately parallel (Figure 5). The preferred direction of orientation of the molecules, depicted as a long arrow, is called the *director*.

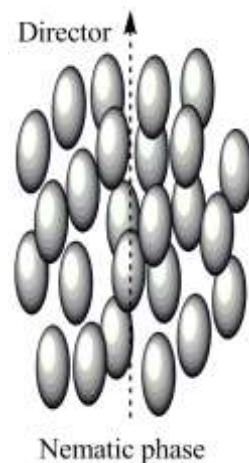


Figure 5. Schematic representation of calamitic nematic liquid crystals.

1.4.3.2 The chiral nematic phase

The first thermotropic liquid crystalline material discovered in 1888 by Austrian botanist Reinitzer, exhibits what is now known as the chiral nematic phase (N^*). Historically, the chiral nematic phase was called the *cholesteric phase* because the first materials exhibiting this phase were cholesterol derivatives. Today this is not the case and there are many different types of chiral materials that exhibit the chiral nematic (cholesteric) phase and these have no resemblance to cholesterol. In fact, a chiral nematic phase can be generated by adding a small quantity of chiral material (not necessarily liquid crystalline) to a nematic material. It is thought that this is achieved by the chiral dopant creating a chiral environment for all of the other achiral molecules and hence a helical macrostructure is generated. The asymmetry of the constituent molecules of the chiral nematic phase causes a slight and gradual rotation of the director. This gradual change describes a helix which has a specific, temperature-dependent pitch (Figure 6). The helical structure has the ability to selectively reflect light of a wavelength equal to that of the helical pitch length. If the pitch length is of the order of the wavelength of visible

light, then colours are selectively reflected. The pitch length is temperature dependent and hence so is the color of the reflected light. This is the basis behind the commercially successful use of chiral nematic materials in thermochromic thermometer devices and other devices that change colour with temperature.

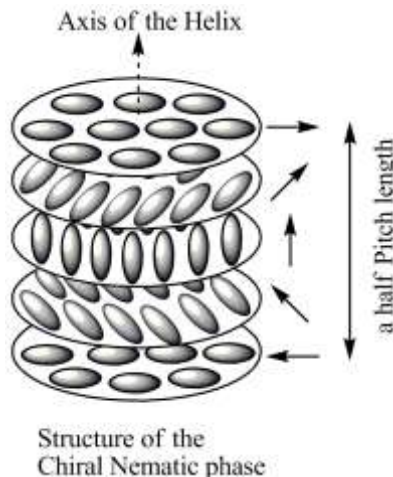


Figure 6. Representation of cholesteric phase.

1.4.3.3 Smectic phases

Rod-like molecules are able to form liquid crystalline phases where in addition to the orientational order, the molecules possess short range positional order as well. The molecules are arranged in layers with well defined layer spacing or periodicity. The smectic phase is denoted by the symbol Sm. There are several types of smectic mesophases, characterized by a variety of molecular arrangements within and between the layers. Although the total number of smectic phases cannot be specified, the following types have been defined: SmA, SmB, SmC, SmF, SmI etc. However, SmA and SmC mesophase are more commonly encountered (Figure 7). In SmA phase the

molecules form layers with their long molecular axes and hence the director parallel to the layer normal. The SmC phase has the same layer structure of the SmA, but the molecules are tilted with respect to the layer normal. In both the phases, there is no positional order among the molecules within the layers. However, they possess 1D layer periodicity (periodical stacking of the layers). SmB, SmF and SmI are more ordered smectic phases in which the molecules possess hexagonal order within the layers. They are called hexatic smectic liquid crystals. Disordered crystals having layer-like structures are often referred to as SmE, SmH, SmK, SmG and SmJ phases but they are more properly defined as lamellar plastic crystals. Tilted smectic mesophases formed by chiral compounds or containing chiral mixtures are designated by the superscript * (SmC*, SmF*, etc.). More recently, a frustrated smectic liquid crystal phase has been discovered that occurs above the temperature of the normal smectic phases in some chiral materials; this phase is called the twist-grain boundary (TGB) phase.

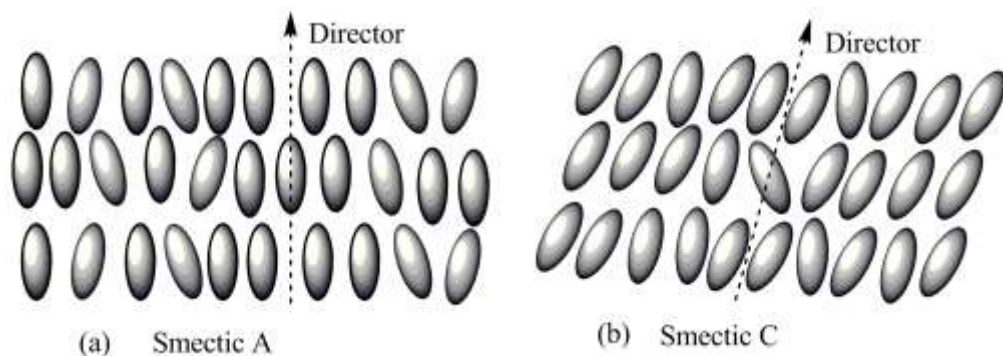


Figure 7. Smectic A and Smectic C liquid crystal phases.

1.4.3.4 Smectic C* phase

When the constituent molecules of the smectic C phase are chiral the phase is called smectic C*. The phase structure is basically the same except that the molecular chirality causes a slight and gradual change in the direction of the molecular tilt (there is no change in the tilt angle with respect to the layer normal). This change in tilt direction from layer to layer gradually describes a helix (Figure 8). Since the tilted molecules of the smectic C* phase are chiral the symmetry of the layers is reduced to a two-fold axis of rotation.

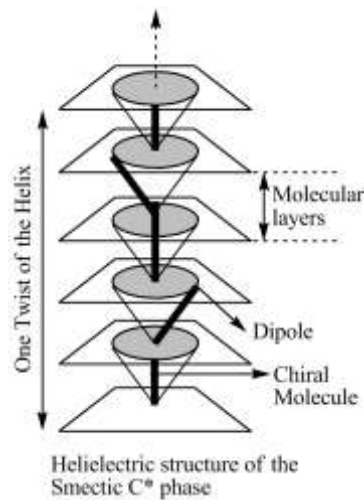


Figure 8. Helielectric structure of smectic C* liquid crystal.

Even though the molecules are undergoing rapid reorientational motion, the overall result of the reduced symmetry is to create an inequivalence in the dipole moment along the C_2 axis. Such dipole inequivalence generates a spontaneous polarization (P_S) along the C_2 axis, the direction of which changes with the changing tilt direction of the helix. Accordingly, P_S is reduced to zero throughout a bulk sample which is not influenced by external forces, hence the SmC* phase is truly defined as helielectric. However, a single

layer of the chiral smectic C phase is ferroelectric and so by unwinding the helix (by external forces such as surface interactions) a true ferroelectric phase is generated [11].

1.4.3.5 Ferro- antiferro- and ferrielectric chiral smectic C phases

Ferroelectricity arises when the naturally helielectric smectic C* phase is unwound. If this unwinding of the helix allows the layer polarizations to point in the same direction then the phase is called ferroelectric. This phase will possess a net bulk polarization. However, the unwinding of the helix can lead to two other phases known as antiferroelectric and ferrielectric phases.

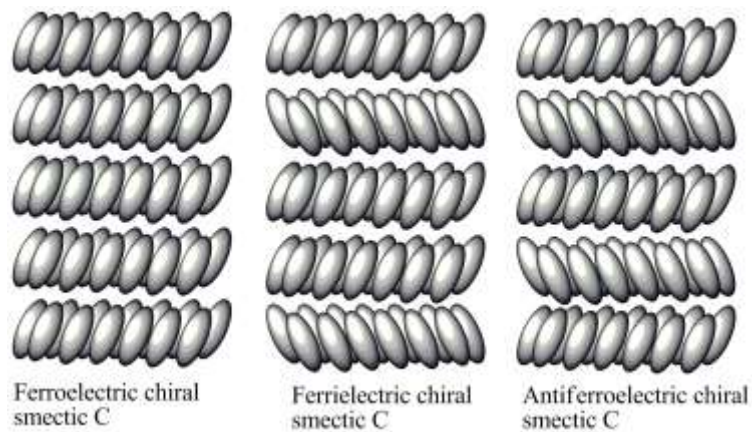


Figure 9. Schematic representation of ferro-, ferri- and antiferroelectric chiral smectic phases.

The suggested structure of the antiferroelectric phase shows that the molecular layers are arranged in such a way that the polarization directions in subsequent layers point in opposite directions which results in an averaging of the spontaneous polarization to zero. Evidence to support this hypothesis comes from the fact that when a strong electric field is applied to this phase the layer ordering is perturbed and the phase returns to a normal

ferroelectric phase. Removal of the field will generate the antiferroelectric phase. In the ferroelectric phase, the layers are stacked in such a way that there is a net overall spontaneous polarization. In this phase, the number of layers of opposite polarization is not equal i.e. more layers are tilted in one direction than the other. The structures are shown in the Figure 9.

1.5 Discotic liquid crystals

Since this thesis mainly deals with **discotic liquid crystals**, they are discussed in greater details later in this chapter after a brief introduction of banana liquid crystals.

1.6 Banana liquid crystals

Molecules incorporating a bent rigid core (banana-shaped molecules) **2** have been synthesized and investigated.

The bend in the rigid cores of the banana liquid crystal compounds leads to a reduction of the rotational disorder of the molecules about their long axes. The reduced symmetry of the rigid segments of such molecules leads to a directed packing of the molecules within layers. The important consequence of the directed packing of such molecules is the occurrence of a polar order parallel to the smectic layers. In order to escape from a macroscopic polarization, the layer structures are modified, and this leads to new mesophase morphologies. Bent core molecules are the first examples which have experimentally shown that antiferroelectric switching with large spontaneous polarization is indeed possible in a liquid crystal phase composed of non-chiral materials. In most of

these mesophases the molecules are additionally tilted (SmCP) and this leads to a further reduction of the phase symmetry. An inherent handedness of such SmCP phase is observed, and this handedness is *geometrical* in nature and does not result from a molecular chirality. This inherent chirality can lead to mesophases with chiral supramolecular structures even though the molecules themselves are achiral. The formation of helical super structures in order to escape from a macroscopic polarization is another way to chirality in such supramolecular systems composed of achiral molecules. Moreover, in some cases macroscopic regions of opposite handedness are spontaneously formed. Due to the absence of molecular chirality both enantiomeric structures are equally probable. These dark conglomerates or dark racemates are optically isotropic phases with local SmCP order. Bent core molecules open the door to novel complex types of molecular self-organization and to the new field of supramolecular stereochemistry. None of the B phases are miscible with any smectic phase of calamitic compounds. Special molecular packing of bent molecules in smectic layers could give rise to ferro-, ferri- or antiferroelectric properties. Bent core mesogens are the first thermotropic liquid crystals for which a biaxial nematic (N_b) phase was unambiguously determined [12]. The occurrence of superstructural chirality in the mesophase of bent-core compounds without having any chiral auxiliary in the molecules is not only of fundamental scientific interest but also of industrial application as this chirality can be switched in external electric fields. Various new applications of these materials include nonlinear optics, flexoelectricity, photoconductivity, molecular electronics and the design of biaxial nematic phase. Figure 10 shows a general template of banana liquid crystal molecules.

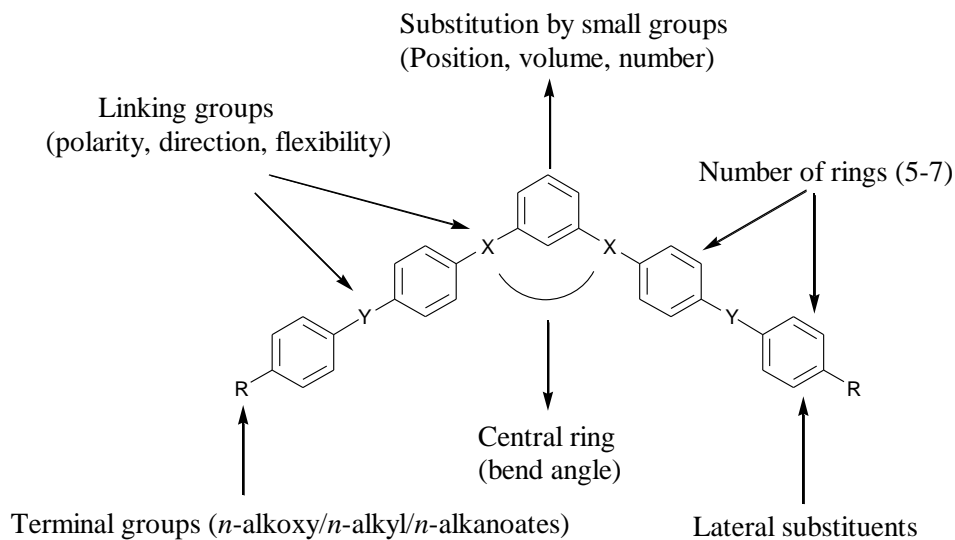


Figure 10. General template for banana liquid crystals.

Bent molecular structures represent a new sub-class of thermotropic liquid crystals, which can display not only classical nematic and/or smectic phases, but also novel types of smectic-like phases called “B” phases and are numbered according to their chronological discovery, from B₁ to the most recent B₈. The symbol B stands for banana- or Bent- or Bow-shaped mesogens. The three vectors (1) layer normal, (2) tilt direction and (3) polar axis (kink direction) make-up an orthogonal system which may be left or right handed. Right and left handed systems are mirror images of one another and hence chiral (Figure 11). If there is a dipole moment associated with the kink this axis becomes the polar axis which is responsible for ferroelectricity. Macroscopic samples are achiral. If chirality alters from layer to layer in a sample, it is called racemic. If there are macroscopic domains with homogeneous chirality, the sample is homochiral.

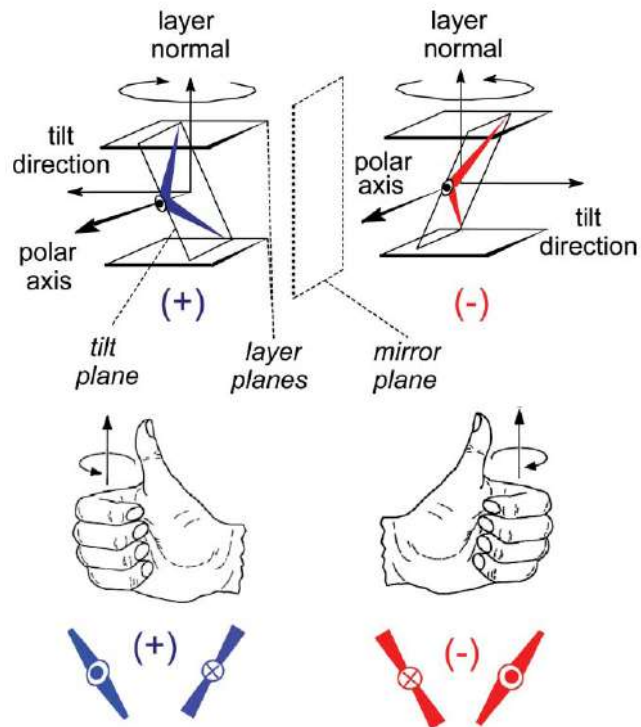


Figure 11. Origin of chirality in banana liquid crystals.

1.7 Polymeric liquid crystals

Basically, there are two types of liquid crystal polymers; main chain LC polymer and side chain LC polymer. Main chain liquid crystal polymers (MCLCPs) consist of repeating mesogenic monomer units. The monomer unit must be anisotropic and difunctional to enable polymerization and the generation of mesophases. Side chain liquid crystal polymers (SCLCPs) consist of mesogenic structural moieties appended from a polymer backbone. The mesogenic units are invariably separated from the polymer backbone by fairly long spacer units which are usually several methylene units or ester units or ether units at the point of attachment. The long flexible spacers in the polymer structure provide adequate mobility for the formation of liquid crystalline phases. Attachment of the calamitic mesogenic units is usually at the terminal position however a few polymers

have their mesogenic units attached at a lateral position. A third class of liquid crystal polymers is called combined liquid crystal polymers. These polymers combine the features of main chain and side chain polymers.

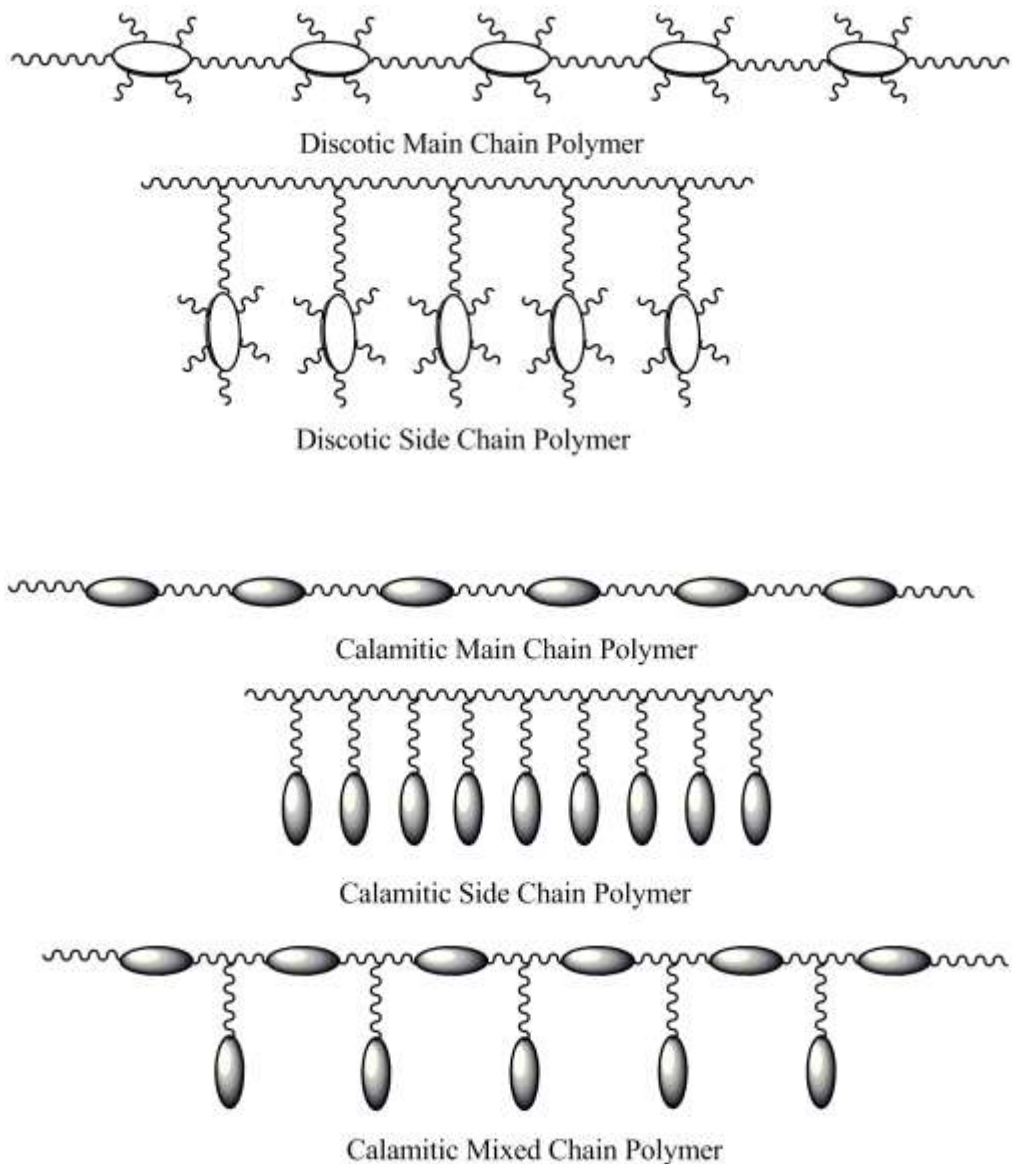


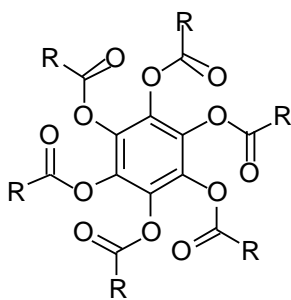
Figure 12. Main chain and side chain liquid crystal polymers.

Side chain mesogenic units can be attached via a spacer unit, to a mesogenic main chain either at the linking unit or at the mesogenic unit. Depending on the shape of the

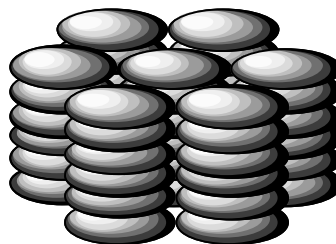
mesogenic units in the polymers they can be classified as calamitic or discotic liquid crystal polymers [13]. They are shown in Figure 12. Moreover in between the low molar mass monomeric and high molar mass polymer LCs there exist monodisperse LC dimers, trimers, higher oligomers and dendrimers which have served as the model compounds to understand the transitional properties of LC polymers.

1.8 Discotic liquid crystals: the discovery

In September 1977, when the rod-like thermotropic liquid crystals started revolutionize commercial display technologies, Sivaramakrishna Chandrasekhar and his colleagues at the Raman Research Institute reported “...*what is probably the first observation of thermotropic mesomorphism in pure, single component systems of relatively simple plate like, or more appropriately disc-like molecules*” [8]. They prepared a number of benzene hexa-*n*-alkanoates (**3**) and from thermodynamic, optical and X-ray studies, it was established that these materials form a new class of liquid crystals in which molecules are stacked one on the top of other in columns that constitute a hexagonal arrangement. This opened a whole new field of fascinating liquid crystal research.



3



It is interesting to mention that Vorländer in 1924 supposed the possibility of the existence of mesophases in leaf-shaped molecules [14] but his attempts to realize any

example with this behaviour had been unsuccessful probably because the molecules, he looked at were devoid of flexible chains. He mentioned in his article that leaf-shaped molecules do not form any liquid crystals at all. Of course, the same molecules surrounded by long aliphatic chains are now well-known for forming columnar mesophases.

In the early 1960s, anisotropic mesophases with nematic texture had been observed during the pyrolysis of graphitizable substances (carbonaceous mesophase) [15]. These mesophases were considered to be built up of flat polyaromatic molecules, however, and not by well-defined organic molecules. They were not stable and homogeneous in nature. Therefore, it was not possible to fully characterize these mesophases.

Self-organization of disc-like molecules to form columnar liquid crystals by Chandrasekhar *et al.* were an entirely new class of liquid crystal, quite different from the classical liquid crystals formed by rod-like molecules that had been known since they were observed by Friedrich Reinitzer in 1888. The disc-like molecules spontaneously self assemble in one-dimensional (1D) stacks, which in turn, self-organize on various two-dimensional (2D) lattices; the third dimension has no translational order (Figure 13).

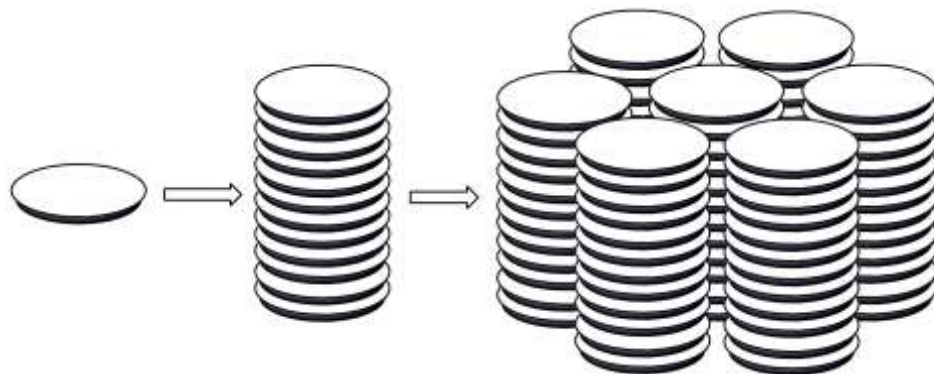


Figure 13. Self assembly of discotic liquid crystals into columnar phase.

1.9 Structure of the liquid crystalline phases formed by discotic mesogens

Most of the discotics exhibit only one type of mesophase but few examples are known to exhibit polymorphism [16]. Mesophases formed by disc-shaped molecules are primarily four types: (i) Nematic, (ii) Smectic, (iii) Columnar and (iv) Cubic. The columnar phase is ubiquitous in discotics followed by nematic phase whereas the other phases are rarely observed.

1.9.1 Nematic Phases of discotic mesogens

The nematic phases of disc-shaped molecules can be subdivided into three different kinds depending on the molecular arrangements. 1. Discotic Nematic (N_D), 2. Chiral Nematic (N_D^*) 3. Columnar nematic (N_{Col}) and 4. Nematic lateral (N_L).

In the discotic nematic phase, the molecules stay more or less parallel, having orientational order but no long range positional order (Figure 14a). The nematic phase of disc-shaped molecules is usually not miscible with the nematic phase of rod-shaped molecules. However, the symmetry of the nematic phase formed by disc-shaped molecules is identical to that formed by rod-shaped molecules. In discotic nematic phase the director is along the short molecular axes of the molecule since the disc normals are orientationally ordered. The phase is denoted by the symbol ' N_D '. Like chiral calamitic nematic or cholesteric phase, chiral discotic nematic mesophase N_D^* also exists. The mesophase occurs in mixtures of discotic nematic and mesomorphic or non-mesomorphic chiral dopants as well as in pure chiral discotic molecules. Chiral discotic nematic phase is characterized by a helical structure. The nematic columnar phase is characterized by a columnar stacking of the molecules. However, these columns do not form two-

dimensional (2D) lattice structures (Figure 14c). They display a positional short-range order and an orientational long-range order. Recently, another nematic phase has been reported, where the disc shaped molecules aggregate into large disc-shaped superstructures, and these aggregates show a nematic arrangement (Figure 14d). The phase is referred as the nematic lateral phase (N_L) due to strong lateral interactions [16].

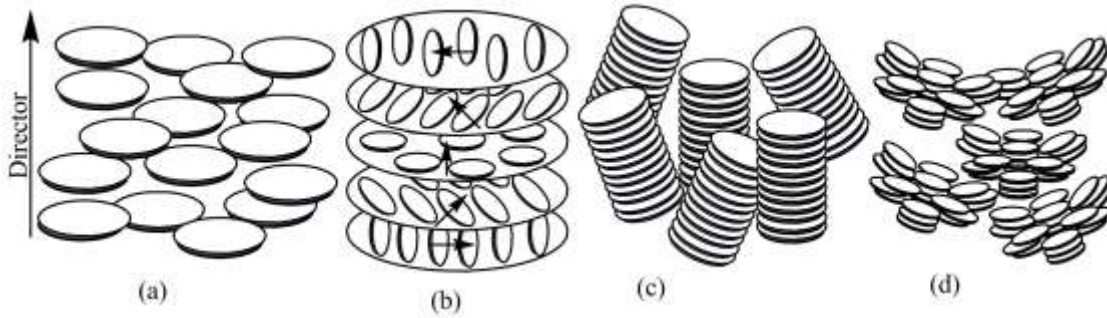


Figure 14. Nematic phases of discotic liquid crystals.

1.9.2 Smectic phases of discotic mesogens

When there is an uneven distribution of the peripheral chains or there is reduced number of peripheral chains, the discotic mesogens exhibit smectic mesophase as shown in the Figure 15. Like the calamitic smectic mesophases, in discotic smectic mesophases the discs are arranged in a layered fashion separated by sub layers of peripheral chains [17]. Since the molecular rotations about their long molecular axes will be restricted in the layers, they are expected to exhibit biaxial smectic phases. Unlike columnar phases, smectic phases are rare in discotic LCs.

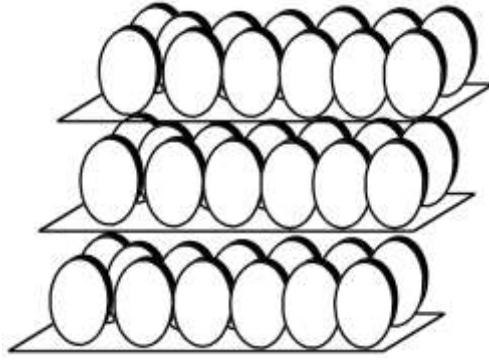


Figure 15. Smectic phase of discotic liquid crystals.

1.9.3 Columnar phases of discotic mesogens

In columnar mesophases, molecules assemble themselves one on the top of the other in columns and these so formed columns self-organize in various two-dimensional lattice. The molecules may be arranged in a regular ordered manner or aperiodically (disordered). Depending on the degree of order in the molecular stacking, orientation of the molecules along the columnar axis, the dynamics of the molecules within the columns and the two-dimensional lattice symmetry of the columnar packing, the columnar mesophases may be classified in seven classes. 1. Columnar hexagonal mesophase (Col_h), 2. Columnar rectangular mesophase (Col_r), 3. Columnar oblique phase (Col_{ob}), 4. Columnar plastic phase (Col_p), 5. Columnar helical phase (H), 6. Columnar square (tetragonal) phase (Col_{tet}), and 7. Columnar lamellar phase (Col_L).

1.9.3.1 The hexagonal columnar mesophase (Col_h)

Columnar hexagonal mesophase is characterized by a hexagonal packing of the molecular columns. Hexagonal mesophases are often denoted as Col_{ho} (Figure 16) or Col_{hd} where h stands for hexagonal and o and d for ordered or disordered stacking of the molecules. In both the cases, fluidity exists; only the correlation lengths are different and,

therefore, it is recommended to discontinue o and d subscripts. The recommended abbreviation for columnar hexagonal phase is “Col_h”.

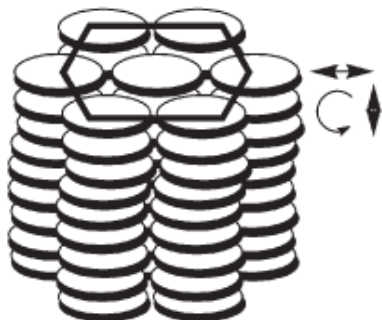


Figure 16. Hexagonal columnar phase.

1.9.3.2 The rectangular columnar mesophase (Col_r)

The columnar rectangular mesophase consist of the stacking of the aromatic cores of the molecules in columns surrounded by disordered aliphatic chains and packed in a rectangular fashion. Three different types of rectangular mesophase Col_r have been identified (Figure 17 & 18). In general, the molecules are tilted with respect to the column axis [18], whereby the cross section, orthogonal to the axis of a column, is elliptic. Depending on the mutual orientation of the molecules (ellipses) and the number of columns per unit cell in the lattice, Col_r phases have been divided into three different types. The symmetry of the 2D lattices are specified by three different planar space group i.e. P2₁/a, P2/a and C2/m (Figure 18a-c) belonging to the subset of space groups without any translational order in the direction of the principal symmetry axis i.e. the direction of the columns. In the lattice with space group P2₁/a, the ellipses are oriented alternatively along two different directions (herringbone packing of elliptical columns), the long axes of the ellipses are orthogonal to the column axis and the lattice contains two columns per

unit cell. The $P2/a$ lattice has elliptical columns having three different orientations and has four columns per unit cell whereas in the $C2/m$ lattice the ellipses are oriented along a unique direction and the unit cell possesses two columns. Stronger core-core interactions are needed for the formation of the rectangular phases because the cores of one column have to ‘know’ how they must be tilted with respect to the cores of the neighboring columns. Therefore, crossover from columnar rectangular to hexagonal mesophases with increasing side-chain lengths has often been observed.

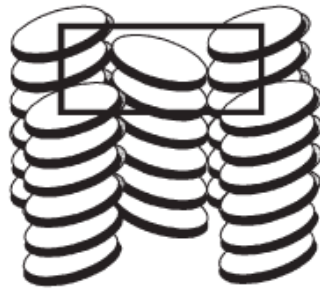


Figure 17. Columnar rectangular phase.

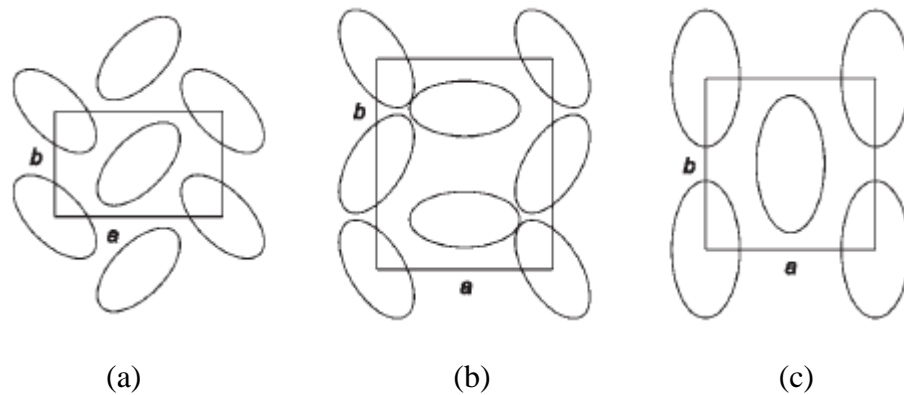


Figure 18. Different types of rectangular columnar phases (a) $Col_r(P2_1/a)$; (b) $Col_r(P2/a)$ and (c) $Col_r(C2/m)$.

1.9.3.3 The columnar oblique mesophase (Col_{ob})

Figure 19 shows the arrangement of the columns in a columnar oblique mesophase, in which the tilted columns are represented by elliptic cross sections. The symmetry of this 2D lattice corresponds to the space group P_1 . Examples for columnar oblique mesophases are rare because of strong core-core interactions [19].

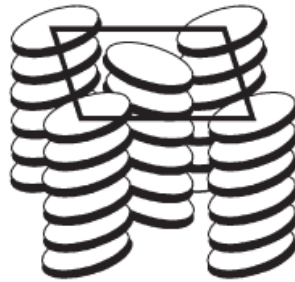


Figure 19. Columnar oblique phase.

1.9.3.4 The columnar plastic mesophase (Col_p)

Columnar plastic phase, denoted as Col_p , has been identified recently in discotic liquid crystals [20].

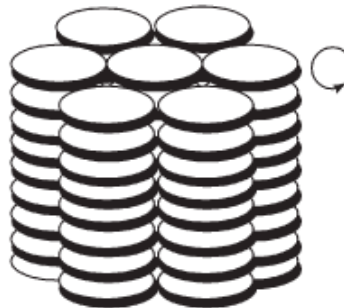


Figure 20. Columnar plastic phase.

This phase is characterized by three-dimensional crystal-like order in a hexagonal lattice, while the discs within the columns are able to rotate about the column axis (Figure 20). In

the case of Col_h phase structural disorders such as non-parallel arrangement of the discs, longitudinal and lateral displacements and rotation around the columnar axis occur, while the motional freedom of discs in the Col_p phase is restricted.

1.9.3.5 The columnar helical (H) phase

An exceptional mesophase structure with helical order has been demonstrated for a triphenylene derivative namely hexahexylthiotriphenylene (HHTT) [21]. In this so-called H phase helical columns develop which interdigitate in groups of three columnar stacks. The H phase found in HHTT is illustrated in Figure 21.

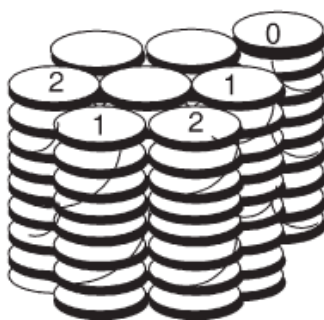


Figure 21. Columnar helical phase.

1.9.3.6 The columnar lamellar mesophase

A layered structure is known to exist for mesophases of certain discotic compounds e.g. bis(*p*-*n*-decylbenzoyl)methanato copper(II), some perylene derivatives, etc. [22]. Such a columnar lamellar mesophase which is denoted by the symbol Col_L is shown in Figure 22. In this phase discotic molecules stack to form columns and these columns are arranged in layers, where the columns in layers can slide. But the columns in different layers do not possess any positional (translational) correlation.



Figure 22. Columnar lamellar phase.

1.9.3.7 The columnar square (tetragonal) phase

The columnar square phase otherwise known as the tetragonal phase (Col_{tet}) is shown in Figure 23. Here the columns are upright and they are arranged in a square lattice. Like columnar hexagonal phase, this phase also exhibit spontaneous homeotropic alignment of the columns. This phase is exhibited by sugar molecules, phthalocyanines and supramolecular fluorinated liquid crystals [23].



Figure 23. Columnar tetragonal phase.

1.10 Cubic phase

Cubic phases are ubiquitous in lyotropic liquid crystals, however some discotic phthalocyanine derivatives [23c-d] exhibit bicontinuous cubic phase which consist of interwoven but not connected branched columns.

1.11 Structure of the discotic mesogens

Since the discovery of the first discotic mesogens, most efforts are aimed at understanding the nature of the molecular parameters that favour the formation of columnar mesophase and control their transition temperatures. It is now well established that molecules forming discotic mesophases are typically made of a central discotic conjugated core substituted by 3-8 saturated chains of three or more carbon atoms. These materials often have two, three, four or six-fold rotational symmetry. However, there are many exceptions and materials with low symmetry, a non-planar, non-aromatic core having shorter number of chains are also documented. The liquid crystallinity results from the microsegregation of the two constituents: the crystalline character is promoted by the interaction between the conjugated cores while the liquid character originates from the melting of the saturated alkyl chains in the mesophase. Discotic molecules organize spontaneously under the form of one-dimensional columns, which can be oriented easily and possess self-healing properties, i.e. the capacity of repairing structural defects in contrast to crystalline materials. The search for such mesophase is mostly ruled by subtle changes in the number, size and nature of the lateral chains in addition to the central core. A general template for discotic mesogens is shown in Figure 24.

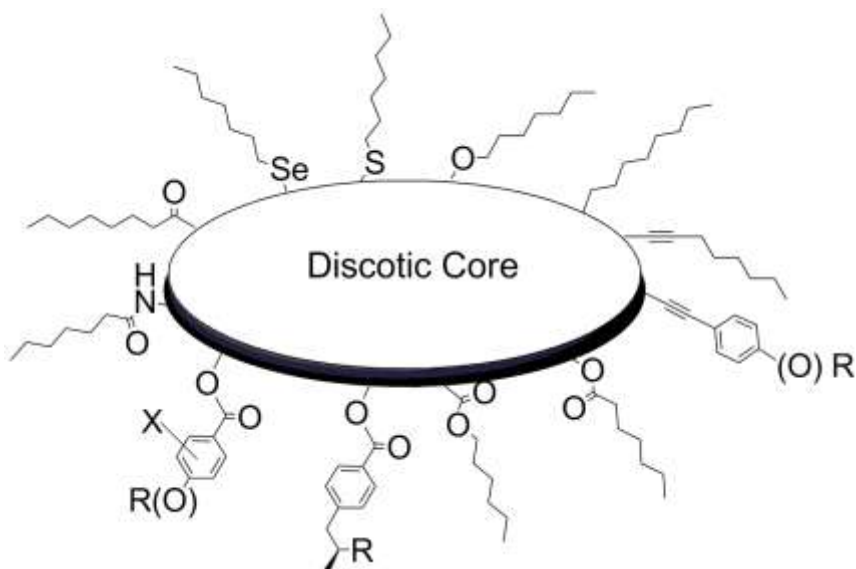


Figure 24. General template of discotic liquid crystals.

By tailoring the shape, size and nature of the central core as well as the type of the attached side chains, compounds with different ability to self-organize into different mesophase morphologies can be obtained.

1.12 Chemistry of discotic liquid crystals

From the synthetic chemistry point of view, strategies to prepare discotic mesogens are fairly straightforward. Assembling an aromatic core followed by nucleophilic or electrophilic aromatic substitutions is most common in the synthesis of discotic liquid crystalline materials. General methods for their synthesis have recently been described in the *Handbook of Liquid Crystals* [1a, 16a]. While preparation of these materials is often but not always simple, their purification is usually difficult and tedious. This is primarily because of incomplete substitution of all the functional groups. Partial substitution of polyfunctional groups gives a mixture of structurally similar products having almost

identical R_f values on a chromatographic plate and their separation is often difficult even by HPLC. It is advisable to push the reaction towards completion by taking excess of the reagent and/or longer reaction time. However, in many cases, excess of the reagent or longer reaction time cause side reactions and thus a complex mixture of the products result. Finding optimum reaction conditions is the crucial part of the synthesis. The chemistry of some of the discotic liquid crystals has been improved significantly in last few years. Highly regio-selective and high yielding methods are now available particularly for the synthesis of triphenylene based discotic liquid crystals. Various options of synthesis pursued to prepare different DLCs are as follows. The simplest route is the attachment of chains to commercially available polyfunctional cores, e.g. esterification of naturally occurring *scyllo*-inositol. However, this option is limited as only a few polyfunctional cores, suitable to prepare DLCs, are commercially available. The direct electrophilic aromatic substitution of polycyclic aromatic hydrocarbons has been used in some cases to generate polyfunctionalized core or directly liquid crystalline materials but because of regioselectivity problem, such examples are also not common. The third option is the preparation of polyfunctional cores directly starting from unprotected functionalized precursor molecules, e.g. one step preparation of hexahydroxy anthraquinone from Gallic acid. However, this option is also limited as many functional groups are sensitive towards the drastic reaction conditions used to build the core. The most common method used to prepare DLCs involves construction of the core with protected functional groups, followed by cleavage of the protecting groups and finally grafting pendant chains. Recently, particularly to prepare discotics with ether linkages, efforts have been made to avoid the protection and deprotection steps and thus, long

aliphatic chains required to induce mesogeneity were attached in the starting molecules and these then transformed directly to liquid crystalline materials using classical or modern synthetic methods. This methodology has also been applied to prepare a number of alkyl substituted DLCs.

1.13 Characterization of discotic liquid crystal phases

The thermotropic phase behavior of discotic liquid crystals is usually studied by using differential scanning calorimetry (DSC), polarized optical microscopy (POM), wide-angle X-ray scattering (WAXS) and solid-state NMR [16c]. DSC is used to determine the temperatures of phase transitions and enthalpy changes related to each transition. The fluid character of mesophases and in many cases the characteristics textures are easily observed by POM. The supramolecular organization and the corresponding packing parameters in each phase can be studied in detail by X-ray diffraction, in particular by 2D-WAXS of macroscopically orientated samples. This technique allows one to obtain a detailed insight into the intra and intercolumnar order. It is possible to determine not only the intercolumnar spacings but also to obtain information about the arrangement of discs within the columns, such as tilting and helical packing and also to provide much more dipper insight into the various microstructures adopted in the self assembly of the mesogens in the mesophase. Solid state NMR is one of the most powerful tools for the study of the molecular dynamics [24]. This technique allows one to derive independent conclusions about the rotation of the core or about peripheral mobility of side chains. Moreover, because of the different electronic environments of the aromatic protons in the intracolumnar packing, the tilted arrangement of the discs in the solid phase can be

determined as well. In general it is necessary to apply all these complementary experimental methods in order to obtain a clear, comprehensive and unambiguous picture of the bulk behavior of discotic mesogens.

The phase transition from crystalline to the LC phase is accompanied by a significant increase in molecular dynamics such as the rotation of the discs around the columnar axis, lateral and axial displacement of the discs etc. The centers of gravity of the molecules in the columnar LC mesophases are positioned along the column axis and columns can slide relative to each other giving rise to the fluid character of the phase. It is important to stress that the molecular fluctuations in the liquid crystalline mesophases support the self-healing of structural defects and hence enhance the charge carrier transport along the columnar stacks.

1.14 DLCs as materials for a new generation of organic electronics

In recent years, the organic electronics, *i.e.* the use of conjugated molecules as active components in electronic devices, is a field of immense scientific research area because of the prospect of creation of new industry, electronic devices such as, light-emitting diodes (LED), field effect transistors (FET), memory elements, sensors, photovoltaic solar cells, etc [16]. The interest in devices is not only because of potential applications but also formidable tools to probe the basic structure-property relationships that governed by the physics and chemistry of organic materials. This challenge creates the need of new organic materials with innovative design and semiconducting behaviour that deviate from conventional conjugated materials [25]. Two of the leading contenders for application in organic (opto)electronic devices are π -bond conjugated polymers and π - π stacked discotic

materials. Molecules with hierarchical self-assembly into supramolecular systems, like discotic liquid crystals which bring order (governs the performance of semiconductor) as well as dynamics (ability to self-healing of structural defects) are currently viewed a new generation of organic semiconductors in devices. The low molecular weight of conjugated liquid crystals associated with discrete mass allows the synthesis of defect-free chemical structures that are amenable to a higher purity level than most conjugated polymers [16].

1.15 Why discotics ?

The two-dimensional chemical structure of discotics creates a new situation that results in a set of unusual features. Majority of DLCs form columnar mesophases probably due to intense π - π interactions of polyaromatic cores. The core-core (intracolumnar) separation in a columnar mesophase is usually of the order of 3.6 Å so that there is considerable overlap of π -orbitals. As flexible long aliphatic chains surround the core, the inter-columnar distance is usually 20-40 Å, depending on the lateral chain length and number of lateral chains. The number of aliphatic chains around the discotic core varies from 3-8 to produce columnar mesophase. Therefore, interactions between neighboring molecules within the same column would be much stronger than interactions between neighboring columns. Consequently, charge migration in these materials is expected to be quasi-one-dimensional. Conductivity along the columns in columnar mesophases has been reported to be several orders of magnitude greater than in the perpendicular direction. Thus the columns may be described as *molecular wires* or more appropriately *molecular cables* since the conducting aromatic cores are surrounded by insulating aliphatic chains in the

columnar phase as shown in the Figure 25. Moreover, the supramolecular order of discotics on/between surfaces (substrates) can be controlled macroscopically by various techniques.

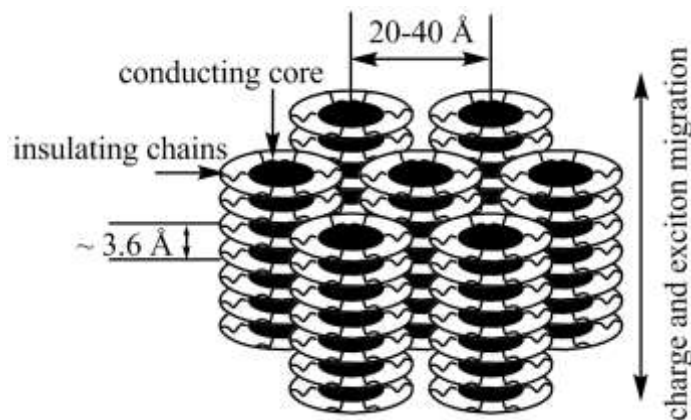


Figure 25. Energy and charge migration in discotic liquid crystals.

1.16 Discotics as semiconductor: molecular concepts, one-dimensional electrical & photoconductivity

As described already, columns in discotic liquid crystals would form molecular wires with conductive channels surrounded by insulating peripheral chains and that's why the columnar liquid crystal may display photoconductivity. Model systems for conductivity studies were based on triphenylene derivatives, which do not usually possess intrinsic charges [16]. To investigate the charge transport along the columns, charges were created by doping or through photogeneration. Vaughan *et al.* [26] doped hexahexylthiotriphenylene (HHTT) **4** with iodine, which increased the conductivity by several orders of magnitude. Boden *et al.* used hexapentyloxytriphenylene **5** with AlCl_3 , which transformed the insulating hexaalkoxytriphenylene **5** into a p-doped

semiconductor, in which the conduction along the columns was three orders of magnitude greater than in perpendicular direction. This result clearly indicates the high anisotropy of conduction in the columnar phase and the columnar phase can be considered as a practical quasi one-dimensional conductor along the columnar axis. The other discotic liquid crystalline materials which have been subjected to the measurement of charge carrier mobility are Porphyrins, Phthalocyanines, Hexabenzocoronenes (HBC) Hexaazatrinaphthylene (HATNA) etc [27]. Carrier mobility as high as $1.0 \text{ cm}^2/\text{Vs}$ is observed in the crystalline phase and in the liquid crystalline phase the value reaches $0.38 \text{ cm}^2/\text{Vs}$ in HBCs. The highest values for Porphyrins and Phthalocyanines in the liquid crystalline phases are 0.07 and $0.08 \text{ cm}^2/\text{Vs}$ respectively and for HATNA the highest is $0.20 \text{ cm}^2/\text{Vs}$. With an increase in core size the carrier mobilities increase but for very large core sizes containing 60 or more carbon atoms in the aromatic core the value decreases because of large amplitude of fluctuation disorder.

For studying charge transport (CT) in discotic liquid crystals the time-of-flight (TOF) technique, which relies on charge photoregeneration, is most widely used [27]. Charges are generated by light irradiation of discotic films in a typical sandwich-cell configuration as shown in Figure 26. A light pulse with a definite wavelength and a short duration is sent, so that the absorption and the following charge generation occurs in a

very thin layer at only the first interface. An electric field is applied to induce a drift of the charges. Depending on the polarity of the applied field, holes or electrons will move across the sample, thus inducing a transient current, which is recorded in an external circuit, and allowing the deduction of the type of the charge carriers involved.

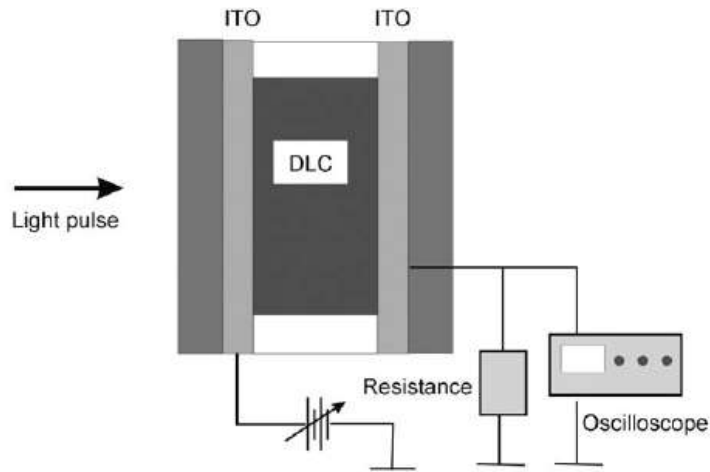


Figure 26. Set up of the TOF experiment.

The time that these charges take to travel between the electrodes allows the mobility μ to be recorded. In fact, μ depends on the applied voltage V and the transit time t_t according to the following equation, where v is the drift velocity, d is the film thickness, and E is the applied electric field.

$$\mu = v/E = d^2/Vt_t$$

The disadvantage of the TOF method is that monodomains with the columns aligned perpendicular to the electrodes (homeotropic alignment) are required. Any defect in the path has a strong effect on the mobility, so the values can underestimate the true transport

potential of the material. Discotics that do not align accordingly might be impossible to investigate with the TOF method.

When samples cannot be properly aligned, the pulse-radiolysis time-resolved microwave conductivity technique (PR-TRMC) has been used [27]. In this technique the material of interest is ionized by a nanosecond pulse of high-energy electrons from a Van de Graaff accelerator. This results in the creation of charge carriers with a uniform and known concentration of the order of micromolar. If the charge carriers formed are mobile this results in an increase in the conductivity of the sample which is monitored with nanosecond time-resolution as a transient decrease in the power of microwaves which propagates through the irradiated medium. A simple schematic representation of the technique is shown in the Figure 27.

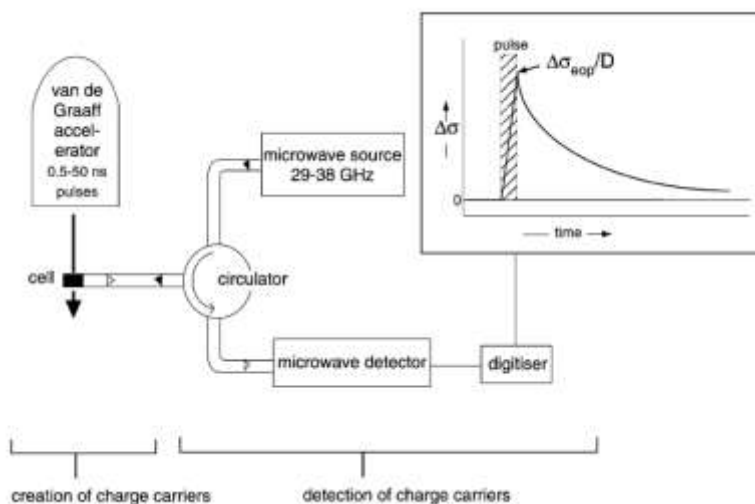


Figure 27. Set up of PR-TRMC experiment.

A PR-TRMC conductivity transient has two characteristics; the magnitude at the end of the pulse, which is proportional to the product of the concentration of carriers formed, and their mobility, and the decay after the pulse, which provides information on

the subsequent recombination and/or trapping of the charge carriers. This has been related by the following equation

$$\Delta\sigma(t) = e \sum [N_i(t) \mu_i]$$

where μ_i is the charge mobility and the N_i is the induced charge-carrier concentration in the sample. The charge carrier mobility in triphenylene discotics, measured by Adam *et al.* using time of flight photoconductivity (TOF) method [28] was confirmed by van de Craats *et al.* using electrode-less pulse-radiolysis time resolved microwave conductivity method [29]

The PR-TRMC technique has its limitations, for example, the individual contributions of the positive and negative charge carriers cannot be separately determined but it is a method that can be readily applied to any material irrespective of its morphology or optical properties, thus allowing a large number and variety of materials to be investigated and compared. Because of the low electric field strength (<100 V/cm) and the ultra high frequency (ca. 30 GHz) the random diffusional motion of charge carriers is only slightly perturbed. This together with the nanosecond time response of detection, ensures that the mobilities determined are effectively zero-field, trap-free values, characteristic of the most well-organised (highest mobility) domains within a sample [27].

Discotic mesophases do not exhibit perfect order; as a result charge carriers tend to localize to an extent that depends on the degree of order. Thus a coherent band like description is inappropriate and a phonon-assisted hopping picture is more suitable as a starting point to describe charge transport in discotics. In this case, the charge carriers are localized on single molecules and jump from disc to disc along the stacks. The frequency

of charge hopping between two adjacent discs can be approximately estimated on the basis of semi classical Marcus theory [30]. For such a self-exchanging electron (hole) transfer process the rate of charge hopping depends on two main parameters: the *reorganization energy* and the intermolecular *transfer integral*. High transfer rates and hence high charge mobility, requires small values for the former and large values for the latter [31]. The reorganization energy is sum of two terms: the inner reorganization energy of the molecule and reorganization energy of the surrounding medium. For discotic liquid crystals in the bulk state the inner reorganization energy plays a significant role since there is no other surrounding medium. The reorganization energy reflects the geometric changes in the molecule when going from the neutral to ionized (ionic or radical) state or vice versa. The intermolecular transfer integral characterizes the strength of the electronic coupling between the molecules; the absolute values can be estimated to a good approximation as half the electronic splitting of the HOMO (LUMO) levels for holes (electrons) in a dimer made of two neutral molecules. For discotics the transfer integral has been shown to be very sensitive to the relative position and orientation of the neighboring molecules. Most favorable for charge transport is the co-facial orientation. For higher temperatures, however, other factors, such as the variation of the order parameter with the temperature and the thermal activation effects, should be taken into account in the model [27].

The chemical structure, symmetry and size of the conjugated core, the shape of the wave function, the nature of the connecting groups between the conjugated core and the flexible alkyl chains, the phase morphology and transition temperatures all play significant role to have a good discotic semiconductor.

1.16.1 Size of the discotic core

Due to efficient π -stacking in relatively larger cores rather than in small aromatic core like benzene, variation of size of the conjugated core to design and explore novel discotic mesogens is one of the main research themes in science. The relatively larger discotic molecules like triphenylenes **4** and **5** have been extensively studied [32]. It has been proposed that increasing the size of conjugated core would reduce the core-core separation and thus enhance the charge mobility [33]. Extraordinary thermal and photochemical stability of phthalocyanines **6** (M = Metal) and porphyrin **7** discotics in the field of dyes and pigments have also been reported [34].

The synthesis of hexa-*peri*-hexabenzocoronene (HBC) derivatives **8** and **9** [35a] have shown an important achievement not only because of highest charge carrier mobility but also to passivate a way to have very large polycyclic aromatic hydrocarbons (PAH). They have an excellent opportunity in charge transport and mobility on the basis of core diameter.

The empirical relationship on the basis of charge mobility value in discotics suggested by van de Craats and Warman is

$$\Sigma\mu_{1D} = 3\exp(-83/n) \text{ cm}^2\text{V}^{-1}\text{s}^{-1}$$

Where $\Sigma\mu_{1D}$ is a mobility sum for holes (μ_+) and electrons (μ_-) along the axis of the columnar stacks and n is the number of atoms in the aromatic core [27].

The experimentally found and calculated values for HBCs and PAHs are reported by Mullen *et al.* [35b]. For relatively small cores the results of PR-TRMC measurements are in good agreement with calculations. For the aromatic cores with 60 and more carbon atoms the measured values are not convenient by the calculation results and interestingly remain insensitive to the core size. This can be the influence of fluctuations (lateral, longitudinal and rotational) on the charge transfer integral, as reported [36]. It can be resulting from the counteracting effects on the overall charge transfer integral of increasing π - π overlap but decreasing average charge density as the core size increases.

1.16.2 Connecting groups

The connecting groups between the aromatic core and the flexible alkyl chains play an important role on charge transport properties. The connecting groups and also flexible peripheral substituents together change the thermotropic behaviour of octa-substituted

phthalocyanines [37]. Changing the oxygen atom of hexahexyloxytriphenylene to sulphur atom results in the formation of a highly ordered helical columnar phase. When connecting groups are involved in some specific non-covalent intermolecular interactions, such as intermolecular hydrogen bonding for example in case of hexamide derivative of hexaazatriphenylene **10**, a inter-disc distance as short as 0.318 nm *i.e.* smaller than the Van der Walls radii of carbon atoms in PAH has been observed [38]. Also connecting groups dramatically influences the reorganization energy for positive and negative polarons of selected conjugated cores with or without substituents, which is modulated by an additional element, the orbital coefficient on the carbon atoms of the π -system directly connected to the heteroatom [39].

1.16.3 Phase behaviour and transition temperatures

Supramolecular order in mesophases is the most important parameter for efficient charge transport. The primary criteria of the material to be most suitable in charge transport, is to be liquid crystalline at ambient temperature and mesophase should be stable over a sufficiently broad temperature range and it should possess single mesophase morphology.

The increase of alkyl chain length, number and branching of the side chains of discotic molecules decreases the transition temperatures. For example, the replacement of normal alkyl chains by branched alkyl chains in hexaalkynylbenzene [40] and tricycloquinazoline [41] produces room temperature discotic nematic and columnar phases, respectively. In hexaalkyl-HBC series of discotic mesogens (**11**), the compound **11a** forms mesophases only above 100 °C with a very high clearing point [42]. On the other hand compound **11b** with longer and more sterically substituents is liquid crystalline at room temperature. Octa-alkoxycarbonyl phthalocyanines with branched chains are reported to be room-temperature liquid crystals in literature [43]. It is clear that introduction of branching produce steric hindrance within the chains and thus has an important influence on the phase behaviour of the discotic molecules. Similar behaviour was observed for the family of tetra-alkoxy phthalocyanines [37]. It clearly appears that the steric hindrance introduced by branching of the side chains has an important influence on the phase behavior of discotic mesogens. However, role of stereoheterogeneity due to branched chains is not negligible, as demonstrated for the HBC derivative **11c**. The temperature of Cr-LC transition for the stereohomogeneous (all-*S*)-**11c** is 15 °C higher than that of **11c** bearing the racemic side chains and comprising multiple

diastereoisomers [44]. Compounds displaying LC properties at all temperatures, while rare, are of considerable interest because of their ready processibility and self-healing properties at room temperature.

1.17 Alignment of discotic liquid crystals

Discotic LCs, as mentioned earlier, can be considered as active components for electronic and optoelectronic devices, such as light-emitting diodes, field-effect transistors and photovoltaic solar cells. The key physical process for these applications is the formation, transport and recombination of electrical charges. In particular the mobility of charge carriers in solid state materials is one of the most important parameters determining device performance. The short range (local) charge transport can be detected by PRTRMC measurements in which the sample is irradiated by a high energy electron beam and the local charge carrier mobility deduced from the change of microwave absorption. However, the value of long range charge carrier mobility can be determined by time of flight (TOF) experiments or directly in a field effect transistor, is usually more important for devices. These electronic mobilities not only depend on the intrinsic electronic properties of the materials but also on the macroscopic order of the molecules in thin and thick films [16, 27]. Therefore the control of their supramolecular order over macroscopic dimensions is a key issue to obtain optimized performance. The control of the molecular arrangement on/between the surfaces is also an important issue during the discotic material processing. For FET, an edge-on organization (Figure 28b) of the discotics in uniaxially oriented columns is required. In this arrangement, charge carriers drift through the columns from the source electrode to the drain electrode, under

controlled gate voltage. In contrast, the large mono-domain face-on arrangement (Figure 28a) of the discs leads to a homeotropic alignment which allows faster charge transport between the top and bottom electrodes and favors the photovoltaic and light emitting performance. So detail studies on the control of the supramolecular order and alignment on/between the surfaces leading to device applications are considered.

1.17.1 Planar alignment of discotics

Generally the alignment of discotic liquid crystals involves two processes, solution processing and melt processing. Good solubility in appropriate solvents and accessible isotropic temperatures of the discotic LCs are promoted by the disorder alkyl chains surrounding the aromatic cores. To achieve thin films with a higher macroscopic order from solution, which allowed device fabrication with improved performance, the zone casting technique has been shown to be very efficient which provides high supramolecular order with edge-on arranged molecules (Figure 29) [45]. Just spin coated samples also exhibit edge-on arrangement of discotics [46]. Discotics possess an apparently lower self-organization in drop cast films. Another innovative way to macroscopically align discotics as a thin film by solution processing is the application of a strong magnetic gradient [47]. The molecules were found to be aligned edge-on with their planes along the magnetic field. Epitaxial growth on pre-oriented and friction-deposited poly (tetrafluoroethylene) PTFE surface layers has been reported for a large variety of materials. Soluble PAHs such as TP and HBC were successfully aligned over large areas [48]. The Langmuir-Blodgett (LB) technique which is one of the most frequently applied alignment methods for TP and PCs has also been applied for the

orientation of HBCs [49]. However, for LB techniques amphiphilic character of discotics is required.

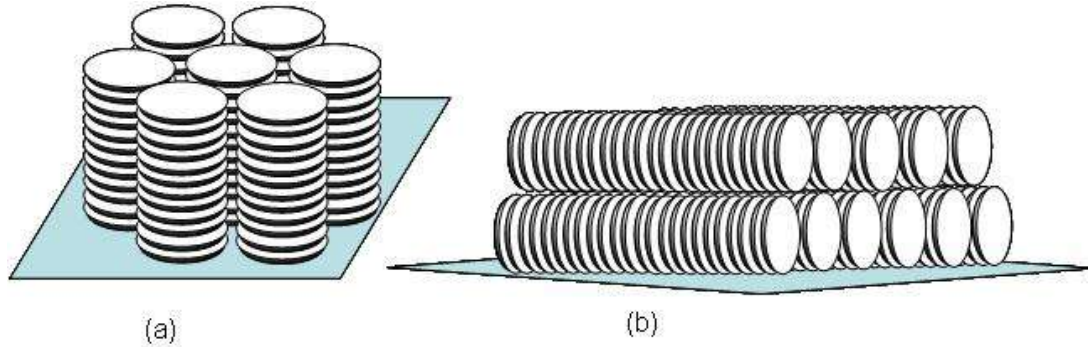


Figure 28. Homeotropic (a) and planar (b) alignment of discotic liquid crystals.

For thermal processing it is necessary to decrease the isotropic phase transition temperature with thermal stability of the discotics. Discotics can be successfully aligned by zone-crystallization technique (Figure 29). The sample was moved at a defined velocity from a hot plate with a temperature above the isotropic phase to a cold plate with a temperature lower than T_i . Between these two plates, the material crystallizes along a temperature gradient as an aligned film. 2D-WAXS revealed a columnar growth along the temperature gradient with edge-on arranged discs. Orientation is in the moving directions of the sample [50].

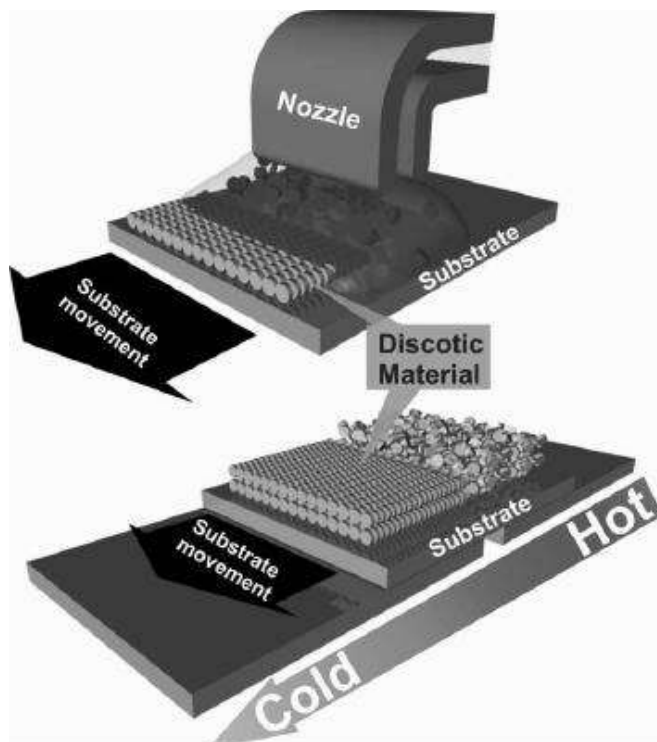


Figure 29. Zone casting (above) and zone crystallization (below) alignment of discotics.

1.17.2 Face-on arrangement (Homeotropic) of discotics

Since in a photovoltaic cell and light emitting diode the active material is sandwiched between two electrodes, a homeotropic alignment with graphene discs in a face-on arrangement might provide an undisturbed pathway for charge carriers between anode and cathode and thus might enhance the device performance. TP and HBC derivatives show spontaneous formation of homeotropic phase even at very rapid cooling rate. The planar molecules adopt a natural face-on arrangement on the substrate surface and grow as vertical columnar stacks. Not much attempt has been made to development of homeotropic alignment techniques, only dependent on spontaneous alignment of discotics. Solution processing, which have been successfully applied to planar alignment, often gives homogeneous or tilted homeotropic alignment with tilt disclination between

the domains. Annealing is used to improve molecular ordering and promote non-tilted homeotropic orientation. It has been shown that homeotropic alignment between two solid surfaces of various natures can be induced by the introduction of appropriate partially fluorinated chains at the periphery of the TP molecules [51]. Homeotropic alignment is indeed induced by specific molecule-surface interactions such as hydrogen bonding or metal coordination. Finally, homeotropic alignment can be created by an external stimulus such as polarized infrared irradiation [52].

1.18 Applications of discotic liquid crystals

After demonstration of electrical and photoconductivity and successful development of alignment techniques the various device characteristics and practical industrial applications have been demonstrated for discotics which are discussed below.

1.18.1 Discotic liquid crystals in display devices

The twisted nematic (TN) and super twisted nematic (STN) display devices have dominated commercial displays since their invention. The liquid crystal layer in these devices is exclusively the calamitic liquid crystal (composed of rod-shaped molecules). The major disadvantage of current LCDs is the narrow and non-uniform viewing cone. The growing emphasis towards higher quality wide viewing angle LCDs has fostered numerous development efforts such as, the multidomain technique [53], the introduction of an optical compensator to reduce the amount of light leakage in the dark state [54], the application of an electric field parallel to the plane of the substrates [55], the so-called ‘amorphous’ twisted nematic liquid crystals [56], etc. The viewing angle of LCDs for gray scale and colour has significantly improved over the past few years due to these

recent developments. However, some additional complex processes are necessary to be used. Very recently, it has been demonstrated that discotic nematic liquid crystals can be utilized instead of calamitic nematic liquid crystals to overcome this problem [57]. The LCD prepared using hexaalkynylbenzene based discotic nematic liquid crystal shows wide and symmetrical viewing angle and no reversal of contrast ratio in any direction [57]. However, because of the very high viscosity of discotic nematic liquid crystal, the device is extremely slow.

The problem of viewing angle, brightness, contrast, sharpness of focus and image inversion associated with classical twisted nematic displays due to positive birefringence of the calamitic nematic liquid crystal layer can be suppressed by the use of compensation films, which should ideally have negative birefringence. The most promising materials for negative birefringence films are discotic nematic liquid crystals. Fuji Photo Films has recently commercialized an optical phase-compensation film using a triphenylene-based cross linked polymer to overcome these problems [58]. These films are usually prepared by aligning the reactive monomer, a triphenylene benzoate ester, with up to six epoxide or acrylate groups homeotropically aligned in the nematic discotic phase followed by photopolymerisation. These compensation films are the most successful commercial application of discotic liquid crystals.

1.18.2 Discotics in Xerographic processes

A commercially available photocopier or laser scanner consists of a rotating cylinder that is covered with a photoconducting surface, which moves over the original document with simultaneous irradiation [59]. The light reflected by the document hits the

photoconducting surface thereby leading to charge separation. An electrostatic image is generated on the cylinder surface. In the next step, the cylinder is covered with black toner particles that preferentially adsorb at the positive charges of the cylinder surface. On rotation of the cylinder over black paper, the toner particles are transferred to the paper and the crude hardcopy is generated and submitted to thermal fixation.

There are several requirements for photoconducting materials for them to be useful for applications. To achieve a high contrast potential for image development, the photoreceptor must be an insulator or have low conductivity in the dark and become conductive on exposure to light. A highly sensitive photoconductor not only requires less energy to generate the electrostatic image, but also increases the speed of the Xerox process. Thus, photosensitivity and dark conductivity of a certain material must be assessed. In addition, the lifetime and processibility of the material must be considered. While copier applications require that the photoconductor is sensitive in the visible region, the corresponding photoconducting materials of laser printers are sensitive in the IR spectra.

Classes of compounds which are particularly well studied for photoconducting devices that operate in the visible region are the perylene bisimides such as compound **12** [60]. On the other hand phthalocyanines have a strong absorption both in the visible and

near infrared region. Eichhorn *et al.* discovered that mixtures, which contained amphotropic phthalocyanines such as **13** with a different substitution pattern, display much higher inter- and intracolumnar order than the single compounds [61]. In addition, macroscopic homeotropic alignment was simply achieved by mechanical shearing, thus providing an easy way to orient the material for laser printers.

1.18.3 Discotics in holographic optical data storage

The principle of optical data storage relies on the *E/Z* isomerisation of dyes such as azobenzenes and stilbenes. The imprinting with two linear polarized laser-light beams induces a reorientation of the chromophores, which results in a change of the refractive index at the irradiated areas. The dye molecules are incorporated in a liquid crystalline matrix, which strongly enhances the change in refractive index. The periodic modulation of the refractive index, induced by writing laser beam, can be read out by a reading laser beam.

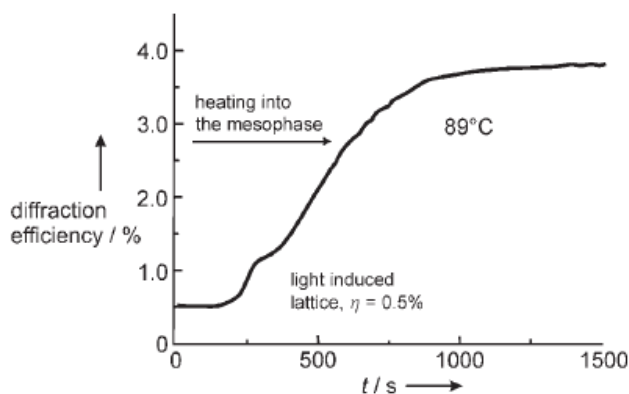


Figure 30. Thermal gain effect of the diffraction efficiency.

The columnar donor-acceptor triple compound **14** bears an azobenzene moiety as the chromophoric group [62]. The strong electron-acceptor TNF in combination with the electron donor pentakis(phenylalkynyl)benzene resulted in the improved stability of the nematic columnar mesophase. As can be seen in the Figure 30, at ambient temperature the refractive index of the photoinduced grating in the material differs by only 0.5%. On heating the sample to the nematic columnar mesophase, the diffraction efficiency increases to 4%. Wendorff, Janietz, and co-workers found that triazomelamine **15** is not only suitable for the light-induced isomerization of the azobenzene units to give rise to photo-reorientation, but also causes surface modulations [63]. The gain effect of these surface modulations was achieved by thermal treatment.

1.18.4 Discotics in organic light-emitting diodes

An OLED is a device, in which light is generated by electrical excitation. In a single-layer OLED, a thin film of an organic emitter is sandwiched between a transparent anode (ITO) and a metallic cathode [64]. A multilayer device (Figure 31) consists of separate hole-transporting layer, emitter layer and electron transporting layer. Electrons and holes, which are injected into the LUMO and HOMO, respectively, drift through the organic film under the influence of the applied electric field. The coulombic attraction between an

electron and hole at the same chromophore site results in the formation of an exciton, a bound electron-hole pair, whose recombination produces luminescence. Efficient devices require the matching of energy levels to minimize the barriers for carrier injection and to trap both electron and holes exclusively in the emitter region. For OLED applications, columnar perylene derivatives have been successfully used. The research groups of Kitzerow and Bock [65] described an all-columnar bilayer OLED that consisted of fluorescent columnar 3,4,9,10-tetra(alkoxycarbonyl)perylene as the luminescent electron transport layer combined with columnar hexaalkoxytriphenylenes as the hole transport layer. A particular advantage of columnar LCs in such devices is their ability to expel defects in an annealing process which leads to increased lifetimes.

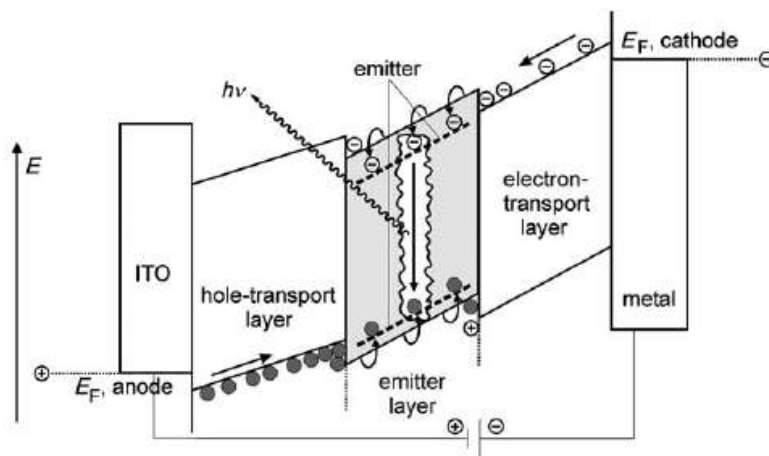


Figure 31. Energy diagram of multilayered diode.

1.18.5 Discotics in organic field-effect transistors

The self-assembly properties of columnar LCs, in combination with their ability to provide anisotropic charge-carrier transport along the channel, makes them viable candidates for OFETs. A typical OFET device is shown in Figure 32.

For a p-type semiconductor, conduction of charge between the source and the drain electrodes is governed by the gate voltage. When the gate is biased negatively, carriers accumulate in the channel between source and drain. The drain current is then proportional to the material mobility [66]. The extraordinary hole mobility for aligned hexa *peri*-hexabenzocoronene ($\mu = 0.5\text{-}1.0 \times 10^{-3} \text{ cm}^2 \text{ V}^{-1} \text{ S}^{-1}$) films on oriented PTFE has been used by the research group of Mullen [67]. By meso-epitaxial solution-growths of the HBC semiconductor devices were built, which displayed on/off ratios of more than 104 and a turn-on voltage of -5 to -10 V. The solution processibility, uniaxial parallel orientation and promising material and device stability under ambient conditions pave the way to the industrial production of these OFETs.

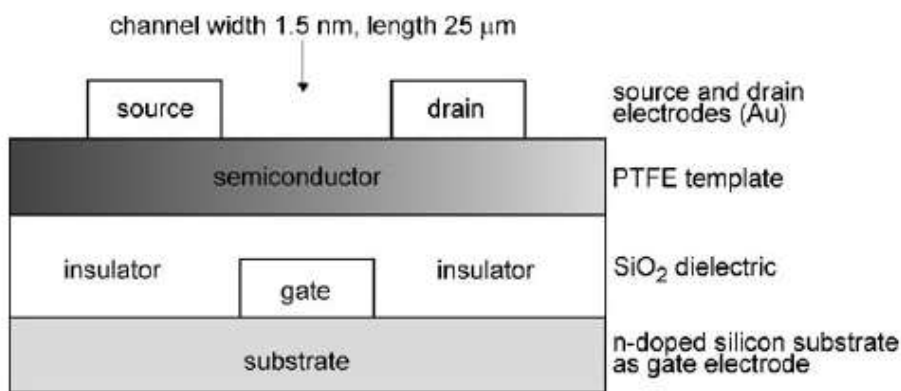


Figure 32. Schematic representation of an organic field effect transistor.

1.18.6 Discotic liquid crystals as photosynthetic light harvesting materials

The light-induced electron-hole generation, separation and migration is an important process for the conversion of light to electric or chemical energy (solar cells; photosynthesis), the latter being the basis of life on earth. The photovoltaic effect requires (a) the absorption of solar radiation and the photogeneration of electrons and holes, and

(b) the charge separation, and the transport of electrons and holes for collection at the cathode and anode, respectively. For a typical blended device under short-circuit conditions, the energy-level diagram is shown in Figure 33 [68].

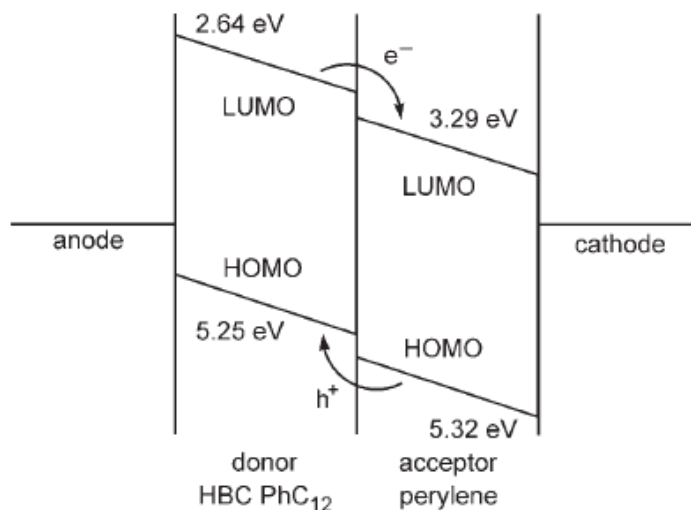


Figure 33. Energy level diagram showing charge separation and transport to electrodes.

Both processes should be highly efficient and charge recombination should be kept as a minimum. Absorption is achieved by exciton formation. Charge separation is achieved by ionization of an exciton over a distributed interface between electron-donating and electron-accepting species. The separated carriers drift to external electrodes in the built in field introduced by dissimilar electrodes. The photosensitivity of semiconducting organic materials can be enhanced by blending donor and acceptor molecules to optimize photoinduced charge separation. Gregg *et al.* studied photovoltaic effects in symmetrical cells filled with discotic liquid crystalline porphyrin complexes [69]. Photovoltaic effect comparable with that of some of the better organic solar cells was found. However, the authors did not study the charge mobility in the mesophases

itself but utilized the liquid crystalline properties to fill the cells and to promote macroscopic order, which on cooling, forms polycrystalline films. Schmit-Mende *et al.* utilized discotic liquid crystalline hexabenzocoronene as the hole transporting layer and a perylene dye to construct a p/n type photovoltaic solar cell [70]. Mullen and coworkers have shown in a seminal contribution [70, 71] that thin film prepared by self-organization of a mixture of columnar LC and crystalline-conjugated materials directly from a xylene solution showed a photovoltaic response with external quantum efficiencies greater than 34% at 490 nm and power efficiencies up to 2%. The formation of vertically segregated nonmesomorphic electron-accepting perylene bismide and the columnar phase forming hole accepting hexa-peribenzocoronene with a high interfacial surface was shown by AFM, STM, and optical polarizing microscopy (Figure 34) [70]. The high efficiencies result from an efficient photoinduced charge transfer between the two molecules and an effective charge transport through the layered structure.

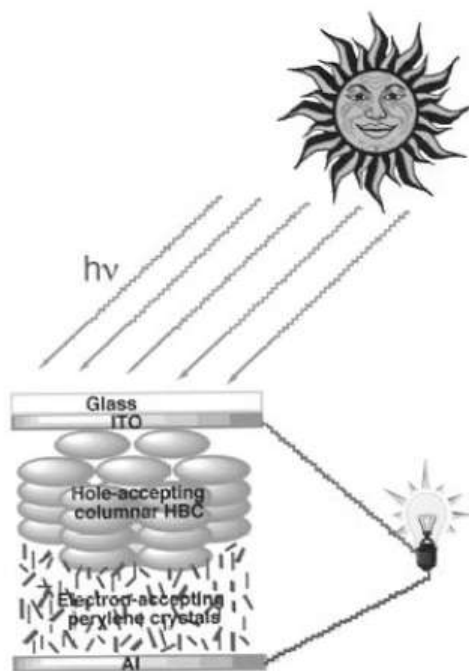


Figure 34. Schematic diagram of a discotic-based photovoltaic solar cell.

1.18.7 Discotics as gas sensors

The free surfaces of liquid crystals are fascinating objects. One can expect extra degrees of freedom near the surface where the absence of interacting neighbors should give rise to new and exciting ordering phenomena. In smectics, the absence of the neighbors on one side actually encourages crystallization. However in discotics, there are more degrees of freedom at the surface which encourage disorder in the stacks. When a lateral field is applied to a homeotropic film, conduction is likely to be dominated by that of the disordered surface since in the bulk it would be perpendicular to the columns. Attempts have been made to study the conductivity of discotic liquid crystal surface films using the interdigitated electrode geometry by filling the cells with homeotropically aligned discotic liquid crystals. If the fluctuation and thermodynamics of liquid crystal surfaces are influenced by exposure to gases the response could be simply and cheaply measured by looking at the conductance change giving a simple gas sensor. Structural changes do not require strong electronic coupling or charge transfer reactions to surface states, so sensor built on these principles could also work for detecting weakly interacting non-polar gases. The adsorbate produces a change in the order of the surface and this in turn changes the conductivity. This is relatively easy to measure. Furthermore, self-organized molecular dynamics prefer to keep charge and uncharged impurities near the free surface of the liquid crystals. Discotic liquid crystals can therefore be used as very sensitive gas sensors for both polar and non-polar molecules [72].

1.18.8 Discotics as precursors of novel carbonaceous nanostructures

The facile formation of ordered columnar superstructures from the discotic molecules in the bulk state and their high stability in the mesophase qualify them as precursors toward novel carbon nanostructures. Therefore, pyrolysis under controlled conditions may maintain the order existing in the mesophase during formation of the carbonaceous materials. Pyrolysis of well-defined discotic molecules in the bulk state produces novel carbon nano and microstructures. Carbon nanotubes (CNTs) without metal catalysts and with desired graphene layer orientations have been prepared by carbonization of the discotic columnar phase. The temperatures are much lower than the normally used graphitization temperature (2000-3000 °C). Recently a template method has been used to fabricate uniform carbon nanotubes by pyrolysis of graphitic molecule hexabenzocoronene (HBC) in porous alumina membranes. Upon carbonization under a controlled heating process the preorganized ordered columnar superstructures can be converted into nanotubes. Mullen *et al.* have produced nanotubes from thermotropic discotic liquid crystals [73]. A unique approach to self-assembled graphitic nanotubes from an amphiphilic hexabenzocoronene is demonstrated. The nanotubes consist of graphitic wall formed from numerous molecular graphene sheets stacked parallel to the longer axis of the tube. The proposed structure of the nanotube consists of helically rolled-up bilayer tapes composed of π -stacked HBC units, where the inner and outer HBC layers are connected by interdigitation of the hydrophobic alkyl chains while the hydrophilic ethylene oxide chains are located on both sides of the tubular wall. The π -stacked HBC units provide a charge carrier transport pathway. Suitable chemical modification of the amphiphilic HBCs results in the formation of nanotubes with various

interesting physical properties [74]. Another remarkable thing about these nanotubes is the formation of discotic columnar mesophase upon heating these graphitic nanotubes.

References

1. (a) *Handbook of Liquid Crystals*, eds. D. Demus, J. Goodby, G. W. Gray, H. W. Spiess, V. Vill, Wiley-VCH, Weinheim, Vol **I-III**, (1998); (b) B. Bahadur (ed.), *Liquid Crystals-Application and Uses*, Vol **I-III**, World Scientific, Singapore (1990); (c) S. Chandrasekhar, *Liquid Crystals*, 2nd ed., Cambridge University Press, Cambridge (1992); (d) P. J. Collings and M. Hird, *Introduction to Liquid Crystals-Chemistry and Physics*, Taylor & Francis Ltd., London (1997); (e) P. J. Collings and S. J. Patel, *Handbook of Liquid Crystal Research*, Oxford University Press, Oxford (1997); (f) H. Kelker and W. Hatz, *Handbook of Liquid Crystals*, VCH, Deerfield Beach, FL, (1980); (g) P. J. Collings, *Nature's delicate Phase of Matter*, Princeton University Press, (1990); (h) P. G. de Gennes and J. Prost, *The Physics of Liquid Crystals*, 2nd ed. Oxford University Press, New York, (1993).
2. A. S. Sonin, *J. Mater. Chem.*, **8**, 2557, (1998).
3. J. L. Serrano, *Metallomesogens-Synthesis, Properties and Application*, VCH Weinheim, (1996).
4. F. Reinitzer, *Monatsh Chem.*, **9**, 421, (1988); for English translation see *Liq. Cryst.*, **5**, 7 (1989).
5. O. Lehmann, *Z. Phys. Chem.*, **4**, 462 (1889).
6. W. Heintz, *J. Prakt. Chem.*, **66**, 1, (1855).
7. D. Vorlander, *Kristallinisch-flussige Substanzen*, Enke, Stuttgart, (1905).

8. S. Chandrasekhar, B. K. Sadashiva and K. A. Suresh, *Pramana*, **9**, 471, (1977).
9. (a) T. Niori, T. Sekine, J. Watanabe, T. Furukawa, H. Takazoe, *J. Mater. Chem.*, **6**, 1231, (1996); (b) G. Pelzi, S. Diele, W. Weissflog, *Adv. Mater.*, **11**, 707, (1999); (c) C. Tschierske, G. Dantlgraber, *Pramana*, **61**, 455, (2003); (d) M. B. Ros, J. L. Serrano, M. R. De la Fuente, C. L. Folcia, *J. Mater. Chem.*, **15**, 5093, (2005); (e) R. A. Reddy, C. Tschierske, *J. Mater. Chem.*, **16**, 907, (2006); (f) H. Takezoe, Y. Takanishi, *Jpn. J. Appl. Phys.*, **45**, 597, (2006); (g) J. Etxebarria, M. B. Ros, *J. Mater. Chem.*, **18**, 2919, (2008).
10. I. Koltover, T. Salditt, J. O. Radler and C. R. Safinya, *Science*, **281**, 78, (1998).
11. (a) S. T. Lagerwall, *Ferroelectric and Antiferroelectric Liquid Crystals*, Wiley – VCH, Weinheim, (1999); (b) J. P. F. Lagerwall and F. Giesselmann, *ChemPhysChem*, **7**, 20, (2006).
12. (a) L. A. Madison, T. J. Dingemans, M. Nakata, E. T. Samulski, *Phys. Rev. Lett.*, **92**, 145505, (2004); (b) B. R. Acharya, A. Primak, S. Kumar, *Phys. Rev. Lett.*, **92**, 145506, (2004).
13. (a) S. Kumar, *Liq. Cryst.*, **32**, 1089, (2005); (b) *Handbook of Liquid Crystals*, eds. D. Demus, J. Goodby, G. W. Gray, H. W. Spiess, V. Vill, Wiley-VCH, Weinheim Vol. **3**, (1998).
14. D. Vorlander, “*Chemische Kristallographic der Flussigkeiten*”, Akademische Verlagsgesellschaft, Leipzig, pp. 34, (1924).
15. (a) G. H. Taylor, *Fuel*, **40**, 465, (1961); (b) J. D. Brooks, G. H. Taylor, *Nature*, **206**, 697, (1965); (c) J. D. Brooks, G. H. Taylor, *Carbon*, **3**, 185, (1985); (d) J. D. Brooks, G. H. Taylor, *Carbon*, **4**, 243, (1968).

16. (a) S. Kumar, *Chem. Soc. Rev.*, **35**, 83, (2006); (b) T. Kato, T. Yasuda, Y. Kamikawa and M. Yoshio, *Chem. Commun.*, 729, (2009); (c) S. Laschat, A. Baro, N. Steinke, F. Giesselmann, C. Hagele, G. Scalia, R. Judele, E. Kapatsina, S. Sauer, A. Schreivogel, M. Tosoni, *Angew. Chem. Int. Ed.*, **46**, 4832, (2007); (d) S. Sergeev, W. Pisula, Y. H. Geerts, *Chem. Soc. Rev.*, **36**, 1902, (2007); (e) J. Wu, W. Pisula, K. Mullen, *Chem. Rev.*, **107**, 718, (2007); (f) Y. Shimizu, K. Oikawa, K. Nakayama, D. Guillon, *J. Mater. Chem.*, **17**, 4223, (2007); (g) N. Boden, R. J. Bushby, J. Clements, B. Movaghar, *J. Mater. Chem.*, **9**, 2081, (1999); (h) R. J. Bushby, O. R. Lozman, *Curr. Opin. Solid State Mater. Sci.*, **6**, 569, (2002); (i) R. J. Bushby, O. R. Lozman, *Curr. Opin. Colloid Interface Sci.*, **7**, 343, (2002); (j) H. Takezoe, K. Kishikawa, E. Gorecka, *J. Mater. Chem.*, **16**, 2412, (2006); (k) K. Ohta, K. Hatsusaka, M. Sugibayashi, M. Ariyoshi, K. Ban, F. Maeda, R. Naito, K. Nishizawa, A. M. van de Craats, J. M. Warman, *Mol. Cryst. Liq. Cryst.*, **397**, 25, (2003); (l) P. H. J. Kouwer, W. F. Jager, W. J. Misj and S. J. Picken, *Macromolecules*, **34**, 7582, (2001); (m) S. Chandrasekhar, *Liq. Cryst.*, **14**, 3, (1993); (n) S. Chandrasekhar and G. S. Ranganath, *Rep. Prog. Phys.*, **53**, 57, (1990).
17. (a) D. W. Bruce, D. A. Dunmur, L. S. Santa, and M. A. Wali, *J. Mater. Chem.*, **2**, 363, (1992); (b) B. Alameddine, O. F. Aebischer, W. Amrein, B. Donnio, R. Deschenaux, D. Guillon, C. Savary, D. Scanu, O. Schidegger, T. A. Jenny, *Chem. Mater.*, **17**, 4798, (2005).
18. (a) A. M. Levelut, *J. Chem. Phys.*, **80**, 149, (1983); (b) F. C. Frank, S. Chandrasekhar, *J. Phys.*, **41**, 1285, (1980).

19. (a) C. Destrade, P. Foucher, H. Esparoux, H. T. Nguyen, A. M. Levelut, J. Malthete, *Mol. Cryst. Liq. Cryst.*, **106**, 121, (1984); (b) F. Morale, R.W. Date, D. Guillon, D. W. Bruce, R. L. Finn, C. Wilson, A. J. Black, M. Schroder, B. Donnio, *Chem. Eur. J.*, **9**, 2484, (2003).
20. B. Glusen, W. Heitz, A. Kettner, J. H. Wendorff, *Liq. Cryst.*, **20**, 627, (1996).
21. (a) E. Fontes, P. A. Heiney, W. H. De Jeu, *Phys. Rev. Lett.*, **61**, 1202, (1988) ; (b) P. A. Heiney, E. Fontes, W. H. De Jeu, A. Riera, P. Carroll, A. B. Smith III, *J. Phys. France*, **50**, 461, (1989).
22. (a) K. Ohta, H. Muroki, A. Takagi, K. I. Hatada, H. Ema, I. Yamamoto, K. Matsuzaki, *Mol. Cryst. Liq. Cryst.*, **140**, 131, (1986); (b) H. Sakashita, A. Nishitani, Y. Sumiya, H. Terauchi, K. Ohta, I. Yamamoto, *Mol. Cryst. Liq. Cryst.*, **163**, 211, (1988).
23. T. Vlad-Bubulak, J. Buchs, A. Kohlmeier, M. Bruma, and D. Janietz, *Chem. Mater.*, **19**, 4460, (2007); (b) K. Ohta, T. Watanabe, H. Hasebe, Y. Morizumi, T. Fujimoto, I. Yamamoto, *Mol. Cryst. Liq. Cryst.*, **196**, 13, (1991); (c) K. Hatsusaka, K. Ohta, I. Yamamoto, H. Shirai, *J. Mater. Chem.*, **11**, 423, (2001); (d) M. Ichihara, A. Suzuki, K. Hatsusaka and K. Ohta, *Liq. Cryst.*, **34**, 555, (2007); (e) K. Praefcke, P. Marquard, B. Kohne, W. Stephan, A. -M. Levelut, E. Watchtel, *Mol. Cryst. Liq. Cryst.*, **203**, 149, (1991).
24. (a) I. Fischbach, F. Ebert, H. W. Spiess and I. Schnell, *ChemPhysChem*, **5**, 895, (2004); (b) M. Lehmann, I. Fischback, H. W. Spiess and H. Meier. *J. Am. Chem. Soc.*, **126**, 772, (2004).

25. (a) *Electronic Materials: The Oligomer Approach*, ed. G. Wegner, K. Mullen, Wiley-VCH, Weinheim (1998); (b) *Semiconducting Polymers: Chemistry, Physics and Engineering*, ed. G. Hadziioannou, P. F. van Hutten, Wiley-VCH, Weinheim (2000).
26. G. B. M. Vaughan, P. A. Heiney, J. P. McCauley, Jr., A. B. Smith III, *Phys. Rev. B*, **46**, 2787, (1992).
27. (a) J. M. Warman, A. M. van de Craats, *Mol. Cryst. Liq. Cryst.*, **396**, 41 (2003).
(b) H. Eichhorn, *J. Porphyrins Phthalocyanines*, **4**, 88, (2000); (c) J. M. Warman, M. P. de Hass, G. Dicker, F. C. Grozema, J. Piris and M. G. Debeje, *Chem. Mater.*, **16**, 4600, (2004); (d) J. M. Warman, J. E. Kroeze, P. G. Schouten, and A. M. van de Craats, *J. Porphyrins Phthalocyanines*, **7**, 342, (2003).
28. (a) M. C. Nuss, P. M. Mankiewich, M. L. O'Malley, E. H. Westerwick, P. B. Littlewood, *Phy. Rev. Lett.*, **66**, 3305, (1991); (b) D. Adam, P. Schuhmacher, J. Simmerer, L. Haussling, K. Siemensmeyer, K. H. Etzbach, H. Ringsdorf, D. Haarer, *Nature*, **371**, 141, (1994).
29. A. M. van de Craats, J. M. Warman, M. P. de Hass, D. Adam, J. Simmerer, D. Haarer, P. Schuhmacher, *Adv. Mater.*, **8**, 823, (1996).
30. R. A. Marcus, *Rev. Mod. Phys.*, **65**, 599, (1993).
31. V. Lemaire, D. A. da Silva Filho, V. Coropceanu, M. Lehmann, Y. Geerts, J. Piris, M. G. Debeje, A. M. van de Craats, K. Senthilkumar, L. D. A. Siebbeles, J. M. Warman, J. -L. Bredas, J. Cornil, *J. Am. Chem. Soc.*, **126**, 3271 (2004).

32. A. N. Cammidge, R. J. Bushby, in *Handbook of Liquid Crystals*, ed. D. Demus, J. W. Goodby, G. W. Gray, H. W. Spiess, V. Vill, Wiley-VCH, Weinheim, Vol. **2B**, Ch. 7, 693, (1998).
33. S. Kumar, J. J. Naidu, D. S. Shankar Rao, *J. Mater. Chem.*, **12**, 1335, (2002).
34. C. -Y. Liu, A. J. Bard, *Acc. Chem. Res.*, **32**, 235, (1999).
35. (a) P. Herwig, C. W. Kayser, K. Mullen, H. W. Spiess, *Adv. Mater.*, **8**, 510 (1996); (b) M. G. Debije, J. Piris, M. P. de Hass, J. M. Warman, Z. Tomovic, C. D. Simpson, M. D. Watson, K. Mullen, *J. Am. Chem. Soc.*, **126**, 4641, (2004).
36. (a) J. Cornil, V. Lemaure, J. P. Calbert, J. L. Bredas, *Adv. Mater.*, **14**, 726, (2002); (b) K. Senthilkumar, F. C. Grozema, F. M. Bickelhaupt, L. D. A. Siebbeles, *J. Chem. Phys.*, **119**, 9809, (2003).
37. (a) J. F. van der Pol, E. Neeleman, J. W. Zwikker, R. J. M. Nolte, W. Drenth, J. Aerts, R. Visser, S. J. Picken, *Liq. Cryst.*, **6**, 577, (1989); (b) K. Ohta, L. Jacquemin, C. Sirlin, L. Bosio, J. Simon, *New J. Chem.*, **12**, 751, (1988); (c) D. Guillon, A. Skoulios, C. Piechocki, J. Simon, P. Weber, *Mol. Cryst. Liq. Cryst.*, **100**, 275, (1983).
38. R. J. Gearba, M. Lehmann, J. Levin, D. A. Ivanov, M. H. J. Koch, J. Barbera, M. G. Debije, J. Piris, Y. H. Geerts, *Adv. Mater.*, **15**, 1614, (2003).
39. J. Tant, Y. H. Geerts, M. Lehmann, V. de Cupere, G. Zucchi, B. W. Laursen, T. Bjornholm, V. Lemaure, V. Marcq, A. Burquel, E. Hennebicq, F. Gardebien, P. Viville, D. Beljonne, R. Lazzaroni, J. Cornil, *J. Phys. Chem. B*, **109**, 20315, (2005).
40. S. Kumar, S. K. Varshney, *Angew. Chem.*, **112**, 3270, (2000).

41. S. Kumar, D. S. Shankar Rao, S. K. Prasad, *J. Mater. Chem.*, **9**, 2751, (1999).
42. W. Pisula, M. Kastler, D. Wasserfallen, T. Pakula, K. Mullen, *J. Am. Chem. Soc.*, **12**, 8074, (2004).
43. S. Sergeev, E. Pouzet, O. Debever, J. Levin, J. Gierschner, J. Cornil, R. Gomez-Aspe, Y. H. Geerts, *J. Mater. Chem.*, **17**, 1777, (2007).
44. A. Fechtenkotter, N. Tchebotareva, M. Watson and K. Mullen, *Tetrahedron*, **57**, 3769, (2001).
45. A. Tracz, T. Pakula, and J. K. Jeszka, *Mater. Sci (Poland)*, **22**, 415, (2004).
46. S. Xiao, M. Myers, Q. Miao, S. Sananur, K. Pang, M. L. Steigerwald, C. Nuckolls, *Angew. Chem. Int. Ed.* **44**, 7390, (2005).
47. I. O. Shklyarevskiy, P. Jonkheijm, N. Stutzmann, D. Wasserberg, H. J. Wondergem, P. C. M. Christianen, A. P. H. J. Schenning, D. M. de Leeuw, Z. Tomovic, J. Wu, K. Mullen, J. C. Maan, *J. Am. Chem. Soc.*, **127**, 16233, (2005).
48. (a) S. Zimmermann, J. H. Wendorff, C. Wedder, *Chem. Mater.*, **14**, 2218, (2002); (b) A. M., van de Craats, N. Stutzmann, O. Bunk, M. M Nielsen, M. Watson, K. Mullen, H. D. Chanzy, H. Sirringhaus, R. H. Friend, *Adv. Mater.*, **15**, 495, (2003).
49. (a) O. Y. Mindyuk, P. A. Heiney, *Adv. Mater.*, **11**, 341, (1999); (b) N. R. Armstrong, *J. Porphyrins Phthalocyanines*, **4**, 414, (2000); (c) N. Reitzel, T. Hassenkam, K. Balashev, T. R. Jensen, P. B. Howes, K. Kjaer, A. Fechtenkotter, N. Tchebotareva, S. Ito, K. Mullen, T. Bjornholm, *Chem. Eur. J.*, **7**, 4894, (2001).

50. (a) W. Pisula, M. Kastler, D. Wasserfallen, T. Pakula, K. Mullen, *J. Am. Chem. Soc.*, **126**, 8074, (2004) ; (b) W. Pisula, M. Kastler, D. Wasserfallen, R. J. Davies, M. –C. Garcia-Gutierrez, K. Mullen, *J. Am. Chem. Soc.*, **128**, 14424, (2006).
51. N. Terasawa, N. Tanigaki, H. Monobe, and K. Kiyohara, *J. Fluorine Chem.*, **127**, 1096, (2006).
52. H. Monobe, K. Awazu, and Y. Shimizu, *Adv. Mater.*, **18**, 607, (2006).
53. T. Sugiyama, T. Hashimoto, K. Katoh, Y. Iimura, S. Kobayashi, *Jpn. J. Appl. Phys.*, **34**, 2396, (1995).
54. H. Mori, *Jpn. J. Appl. Phys.*, **36**, 1068, (1997).
55. M. Oh-e, M. Yoneya, K. Kondo, *J. Appl. Phys.*, **82**, 528, (1997).
56. Y. Toko, T. Sugiyama, K. Katoh, Y. Iimura, S. Kobayashi, *J. Appl. Phys.*, **74**, 2071, (1993).
57. S. Chandrasekhar, S. Krishna Prasad, G. G. Nair, D. S. Shankar Rao, S. Kumar, M. Manikam, *Euro Display '99, The 19th International Display Research Conference Late-news papers* (Berlin-Germany), pp.9 (1999).
58. (a) K. Kawata, *Chem. Rec.*, **2**, 59, (2002); (b) H. Mori, Y. Ioh, Y. Nishiura, T. Nakamura, Y. Shinagawa, *Jpn. J. Appl. Phys.*, **36**, 143, (1997); (c) F. Leenhouts, *Jpn. J. Appl. Phys.*, **39**, L741, (2000).
59. K. –Y. Law, *Chem. Rev.*, **93**, 449, (1993).
60. F. Wurthner, C. Thalacker, S. Diele, C. Tschierske, *Chem. Eur. J.*, **7**, 2245, (2001).
61. H. Eichhorn, D. W. Bruce, D. Wöhrle, *Adv. Mater.*, **10**, 419, (1998).

62. (a) D. Hertel, C. D. Muller, K. Meerholz, *Chem. Unserer Zeit.*, **39**, 336, (2005).
(b) A. Stracke, J. H. Wendroff, D. Janietz, S. Mahlstedt, *Adv. Mater.*, **11**, 667 (1999).
63. A. Stracke, J. H. Wendroff, D. Goldmann, D. Janietz, B. Stiller, *Adv. Mater.*, **12**, 282, (2000).
64. M. O'Neill, S. M. Kelly, *Adv. Mater.*, **15**, 1135, (2003).
65. (a) S. Benning, H. –S. Kitzerow, H. Bock, M. –F. Achard, *Liq. Cryst.*, **27**, 901, (2000); (b) T. Hassheider, S. A. Benning, H. –S. Kitzerow, M. –F. Achard, H. Bock, *Angew. Chem.*, **113**, 2119, (2001); (c) I. Seguy, P. Destruel, H. Bock, *Synth. Met.*, **111**, 15, (2000).
66. N. Boden, R. J. Bushby, J. Clements, B. Movaghar, *J. Mater. Chem.*, **9**, 2081 (1999).
67. W. Pisula, A. Menon, M. Stepputat, I. Lieberwirth, U. Kolb, A. Tracz, H. Sirringhaus, T. Pakula and K. Mullen, *Adv. Mater*, **17**, 684, (2005).
68. (a) S. Kumar, *Curr. Sci.*, **82**, 256, (2002) ; (b) N. R. Armstrong, B. Kippelen, D. F. O'Brien, S. M. Marder, J. –L. Bredas, *Proceedings-NCPV Program Review Meeting, Lakewood*, 328, (2001).
69. B. A. Gregg, M. A. Fox, A. J. Bard, *J. Phys. Chem.*, **94**, 1586, (1990).
70. L. Schmidt-Mende, A. Fechtenkotter, K. Mullen, E. Moons, R. H. Friend, J. D. Mackenzie, *Science*, **293**, 1119, (2001).
71. (a) J. Jung, A. Rybak, A. Slazak, S. Bialecki, P. Miskiewicz, I. Glowacki, J. Ulanski, S. Rosselli, A. Yasuda, G. Nelles, Z. Tomovic, M. D. Watson and K.

- Mullen, *Synth. Met.*, **155**, 150, (2005); (b) J. P. Schmidtke, R. H. Friend, M. Kastler and K. Mullen, *J. Chem. Phys.*, **124**, 174704, (2006).
72. (a) J. Clements, N. Boden, T. Gibson, R. Chandler, J. Hulbert and E. A. Ruck-Keene, *Sens. Actuators*, **47**, 37, (1998); (b) N. Boden, R. J. Bushby and A. N. Cammidge, *J. Am. Chem. Soc.*, **117**, 924, (1995).
73. (a) L. Zhi, J. Wu, J. Li, U. Kolb and K. Mullen, *Angew. Chem. Int. Ed.*, **44**, 2120, (2005); (b) J. Wu, B. E. Hamaoui, J. Li, L. Zhi, U. Kolb and K. Mullen, *Small*, **1**, 210, (2005); (c) L. Gherghe, C. Kubel, G. Lieser, H. -J. Rader and K. Mullen, *J. Am. Chem. Soc.*, **124**, 13130, (2002).
74. (a) J. P. Hill, W. Jin, A. Kosaka, T. Fukushima, H. Ichihara, T. Shimomura, K. Ito, T. Hashizume, N. Ishii and T. Aida, *Science*, **304**, 1481, (2004). (b) W. Jin, Y. Yamamoto, T. Fukushima, N. Ishii, J. Kim, K. Kato, M. Takata and T. Aida, *J. Am. Chem. Soc.*, **130**, 9434, (2008).

CHAPTER 2

Green chemistry approach to the synthesis of liquid crystalline materials

2.1 Part A: Microwave-assisted facile synthesis of alkoxybiphenyls and their dimers

2.1.1 Introduction

Until recently, heating reaction mixtures on a laboratory scale was typically performed using isomantles, oilbaths or hot plates. This traditional (classical) form of heating is a rather slow and inefficient method for transferring energy into a reaction mixture, since it depends on convection currents and on the thermal conductivity of the various materials that must be penetrated, and often results in the temperature of the reaction vessel being higher than that of the reaction mixture.

In contrast, microwave (MW) irradiation produces efficient internal heating by directly coupling of microwave energy with the molecules that are present in the reaction mixture. Microwave irradiation triggers heating by two main mechanisms - dipolar polarization and ionic conduction. Whereas the dipoles in the reaction mixture (polar solvents) are involved in the dipolar polarization effect, the charged particles in a sample (usually ions) are affected by ionic conduction. When irradiated at microwave frequencies, the dipoles or ions of the sample align in the applied electric field. As the applied field oscillates the dipole or ion field attempts to realign itself with the alternating electric field and, in the process, energy is lost in the form of heat through molecular

friction and dielectric loss. The ability of a specific material or solvent to convert microwave energy into heat at a given frequency and temperature is determined by the so-called loss tangent ($\tan \delta$) and in general a reaction medium with a high $\tan \delta$ at the standard operating frequency of a microwave synthesis reactor (2.45 GHz) is required for good absorption and consequently, for efficient heating. For low MW absorbing solvents, polar additives such as ionic liquids or passive heating elements made out of strongly microwave absorbing materials can be added to otherwise low absorbing reaction mixtures in order to increase the absorbance level of the medium. Since the reaction vessels employed in microwave chemistry are made out of essentially microwave transparent materials such as glass or Teflon, only the reaction-mixture not the reaction-vessel is heated. The use of microwave heating in organic synthesis was introduced in 1986 by the group of Gedye and Giguere [1]. Although many of the pioneering experiments in microwave assisted synthesis have been carried out in domestic microwave oven, the recent trend is to use dedicated microwave reactors specifically designed for synthetic applications. These instruments feature built-in magnetic stirrer, direct temperature control of the reaction mixture with the aid of internal fibre-optic probes or external infrared sensors and software that enables on-line temperature/pressure control by regulation of microwave power output.

This non-classical heating technique using microwaves, termed “Bunsen burner of the 21st century”, is rapidly becoming popular and is dramatically reducing reaction times. The significant outcomes of microwave-assisted ‘green chemistry’ endeavors have resulted in the development of synthetic protocols for drugs and fine chemicals synthesis that are relatively more sustainable. Since the reaction times are reduced from days and

hours to minutes and seconds, microwave assisted organic synthesis is considered as “Chemistry at the Speed of Light”. Though almost all types of organic reactions have been performed using the efficiency of microwave flash heating [2] this non-classical technique has not been much explored for the synthesis of liquid crystalline materials.

Liquid crystal displays (LCDs) have played a vital role in information technology. The twisted nematic (TN) and supertwisted nematic (STN) display devices are dominating commercial displays since their invention. The liquid crystal layer in these devices is made-up of a complex mixture of calamitic liquid crystals (composed of rod-shaped molecules). Alkyl- and alkoxybiphenyls are indispensable ingredients of these mixtures (Figure 1). These revolutionary materials, prepared by Gray *et al.*, were the first known low-melting stable nematic LCs [3]. Because of their commercial importance, a number of cyanobiphenyl derivatives have been extensively studied for various physical properties [4].

Figure 1. The calamitic liquid crystal mixture E7 used in commercial liquid crystal display (LCD) devices consists of alkyl- and alkoxybiphenyls and alkylcyanoterphenyl in a definite proportion.

On the other hand, compounds composed of two mesogenic units linked by a flexible spacer, commonly known as liquid crystalline dimers, or dimesogens, are interesting materials for their potential use as model compounds to understand the more complex semi-flexible polymeric liquid crystal systems. Liquid crystal dimers are the lowest possible oligomers exhibiting characteristic properties, such as, thermal behaviour, glass transition, etc., of polymer liquid crystals with retaining the fluidity of low molar mass liquid crystals and hence are promising systems for many practical applications [5]. Hitherto the most extensively studied series of liquid crystalline dimers is the α,ω -bis(4'-cyanobiphenyl-4-yloxy)alkanes **b** (Figure 2) [5, 6]. The interest in this series arises because they may be considered to be the dimeric analogous of the 4-n-alkoxy-4-cyanobiphenyls **a** (Figure 2) which is probably the most widely studied series of conventional low-molar mass liquid crystals. The dramatic odd-even effect, depending on the length and parity of the spacer, exhibited by the transitional properties viz temperature, entropy, enthalpy and orientational order parameter at N-I transitions have been well studied and accounted for as well [5, 6]. This is the only series for which a large range of spacer chain lengths, spanning a single to twenty two methylene units have been prepared. All 22 homologues belonging to this series exhibit nematic behavior and their melting point and nematic-isotropic transition temperatures and associated entropy exhibit dramatic odd-even effect. The magnitude of the alternations seen for the nematic-isotropic transition temperatures and associated entropy changes as the length and parity of the spacer are varied is strongly dependent on the nature of the group linking the spacer to the mesogenic units. Accordingly various dimers **c** (Figure 2) differing in the

nature of the spacer i.e. oligo(ethylene oxide) and siloxane-containing chains have been prepared and studied [7].

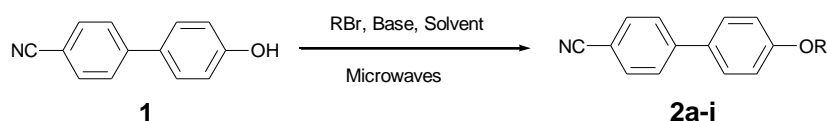
Figure 2. Alkoxy cyanobiphenyls **a** and their dimers **b,c** containing different spacers.

While alkoxy cyanobiphenyls have traditionally been prepared by the cyanation of 4'-alkoxy-4-bromobiphenyls or by the alkylation of the 4'-hydroxy-4-biphenylcarbonitriles [5], α,ω -bis(4'-cyanobiphenyl-4-yloxy)alkanes have been generally prepared by a single-step alkylation of 4'-hydroxy-4-biphenylcarbonitrile with α,ω -dibromoalkanes. Alkylation of the 4'-hydroxy-4-biphenylcarbonitrile with an appropriate alkyl halide or dihalide is the key reaction to produce various liquid crystalline alkoxy cyanobiphenyls and their dimers. This reaction is usually accomplished by heating 4'-hydroxy-4-biphenylcarbonitriles with an appropriate alkyl halide in polar solvents for 24 hours in moderate yield [8]. Here, in this part of the chapter, we have observed that this reaction could be finished in about one minute in very high yield by using microwave heating. This first half of this chapter deals with the synthesis of archetypal calamitic liquid crystals and their dimers using microwave dielectric heating. The reaction step

chosen here is the most often and commonly used synthetic step in liquid crystal synthesis i.e. the Williamson etherification of phenols. First, the reaction conditions are optimized with one compound and then the rest of the compounds were synthesized following the optimum reaction condition which ensures the high reproducibility of the method though a domestic microwave oven has been employed for the synthesis [9].

2.1.2 Results and discussion

The preparation of alkoxy cyanobiphenyls **2** using microwave heating is outlined in Scheme 1.



Scheme 1. Synthesis of alkoxy cyanobiphenyls using microwave irradiation.

The 4'-hydroxy-4-biphenylcarbonitrile **1** was prepared following literature method [8]. Alkylation was carried out using an unmodified house-hold microwave oven (LG, MS-192W). However, commercial microwave reactors for organic reactions are now available which provide adequate mixing and control of reaction parameters such as temperature and pressure [2]. We examined the effect of microwave power on a set of reactions using 4'-hydroxy-4-biphenylcarbonitrile, alkyl bromide and base in different solvents. The initial optimization of reaction conditions was performed using octyl bromide under different reaction conditions and the results are summarized in Table 1.

Table 1. Optimization of reaction conditions for preparation of 4'-(octyloxy)[1,1'-biphenyl]-4-carbonitrile (**2e**) using microwave irradiation.

Entry	Base	Solvent	MW Power	Time/s	Yield (%)
1	Cs ₂ CO ₃	NMP	360 W	30	80
2	Cs ₂ CO ₃	NMP	600 W	30	94
3	Cs ₂ CO ₃	NMP	800 W	30	90
4	Cs ₂ CO ₃	NMP	800 W	20	85
5	Cs ₂ CO ₃	NMP	360 W	30 x 2	98
6*	Cs ₂ CO ₃	NMP	360 W	30 x 2	79
7*	Cs ₂ CO ₃	NMP	360 W	30 x 4	94
8	Cs ₂ CO ₃	DMSO	360 W	30 x 2	90
9	Cs ₂ CO ₃	DMSO	600 W	30	80
10	Cs ₂ CO ₃	DMF	360 W	30 x 2	93
11	Cs ₂ CO ₃	DMF	600 W	30	88
12	Cs ₂ CO ₃	PEG	360 W	30 x 2	58
13	Cs ₂ CO ₃	PEG	600 W	30	80
14	K ₂ CO ₃	NMP	360 W	30 x 2	93
15	K ₂ CO ₃	NMP	600 W	30	90
16	K ₂ CO ₃	NMP	600 W	30 x 2	96
17	K ₂ CO ₃	DMSO	360 W	30 x 2	60
18	K ₂ CO ₃	DMF	360 W	30 x 2	64
19	Na ₂ CO ₃	NMP	360 W	30 x 2	82
20	Na ₂ CO ₃	NMP	600 W	30	41
21	Na ₂ CO ₃	DMSO	360 W	30 x 2	40
22	Na ₂ CO ₃	DMF	360 W	30 x 2	54
23	KOH	NMP	360 W	30 x 2	78
24	KOH	NMP	600 W	30	82

* 1.2 equivalent of octyl bromide was used. In all other reactions 2.0 equivalent of base and octyl bromide were used.

As can be seen from the Table 1, irradiation of the reaction mixture at 360 W for 30 s yielded 80% product **2e** (entry 1). Further irradiation of the reaction mixture for another 30 s increased the yield to 98% (entry 5). Enhancing the microwave power to 600 W produced 94% of the product in 30 s (entry 2). However, a further increase in the microwave power (800 W) furnished lower amount of the product (entry 3). Irradiation of the reaction mixture at this power for a shorter period (20 s) also gave poor yield (entry 4). When 1-bromooctane was used in close to an equimolar ratio (1.2 equiv) under the conditions of entry 5 only 79% of the product could be isolated (entry 6). However, irradiation of the same reaction mixture four times, i.e., 30 s X 4 with an interval of about 1 minute yielded 94% of the product (entry 7). Replacing the solvent NMP by other polar solvent like PEG, DMSO or DMF having higher or lower $\tan\delta$ [3] resulted in slightly lower yields of the product (entry 8-13). Changing the base from cesium carbonate to potassium carbonate, sodium carbonate or potassium hydroxide also produced lower amounts of the product in different solvents (entry 14-24). In all examples, fairly good to excellent yields could be achieved in less than 60 s. This indicates a dramatic reduction in the reaction time as compared with the conventional thermal process. The reaction conditions described in the entry 5 were found to be the optimal reaction conditions for the alkylation of hydroxycyanobiphenyl. When similar reactions were performed at 140 °C with an oil bath for the same time intervals, less than 15% yields were obtained. The purity and identity of the compound **2e** was confirmed by spectral techniques and comparing with authentic samples.

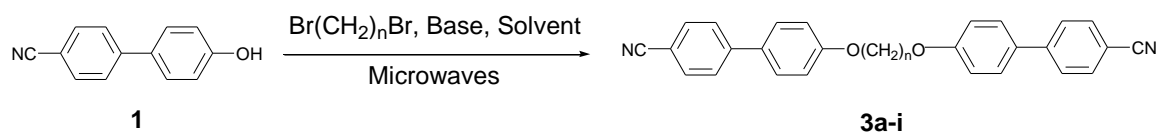
The versatility of the procedure has been demonstrated by the preparation of a number of alkoxybiphenyls as shown in Table 2. As can be seen from this Table 2 that while higher alkyl bromides (from octylbromide to dodecylbromide) afforded excellent yields, lower homologues furnished little smaller amount of products. This could be due to the faster evaporation of these relatively low-boiling alkyl bromides.

Table 2. Microwave-assisted preparation of alkoxybiphenyls.

$\text{RBr, Cs}_2\text{CO}_3, \text{NMP} \downarrow 360 \text{ W, } 2 \times 30 \text{ s}$

Entry	RBr	Product	Yield (%)
1	C ₁₂ H ₂₅ Br	2a	98
2	C ₁₁ H ₂₃ Br	2b	97
3	C ₁₀ H ₂₁ Br	2c	98
4	C ₉ H ₁₉ Br	2d	96
5	C ₈ H ₁₇ Br	2e	98
6	C ₇ H ₁₅ Br	2f	63
7	C ₆ H ₁₃ Br	2g	77
8	C ₅ H ₁₁ Br	2h	75
9	C ₄ H ₉ Br	2i	80

The synthesis of alkoxy cyanobiphenyl dimers **3** using microwave heating is outlined in Scheme 2. For the preparation of dimers, the initial optimization of reaction conditions was performed using 1,6-dibromohexane under different reaction conditions and the results are summarized in Table 3.



Scheme 2. Synthesis of alkoxy cyanobiphenyl dimers using microwaves.

Table 3. Optimization of reaction conditions for preparation of alkoxy cyanobiphenyl dimers using 1,6-dibromohexane and microwaves.

Entry	Base	Solvent	MW Power	Time/s	Yield (%)
1*	Cs ₂ CO ₃	NMP	360 W	30 x 2	63
2	Cs ₂ CO ₃	NMP	360 W	30	55
3	Cs ₂ CO ₃	NMP	360 W	30 x 2	64
4	Cs ₂ CO ₃	NMP	360 W	30 x 3	63
5	Cs ₂ CO ₃	NMP	360 W	30 x 4	61
6	K ₂ CO ₃	NMP	360 W	30 x 2	50
7	Cs ₂ CO ₃	DMSO	360 W	30 x 2	51
8	Cs ₂ CO ₃	DMF	360 W	30 x 2	39
9	Cs ₂ CO ₃	NMP	600 W	30	66
10	Cs ₂ CO ₃	NMP	600 W	30 x 2	66
11**	Cs ₂ CO ₃	NMP	360 W	30 x 2	65
12***	Cs ₂ CO ₃	NMP	360 W	30 x 2	-

* Exactly 2:1 equivalents of hydroxycyanobiphenyl and dibromide were used.

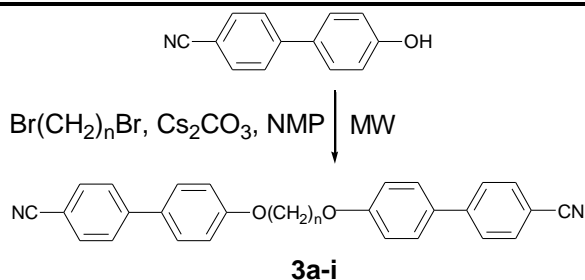
** Hydroxycyanobiphenyl and dibromide were used in 4:1 ratio.

*** Hydroxycyanobiphenyl and dibromide were used in 1:4 ratio.

As can be seen from Table 3, irradiation of the reaction mixture at 360 W for 30+30s with exactly 1:2 equivalents of 1,6-dibromohexane and 4'-hydroxy-4-biphenylcarbonitrile furnished 63% yield (entry 1) but the formation of ω -bromohexyloxy cyanobiphenyl was competing. So a slightly higher amount of 4'-hydroxy-4-biphenyl carbonitrile *i.e.* 1:2.2 equivalents was used (entry 2-10). When irradiated for 30 s the yield was 55% (entry 2) which increased to 64% on further irradiation of the same sample for another 30 s (entry 3). However, further increase in number of pulses furnished slightly lower yields (entry 4 and 5). When the base was changed from cesium carbonate to potassium carbonate there was a decrease in the product amount (entry 6). Changing the solvent from NMP to DMSO or DMF also resulted in the decrease of the product (entry 7 and 8). When we used excess of 4'-hydroxy-4-biphenylcarbonitrile (entry 11) there was no increase in product amount but the excess amount could be recovered almost quantitatively, which shows the non-destructiveness of the process. When excess of dibromide was used, exclusively the ω -bromohexyloxy cyanobiphenyl (80%) was formed (entry 12). The ω -bromoalkoxycyanobiphenyl is a key intermediate in the synthesis of various other liquid crystalline materials, such as, trimers, tetramers [10] and terminally functionalized alkoxy cyanobiphenyls [11]. This shows that this process can be efficiently used for the synthesis of such compounds. When the microwave power was changed to 600 W, irradiation for 30 s produced 66% product (entry 9). Increasing the number of pulses did not increase the product amount (entry 10). So it is clear that the optimum conditions for the preparation of alkoxy cyanobiphenyl dimers are: two 30 seconds irradiation at 360 W or a 30 seconds irradiation at 600W using NMP as solvent and cesium carbonate as base.

A number of dimers were prepared using these reaction conditions and the results are shown in Table 4. In all the cases good yield of the product was obtained which renders this method attractive.

Table 4. Microwave-assisted synthesis of alkoxybiphenyl dimers **3**.



Entry	n	Product	Yield (%)	
			600 W, 30s	360W, 30s X 2
1	4	3a	61	65
2	5	3b	71	66
3	6	3c	66	64
4	7	3d	61	58
5	8	3e	63	68
6	9	3f	69	71
7	10	3g	68	69
8	11	3h	69	62
9	12	3i	74	75

While the phase transition temperatures of monomers were found to be identical with literature data, the phase transition temperatures of all the dimers were found

slightly higher than the reported values and thus demonstrate the cleanness of the procedure. Phase transition temperature data of the dimers are collected in the Table 5. The numbers in parenthesis indicate the highest transition temperature reported in the literature [5, 6].

Table 5. Phase transition temperatures of alkoxybiphenyl dimers **3a-i** prepared using MW protocol. The numbers in parenthesis represent the highest transition temperature reported in the literature [5, 6].

Compound	Thermal transitions
3a	Cr 211.2 (210.3) N 253 (251.4) I
3b	Cr 141.4 (138.3) N 188.6 (184.1) I
3c	Cr 192.7 (192) N 224.3 (221.2) I
3d	Cr 140.1 (137) N 182.7 (181) I
3e	Cr 178.6 (176.7) N 203.3 (202.8) I
3f	Cr 136.6 (136.4) N 174 (174.9) I
3g	Cr 167.7 (165.8) N 186.4 (185.4) I
3h	Cr 127.6 (124.3) N 166.5 (164.1) I
3i	Cr 156.3 (152.7) N 173.5 (170.5) I

As can be observed from the Table 5 that the transition temperatures of the dimers prepared by MW protocol also exhibit the odd-even effect which matches with the literature behavior. The dramatic odd-even effects seen in the transitional properties of

dimers on varying the length and parity of the spacer are most often attributed to the dependence of the molecular shape on the number of atoms linking the two mesogenic units, and by considering the spacer to exist in its all-*trans* confirmation. An even-membered dimer has a zigzag shape in which the mesogenic units are anti-parallel whereas an odd-membered dimer has a bent shape in which the mesogenic units are inclined to each other. The structure of an even-membered dimer is then considered to be more compatible with the molecular organization found in the nematic phase than is the bent shape seen for odd-membered dimers. It is this greater compatibility which results in the higher nematic-isotropic transition temperatures and entropies found for the even members [5].

2.1.3 Conclusions

We have introduced an efficient, simple, rapid, economically and environmentally acceptable “green chemistry” approach to the synthesis of various commercially important alkoxybiphenyls and their dimeric calamitic liquid crystals. The present facile and clean protocol can be employed for the synthesis of many other liquid crystalline materials. However, at the moment, this procedure is best suitable to quickly prepare a few hundred milligrams of the material for laboratory use only. A lot of development work is required to reach commercial scale.

2.2 Part B: Microwave-assisted synthesis of monohydroxy-functionalised triphenylenes and their novel liquid crystalline derivatives

There has been an ever increasing interest in the field of discotic liquid crystals in general and in triphenylene-based discotic mesogens in particular, since their discovery [12]. Triphenylene derivatives are the most widely synthesized and studied materials in the family of discotic liquid crystals, because they exhibit a variety of mesophase, their derivatives are thermally and chemically stable, and their chemistry is fairly accessible [13]. Scaled up and improved synthetic routes to the hexaalkoxytriphenylenes, the so-called “working horse” of liquid crystal chemists, has been well documented. The search for columnar mesophases in triphenylene is mostly ruled by subtle changes in the number, size and nature of the lateral chains and it has been found that the discotic core is tolerant to various substitution changes without sacrificing the mesophase forming ability. Therefore by tuning the type of attached side chains, compounds with different ability to self organize into different mesophase morphologies can be tailor-made from triphenylene [13]. Triphenylenes exhibit diverse mesophase morphologies such as helical, plastic, columnar, smectic and nematic in addition to crystalline and stable isotropic phases. Variety of monomeric, polymeric and monodisperse oligomeric liquid crystals have been prepared from this core [13]. Some of the oligomers form super cooled glassy phase and some of them even form super lattice of columnar superstructures [12]. However because of synthetic problems in obtaining mono-functionalized triphenylenes, which are valuable precursor molecules for the synthesis of a variety of discotic dimers,

oligomers, polymers, networks, dendrimers and mixed tail derivatives, the potential utility of these materials has not yet been fully explored. Physical properties of these non-conventional liquid crystals are significantly different to those of conventional low molar mass liquid crystals [13]. A few methods have been developed for the synthesis of mono-functionalised triphenylenes, but most of these methods involve expensive and/or hazardous reagents.

The synthesis of mono-functionalised triphenylenes can be achieved in different ways. One of the earliest reported methods of monohydroxypentaalkoxytriphenylene synthesis involves partial alkylation of hexaacetoxypentatriphenylene to monoacetyl-pentaalkoxytriphenylene in low yield [14]. This can be hydrolyzed to monohydroxytriphenylene. A non selective cleave of one of the alkoxy groups of hexaalkoxytriphenylenes using a calculated amount of 9-Br-BBN gives a mixture of products containing the unreacted hexaalkoxytriphenylenes, monohydroxy triphenylene and a minor amount of dihydroxytriphenylene [15]. A selective cleavage of the methyl ether of monomethoxy-pentaalkoxytriphenylene with lithium diphenylphosphide affords the monohydroxytriphenylene in high yields [16]. The synthesis of monohydroxytriphenylene by directly coupling tetraalkoxybiphenyl and alkoxy phenol using Molybdenum(V) chloride has been reported, but the reaction is sluggish and the isolation of the product was difficult [17]. It has been previously reported that this compound can be obtained as a side product in the oxidative trimerization of dialkoxy benzene with MoCl_5 in about 25% yield. Bromo-catecholborane (Cat-B-Br) an alternative to 9-Br-BBN, has been found to give almost 70% of mono-functionalised

triphenylene. This reaction is highly efficient for the preparation of mono- di- and trifunctionalised derivatives, but the reagent is expensive and moisture sensitive [18].

Recently, an economic and convenient method for the preparation of monohydroxy functionalized triphenylene using ferric chloride in nitromethane is also reported [19]. Though it is a one step process, the over all yield in the reaction does not go above 20%. Because of these problems, we started looking for an alternative, inexpensive and less hazards method to produce these mono functionalized materials. We have found that ionic reagents can be used to prepare these various monohydroxy functionalised triphenylenes in moderate yield. This methodology avoids all types of toxic, volatile and hazardous reagents [20].

Developing green chemistry methodologies is one of the main themes of modern synthetic chemistry. In this context, the use of ionic liquids and microwaves are powerful tools. Ionic liquids a class of organic salts with usually low melting points, have attracted considerable attention. Due to their unique characteristics such as non-volatility, thermal stability, non-flammability, very low vapor pressure, reusability, and diverse solvating ability, they can be used as environmentally benign solvent media to replace conventional volatile organic solvents in many chemical processes. Ionic liquids serve the dual purpose of solvent as well as reagents in many reactions, and allow easy isolation of products [21]. On the other hand, microwave assisted high-speed chemical synthesis has attracted much attention in the past decade. As mentioned earlier, this is due to the fact that reactions proceed faster and more selective than conventional thermal conditions and because of operational simplicity, high yield of products and cleaner reactions with easier work up.

In this part of the chapter, we present a convenient, economic and environmentally benign green chemical method for the synthesis of monohydroxypentaalkoxytriphenylenes (Figure 3) by using pyridinium and imidazolium-based ionic reagents under microwave heating conditions [20] and subsequently these monofunctionalised triphenylenes have been converted into novel non-symmetrical hexaalkoxytriphenylenes by using branched alkyl chains [22].

Figure 3. Monohydroxy functionalized triphenylenes prepared by microwaves and ionic reagents.

Owing to its electron rich core triphenylene derivatives act as a p-type semiconductor [23, 24], however by replacing some of the carbon atoms from the carbocyclic aromatic core by electronegative hetero atoms such as nitrogen, n-type semiconductors can be made e.g. hexaazatriphenylenes [25]. Charge carrier transport and photoconductivity in the columnar phase of triphenylenes has been studied extensively and accounted for as well. The various other non-covalent supramolecular interactions such as hydrogen bonding, charge-transfer, ionic, complementary polytopic interaction (CPI) etc. have been introduced to induce and/or stabilize mesophases in triphenylenes in addition to strong π - π interactions. Furthermore, stimuli-responsive discotic liquid crystals that change the self-assembled LC structure by external stimuli such as ions have

been reported for triphenylene derivatives [12]. Triphenylenes possess the propensity for self-alignment on various substrates to give homeotropic or planar alignment which is crucial for various opto-electronic applications of these intriguing materials. The structure-property relationship is relatively well understood in triphenylenes [13] and the present focus is on structure-(device)performance of these fascinating materials. The successful practical commercial application of discotic liquid crystals is centered on triphenylene derivatives. Owing to its transparency to visible light, this has found application as optical compensation films for improving the viewing angle characteristics and hence contrast ratio of current thin film transistor liquid crystal display (TFT-LCD) devices. Thin polymerized films of nematic triphenylenes provide wide viewing angle liquid crystal displays with very good contrast ratio [26]. Since for other opto-electronic practical applications, discotic compounds should have lower melting points and wide mesophase range, there have been efforts to bring down the transition temperatures and stabilize the mesophases. Unsymmetrical peripheral substitution affects the phase behavior markedly. The symmetry of a discotic molecule can be reduced in different ways; like for example by core asymmetric substitution or by introducing an extra group or alkyl chain in a triphenylene molecule, or by side chain asymmetry by attaching alkyl chains of different length in the periphery, or by changing the mode of attachment of the peripheral chains, e.g. mixed ether-ester derivatives. In hexaalkoxytriphenylenes **4** the strategy has been to use alkyl chains of different chain length. Tinh *et al.* **5** [27], Allen *et al.* **6, 7**, [28] Paraschiva *et al.* [29] **8** and Goodby *et al.* **9** [30] have prepared hexaalkoxy substituted triphenylenes with different alkyl chain lengths to understand the effect of unsymmetrical chains on mesomorphism. They found that introduction of dissymmetric

side chains do not affect the nature of the columnar phase but results in reduction of mesophase stability by lowering the isotropic transition temperatures. Similar results have been found in heptasubstituted triphenylenes **10**, **11** [31].

A number of research groups have recently demonstrated that when branching points are introduced into the aliphatic side chains of DLCs the temperature range of the mesophase was widened and the transition temperatures were lowered without altering the nature of the mesophase [32]. In some of the cases it has been possible to obtain room temperature DLCs with very broad range of mesophase [33].

In order to obtain low temperature and stable liquid crystalline electron rich triphenylene derivatives we have replaced one of the alkyl chains of hexaalkoxytriphenylenes by branched alkyl chains *viz.* 2-ethyl hexyl and 3,7-dimethyl octyl and studied the mesophase behavior of novel triphenylene derivatives [22]. The monohydroxy functionalized precursors (Figure 3) have been prepared from symmetrical

hexaalkoxy triphenylenes **13** by using microwave irradiation and ionic reagents. The monohydroxy functionalized pentalkoxytriphenylenes have been converted into unsymmetrical hexaalkoxytriphenylenes with the help of microwave dielectric heating.

2.2.1 Results and discussion

The synthesis of monohydroxypentaalkoxytriphenylenes **14** using ionic reagents **I-V** is shown in Scheme 3.

Scheme 3. Synthesis of monohydroxypentaalkoxytriphenylenes using ionic reagents.

When different hexaalkoxytriphenylenes **13** [R=-C₄H₉ (H4TP), -C₅H₁₁ (H5TP), -C₆H₁₃ (H6TP)] were treated with various ionic reagents (**I-V**), monohydroxy-functionalised triphenylenes **14** were formed in moderate yields. The ionic reagents were prepared following literature methods [34]. We have used different equivalents of the reagents **I-V** under different microwave powers and for various reaction times. While reagents **I**, **III** and **IV** did not give any monohydroxy-functionalised triphenylene under

microwave heating condition for more than 5-10 min, the reagents **II** and **V** produced the desired product. The results are summarized in Table 6 and 7.

Table 6. Preparation of monohydroxy-pentaalkoxytriphenylene **14** using reagent **V** under microwave heating.

Entry	13	V (Equi.)	MW Power	Time (min)	14 (%)	Rec. 13 (%)	Yield ^a (%)
1	H4TP	4	160	3	12	70	40
2	H4TP	2	360	5	23	53	49
3	H4TP	2	360	10	22	44	39
4	H4TP	4	360	5	21	43	37
5	H4TP	6	360	5	23	38	37
6	H4TP	3	360	5	25	57	58
7	H4TP	2	600	3	24	51	49
8	H4TP	3	600	3	26	46	48
9	H4TP	4	600	5	25	43	44
10	H4TP	6	600	3	24	45	44
11	H4TP	6	600	5	24	41	40
12	H4TP	2	800	3	20	52	42
13	H4TP	2	800	1	19	66	56
14	H4TP	2	800	5	22	45	40
15	H4TP	4	800	3	22	45	40
16	H4TP	4	360	3	17	60	42
17	H5TP	3	360	3	4	90	40
18	H5TP	3	360	5	30	54	65
19	H5TP	6	360	5	23	47	43
20	H5TP	3	600	5	28	52	59
21	H5TP	3	600	3	26	56	59
22	H5TP	3	800	3	27	54	59
23	H6TP	3	360	3	10	83	59
24	H6TP	3	360	5	29	41	49
25	H6TP	3	600	3	30	50	60
26	H6TP	3	600	5	29	40	60
27	H6TP	6	360	5	2	38	3
28	H6TP	3	800	3	27	52	56

^a yield of **14** based on consumed material **13** in the Tables 6 and 7.

It is interesting to note that no side product was formed in the reaction and the unreacted triphenylene can be recovered easily and can be recycled. It is clear from the tables that longer chain aryl-alkyl ethers gives lower yield of the product. This could be because of the increased steric hindrance of longer alkyl chains.

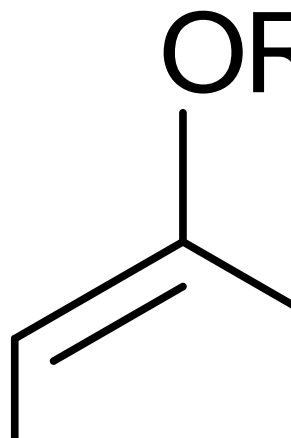
Table 7. Preparation of monohydroxy-pentaalkoxytriphenylene **14** using reagent **II** under microwave irradiation conditions.

Entry	13	II	MW	Time	14	Rec. 13	Yield ^a
		(Equi.)	Power	(min)	(%)	(%)	(%)
1	H4TP	3	360	5	36	27	49
2	H4TP	3	600	3	26	54	57
3	H4TP	3	800	3	28	51	57
4	H4TP	3	800	1	24	62	63
5	H4TP	3	600	5	28	45	51
6	H4TP	3	360	2	23	55	51
7	H4TP	3	360	3	28	48	54
8	H4TP	6	360	3	22	43	38
9	H5TP	3	360	3	22	55	49
10	H5TP	3	360	5	34	38	55
11	H5TP	3	600	3	26	57	61
12	H5TP	3	600	5	30	51	62
13	H6TP	3	360	5	25	54	55
14	H6TP	3	600	3	28	53	59

^a yield of **14** based on consumed material **13** in the Tables 6 and 7.

As can be seen from Table 6 and 7, irradiation of the reaction mixture at 600W for 3 min. using 3 equivalent of the reagent generally furnished good yield of the products. When the reaction mixture is irradiated with 360W, it takes longer time i.e. 5min. to furnish good yield of the products. Enhancing the microwave power to 800W did not increase the yield significantly. The identity and purity of the products were characterized by their spectral data, phase behavior and by comparison with authentic samples.

The synthesis of unsymmetrical hexaalkoxy triphenylenes **15** and **16** from **14** is shown in Scheme 4.



Scheme 4. Synthetic route of unsymmetrical hexaalkoxytriphenylenes from monohydroxypentaalkoxytriphenylenes.

The racemic branched chain alkyl bromides were prepared from their corresponding alcohols using N-bromosuccinimide and triphenylphosphine[32, 33]. The unsymmetrical hexaalkoxytriphenylenes have been prepared in very good yield within 3-4

min by using microwave dielectric heating which is simple, efficient, rapid and economic. The purity and identity of the products were characterized from their spectral features (FTIR, ^1H NMR ^{13}C NMR etc.) and elemental analysis. The FTIR spectrum of compound **15a** is shown in Figure 4. The absence of phenolic hydroxyl absorption peak at around 3500 cm^{-1} in the IR spectra of all the hexaalkoxytriphenylenes suggests that the hydroxyl group of **14** has been successfully alkylated by microwaves. The ^1H NMR of all the unsymmetrical hexaethers show a single aromatic peak at δ 7.8 ppm integrating for six protons in addition to phenoxyethylene, methylene and methyl resonances (Figure 5). The resonance peak corresponding to the hydroxyl group of **14**, which appears at δ 5.9 ppm is completely absent in the ^1H NMR spectra of hexaethers **15** and **16**. The ^{13}C NMR spectra of the hexaethers **15** and **16** exhibit only three aromatic carbon resonances at *ca.* δ 149, 124, 108 ppm characteristics of hexaalkoxy-substituted triphenylenes, two aryloxy methylene-carbon at *ca.* 72 and 69 ppm in addition to the methylene and methyl-carbon resonances (Figure 6). These spectral features (IR and NMR) and the actual combustion analysis data obtained for the hexaethers of triphenylene confirm the structure as well as high purity of the novel discotic compounds unambiguously.

2.2.2 Thermal behavior of unsymmetrical triphenylenes

The phase transition temperatures of all the compounds were initially established from the polarizing optical microscopy and then measured accurately by differential scanning calorimetry along with their associated enthalpy changes (Table 8). All the compounds exhibit enantiotropic liquid crystalline behavior. These materials display characteristic defect textures for the columnar hexagonal mesophase, example of which is shown in

Figure 7. As a typical example the DSC thermogram of compound **16c** is shown in Figure 8. The Cr-Col_h and Col_h-I transitions upon heating and I-Col_h transition upon cooling are seen. As can be seen from the Table 8, both the melting and clearing temperatures of all these materials are lower than their symmetrical counterparts [35].

Table 8. Phase transition temperatures °C (peak temperatures) and enthalpies (kJ/mol. in parentheses) of triphenylene derivatives **15a-e** and **16a-e**. Cr = crystal, Col_h = hexagonal columnar, I = isotropic

Compound	Heating Scan	Cooling Scan
15a	Cr 71.6 (28.8) Col _h 95(8.4) I	I 93.5 (8.4) Col _h 40.2 (22.6) Cr
15b	Cr 54.3 (32.5) Col _h 88.1(6.4) I	I 86.7 (6.3) Col _h 29.8 (27) Cr
15c	Cr 53.3 (37.4) Col _h 74.5 (4.7) I	I 72.6 (4.6) Col _h 35.1 (36.3) Cr
15d	Cr 48.7 (51.5) Col _h 68.8 (4.4) I	I 67.2 (4.4) Col _h 32 (45.2) Cr
15e	Cr 51 (43.5) Col _h 58.5 (3.2) I	I 56.6 (3.3) Col _h 33.5 (46.8) Cr
16a	Cr 51.8 (28.9) Col _h 80.1 (6.1) I	I 78.4 (6.2) Col _h
16b	Cr 39.7 (30.8) Col _h 88.6 (6.8) I	I 86.7 (6.5) Col _h
16c	Cr 44 (36.8) Col _h 84.4 (5.5) I	I 82.9 (5.4) Col _h
16d	Cr 42.7 (47.2) Col _h 86.3 (5.3) I	I 84.4 (4.9) Col _h
16e	Cr 51.7 (57) Col _h 80.5 (4.9) I	I 78.1 (4.6) Col _h 32.8 (50.3) Cr

On an average about 15 °C lowering in melting point and 25 °C lowering in isotropic temperature was found for the compounds of series **1 (15a-e)**. In series **2 (16a-e)** the melting points of the compounds are lowered by about 25 °C. This could be because of the disordering introduced by the branched alkyl chain into the periphery. The crystal to mesophase transition enthalpy increases as the chain length is increased in both the series. This could be due to the fact that with increase in chain length the molecules become more symmetric in shape and hence more favorable packing in the crystalline phase. The compounds **15c** and **16e** show sharp crystallization while cooling. It may be due to their symmetrical molecular shape but other members show slow crystallization. It should be noted that **16e** is the only member of that series which crystallizes but other members exhibit columnar mesophase down to room temperature. The transition enthalpies for mesophase to isotropic transition decreases with increase in chain length, this could be due to the extra steric crowding of the branched alkyl chains. Both **15b** and **16b** exhibit the highest mesophase range in their respective series where as H4TP exhibits the highest mesophase range in the symmetrical hexaalkoxytriphenylenes. This is due to the fact that H4TP forms a highly ordered plastic columnar phase [36]. It is interesting to note that both melting and clearing temperatures for the compounds **16a-e** show very strong odd-even effect (Figure 9). The members containing odd number of carbon atoms in their periphery (except the branched chain) exhibit lower melting points then having even number of carbon atoms in their periphery which is reverse to the clearing temperatures. This could be due to favorable packing of the molecules containing even number of carbon atoms in their crystalline state where as the packing of the molecules is favorable in the mesophase in case of the members containing odd number of carbon atoms in the

alkoxy chains. The compounds **16c-e** display broader mesophase range than their symmetrical counter parts though their clearing temperatures are less than the symmetrical ones. This is because the melting transition temperatures are lowered more as compared to the clearing temperatures for these compounds and hence resulting in broad mesophase range. The mesophase stability for the series **15a-e** is less than the series **16a-e** (Figure 9). This could be because of the more proximity of the ethyl group to the aromatic core of the discotic molecules and hence making unstacking of the molecules in the columns easy.

2.2.3 X-ray diffraction studies

X-ray diffraction patterns for all the compounds were recorded in the columnar phase 10 °C below the isotropic temperature while cooling from the isotropic phase. A representative diffraction pattern obtained for the compound **15a** (Figure 10) and its one-dimensional intensity vs. 2θ profile obtained by integrating over the entire χ (0-360°) range are shown in Figure 11. Qualitatively similar patterns were obtained for the other compounds. The overall features observed are consistent with the structure of the Col_h phase. In the low-angle region, four sharp peaks, one very strong and three weak reflections are seen whose d-spacings are in the ratio of 1 : 1/√3 : 1/√4 : 1/√7. Identifying the first peak with the Miller index 100, the ratios conform to the expected values from a two-dimensional hexagonal lattice. In the wide-angle region two diffuse reflections are seen. The broad one centered at 4.66Å corresponds to the liquid-like order of the aliphatic chains. The relatively sharper one seen at higher 2θ value and well separated from the broad one is due to the staking of the molecular cores one on top of the other. As it is a

diffuse peak it suggests that the staking of the discs within each column is correlated over short distances only. The average staking distance (core-core separation) was found to be 3.64Å and falls in the range observed for a number of materials exhibiting the columnar phase. It should be noted here that H4TP forms a highly ordered plastic columnar phase [36] but the compounds **15a** and **16a** form normal hexagonal columnar phase. The intercolumnar distance for H4TP is 18.59Å [37] where as this distance is 19.26Å and 19.74Å respectively for **15a** and **16a**. This could be because of the interdigitation of the long branched chain alkoxy groups which restricts the molecular rotation within the column and hence destroy the plastic columnar phase. The hexagonal columnar structure of the compounds is corroborated by the appearance of six symmetrically positioned spots (Figure 12) in the diffraction pattern of the compound **15c** without any pretreatment for alignment of the columnar phase or application of any external force. This type of pattern can be obtained from aligned samples by passing the X-ray beam along the column axis in the columnar mesophase. So this could be because of formation of large homeotropic domains by branched chain discotic compounds as found earlier [32]. The miller indices of 100 reflections (d_{100}) and the corresponding inter columnar distances along with the inter disc distances (intracolumnar) for all the compounds are listed in Table 9. The intercolumnar spacing for a hexagonal lattice is obtained by division of d_{100} by $(\cos 30^\circ)$. As can be seen from the Table 9, for compounds of both the series the inter columnar distances increase monotonically with increase in the chain lengths. As expected the compounds of the series-2 show slightly higher intercolumnar distances (Figure 13) than the compounds of the series-1 because the 3, 7-dimethyl octyloxy chain is longer than the 2-ethyl hexyloxy chain. The intercolumnar distances are intermediate

between their symmetrical counterparts and their fully extended all-*trans* structure which suggests some degree of interdigitation of the alkyl chains [38].

Table 9. Layer spacing and intercolumnar distances for the mesophase of series **15a-e** and **16a-e**, deduced from X-ray measurements in the mesophase.

Compound	<i>d</i> -spacing/Å	Intercolumn distance/Å	Interdisc distance/Å
15a	16.68	19.26	3.64
15b	17.65	20.38	3.67
15c	18.01	20.79	3.67
15d	19.31	22.29	3.67
15e	20.01	23.10	3.66
16a	17.10	19.74	3.64
16b	17.72	20.46	3.65
16c	18.73	21.62	3.66
16d	19.57	22.59	3.63
16e	20.33	23.47	3.64

The compounds **15c** (20.79Å) and **16e** (23.47Å) have intercolumnar distances similar to H6TP (21.17Å) [29] and H8TP (23.4Å) [38] suggesting there is little interdigitation of the alkyl chains in these two compounds. This could be due to their relatively more symmetrical structure than the other compounds.

2.2.4 Conclusions

In conclusion, 30-40% yields of the valuable mono-functionalized triphenylenes can be isolated using simple ionic liquids in microwave flash heating conditions. Using microwave flash heating, these materials can be prepared in a few minutes in moderate yield. In all cases, no side reaction occurred and the unreacted starting material can be isolated easily, and can be recycled. The process reported here is an economic and green synthesis method for the preparation of monohydroxy-pentaalkoxy triphenylene derivatives.

We have also prepared two novel series of triphenylene-based DLCs having a branched-alkyl chain and five normal alkyl chains using microwave dielectric heating from monohydroxy functionalized triphenylenes. Mesophase behavior of the compounds has been characterized by polarizing optical microscopy, differential scanning calorimetry and mesophase structure has been characterized by X-ray diffractometry. The introduction of branched-alkyl chain produces materials having low clearing temperature ($< 100\text{ }^{\circ}\text{C}$) and wide mesophase range. From X-ray studies, it was observed that these compounds have a tendency of homeotropic alignment without any pretreatment for alignment of the columnar phase or application of any external force. The manipulation of the molecular architecture provides the opportunity to obtain homeotropically aligned films of self-assembled materials with low clearing temperature and wide mesophase range which is essential for the implementation of these kinds of materials in electronic devices like organic light emitting diodes, photovoltaic solar cells, gas sensors, etc.

2.3 Experimental

2.3.1 General information

Chemicals and solvents (AR quality) were used without purification. All reactions were monitored by employing TLC technique using appropriate solvent system for development. All solvent extracts were washed with water and dried over anhydrous sodium sulphate and concentrated at reduced pressure on a Buchi rotary evaporator. Yields reported are isolated yields of pure materials. The purity of all the compounds was confirmed from their homogenous nature of a TLC plate, NMR spectrum and elemental analysis. Microwave irradiation was performed in an unmodified household microwave oven. (LG, MS-192W). Column chromatographic separation was performed on silica gel (100-200 mesh). ^1H NMR spectra and ^{13}C NMR spectra were recorded in CDCl_3 on a 400 MHz (Bruker AMX 400) spectrometer. All chemical shifts are reported in δ (ppm) units down field from tetramethylsilane (TMS) and J values are reported in Hz. FT-IR spectra were recorded as KBr discs on Shimadzu FTIR-8400. Elemental analysis was performed on Carlo-Erba Flash 1112 analyser. Transition temperatures were observed using a Mettler FP82HT hot stage and FP90 central processor in conjunction with an OLYMPUS BX51 polarizing microscope. Transition temperatures and associated enthalpies were measured by differential scanning calorimetry by heating and cooling at the scan rate of 5 $^\circ\text{C}$ per minute (Perkin- Elmer Model Pyris 1D with Intracooler 2P cooling system). X-ray diffraction measurements were carried out using $\text{Cu-K}\alpha$ radiation ($\lambda=1.54\text{\AA}$) generated from a 4 kW rotating anode generator (Rigaku Ultrax-18) equipped with a graphite crystal monochromator. Samples were filled in Hampton research capillaries (0.5 or 0.7 mm diameter) from isotropic phase, sealed and held on a heater. For all the samples, X-

ray diffraction was carried out at room-temperature (25 °C) and diffraction patterns of the mesophase were recorded on a two dimensional image plate (Marresearch).

2.3.2 General procedure for the synthesis of 4'-alkoxy-4-cyanobiphenyls

In a typical reaction, 4'-hydroxy-4-biphenylcarbonitrile (50 mg, 0.26 mmol), 1-bromooctane (98 mg, 0.5 mmol) and cesium carbonate (165 mg, 0.5 mmol) were mixed in N-methyl-pyrrolidinone (NMP, 0.2 ml) in a small glass vial and loosely covered with a rubber septum. The mixture was heated in an unmodified household microwave oven at 360 W for 30 seconds (this has been reported [3] that under similar conditions the bulk temperature reaches to about 100 °C). The vial was taken out and water (2 ml) was added. The resultant precipitate was filtered off and dried. It was purified by passing through a short bed of silica gel and eluting the product in hexane-ethyl acetate to afford 63 mg (80%) of the pure product. In the case of more than 30 s heating, after the first 30 s irradiation, the vial was taken out of the oven and placed back after about one minute and irradiated again for 30 s. A 30 + 30 s heating followed by above-mentioned work-up furnished 77 mg (98%) of the product. The yield represents the isolated pure product in hand in all the cases. The product can also be isolated in almost similar yield by simple crystallization as no other side product forms but the quality of the product is not as good as in the case of chromatographic purification.

2.3.3 General procedure for the synthesis of α,ω -bis(4'-cyanobiphenyl-4-yloxy)alkanes

To a mixture of 0.2 mmol dibromoalkane, 0.44 mmol of 4'-hydroxy-4-biphenylcarbonitrile and 0.8 mmol of base in a glass vial, a few drops of solvents were added. It was irradiated as mentioned above. The product was extracted with dichloromethane and purified by passing through a silica column. All the products were characterized from their spectral data and thermal behaviour.

2.3.4 General procedure for the synthesis of monohydroxy pentaalkoxytriphenylenes

H4TP **13a** (330 mg, 0.5 mmol) was taken in a glass vial, [bmim]Br **V** (330 mg, 1.5 mmol) was added, and the mixture was thoroughly mixed and irradiated for one minute under the desired microwave power. The vial was taken out and once again kept back for one minute and this procedure was continued up to desired time. Then the vial was cooled to room temperature. The mixture was dissolved in dichloromethane and then passed through a neutral alumina column to isolate the pure product and unreacted starting material.

Selected data are as follows.

14a: ^1H NMR (400 MHz, CDCl_3): δ 7.96 (s, 1H), 7.83 (m, 4H), 7.78 (s, 1H), 5.90 (br s, 1H), 4.24 (m, 10H), 1.94 (m, 10H), 1.58 (m, 10H), 1.04 (t, $J = 7.2$ Hz, 15H); ^{13}C NMR (100 MHz, CDCl_3): δ 149.0, 148.8, 145.9, 145.3, 124.0, 123.7, 123.3, 123.0, 107.3, 106.6, 104.4, 69.6, 69.3, 68.8, 31.5, 19.4, 14.0; IR (KBr, all the derivatives **14a-c** showed similar spectra): ν_{max} 3545, 2953, 2928, 2858, 1616, 1518 1437, 1389, 1352, 1261, 1171,

1074, 835 cm^{-1} ; UV-vis data (CHCl_3 , all the derivatives **14a-c** show similar spectrum): λ_{max} 276.8, 303.2, 344.0 nm; DSC (peak temperature in $^{\circ}\text{C}$ and associated enthalpy changes J /g in parentheses, Cr = crystals, I = isotropic): Cr 112.0 (56) I; Elemental analysis: calculated for $\text{C}_{38}\text{H}_{52}\text{O}_6$, C 75.47, H 8.66%; found C 75.18, H 9.10%.

14b: ^1H NMR (400 MHz, CDCl_3): δ 7.96 (s, 1H), 7.83 (m, 4H), 7.78 (s, 1H), 5.90 (br s, 1H), 4.24 (m, 10H), 1.94 (m, 10H), 1.50 (m, 20H), 0.98 (m, 15H); ^{13}C NMR (100 MHz, CDCl_3): δ 149.2, 149.0, 148.8, 145.9, 145.3, 124.0, 123.7, 123.3, 123.0, 107.6, 107.3, 106.5, 104.3, 69.9, 69.6, 69.1, 29.2, 29.0, 28.4, 22.6, 14.1; DSC: Cr 64 (28) Cr 82 (27) I; Elemental analysis: calculated for $\text{C}_{43}\text{H}_{62}\text{O}_6$, C 76.52, H 9.26%; found C 76.29 H 9.60%.

14c: ^1H NMR (400 MHz, CDCl_3): δ 7.96 (s, 1H), 7.83 (m, 4H), 7.78 (s, 1H), 5.90 (br s, 1H), 4.29 (m, 10H), 1.94 (m, 10H), 1.57 (m, 10H), 1.40 (m, 20H), 0.93 (m, 15H); ^{13}C NMR (100 MHz, CDCl_3): δ 149.1, 148.8, 145.9, 145.3, 124.0, 123.7, 123.2, 123.0, 107.7, 107.5, 107.3, 106.5, 104.4, 69.9, 69.7, 69.2, 31.7, 29.4, 29.3, 25.8, 22.7, 14.1; DSC: Cr 65 (63) I; Elemental analysis: calculated for $\text{C}_{48}\text{H}_{72}\text{O}_6$, C 77.38, H 9.74%; found C 77.31 H 9.98%.

2.3.5 General procedure for the synthesis of unsymmetrical triphenylene derivatives

To a mixture of monohydroxy-pentaalkoxytriphenylene **14** (0.15 mmol), cesium carbonate (0.3 mmol) and appropriate branched chain alkyl bromide (0.3 mmol) in a small glass vial was added few drops of NMP (0.2 ml). The vial was loosely covered with a rubber septum (Aldrich) and then irradiated under microwave for 30 seconds. The vial was taken out and again kept back after about one minute. The process was continued 6-8 times until the reaction gets completed (monitored by TLC). The reaction mixture was

cooled and worked up by adding water followed by extraction with dichloromethane. The crude product was purified by column chromatography (silica gel, ethyl acetate-petroleum ether 1:20) and crystallized from methanol in about 79-87% yield.

IR data. (ν_{\max}) **15a**: 3101, 2956, 2931, 2868, 2742, 1616, 1517, 1438, 1263, 1172, 1070, 1033, 960, 835, 599 cm^{-1} . **16a**: 3101, 2956, 2927, 2868, 1616, 1518, 1438, 1386, 1263, 1172, 1070, 1033 962, 835, 599 cm^{-1} . All other derivatives give similar spectra.

^1H NMR data. **15a**: δ_{H} 7.84 (s, 6H, ArH), 4.25 (t, 10H, $J = 6.2$, ArOCH_2), 4.12 (d, 2H, $J = 5.7$, ArOCH_2), 1.9 (quintet, 12H, $J = 6.5$, $\text{CH}_2\text{CH}_2\text{CH}_2$), 1.7-1.4 (m, 17H, CH, CH_2), 1.1 (m, 18H, CH_3), 0.9 (t, 3H, $J = 7$, CH_3); **16a**: δ 7.84 (s, 6H, ArH), 4.24 (t, 12H, $J = 6.4$, ArOCH_2), 1.9 (quintet, 12H, $J = 6.7$, $\text{CH}_2\text{CH}_2\text{CH}_2$), 1.8-1.2 (m, 18H, CH, CH_2), 1.0 (m, 18H, CH_3), 0.9 (d, 6H, $J = 6.6$, CH_3). All other compounds give similar spectra having more number of hydrogens in the aliphatic region.

^{13}C NMR data. **15a**: δ_{C} 149.1, 123.7, 107.6, 72.3, 69.5, 39.7, 31.5, 30.8, 29.2, 24.1, 23.1, 19.4, 13.9, 11.3. **16a**: 149.0, 123.7, 107.5, 69.4, 68.1, 39.3, 37.5, 36.4, 31.5, 30.0, 28.0, 24.8, 22.6, 19.8, 13.9. All other compounds give similar spectra.

Elemental analysis: **15a**, Found: C, 76.6; H, 9.7. $\text{C}_{46}\text{H}_{68}\text{O}_6$ requires C, 77; H, 9.6%; **15b**, Found: C, 77.5; H, 9.8. $\text{C}_{51}\text{H}_{78}\text{O}_6$ requires C, 77.8; H, 9.9%; **15c**, Found: C, 78.1; H, 10.6. $\text{C}_{56}\text{H}_{88}\text{O}_6$ requires C, 78.5; H, 10.4%; **15d**, Found: C, 78.7; H, 11.0. $\text{C}_{61}\text{H}_{98}\text{O}_6$ requires C, 79.0; H, 10.7%; **15e**, Found: C, 79.1; H, 10.9. $\text{C}_{66}\text{H}_{108}\text{O}_6$ requires C, 79.5; H, 10.9%; **16a**, Found: C, 77.0; H, 9.75. $\text{C}_{48}\text{H}_{72}\text{O}_6$ requires C, 77.4; H, 9.74%; **16b**, Found: C, 77.7; H, 10.5. $\text{C}_{53}\text{H}_{82}\text{O}_6$ requires C, 78.1; H, 10.1%; **16c**, Found: C, 78.3; H, 10.9. $\text{C}_{58}\text{H}_{92}\text{O}_6$ requires C, 78.7; H, 10.5%; **16d**, Found: C, 79.0; H, 11.2. $\text{C}_{63}\text{H}_{102}\text{O}_6$ requires C, 79.2; H, 10.7%; **16e**, Found: C, 79.2; H, 11.1. $\text{C}_{68}\text{H}_{112}\text{O}_6$ requires C, 79.6; H, 11.0%.

References

1. (a) R. Gedye, F. Smith, K. Westaway, H. Ali, L. Baldisers, L. Laberge and J. Rousell, *Tetrahedron. Lett.*, **27**, 279, (1986); (b) R. J. Giguere, T. L. Bray, S. M. Duncan and G. Majetich, *Tetrahedron. Lett.*, **27**, 4945, (1986).
2. (a) C. O. Kappe, *Chem. Soc. Rev.*, **37**, 1127, (2008); (b) V. Polshettiwar and R. S. Varma, *Acc. Chem. Res.*, **41**, 629, (2008); (c) M. A. Herrero, J. M. Kremsner and C. O. Kappe, *J. Org. Chem.*, **73**, 36, (2008); (d) C. O. Kappe, *Angew. Chem. Int. Ed.*, **43**, 6250, (2004); (e) F. Wiesbrock, R. Hoogenboom and U. S. Schubert, *Macromol. Rapid Commun.*, **25**, 1739, (2004); (f) M. Nuchter, B. Ondruschka, W. Bonrath and A. Gum, *Green Chem.*, **6**, 128, (2004); (g) A. K Bose, M. S. Manhas, S. N. Ganguly, A. H Sharma and B. K Banik, *Synthesis*, 1578, (2002); (h) A. de la Hoz, A. Diaz-Ortiz and A. Moreno, *Chem. Soc. Rev.*, **34**, 164, (2005); (i) V. Molteni and D. A. Ellis, *Curr. Org. Synth.*, **2**, 333, (2005); (j) M. Larhed, C. Moberg, and A. Hallberg, *Acc. Chem. Res.*, **35**, 717, (2002); (k) D. Bogdal, *Microwave-Assisted Organic Synthesis-One Hundred Reaction Procedures*. Elsevier, Amsterdam, (2005); (l) O. C. Kappe and A. Stadler, *Microwaves in Organic and Medicinal Chemistry*. Wiley-VCH, Weinheim, (2005); (m) E. Van der Eycken, and C. O. Kappe, (Eds.), *Microwave-Assisted Synthesis of Heterocycles*. Springer, Heidelberg, (2006). (n) *Microwaves in Organic Synthesis*, A. Loupy (ed.), Wiley-VCH, Weinheim, (2002). (o) *Microwave Synthesis: Chemistry at the Speed of Light*. CEM Publishing, Matthews NC, (2002).

3. (a) G. W. Gray, K. J. Harrison and J. A. Nash, *Electron. Lett.*, **9**, 130 (1973); (b) G. W. Gray, K. J. Harrison, J. A. Nash, J. Constant, J. S. Hulme, J. Kirton and E. P. Raynes, in *Liquid Crystals and Ordered Fluids*, Vol. **2**, edited by R. S. Porter, J. F. Johnson Plenum, New York, p.617, (1973).
4. (a) D. A. Dunmur, A. Fukuda and G. R. Luckhurst (editors), *Physical Properties of Liquid Crystals: Nematics*, INSPEC, London, (2001); (b) D. Demus, J. Goodby, G. W. Gray, H. -W. Spiess and V. Vill, (Editors), *Handbook of Liquid Crystals*, Vol. **1** and **2**, Wiley-VCH, Weinheim, (1998).
5. (a) C. T. Imrie and P. A. Henderson, *Chem. Soc. Rev.*, **36**, 2096, (2007); (b) C. T. Imrie, and P. A. Henderson, *Current Opinion in Colloid & Interface Science*, **7**, 298, (2002); (c) C. T. Imrie, *Structure and Bonding*, edited by D. M. P. Mingos, Springer-Verlag, Berlin, p. 149, (2001); (d) C. T. Imrie and G. R. Luckhurst, *Handbook of Liquid Crystals*, Vol. 2B, edited by D. Demus, J. Goodby, G. W. Gray, H. -W. Spiess and V. Vill, Wiley-VCH, Weinheim, Chap. X, (1998).
6. (a) J. W. Emsley, G. R. Luckhurst, G. N. Shilestone and I. Sage, *Mol. Cryst. Liq. Cryst. Letters*, **102**, 223, (1984); (b) A. C. Griffin, S. R. Vaidya, R. S. L. Hung and S. Gorman, *Mol. Cryst. Liq. Cryst. Letters*, **1**,131, (1985); (c) J. W. Emsley, G. R. Luckhurst and G. N. Shilestone, *Mol. Phys.*, **53**, 1023, (1984); (d) A. Abe and H. Furuya, *Polymer Bulletin*, **19**, 403, (1988); (e) N. V. Tsvetkov, V. V. Zuev, I. V. Ksenofontov and V. N. Tsvetkov, *Liq. Cryst.*, **25**, 727, (1998); (f) D. Ionescu, G. R. Luckhurst and D. S. de Silva, *Liq. Cryst.*, **23**, 833, (1997), (g) N. V. Tsvetkov, V. V. Zuev, I. V. Ksenofontov and V. N. Tsvetkov, *Mol. Cryst. Liq. Cryst.*, **331**, 41, (1999); (h) V. N. Tsvetkov, N. V. Tsvetkov, S. A. Didenko and V.

- V. Zuev, *Mol. Cryst. Liq. Cryst.*, **265**, 341, (1995); (i) P. J. Barnes, A. G. Douglass, S. K. Heeks and G. R. Luckhurst, *Liq. Cryst.*, **13**, 603, (1993); (j) A. Ferrarini, G. R. Luckhurst, P. L. Nordio, S. J. Roskilly, *Chem. Phys. Lett.*, **214**, 409 (1993).
7. (a) D. Creed, J. R. D. Gross, S. L. Sullivan, A. C. Griffin, and C. E. Hoyle, *Mol. Cryst. Liq. Cryst.*, **149**, 185, (1987); (b) J. R. Willmott, C. J. Davenport, J. Newton and H. J. Coles, *Mol. Cryst. Liq. Cryst.*, **434**, 537, (2005).
8. V. Percec and M. Lee, *Macromolecules*, **24**, 2780, (1991).
9. H. K. Bisoyi and S. Kumar, *Phase Transitions*, **79**, 285, (2006).
10. (a) C. T. Imrie and G. R. Luckhurst, *J. Mater. Chem.*, **8**, 1339, (1998); (b) C. T. Imrie, D. Stewart, C. Remy, D. W. Christie, I. W. Hamley and R. Harding, *J. Mater. Chem.*, **9**, 2321, (1999).
11. S. Kumar and S.K. Pal, *Liq. Cryst.*, **32**, 659, (2005).
12. (a) S. Kumar, *Chem. Soc. Rev.*, **35**, 83, (2006); (b) F. Vera, J. L. Serrano and T. Sierra, *Chem. Soc. Rev.*, **38**, 781, (2009); (c) T. Kato, T. Yasuda, Y. Kamikawa and M. Yoshio, *Chem. Commun.*, 729, (2009); (d) S. Laschat, A. Baro, N. Steinke, F. Giesselmann, C. Hagele, G. Scalia, R. Judele, E. Kapatsina, S. Sauer, A. Schreivogel and M. Tosoni, *Angew. Chem. Int. Ed.*, **46**, 4832, (2007); (e) S. Sergeyev, W. Pisula and Y. H. Geerts, *Chem. Soc. Rev.*, **36**, 1902, (2007); (f) J. Wu, W. Pisula and K. Müllen, *Chem. Rev.*, **107**, 718, (2007); (g) A. Zecler, B. Donnio, C. Bourgogne, F. D. Cukiernik and D. Guillon, *Chem Mater.*, **19**, 1992, (2007).

13. (a) S. Kumar, *Liq. Cryst.*, **32**, 1089, (2005); (b) S. Kumar, *Liq. Cryst.*, **31**, 1037, (2004).
14. W. Kreuder and H. Ringsdorf, *Makromol. Chem. Rapid. Commun.*, **4**, 807, (1983).
15. F. Closs, L. Haussling, P. Henderson, H. Ringsdorf and P. Schuhmacher, *J. Chem. Soc. Perkin Trans. 1*, 1059 (1995).
16. (a) P. Henderson, H. Ringsdorf and P. Schuhmacher, *Liq. Cryst.*, **18**, 191, (1995); (b) N. Boden, R. J. Bushby, A. N. Cammidge, A. EI-Mansoury, P. S. Martin and Z. Lu, *J. Mater. Chem.*, **9**, 1391, (1999).
17. S. Kumar and M. Manickam, *Chem. Commun.*, 1615, (1997).
18. S. Kumar and M. Manickam, *Synthesis*, 1119, (1998).
19. S. Kumar and B. Lakshmi, *Tetrahedron Lett.*, **46**, 2603, (2005).
20. S. K. Pal, H. K. Bisoyi and S. Kumar, *Tetrahedron*, **63**, 6874, (2007).
21. (a) T. Welton, *Chem. Rev.*, **99**, 2071, (1999); (b) P. Wasserscheid and W. Kein, *Angew. Chem. Int. Ed.*, **39**, 3772, (2000); (c) R. Sheldon, *Chem. Commun.*, 2399, (2001); (d) J. Dupont, R. F. de Souza, and P. A. Z. Suarez, *Chem. Rev.*, **102**, 3667, (2002); (e) A. Corma, and H. Garcia, *Chem. Rev.*, **103**, 4307, (2003); (f) C. E. Song, *Chem. Commun.*, 1033, (2004); (g) *Ionic Liquids in Synthesis*, P. Wasserscheid and T. Welton (eds), Wiley-VCH, Weinheim, (2002); (h) *Ionic Liquids: Industrial Application to Green Chemistry*, R. D. Rogers and K. R. Seddon (eds), ACS Symposium Series 818; American Chemical Society: Washington, DC, (2002).
22. H. K. Bisoyi and S. Kumar, *J. Phys. Org. Chem.*, **21**, 47, (2008).

23. A. N. Cammidge, *Phil. Trans. R. Soc. A*, **364**, 2697, (2006).
24. S. Chandrasekhar and G. S. Ranganath, *Rep. Prog. Phys.*, **53**, 57, (1990).
25. (a) M. Palma, J. Levin, O. Debever, Y. Geerts, M. Lehmann and P. Samori, *Soft Matter*, **4**, 303, (2008); (b) R. I. Gearba, M. Lehman, J. Levin, D. A. Ivanov, M. H. J. Koch, J. Barbera, M. G. Debijs, J. Piris, Y. H. Geerts, *Adv. Mater.*, **15**, 1614, (2003).
26. (a) K. Kawata, *Chem. Rec.*, **2**, 59, (2000); (b) H. Mori, *Jpn. J. Appl. Phys.*, **36**, 1068, (1997).
27. N. H. Tinh, M. C. Bernaud, G. Sigaud, C. Destrade, *Mol. Cryst. Liq. Cryst.*, **65**, 307, (1981).
28. M. T. Allen, S. Diele, K. D. M. Harris, T. Hegmann, B. M. Kariuki, D. Lose, J. A. Preece and C. Tschierske, *J. Mater. Chem.*, **11**, 302, (2001).
29. I. Paraschiva, P. Delforterie, M. Giesbers, M. A. Posthumus, A. T. M. Macelis, H. Zuilhof, E. Sudholter, Jr, *Liq. Cryst.*, **32**, 977, (2005).
30. S. J. Cross, J. W. Goodby, A. M. Hall, M. Hird, S. M. Kelly, K. J. Toyne and C. Wu, *Liq. Cryst.*, **25**, 1, (1998).
31. S. Kumar, M. Manickam, S. K. Varshney, D. S. S. Rao and S. K. Prasad, *J. Mater. Chem.*, **10**, 2483, (2000).
32. (a) D. M. Collard and C. P. Lillya, *J. Am. Chem. Soc.*, **111**, 1829, (1989); (b) D. M. Collard and C. P. Lillya, *J. Am. Chem. Soc.*, **113**, 8577, (1991); (c) P. G. Schouten, J. M. Warman, M. P. de Hass, C. F. van Nostrum, G. H. Gelinck, R. J. M. Nolte, M. J. Copyn, J. W. Zwikker, M. K. Engel, M. Hanack, Y. H. Chang and W. T. Ford, *J. Am. Chem. Soc.*, **116**, 6880, (1994); (d) P. G. Schouten, J. F. van

- der Pol, J. W. Zwikker, W. Drenth and S. J. Picken, *Mol. Cryst. Liq. Cryst.*, **195**, 291, (1991); (e) K. Ohta, T. Watanabe, H. Hasebe, Y. Morizumi, T. Fujimoto and I. Yamamoto, *Mol. Cryst. Liq. Cryst.*, **196**, 13, (1991); (f) K. Ohta, Y. Morizumi, H. Ema, T. Fujimoto and I. Yamamoto, *Mol. Cryst. Liq. Cryst.*, **208**, 55, (1991); (g) W. Pisula, M. Kastler, D. Wasserfallen, T. Pakula and K. Müllen, *J. Am. Chem. Soc.*, **126**, 8074, (2004); (h) M. Kastler, W. Pisula, F. Laquai, A. Kumar, R. J. Davies, S. Balushev, M. –C. Garcia-Guierrez, D. Wasserfallen, H. –J. Butt, C. Riekel, G. Wegner and K. Müllen, *Adv. Mater.*, **18**, 2255, (2006); (i) W. Pisula, Z. Tomovic, B. E. Hamaoui, M. W. Watson, T. Pakula and K. Müllen. *Adv. Funct. Mater.*, **15**, 893, (2005).
33. (a) S. Kumar and S. K. Varshney, *Angew. Chem. Int. Ed.*, **39**, 3140, (2000); (b) S. Kumar, S. K. Varshney and D. Chauhan, *Mol. Cryst. Liq. Cryst.*, **396**, 241, (2003); (c) S. Kumar, D. S. S. Rao and S. K. Prasad, *J. Mater. Chem.* **9**, 2751, (1999).
34. (a) N. L. Lancaster, P. A. Salter, T. Welton and G. B. Young, *J. Org. Chem.* **67**, 8855, (2002); (b) R. A. Mackay and E. J. Poziomek, *J. Am. Chem. Soc.*, **92**, 2432, (1970); (c) S. Alumni, T. D. Giacco, P. D. Maria, A. Fontana, G. Gasbarri and L. Ottavi, *J. Org. Chem.*, **69**, 6121, (2004).
35. C. Destrade, M. C. Mondon and J. Malthete, *J. Phys. Supp. C3*, **40**, 17, (1979).
36. J. Simmerer, B. Glusen, W. Paulus, A. Kettner, P. Schuhmacher, D. Adam, K. H. Ezbach, K. Siemensmeyer, J. H. Wendorf, H. Ringsdorf and D. Haarer, *Adv. Mater.*, **8**, 815, (1996).

37. E. O. Arikainen, N. Boden, R. J. Bushby, J. Clements, B. Movaghar and A. Wood, *J. Mater. Chem.*, **5**, 2161, (1995).
38. C. Destrade, N. H. Tinh, H. Gasparoux, J. Malthete and A. M. Levelut, *Mol. Cryst. Liq. Cryst.*, **71**, 111, (1981).

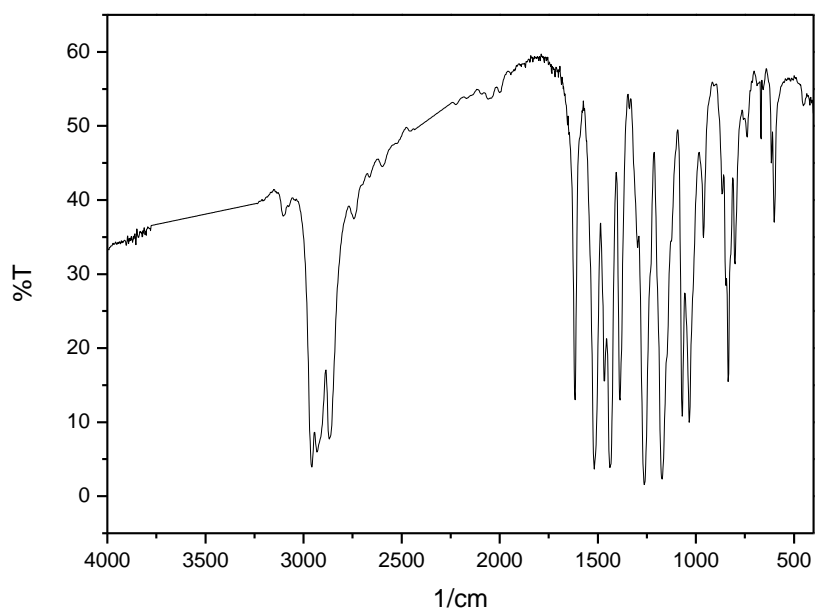


Figure 4. FT-IR spectrum of compound **15a**.

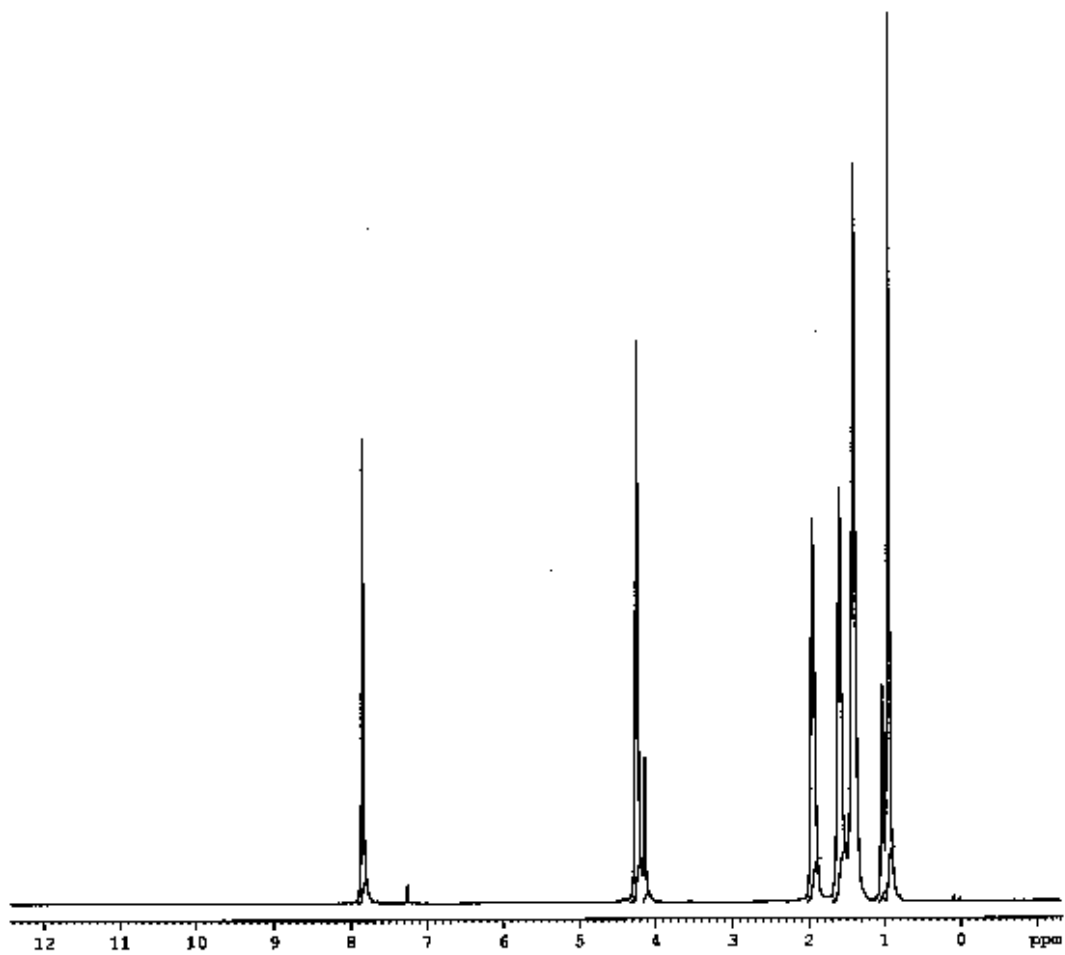


Figure 5. ^1H NMR spectrum of compound **15c**.

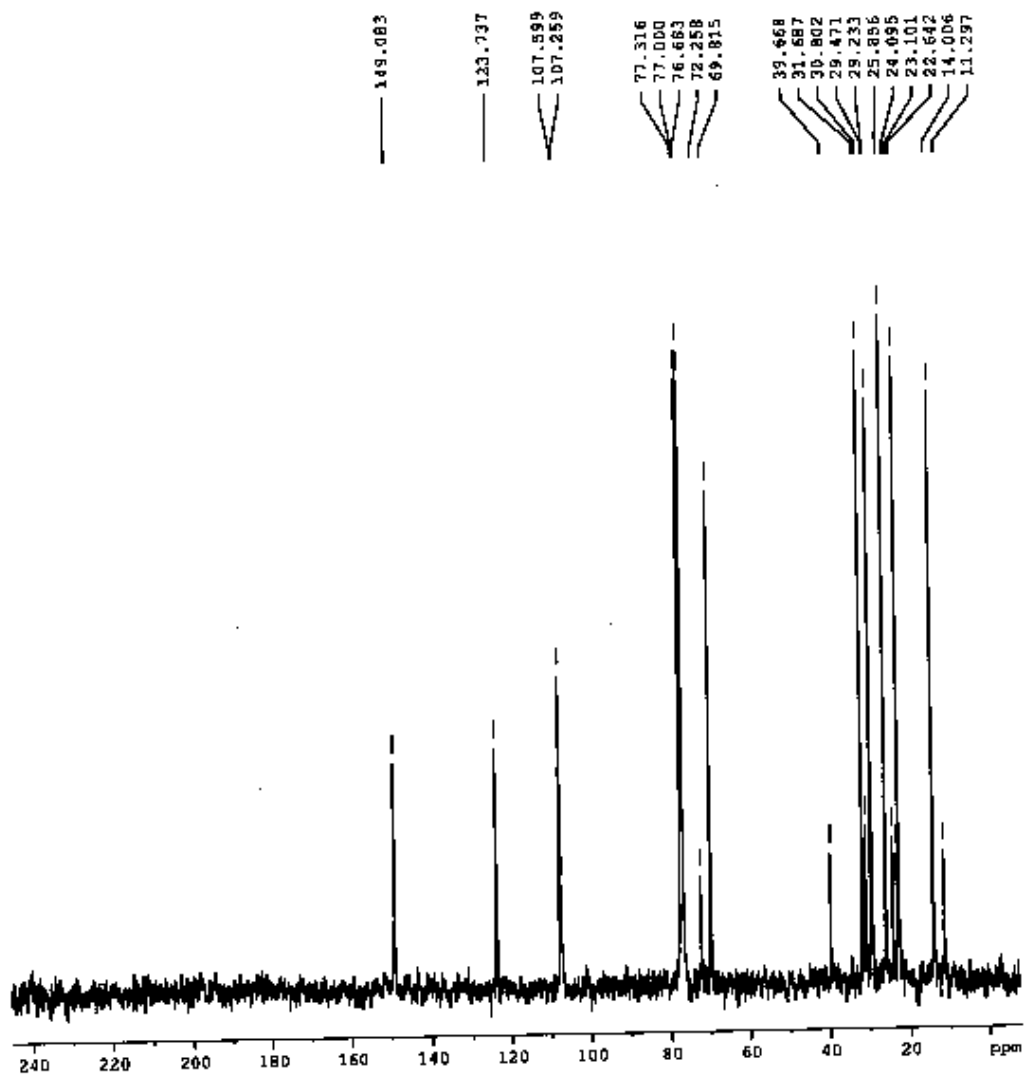


Figure 6. ^{13}C NMR spectrum of compound 15c.

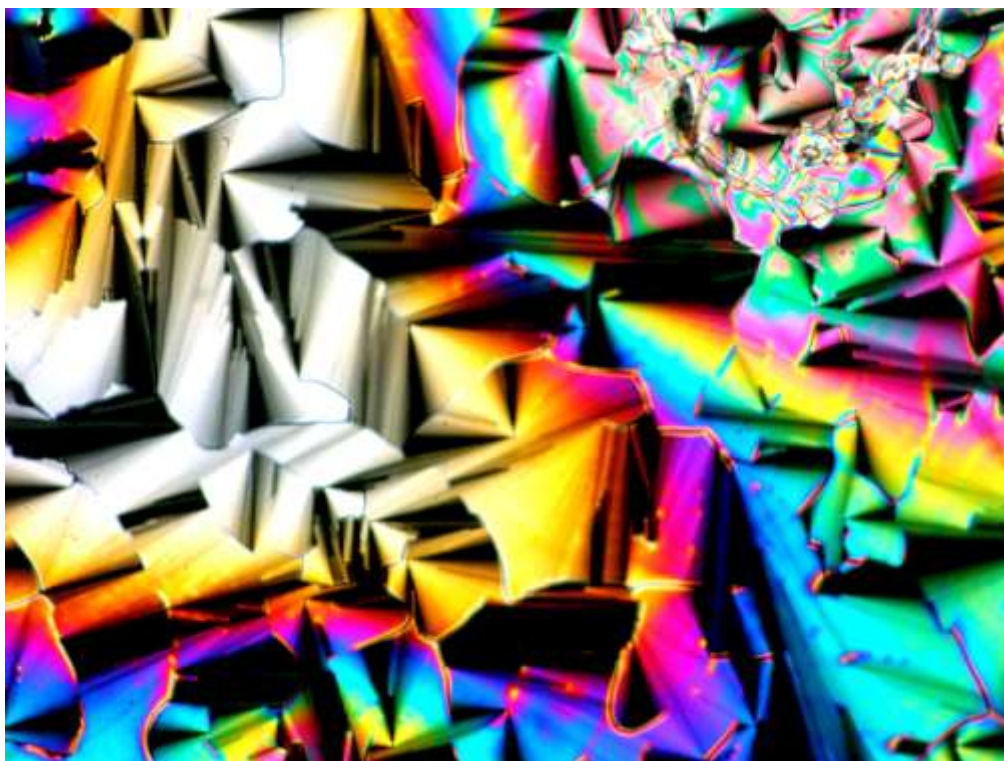


Figure 7. Optical microscopic texture of the compound **16d** under crossed polarizer at 75 °C on cooling from the isotropic liquid (magnification X 200).

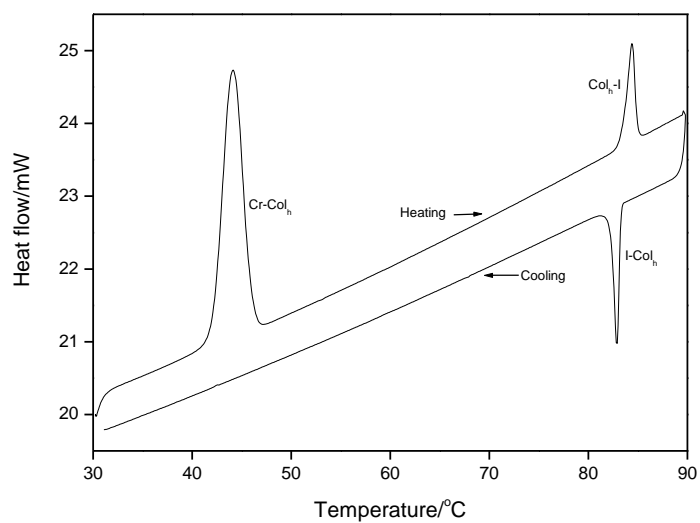
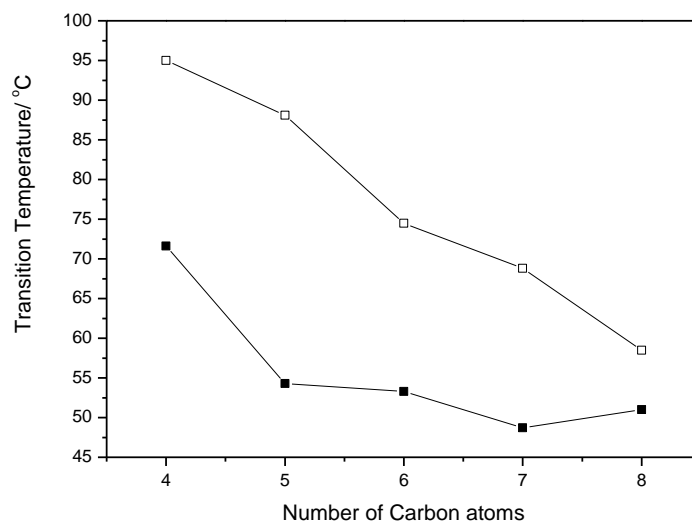
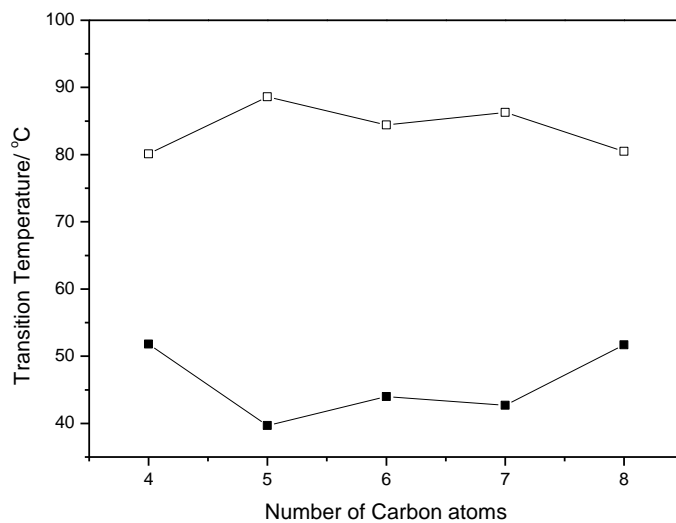


Figure 8. DSC thermogram of the compound **16c** on heating and cooling cycles (scan rate 5 °C/min.)



(a)



(b)

Figure 9. Variation of melting and clearing temperatures with number of carbon atoms in the alkyl chains. (a) Melting (■) and clearing (◻) temperatures of the series-1 . (b) Melting (■) and clearing (◻) temperatures of the series-2.



Figure 10. X-ray diffraction pattern of the compound **15a** in the mesophase.

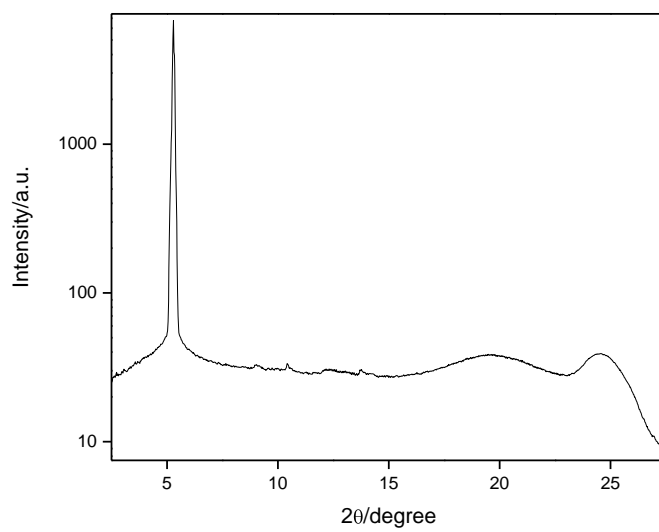


Figure 11. Intensity- 2θ graph derived from the above pattern of the compound **15a**.

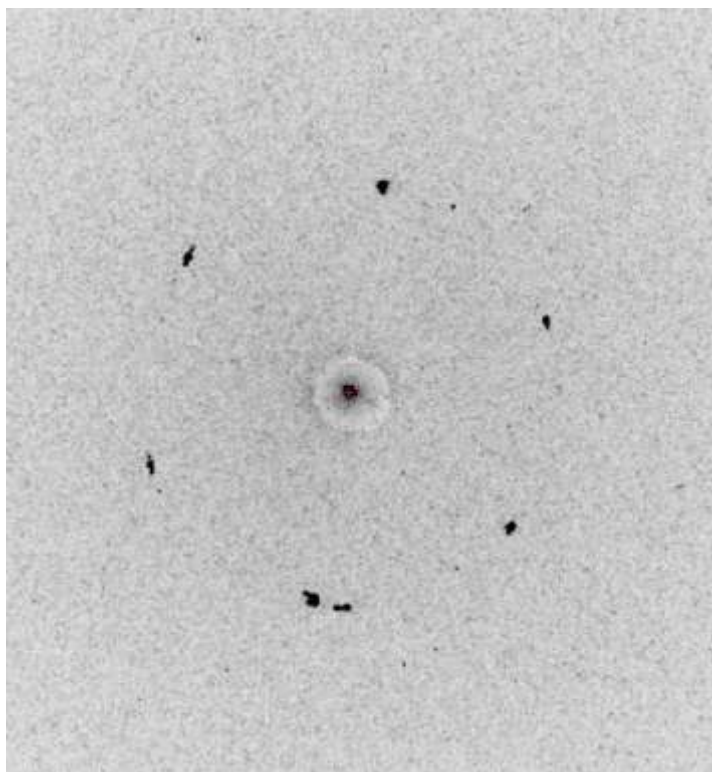


Figure 12. X-ray diffraction pattern of the compound **15c** in the mesophase. Note that no special technique was used for the alignment of the sample.

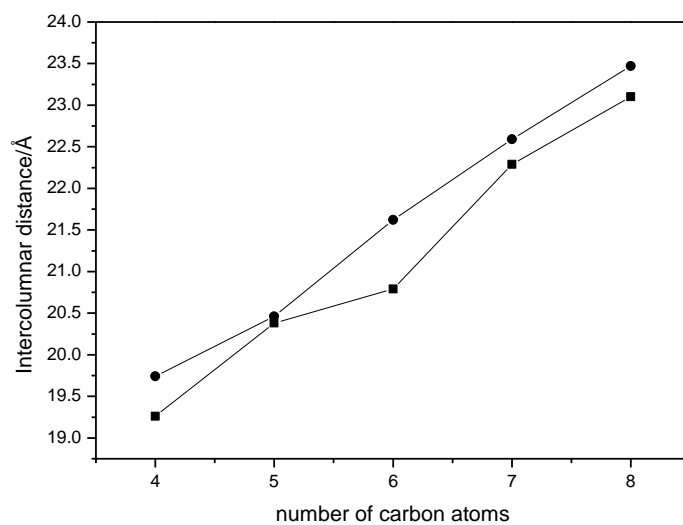


Figure 13. Variation of intercolumnar distances with number of carbon atoms (◼) inter columnar distance of the series-1 (●) inter columnar distance of the series-2.

CHAPTER 3

Microwave-assisted facile synthesis of rufigallol and its novel room-temperature liquid crystalline derivatives

3.1 Introduction

Rufigallol (1,2,3,5,6,7-hexahydroxy-9,10-anthraquinone) is a molecule of both biological and materials science interest [1]. Recently, it has been reported as a novel oxidant drug [2, 3]. A remarkable synergistic antimalarial interaction between rufigallol and the structurally similar compound exifone has been described [4]. It is believed that rufigallol acts in pro-oxidant fashion to produce oxygen radicals inside parasitized erythrocytes [4]. The 1,2,3,5,6,7-hexahydroxy-9,10-anthraquinone (rufigallol) has recently been identified as an active antimalarial compound [2-4]. Rufigallol has also been recognized for its vitamin K activity [5].

Robiquet reported the synthesis of rufigallol in very poor yield by the action of sulphuric acid on gallic acid as early as in 1836 [6]. Its structure was advanced by Klobukowsky [7]. Grimshaw and Haworth reported the purification of rufigallol in 1956 [8]. Since then little further work has appeared and no new efficient method to prepare rufigallol has been reported.

Rufigallol has been found to function as the core fragment for a remarkable family of discotic liquid crystals [1]. Rufigallol derivatives are one of the earliest systems reported to form columnar mesophases. They are interesting materials as these molecules have an elongated core with a two-fold symmetry axis, they are colored, they exhibit an important polymorphism, the core is electron-deficient in nature, they are thermally stable and their chemistry is fairly easy. Billard and co-workers reported the first discotic liquid crystalline hexaesters of rufigallol [9] in 1980 and since then about 100 different discotic liquid crystalline derivatives of this molecule have been prepared and studied for various physical properties [1].

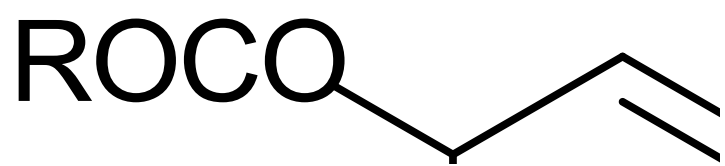
As in traditional inorganic semiconductors, DLCs can function either as p-type or n-type organic semiconductors [10, 11]. The most widely synthesized and studied discotic liquid crystals are electron rich π -conjugated materials and are better hole carriers (p-type semiconductors). Few examples of electron deficient (n-type) DLCs such as bis(dithiolene) nickel complex **1** [12], perylene **2** [13], tricycloquinazoline **3** [14], hexaazatrinaphthylene **4** [15], hexaazatriphenylene **5** [16], triazine derivatives **6** [17], fluorine substituted hexabenzocoronene **7** [18], etc., are reported in the literature which are very less as compared to p-type DLCs. Thus novel n-type liquid crystalline materials are required as electron transporting layers for organic light emitting diodes (OLED) and organic photovoltaic (OPV) solar cells as has already been demonstrated [19].

In the design of discotic liquid crystals the use of branched alkyl chains to modify thermal properties has been well documented [20]. It is realized that the use of branched alkyl chains generally do not change the nature of the mesophase, reduce the transition temperatures, broaden the mesophase range and help in obtaining room-temperature

liquid crystalline materials. This strategy has been applied to alkynylbenzenes **8** [21] hexabenzocoronenes **9** [22], tricycloquinazolines **10** [23], and phthalocyanines **11**, **12** [24,25], to obtain room-temperature liquid crystalline phases, which could be due to steric crowding and stereoheterogeneity introduced by the racemic branched alkyl chains. The various known liquid crystalline derivatives of electron deficient rufigallol are as follows; hexa-n alkanoates **13** [26], octaalkanoates **14** [27], hexa-n-alkoxy rufigallol **15** [28], monohydroxy pentaalkoxy rufigallol **16** [29], mixed-tail hexaalkoxy rufigallol **17-19** [30-32], rufigallol based discotic metallomesogens **20** [33], rufigallol based discotic dimers **21** [34], donor-acceptor dyads **22** [35], donor-acceptor-donor triads **23** [36],

rufigallol based discotic-calamitic hybrids **24** [37], rufigallol based discotic main chain polymers **25** [38] etc.

The various physical property studies of rufigallol derivatives include confinement and hydrostatic pressure effect on phase behavior, DC and AC conductivity studies etc. Covazier and Zhao investigated the confinement effect on the phase behavior of rufigallol- hexa-n- octanoate [39]. Millipore membranes of various pore sizes were taken as the confinement media. The suppression of the monotropic phase inside the membrane of smaller pore size was observed. However, the confinement does not impart any effect on the overall crystallization mechanism. This material was also dispersed in different polymers like polystyrene, poly(methyl methacrylate) and poly(ethyl methacrylate). It is reported that the orientation of discotic molecules can be achieved by



C

the stretching of polymer dispersed discotic liquid crystal films [40]. Maeda *et al.* studied the phase behavior of three hexaalkoxy-rufigallols under hydrostatic pressure using a high pressure differential thermal analyzer [41]. Under pressure, on one hand, induction of Col_r phase in hexaoctyloxy-rufigallol was observed. On the other hand, the stable Col_r phase of hexahexyloxy-rufigallol has a decreased temperature range with increasing pressure and then the Col_r phase disappears under higher pressure. The temperature dependent dielectric spectroscopy of four homologues hexaalkoxy rufigallols in the frequency range of 10 Hz to 10 MHz has recently been carried out by Gupta *et al.* [42]. The dielectric anisotropy has been found to be positive throughout the entire range of the Col_h phase for all of the four compounds of this series. No relaxation phenomena are found in the frequency range of measurement i.e. 10 Hz to 10 MHz. They have also measured the DC conductivity of these compounds which was found in the range of 10^{-10} - 10^{-11} Sm⁻¹. Chandrasekhar *et al.* measured AC conductivity of hexapentyloxy-rufigallol doped with a small amount of an electron donor anthracene [43]. The conductivity was found to be nearly seven orders of magnitude higher in the columnar phase relative to that in the isotropic phase, as well as that in the columnar phase in the undoped state. Thermoelectric power studies confirmed the nature of the charge carrier as electrons in anthracene-doped hexapentyloxy-rufigallol [43].

While a large number of discotic liquid crystals have been derived from rufigallol, most of them display mesophase at higher temperatures. For any device application, the stability of the mesophase at ambient temperature is required and the mesophase should be stable over a wide temperature range and should possess a single mesophase structure. Efforts have been made to prepare a variety of room-temperature electron-rich DLCs,

however, room-temperature electron-deficient DLCs are rare. Therefore, it is of great practical interest to prepare rufigallol-based room-temperature electron-deficient DLCs.

As described in previous chapter, microwave-assisted high-speed chemical synthesis has attracted a considerable amount of attention in the past decade. Almost all types of organic reactions have been performed using the efficiency of microwave-flash heating. This is not only due to the fact that reactions proceed significantly faster and more selective than under conventional thermal conditions but also because of the operational simplicity, high yield of products and cleaner reactions with easier work-up [44]. Though a large variety of organic molecules have been prepared using microwave dielectric heating, this technique has not been much explored for the synthesis of liquid crystalline materials.

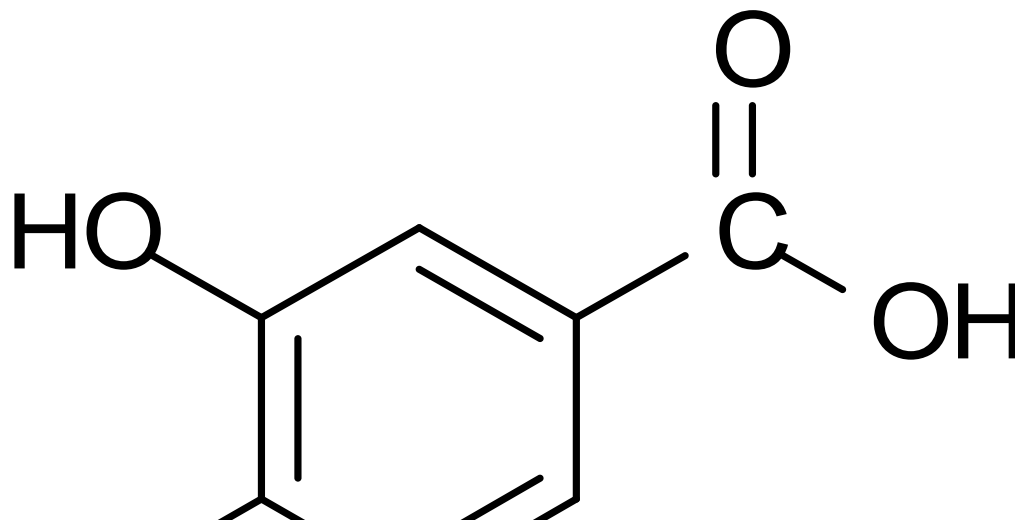
Here, in this chapter, we describe the self-condensation of the gallic acid in the presence of sulphuric acid which can be achieved in high yield in about one minute by using microwave heating. The resultant rufigallol was converted to novel unsymmetrical room-temperature discotic liquid crystalline derivatives by substituting with normal and branched-alkyl chains [45, 46].

3.2 Results and discussion

3.2.1 Microwave assisted synthesis of rufigallol

The synthetic scheme of rufigallol and its novel room-temperature derivatives are shown in Scheme 1. Rufigallol **27** is prepared by the self-condensation of gallic acid **26** monohydrate in sulfuric acid under microwave irradiation as shown in Scheme 1. The

condensation was carried out using an unmodified domestic microwave oven (LG, MS-192W).



Scheme 1. Synthesis of rufigallol and its novel liquid crystalline derivatives. *Reagents and conditions:* (i) H_2SO_4 , MW, 90 sec., 84%; (ii) RBr , DMSO, NaOH; (iii) $\text{R}'\text{Br}$, Cs_2CO_3 , NMP, MW, 3 min.; (iv) $\text{R}'\text{Br}$, NaOH, DMSO; (v) RBr , Cs_2CO_3 , NMP, MW, 3-4 min.

Irradiation (360W) of gallic acid monohydrate (2.0 g) in 6.0 mL of concentrated H_2SO_4 for 90 sec. yielded 1.36 g (84%) of crude rufigallol. The product was isolated simply by adding the mixture to ice-water followed by filtration of the solid product. The various yields of rufigallol against 2.0 gm of gallic acid monohydrate are shown in Table 1.

Table 1 The various yields of rufigallol **27** against 2.0 gm of gallic acid monohydrate **26**.

Entry	Acid (mL)	Time (sec.)	HHA 27 (gm)	Yield (%)
1	4	15x2	0.4	25
2	4	15x4	0.88	54
3	4	15x6	1.27	78
4	5	15x3	1.2	74
5	5	15x4	1.24	76
6	5	15x5	1.28	79
7	5	15x6	1.30	80
8	6	15x4	1.28	79
9	6	15x5	1.35	83
10	6	15x6	1.37	84

This crude product was converted to its hexaacetate (60%) by treatment with acetic anhydride. Hydrolysis of the analytically pure hexaacetate furnished pure rufigallol in an overall yield of about 50%.

3.2.2 Synthesis of hexaethers of rufigallol and their characterization

In order to prepare novel room-temperature rufigallol discotics, we initially replaced all six peripheral n-alkyl chains with 3,7-dimethyloctyl chains **32**. The reaction of rufigallol with excess of 1-bromo-3, 7-dimethyloctane in the presence of cesium carbonate under microwave heating produced the hexa branched alkyl chain substituted derivative **32**

within 3 min. However, it was found to be non-liquid crystalline viscous oil. The replacement of two or four n-alkyl chains with branched alkyl chains under similar reaction conditions afforded novel unsymmetrical room-temperature liquid crystalline rufigallol derivatives **29** and **31** (Scheme 1). The synthesis of the unsymmetrical hexaethers was achieved by a two-step alkylation process. The unequal reactivity of the six phenolic groups, two of which are less reactive by virtue of being intra molecularly hydrogen bonded to the adjacent quinone carbonyls, was exploited. Etherification of rufigallol **27** under mild conditions produced 1,5-dihydroxy-2,3,6,7-tetraalkoxy-9,10-anthraquinone (**28** and **30**) without alkylating the hydrogen bonded C-1 and C-5 positions [30]. These tetraalkoxy derivatives were further alkylated with the help of microwave dielectric heating as shown in the Scheme 1 under mild basic conditions to give the unsymmetrical hexaethers in very good yield within 3-4 minutes which is simple, efficient, rapid and economic. Under classical reaction conditions no product could be obtained with in this much time. The optimized yield under microwave dielectric heating condition is 90% in 4 minutes whereas under classical thermal heating conditions the yield is 65% after 20 hours of reaction at 100 °C with identical reaction mixtures.

The chemical structures and purity of all the compounds have been characterized by FT-IR, ¹H NMR, ¹³C NMR and elemental analysis etc. The IR spectra of recrystallised tetraethers **28** and **30** (Figure 1) showed an absorption peak at 1616 cm⁻¹, characteristic of an intramolecularly hydrogen-bonded anthraquinone carbonyl moiety in addition to other aromatic, methylene and methyl absorption peaks. The ¹H NMR of others **28** and the branched chain tetraether **30** (Figure 2) showed a singlet resonance at δ 12.7 ppm integrating for two protons, characteristic of an intramolecularly hydrogen-bonded

phenoxy hydrogen and another singlet resonance at δ 7.4 ppm corresponding to the two aromatic protons in addition to the phoxymethylene, methylene and methyl resonances. The tetraether by virtue of its C_2 symmetry, exhibits only a single aromatic proton signal and single phenolic proton signal. The ^{13}C NMR spectrum of branched chain tetraether **30** (Figure 3) exhibited an intramolecularly hydrogen-bonded quinone-carbonyl-carbon resonance at δ 186 ppm, six aromatic carbon resonances at *ca.* 158, 157, 141, 129, 112, 105 ppm, aryloxy methylene-carbon at *ca.* 72 and 68 ppm in addition to the methylene and methyl-carbon resonances. These spectral features (IR and NMR) and the actual combustion analysis data obtained for the tetraethers confirm the structure as well as purity of the tetraethers unambiguously.

The IR spectra (Figure 4 and 5) of the unsymmetrical hexaethers **29** and **31** showed an absorption peak at 1666 cm^{-1} , characteristic of a non-hydrogen-bonded anthraquinone-carbonyl moiety. The 1H NMR spectra of these ethers, by virtue of their symmetry, exhibited a singlet at δ 7.6 ppm integrating for two protons corresponding to the aromatic protons in addition to the phoxymethylene, methylene and methyl proton resonances (Figure 6 and 7). It is important to note that the difference in the chemical shift between an aromatic proton present in an aromatic ring bearing a hydrogen-bonded phenolic group (tetraethers δ 7.4) and the aromatic proton present in a corresponding alkylated product (hexaethers δ 7.6). 1H NMR spectra of all the hexaethers synthesized were carefully analysed and found that there was no resonance appeared at δ 12.7 ppm and the only aromatic resonance found was at δ 7.6 ppm. Finally, all the hexaethers synthesized were characterized by ^{13}C NMR spectra in order to confirm the structure and purity of these homologues. The ^{13}C NMR spectra of these ethers (Figure 8 and 9)

showed six aromatic-carbon resonances at *ca.* 157, 154, 147, 133, 120, 107 ppm, only one quinone-carbonyl-carbon resonance at δ 181 ppm and three aryloxymethylene-carbon resonance at *ca.* 74, 73, 69 ppm in addition to methylene and methyl-carbon resonances. These spectral features and the actual combustion analysis data obtained for these hexaethers confirm the structure as well as purity of each and every hexaether synthesized here unambiguously.

3.2.3 Mesophase behavior of the novel rufigallol derivatives

The phase transition temperatures of all the compounds were initially established from the polarizing optical microscopy (POM) and then measured accurately by differential scanning calorimetry (DSC) along with their associated enthalpy changes which are listed in Table 2. These materials under crossed polarizers display characteristic defect textures for the columnar hexagonal mesophase upon cooling from isotropic melt, examples of which are shown in Figure 10, 11 and 12. The solvent precipitated samples which exhibit liquid crystalline behavior at room-temperature do not exhibit any characteristic texture at room-temperature itself but when cooled from isotropic liquid they show characteristic broken fan and mosaic textures of discotic columnar phases. However, these compounds possess sufficient mobility at room temperature so that they can be easily disturbed by mechanical shearing (samples were sheared by pressing the cover slip of the sample slides under the microscope). As compared to the compounds of *Series I* the compounds of *Series II* possess more fluidity at room temperature as has been observed under polarizing optical microscope. Surprisingly the branched chain substituted tetraalkoxy-dihydroxy compound **30** exhibits liquid crystalline behavior at room temperature contrary to its straight chain analogous **28** which do not show any liquid crystalline property

except compound **28a** which exhibits a metastable monotropic mesophase [31], this could be because the branched chains fill the necessary space around the core to induce mesomorphism (space filling effect) in compound **30**.

Table 2. Phase transition temperatures (peak, °C) and associated enthalpy changes (kJ/mol, in parentheses) of novel rufigallol based discotics, Cr = Crystal, Col_h = Hexagonal columnar phase, M = unidentified phase, I = Isotropic phase.

Compound (n)	Heating	Cooling
29a (4)	Cr 54.7 (18.4) Col _h 65.8 (7.6) I	I 63.9 (7.7) Col _h 12.4 (5.0) M
29b (5)	Col _h 75.2 (9.3) I	I 73.2 (9.1) Col _h
29c (6)	Col _h 77.7 (9.8) I	I 76.0 (9.9) Col _h
29d (7)	Col _h 78.7 (9.7) I	I 76.4 (9.6) Col _h
29e (8)	Col _h 72.3 (9.2) I	I 70.4 (9.2) Col _h
29f (9)	Col _h 67.4 (8.0) I	I 65.4 (8.0) Col _h
29g (10)	Cr 37.6 (14.3) Col _h 61.0 (8.0) I	I 59.0 (7.9) Col _h
29h (11)	Cr 42.0 (56.5) Col _h 54.7 (5.7) I	I 51.7 (5.7) Col _h -28 (9.8) M
29i (12)	Cr 39.8 (47.8) I	I 30.5 (2.0) Col _h 9.0 (56.6) Cr
30	Col _h 115.7 (5.5) I	I 114.1 (5.4) Col _h
31a (5)	Cr 52.6 (34.9) I	I 33.1 (5.8) Col _h
31b (6)	Cr 57.2 (34.5) I	I 41.3 (6.3) Col _h
31c (7)	Col _h 52.6 (8.3) I	I 50.7 (8.3) Col _h
31d (8)	Col _h 56.8 (8.9) I	I 54.6 (8.9) Col _h
31e (9)	Col _h 59.7 (9.9) I	I 57.8 (9.9) Col _h
31f (10)	Col _h 59.6 (10.1) I	I 57.6 (10.0) Col _h
31g (11)	Col _h 56.1 (9.4) I	I 53.9 (9.2) Col _h
31h (12)	Col _h 52.7 (9.1) I	I 50.4 (8.5) Col _h
31i (14)	Col _h 39.2 (6.4) I	I 36.1 (6.7) Col _h

Compound **30** also displays large homeotropic domains when cooled from the isotropic state as shown in Figure 11. As typical examples, the DSC thermograms of compound **29**, **30**, and **31** are shown in Figure 13, 14 and 15. The compound **30** shows only one transition Col-I at 115.7 °C while heating and I-Col transition at 114 °C while cooling, which is the widest mesophase range among all the rufigallol derivatives known to date [1]. In *Series I*, the compound **29a** shows a crystalline phase at room temperature and on heating it melts to columnar liquid crystalline phase at 54.7 °C which clears to an isotropic liquid at 65.8 °C, upon cooling it shows two transitions, I- Col transition at 63.9 °C and another transition at 12.4 °C. The second transition is suspected to be a transition to another mesophase because of the transition enthalpy value i.e. 5 kJ/mol which is of similar magnitude as that of columnar phase transitions. Compounds **29b-29f** display columnar mesophase behavior at room temperature as is evident from a single thermal transition in their DSC thermograms while heating and cooling, which is assigned to columnar hexagonal to isotropic and isotropic to columnar hexagonal phase transitions respectively. These compounds do not crystallize even after cooling to -30 °C. The compounds **29g-i** are crystalline at room temperature, **29g** upon heating passes to columnar phase at 37.6 °C and at 61 °C it clears to isotropic phase while cooling the mesophase transition is at 59 °C and the phase is stable down to room temperature and the sample does not crystallize. Compound **29h** exhibits similar behavior as that of **29a** whereas the compound **29i** shows a monotropic columnar hexagonal phase below 31 °C and crystallizes at 9 °C. In *Series II*, except compounds **31a** and **31b** all the other compounds display columnar mesophase at room temperature and none of them show

any sign of crystallization upon cooling to $-30\text{ }^{\circ}\text{C}$ as shown in Table 2. Compounds **31a** and **31b** are crystalline at room temperature and exhibit monotropic columnar hexagonal phases while cooling from the isotropic state similar to the compound **29i** but they do not crystallize immediately upon cooling to low temperature. So the compounds **29b-29f**, **30** and **31c-i** are truly room-temperature liquid crystals exhibiting only one columnar phase over a wide range of temperature. These compounds will be suitable electron transport candidates while considering the potential application of discotic liquid crystals for light emitting diodes and photovoltaic solar cells. The variation of transition temperatures ($T_{\text{Col-I}}$) and transition enthalpies ($\Delta H_{\text{Col-I}}$) with the number of carbon atoms in the normal alkoxy chains for the compounds of both the series are shown in the Figure 16 and Figure 17 respectively. Both the transitional properties increase marginally as the number of carbon atoms increase and attain the maximum value about the middle of the series and then the values fall as the number of carbon atoms are further increased in the homologues series. The extent of order present in the mesophase is often characterized by the isotropization enthalpy and isotropization entropy. The branched alkyl chains exert two contrasting effects, one space-filling effect and the other is steric effect. So depending on the balance of these competing factors the mesophase order may increase or decrease. Thus within a series, the mesophase order may vary in a non-linear fashion depending on the relative contributions of these competing factors for each member of the series. In addition, there is the rigidity of the n-alkyl chains which also contributes towards the order of the compounds so also symmetry in terms of the alkyl chain lengths whereas stereoheterogeneity of the branched chains contribute towards the mesophase disorder. So as we move towards longer chain lengths the molecules approach towards

symmetry and then again deviate from symmetry in terms of alkyl chain lengths. Accordingly the order in the mesophase marginally increases, attains the maximum value and then decreases. It should be noted that the flexibility of the longer alkyl chains also contributes for the mesophase disorder in the higher members of the homologues series. In *Series II* since the molecules possess four branched alkyl chains the steric effect exerted by the branch points might dominate over the space-filling effect of the branch points and this could be the reason for lower clearing temperatures and more fluidity of these compounds as compared to the members of *Series I*. The competition between steric effect and symmetric approach in the lower members of the *Series II* is just in favour of the later so with increase in the chain length the stability of the mesophase increases, attains the maximum value and then decreases in the higher homologues where both steric effect of the branched alkyl chains and bending of the longer alkyl chains contribute for the mesophase disorderness.

3.2.4 X-ray diffraction study

In order to reveal the mesophase structure and hence the supramolecular organization of these compounds, X-ray diffraction experiments were carried out using unoriented samples taken in glass capillaries at room-temperature. The X-ray diffraction patterns of the mesophase exhibited by all the samples belonging to both the series is supportive of a discotic hexagonal columnar arrangement. As typical examples, the X-ray diffraction pattern of compound **29e**, **30** and **31d** and the intensity vs theta (θ) graphs derived from these patterns are shown in the Figure 18-20. Four sharp rings, one strong (d_{10}) and three weak reflections are seen in the pattern as well as in the plot in the small angle region. Qualitatively, all the compounds show similar X-ray diffraction patterns. The d -spacings

of these four rings are in the ratio $1: 1/\sqrt{3}: 1/\sqrt{4}: 1/\sqrt{7}$ and they can be indexed as 10, 11, 20, 21 reflections of a two-dimensional hexagonal lattice. A fairly narrow diffraction ring corresponding to the spacing of 3.7 Å which corresponds to interdisc (intracolumnar = d_{01}) spacing within a column and a broad diffuse reflection at ~ 4.6 Å suggesting a liquid like structure of the alkyl chains are also seen in the wide angle region. So the discotic molecules stack one on top of the other to form the columns and these columns in turn arrange themselves in two dimensional hexagonal fashions for both the series of compounds. In the columns the insulating alkyl chains surround the conducting aromatic cores because of nano phase-segregation. The intercolumnar distances calculated using the relation $d_{10}/\cos 30^\circ$ for all the compounds are listed in Table 3. In both the series it is evident that as ‘n’ increases the diameter of the cylindrical columns formed by the discotic molecules also increases as shown in the Figure 21. The intercolumnar distances varies from 20-26 Å where as the intracolumnar distance is around 3.7 Å which is usually observed for discotic columnar mesophases. The compound **30** also exhibits the same feature as described above but the intracolumnar core-core separation in this material is 3.43 Å and the peak is narrow and relatively strong at room temperature suggesting high intracolumnar order in this particular compound. This high intracolumnar order could be due to the added intermolecular interactions by two additional hydrogen bonded rings in the molecular core of compound **30**. The position of the peak d_{01} (d_{intra}) is temperature dependent such that d_{intra} increases on increasing the temperature. However, the core-core distance in compound **30** is 3.43 Å at 25 °C, whereas close to isotropic temperature the core-core distance is 3.49 Å (105 °C) indicating relatively strong intracolumnar order in this compound. For other compounds which were investigated at higher temperatures it

was found that the d_{01} peaks become broader with increasing temperature, indicating a decrease in the degree of ordering along the columns.

Table 3. d -spacings and inter and intracolumnar distances for the mesophase of *Series I* and *Series II*, deduced from X-ray measurements at 25 °C.

Compound (n)	d -spacing/Å	Intercolumn dist./Å	Interdisc dist./Å
29a (4)	17.5	20.2	3.65
29b (5)	18.2	21.0	3.69
29c (6)	19.0	21.9	3.64
29d (7)	19.7	22.7	3.66
29e (8)	20.3	23.4	3.67
29f (9)	20.9	24.0	3.67
29g (10)	21.3	24.6	3.69
29h (11)	22.0	25.3	3.68
29i (12)	22.6	26.1	3.69
30	19.4	22.4	3.43
31a (5)	19.6	22.6	3.68
31b (6)	19.9	22.9	3.69
31c (7)	20.1	23.2	3.69
31d (8)	20.5	23.7	3.69
31e (9)	21.0	24.2	3.69
31f (10)	21.3	24.6	3.69
31g (11)	21.5	24.8	-
31h (12)	21.8	25.1	-
31i (14)	22.3	25.7	-

This observation may be interpreted on the basis that the average length of the order domains along the column decreases as temperature is increased. Further more, increasing n , we note that the width of the (01) peak increases even at room temperature, suggesting the decrease in intracolumnar order with increasing the chain length around the discotic core. As can be seen from the Figure 21 the intercolumnar distances for both the series increase, as anticipated, with increase in the number of carbon atoms in the alkyl chains. From the Figure 21 it is very clear that the lower members of the *Series I* possess less value of intercolumnar distances when compared with the corresponding members of the *Series II* but the trend reverses as the number of carbon atoms in the alkyl chains increases. This could be because of the fact that in *Series I* the molecules contain four shorter n-alkyl chains and two longer alkyl (3,7-dimethyloctyl) chains so the effective diameter of the molecules are decided by the shorter chains whereas in *Series II* the molecules contain four longer alkyl (3,7-dimethyloctyl) chains and two shorter n-alkyl chains and hence the effective molecular diameter is decided by the longer chains which explains the difference of intercolumnar distances in the lower members. The story reverses in the higher members. It is very clear from the Figure 21 that *Series I* and *Series II* show different slopes. The reason for the difference in slopes may be due to the different positions of the n-alkyl chains in the molecules. For *Series I*, n-alkyls are on the side and the branched chains are on the lateral but the situation is reversed for *Series II*. The effective dimensions of both the series are mainly determined by the side chains rather than lateral chains which explain the difference in slopes. The bending of the longer alkyl chains, in part, will lead to a decrease of the core-core overlap between discs in the columns. Therefore the π - π interactions will be diminished and hence the d_{01} peak

broadens with increase in the number of carbon atoms in the alkyl chains. For compounds **31g-31i** this peak is not discernable even after longer exposure time, this could be because of the combined effect of the bending of the longer alkyl chains and the steric effect of the branched alkyl chains for the intracolumnar disorder.

3.3 Conclusions

In conclusion, we have developed an efficient, simple, rapid and economic methodology for the synthesis of rufigallol by using microwave dielectric heating. We have synthesized two novel series of rufigallol based room-temperature discotic liquid crystals with the help of microwave dielectric heating within few minutes under mild basic conditions in very good yield. The columnar mesophase behavior of all the compounds has been investigated by polarizing optical microscopy and differential scanning calorimetry. The mesophase stability decreases as the length of the alkyl chain increases in both the series. All the compounds exhibit columnar hexagonal mesophase over a broad range of temperature. The columnar hexagonal structure of the mesophase was established by X-ray diffraction studies. As anticipated, the intercolumnar distance increases with increase in the alkyl chain length in both the series. Compound **30** being a difunctional molecule can be used to prepare various discotic oligomers and polymers. These electron-deficient room-temperature discotic liquid crystals may find applications in light emitting diodes, photovoltaic solar cells, thin film transistors, etc.

3.4 Experimental

3.4.1 General information

General information has been described in chapter 2.

3.4.2 Synthesis of rufigallol and its liquid crystalline derivatives

Synthesis of rufigallol 27, 1,2,3,5,6,7-hexahydroxyanthracene-9,10-dione: Gallic acid **26** (2.0 g) and sulfuric acid (6 mL) were taken in a glass vial, which was loosely sealed with a rubber septum and then irradiated in a microwave oven for 15 sec. The vial was removed from the oven and left to stand for about 1 min. This process was repeated six times and then the reaction mixture was poured into ice-water. The resultant solid was collected by filtration and washed repeatedly with water until neutral and then dried to afford rufigallol **27** 1.37g (84%).

Tetraalkoxy rufigallols **28** and **30** were prepared following the literature procedure [30]. To a stirred solution of NaOH (4 eq.) in dry DMSO (50 ml) added crude rufigallol (5 g, 0.164 mmol) and appropriate (normal or branched) alkylbromide (4.4 eq.), and the mixture was heated to 70 °C and held at the same temperature under N₂ for 18h. The reaction mixture was cooled, diluted with aq. HCl and extracted with chloroform (80 ml X 5). The combined chloroform extracts were washed with water and dried over anhydrous Na₂SO₄. Product was crystallized from EtOH:CHCl₃ (4:6). Yield 45 % (yellow solid).

Synthesis of 29c: In a vial containing tetrahexyloxy-rufigallol **28c** (0.1g, 0.156 mmol), cesium carbonate (0.2g, 0.62 mmol) and 3,7-dimethyl-1-bromooctane (0.14g, 0.62 mmol) was added NMP (0.5 mL), the vial was loosely sealed with a rubber septum and then irradiated in a microwave oven for 30s. The vial was removed from the oven and left to stand for about 1 min, this process was repeated six times. The reaction mixture was poured into cold water and the product was extracted with dichloromethane. The organic

extract was dried, concentrated and the product was purified by column chromatography over silica gel to afford 88% of the product. Other members of the series were synthesized with the same procedure.

Synthesis of 31: In a vial containing **30** (0.1 mmol), cesium carbonate (0.6 mmol), and n-alkyl bromide (0.6 mmol) was added NMP (0.5 mL). The vial was loosely sealed with a rubber septum and then irradiated in a microwave oven for 30s. The vial was removed from the oven and left to stand for about 1 minute and again irradiated for 30s. This process was repeated for 6 to 8 times till the reaction completes (TLC monitoring). The reaction mixture was poured into cold water and the product was extracted with dichloromethane. The organic extract was dried, concentrated and the product was purified by column chromatography over neutral alumina. Finally the product was crystallized from chloroform by adding excess of ethanol to afford 80-90% of **31**.

29e: 1,5-bis(3,7-dimethyloctyloxy)-2,3,6,7-tetrakis(octyloxy)anthracene-9,10-dione.

¹H NMR (400 MHz; CDCl₃; Me₄Si) δ_H 7.6 (s, 2H, Ar-H), 4.1 (m, 12H, ArOCH₂), 1.1-2.1 (m, 68H, aliphatic CH and CH₂), 0.96 (d, 6H, *J* = 6.2 Hz, CH₃), 0.92 (t, 12H, *J* = 6.7 Hz, CH₃), 0.86 (d, 12H, *J* = 6.6 Hz, CH₃). Derivatives **29a-29i** showed similar spectra except for different numbers of aliphatic protons.

29e, ¹³C NMR (100 MHz; CDCl₃; Me₄Si) δ_C 181.1, 157.4, 153.9, 146.9, 132.6, 120.3, 106.9, 74.0, 73.1, 69.1, 39.3, 37.4, 31.7, 30.3, 29.8, 29.4, 29.2, 29.0, 27.9, 26.0, 24.6, 22.6, 19.6, 14.0. Derivatives **29a-29i** showed similar spectra.

29e, FT-IR ν_{max}(KBr)/cm⁻¹ 2924, 2852, 1666, 1572, 1464, 1377, 1319, 1265, 1130, 1096, 1040, 978, 876, 721; All other derivatives give similar spectra.

30: 2,3,6,7-tetrakis(3,7-dimethyloctyloxy)-1,5-dihydroxyanthracene-9,10-dione.

¹H NMR (400 MHz; CDCl₃; Me₄Si) δ_H 12.76 (s, 2H, Ar-OH), 7.4 (s, 2H, Ar-H), 4.23-4.13 (m, 8H, ArOCH₂), 1.9-1.1 (m, 40H, aliphatic CH₂ and -CH), 0.98 (d, 6H, *J* = 6.3 Hz, -CH-CH₃), 0.95 (d, 6H, *J* = 6.6 Hz, -CH-CH₃), 0.88 (d, 12H, *J* = 4.5 Hz, -CH-(CH₃)₂), 0.85 (d, 12H, *J* = 4.5 Hz, -CH-(CH₃)₂).

¹³C NMR (100 MHz; CDCl₃; Me₄Si) δ_C 186.4, 158.1, 157.3, 141.2, 128.9, 111.8, 104.8, 72.1, 67.8, 39.3, 37.3, 36.1, 31.1, 29.8, 29.7, 28.8, 28.0, 24.7, 22.6, 19.6.

FT-IR ν_{max}(KBr)/cm⁻¹ 2922, 2854, 1616, 1569, 1506, 1456, 1427, 1365, 1315, 1280, 1226, 1138, 1095, 1045, 950, 864, 802, 723.

31d: 2,3,6,7-tetrakis(3,7-dimethyloctyloxy)-1,5-bis(octyloxy)anthracene-9,10-dione.

¹H NMR (400 MHz; CDCl₃; Me₄Si) δ_H 7.6 (s, 2H, Ar-H), 4.0-4.2 (m, 12H, ArOCH₂), 1.1-1.9 (m, 64H, aliphatic CH and CH₂), 0.98 (d, 6H, *J* = 6.2 Hz, CH₃), 0.94 (d, 6H, *J* = 6.5 Hz, CH₃), 0.86 (m, 30H, CH₃). Derivatives **31a-31i** showed similar spectra except for different numbers of aliphatic protons.

31d, ¹³C NMR (100 MHz; CDCl₃; Me₄Si) δ_C 181.2, 157.5, 153.9, 147.0, 132.7, 120.4, 117.7, 107.0, 74.7, 72.4, 67.5, 39.2, 37.3, 36.1, 31.8, 30.3, 29.7, 29.5, 29.3, 27.9, 26.0, 24.7, 22.6, 19.6, 14.0. Derivatives **31a-31i** showed similar spectra.

31d, FT-IR ν_{max}(KBr)/cm⁻¹ 2924, 2852, 1666, 1572, 1508, 1466, 1377, 1319, 1267, 1130, 1094, 1045, 954, 874, 721. Derivatives **31a-31i** showed similar spectra.

Elemental analysis. **29a**, Found: C, 74.69; H, 9.60. C₅₀H₈₀O₈ requires C, 74.22; H, 9.97%; **29b**, Found: C, 75.44; H, 10.54. C₅₄H₈₈O₈ requires C, 74.96; H, 10.25%; **29c**, Found: C, 75.87; H, 10.26. C₅₈H₉₆O₈ requires C, 75.61; H, 10.50%; **29d**, Found, C, 75.92; H, 11.0. C₆₂H₁₀₄O₈ requires C, 76.18; H, 10.72%; **29e**, Found, C, 76.47; H, 11.25.

$C_{66}H_{112}O_8$ requires C, 76.69; H, 10.92%: **29f**, Found, C, 77.29; H, 11.09. $C_{70}H_{120}O_8$ requires C, 77.15; H, 11.10%: **29g**, Found: C, 77.48; H, 10.95. $C_{74}H_{128}O_8$ requires C, 77.57; H, 11.26%: **29h**, Found, C, 77.65; H, 11.25. $C_{78}H_{136}O_8$ requires C, 77.95; H, 11.41%: **29i**, Found, C, 78.05; H, 11.36. $C_{82}H_{144}O_8$ requires C, 78.29; H, 11.54%: **30**, Found: C, 75.0; H, 10.71. $C_{54}H_{88}O_8$ requires C, 74.96; H, 10.25%: **31a**, Found: C, 76.74; H, 11.26. $C_{64}H_{108}O_8$ requires C, 76.45; H 10.83%: **31b**, Found: C, 76.81; H, 11.64. $C_{66}H_{112}O_8$ requires C, 76.69; H, 10.92%: **31c**, Found: C, 76.84; H, 11.27. $C_{68}H_{116}O_8$ requires C, 76.93; H, 11.01%: **31d**, Found: C, 77.30; H, 10.86. $C_{70}H_{120}O_8$ requires C, 77.15; H, 11.1%: **31e**, Found: C, 77.30; H, 11.53. $C_{72}H_{124}O_8$ requires C, 77.37; H, 11.18%: **31f**, Found: C, 77.85; H, 11.80, $C_{74}H_{128}O_8$ requires C, 77.57; H, 11.26%: **31g**, Found: C, 77.60; H, 11.81. $C_{76}H_{132}O_8$ requires C, 77.76; H, 11.33%: **31h**, Found, C, 77.84; H, 11.82. $C_{78}H_{136}O_8$ requires C, 77.95; H, 11.41%: **31i**, Found, C, 77.92; H, 11.35. $C_{82}H_{144}O_8$ requires C, 78.29; H, 11.54%.

References

1. S. Kumar, *Phase Transitions*, **81**, 113, (2008).
2. M. V. Ignatushchenko, R. W. Winter and M. Riscoe, *Am. J. Trop. Med. Hyg.*, **62**, 77, (2000).
3. J. Ziegler, R. Linck and D. W. Wright, *Current Med. Chem.*, **8**, 171, (2001).
4. R. W. Winter, K. A. Cornell, L. L. Johnson, M. Ignatushchenko, D. J. Hinrichs, M. K. Riscoe, *Antimicrob. Agents Chemother.*, **40**, 1408, (1996).
5. G. J. Martin and C. F. Lischer, *J. Biol. Chem.*, **137**, 169, (1941).
6. Robiquet, *Annalen*, **19**, 204, (1836).

7. W. Klobukowsky, *Chem. Ber.*, **10**, 880, (1877).
8. J. Grimshaw, and R. D. Haworth, *J. Chem. Soc.*, **56**, 4225, (1956).
9. A. Queguiner, A. Zann, J. C. Dubois, J. Billard, *Proceedings of International Conference on Liquid Crystals*, Bangalore, Heyden and Son, London (Edited by S. Chandrasekhar). P. 34, (1980).
10. (a) S. Kumar, *Liq. Cryst.*, **32**, 1089, (2005); (b) S. Kumar, *Liq. Cryst.*, **31**, 1037, (2004).
11. (a) S. Kumar, *Chem. Soc. Rev.*, **35**, 83, (2006); (b) F. Vera, J. L. Serrano and T. Sierra, *Chem. Soc. Rev.*, **38**, 781, (2009); (c) T. Kato, T. Yasuda, Y. Kamikawa and M. Yoshio, *Chem. Commun.*, 729, (2009); (d) S. Laschat, A. Baro, N. Steinke, F. Giesselmann, C. Hagele, G. Scalia, R. Judele, E. Kapatsina, S. Sauer, A. Schreivogel and M. Tosoni, *Angew. Chem. Int. Ed.*, **46**, 4832, (2007); (e) S. Sergeyev, W. Pisula and Y. H. Geerts, *Chem. Soc. Rev.*, **36**, 1902, (2007); (f) J. Wu, W. Pisula and K. Müllen, *Chem. Rev.*, **107**, 718, (2007).
12. K. Ohta, H. Hasebe, H. Ema, M. Moriya, T. Fujimoto, and I. Yamamoto, *Mol. Cryst. Liq. Cryst.*, **208**, 21, (1991).
13. (a) C. Goltner, D. Pressner, K. Mullen and H. W. Spiess, *Angew. Chem. Int. Ed.*, **32**, 1660, (1993); (b) D. Pressner, C. Goltner, H. W. Spiess and K. Mullen, *Ber. Bunsen. Phys. Chem.*, **97**, 1362, (1993); (c) S. Benning, H. S. Kitzerow, H. Bock, and M.F. Achard, *Liq. Cryst.*, **27**, 901, (2000); (d) F. Wurthner, C. Thalacker, S. Diele and C. Tschierske, *Chem. Eur. J.*, **7**, 2245, (2001).
14. (a) S. Kumar, E. J. Watchtel, E. Keinan, *J. Org. Chem.*, **58**, 3821, (1993); (b) E. Keinan, S. Kumar, S. P. Singh, R. Garlando, E. J. Watchtel, *Liq. Cryst.*, **11**, 157,

- (1993); (c) N. Boden, R. J. Bushby, K. Donovan, Q. Liu, Z. Lu, T. Kreouzis, and A. Wood, *Liq. Cryst.*, **28**, 1739, (2001).
15. K. Pieterse, P. A. van Hal, R. Kleppinger, J. A. J. M. Vekemans, R. A. J. Janssen, and E. W. Meijet, *Chem. Mater.*, **13**, 2675, (2001).
16. (a) M. Palma, J. Levin, O. Debever, Y. Geerts, M. Lehmann and P. Samori, *Soft Matter*, **4**, 303, (2008); (b) R. I. Gearba, M. Lehman, J. Levin, D. A. Ivanov, M. H. J. Koch, J. Barbera, M. G. Debije, J. Piris, Y. H. Geerts, *Adv. Mater.*, **15**, 1614, (2003).
17. H. Lee, D. Kim, H. -K. Lee, W. Qiu, N. -K. Oh, W. -C. Zin, and K. Kim, *Tetrahedron Lett.*, **45**, 1019, (2004).
18. Q. Zhang, P. Prins, S. C. Jones, S. Barlow, T. Kondo, Z. An, L. D. A. Siebbeles and S. R. Marder, *Org. Lett.*, **7**, 5019, (2005).
19. (a) L. Schimdt-Mende, A. Fechtenkotter, K. Mullen, E. Moons, R. H. Friend and J. D. Mackenzie, , **293**, 1119, (2001); (b) I. Seguy, P. Destruel and H. Bock, *Synth. Met.*, **111-112** , 15, (2000).
20. (a) D. M. Collard and C. P. Lillya, *J. Am. Chem. Soc.*, **111**, 1829, (1989); (b) D. M. Collard and C. P. Lillya, *J. Am. Chem. Soc.*, **113**, 8577, (1991); (c) P. G. Schouten, J. M. Warman, M. P. de Hass, C. F. van Nostrum, G. H. Gelinck, R. J. M. Nolte, M. J. Copyn, J. W. Zwikker, M. K. Engel, M. Hanack, Y. H. Chang and W. T. Ford, *J. Am. Chem. Soc.*, **116**, 6880, (1994); (d) P. G. Schouten, J. F. van der Pol, J. W. Zwikker, W. Drenth and S. J. Picken, *Mol. Cryst. Liq. Cryst.*, **195**, 291, (1991); (e) K. Ohta, T. Watanabe, H. Hasebe, Y. Morizumi, T. Fujimoto and I. Yamamoto, *Mol. Cryst. Liq. Cryst.*, **196**, 13, (1991); (f) K. Ohta, Y. Morizumi,

- H. Ema, T. Fujimoto and I. Yamamoto, *Mol. Cryst. Liq. Cryst.*, **208**, 55, (1991); (g) W. Pisula, M. Kastler, D. Wasserfallen, T. Pakula and K. Müllen, *J. Am. Chem. Soc.*, **126**, 8074, (2004); (h) M. Kastler, W. Pisula, F. Laquai, A. Kumar, R. J. Davies, S. Balushev, M. –C. Garcia-Guierrez, D. Wasserfallen, H. –J. Butt, C. Riekel, G. Wegner and K. Müllen, *Adv. Mater.*, **18**, 2255, (2006); (i) W. Pisula, Z. Tomovic, B. E. Hamaoui, M. W. Watson, T. Pakula and K. Müllen. *Adv. Funct. Mater.*, **15**, 893, (2005).
21. (a) S. Kumar and S. K. Varshney, *Angew. Chem. Int. Ed.*, **39**, 3140, (2000); (b) S. Kumar, S. K. Varshney and D. Chauhan, *Mol. Cryst. Liq. Cryst.*, **396**, 241, (2003).
22. (a) C. Liu, A. Fechtenkotter, M. D. Watson, K. Mullen and A. J. Bard, *Chem. Mater.*, **15**, 124, (2003); (b) W. Pisula, M. Kastler, D. Wasserfallen, M. Mondeshki, J. Paris, I. Schnell and K. Müllen, *Chem. Mater.*, **18**, 3634, (2006).
23. S. Kumar, D. S. S. Rao and S. K. Prasad, *J. Mater. Chem.*, **9**, 2751, (1999).
24. R. I. Gearba, A. I. Bondar, B. Goderis, W. Bras, and D. A. Ivanov, *Chem. Mater.*, **17**, 2825, (2005).
25. S. Sergeyeve, E. Pouzet, O. Debever, J. Levin, J. Gierschner, J. Cornil, R. G. Aspe and Y. H. Geerts, *J. Mater. Chem.*, **17**, 1777, (2007).
26. (a) C. Carfagna, A. Roviello and A. Sirigu, *Mol. Cryst. Liq. Cryst.*, **122**, 151, (1985); (b) J. Billard, J. C. Dubois, C. Vaucher and A. M. Levelut, *Mol. Cryst. Liq. Cryst.*, **66**, 115, (1981).
27. J. Billard, Z. Luz, R. Poupko, and H. Zimmermann, *Liq. Cryst.*, **16**, 333, (1994).
28. C. Carfagna, P. Iannelli, A. Roviello, A. Sirigu, *Liq. Cryst.*, **2**, 611, (1987).

29. (a) S. Kumar, J. J. Naidu and S. K. Varshney, *Liq. Cryst.*, **30**, 319, (2003); (b) K. Krishnan and V. S. K. Balaguruswamy, *Liq. Cryst.*, **27**, 991, (2000).
30. (a) K. S. Raja, S. Ramakrishnan and V. A. Raghunathan, *Chem. Mater.*, **9**, 1630, (1997); (b) K. Krishnan and V. S. K. Balaguruswamy, *Mol. Cryst. Liq. Cryst.*, **350**, 1, (2000).
31. V. Prasad, K. Krishnan, and V. S. K. Balaguruswamy, *Liq. Cryst.*, **27**, 1075, (2000).
32. (a) V. Prasad, *Liq. Cryst.*, **28**, 647, (2001); (b) V. Prasad and D. S. S. Rao, *Mol. Cryst. Liq. Cryst.*, **350**, 51, (2000).
33. (a) J. J. Naidu and S. Kumar, *Mol. Cryst. Liq. Cryst.*, **397**, 17/[317], (2003); (b) S. Kumar and J. J. Naidu, *Liq. Cryst.*, **29**, 1369, (2002).
34. K. Krishnan and V. S. K. Balaguruswamy, *Liq. Cryst.*, **28**, 321, (2001).
35. S. Kumar, J. J. Naidu and S. K. Varshney, *Mol. Cryst. Liq. Cryst.*, **411**, 355, (2004).
36. S. K. Gupta, V. A. Raghunathan and S. Kumar, *New J. Chem.*, **33**, 112, (2009).
37. S. K. Pal, S. Kumar and J. Seth, *Liq. Cryst.*, **35**, 521, (2008).
38. K. S. Raja, V. A. Raghunathan and S. Ramakrishnan, *Macromolecules*, **31**, 3807, (1998).
39. L. Corvazier and Y. Zhao, *Liq. Cryst.*, **27**, 137, (2000).
40. Y. Chenard, N. Paiement and Y. Zhao, *Liq. Cryst.* **27**, 459, (2000).
41. Y. Maeda, H. Yokoyama and S. Kumar, *Liq. Cryst.*, **32**, 833, (2005).
42. M. Gupta, R. Dhar, V. K. Agarwal and S. Kumar, *Proceedings of the 16th Conference on Liquid Crystals*, Warszawa, 109, (2007).

43. S. Chandrasekhar, V. S. K. Balaguruswamy, *Proc. Royal Soc. Lond. A*, **458**, 1783, (2002).
44. (a) C. O. Kappe, *Chem. Soc. Rev.* **37**, 1127, (2008); (b) V. Polshettiwar and R. S. Varma, *Acc. Chem. Res.*, **41**, 629, (2008); (c) M. A. Herrero, J. M. Kremsner and C. O. Kappe, *J. Org. Chem.*, **73**, 36, (2008); (d) C. O. Kappe, *Angew. Chem. Int. Ed.*, **43**, 6250, (2004); (e) F. Wiesbrock, R. Hoogenboom and U. S. Schubert, *Macromol. Rapid Commun.*, **25**, 1739, (2004); (f) M. Nuchter, B. Ondruschka, W. Bonrath and A. Gum, *Green Chem.*, **6**, 128, (2004); (g) A. K Bose, M. S. Manhas, S. N. Ganguly, A. H Sharma and B. K Banik, *Synthesis*, 1578, (2002); (h) A. de la Hoz, A. Diaz-Ortiz and A. Moreno, *Chem. Soc. Rev.*, **34**, 164, (2005); (i) V. Molteni and D. A. Ellis, *Curr. Org. Synth.*, **2**, 333, (2005); (j) M. Larhed, C. Moberg, and A. Hallberg, *Acc. Chem. Res.*, **35**, 717, (2002); (k) D. Bogdal, *Microwave-Assisted Organic Synthesis-One Hundred Reaction Procedures*. Elsevier, Amsterdam, (2005); (l) O. C. Kappe and A. Stadler, *Microwaves in Organic and Medicinal Chemistry*. Wiley-VCH, Weinheim, (2005); (m) E. Van der Eycken, and C. O. Kappe, (Eds.), *Microwave-Assisted Synthesis of Heterocycles*. Springer, Heidelberg, (2006). (n) *Microwaves in Organic Synthesis*, A. Loupy (ed.), Wiley-VCH, Weinheim, (2002). (o) *Microwave Synthesis: Chemistry at the Speed of Light*. CEM Publishing, Matthews NC, (2002).
45. H. K. Bisoyi and S. Kumar, *New J. Chem.*, **32**, 1974, (2008).
46. H. K. Bisoyi and S. Kumar, *Tetrahedron Lett.*, **48**, 4399, (2007).

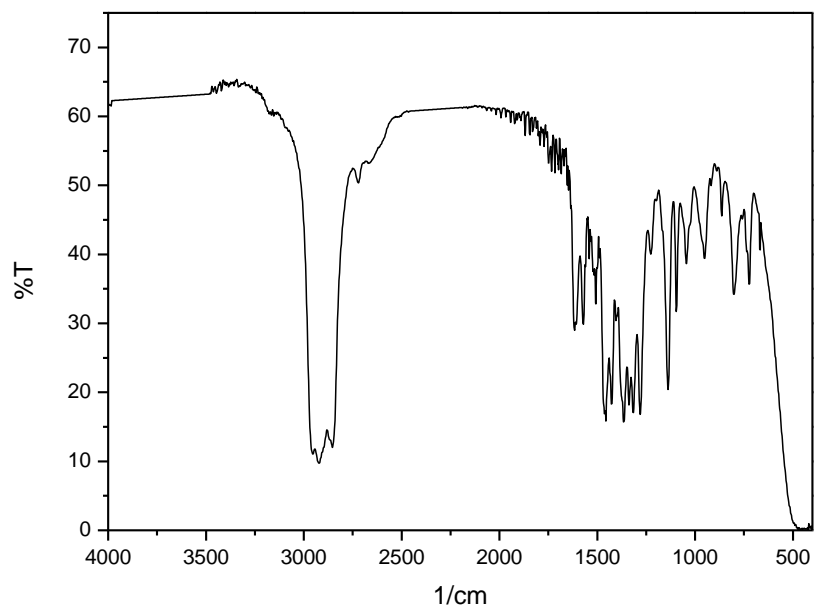


Figure 1. FT-IR spectrum of compound **30**.

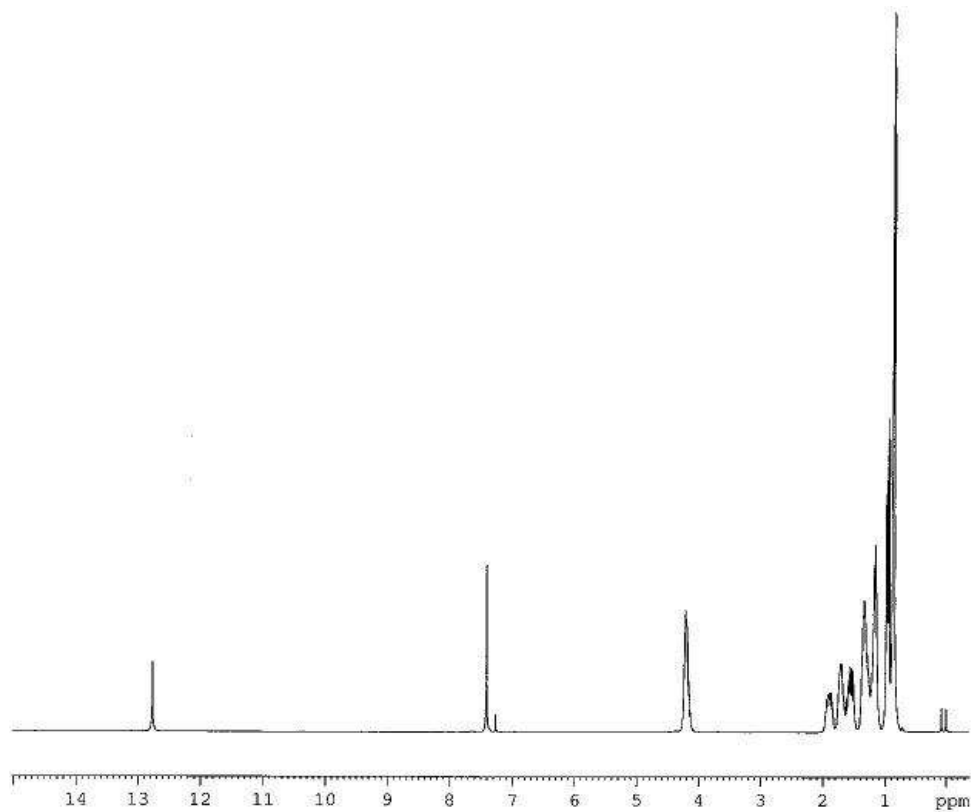
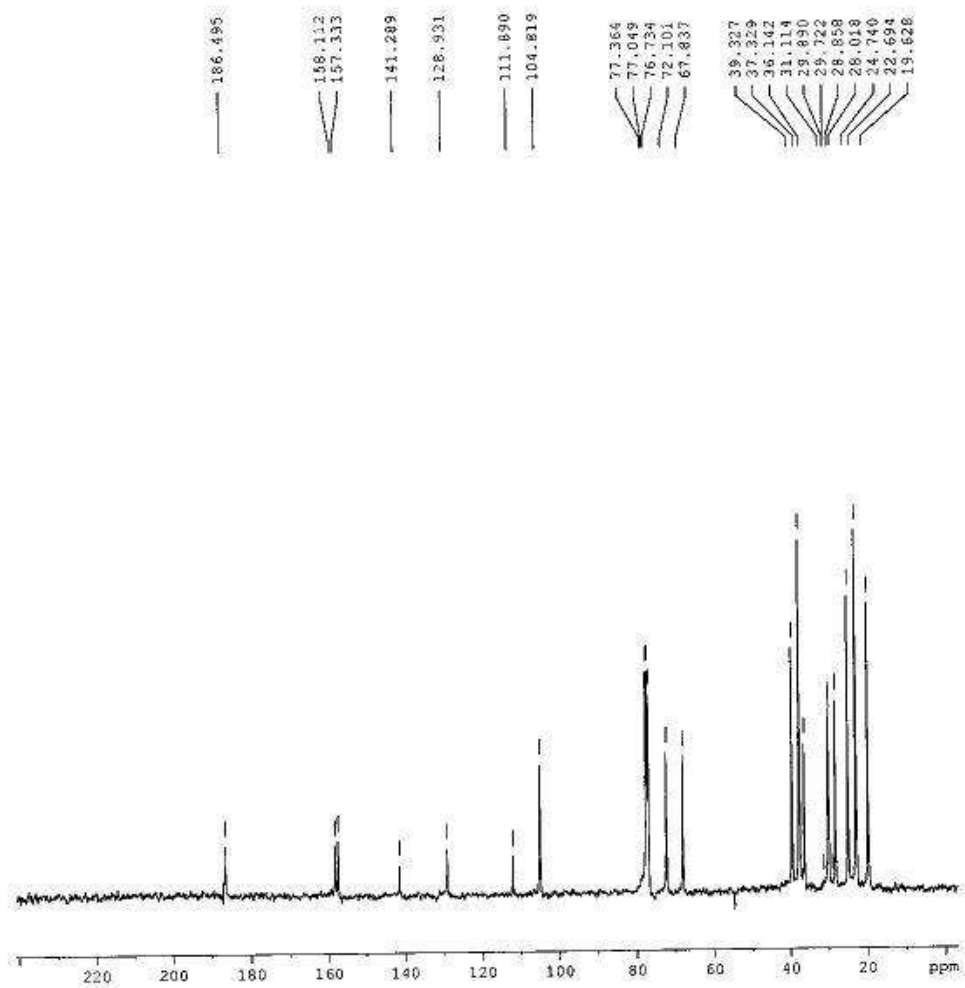


Figure 2. ¹H NMR spectrum of compound **30**.



(c)

Figure 3. ¹³C NMR spectrum of compound 30.

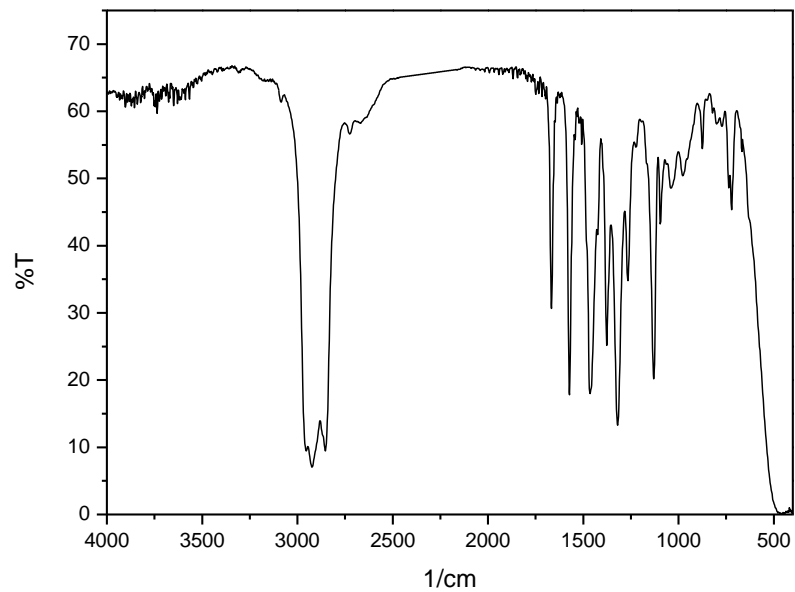


Figure 4. FT-IR spectrum of compound **29g**.

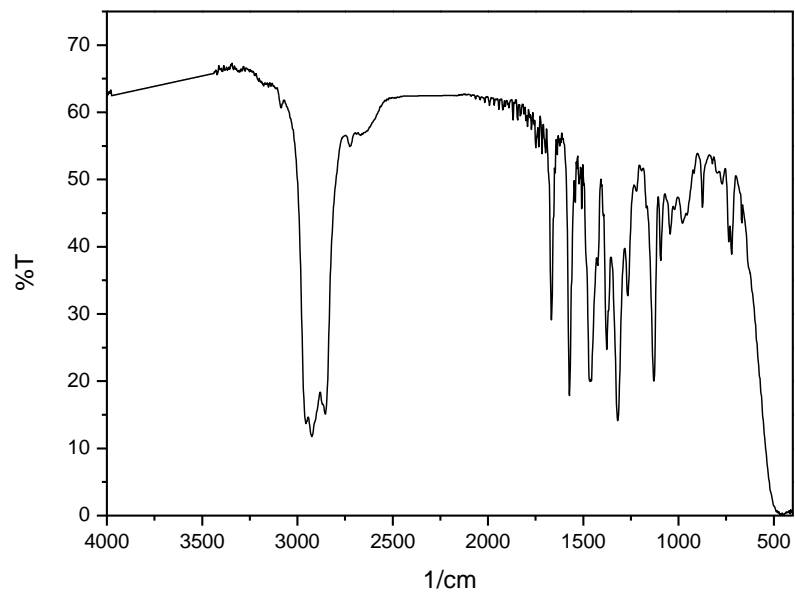


Figure 5. FT-IR Spectrum of Compound **31f**.

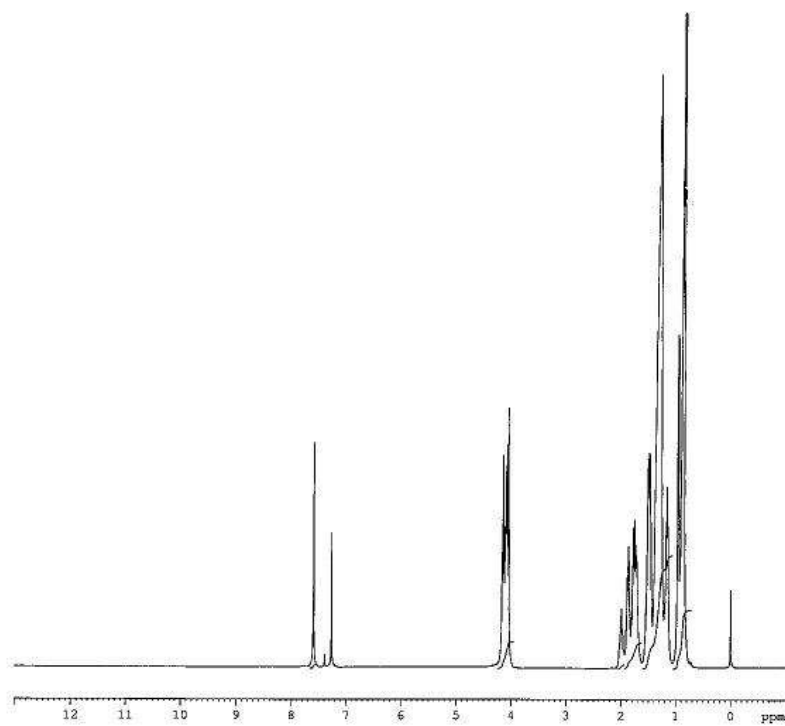


Figure 6. ^1H NMR spectrum of compound **29e**.

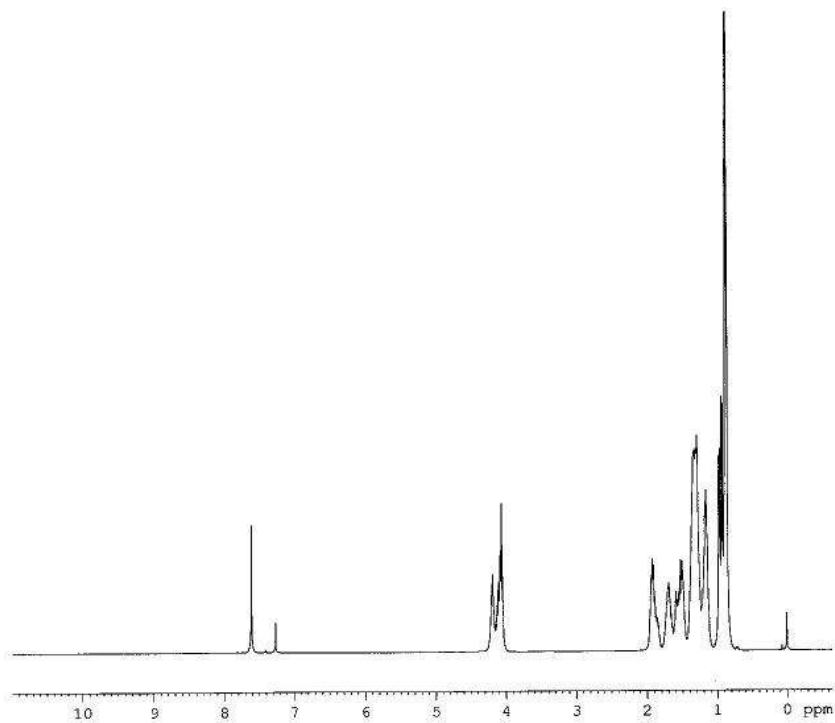


Figure 7. ^1H NMR spectrum of compound **31d**.

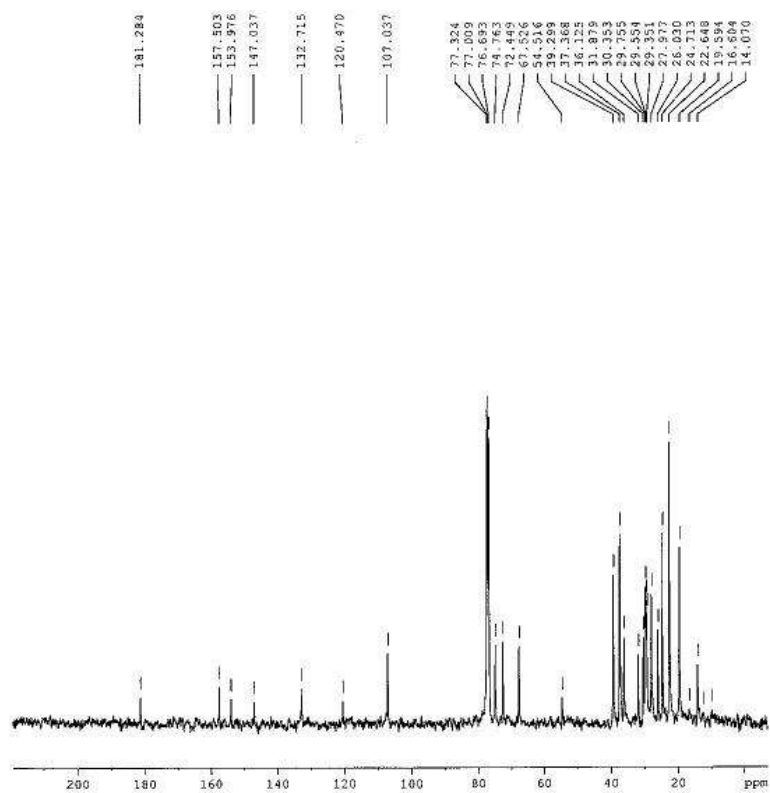


Figure 8. ^{13}C NMR spectrum of compound **29e**.

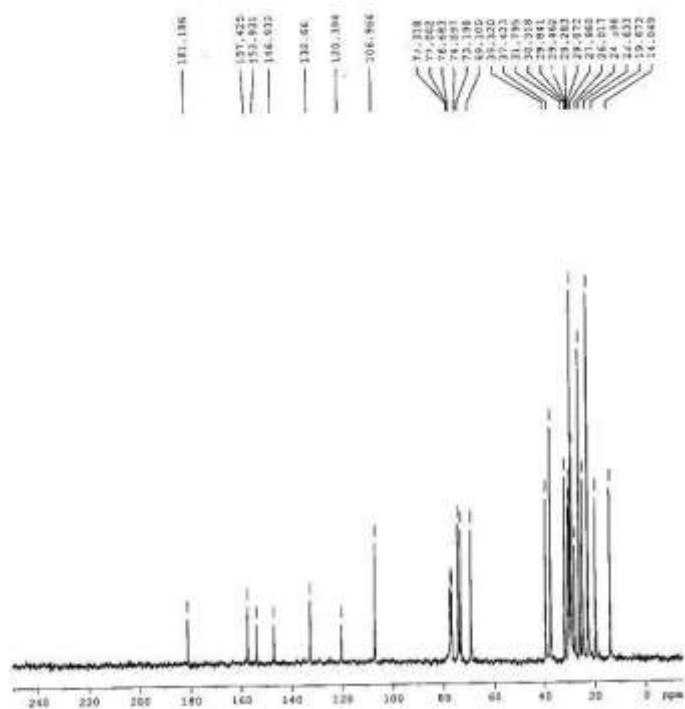


Figure 9. ^{13}C NMR spectrum of compound **31d**.

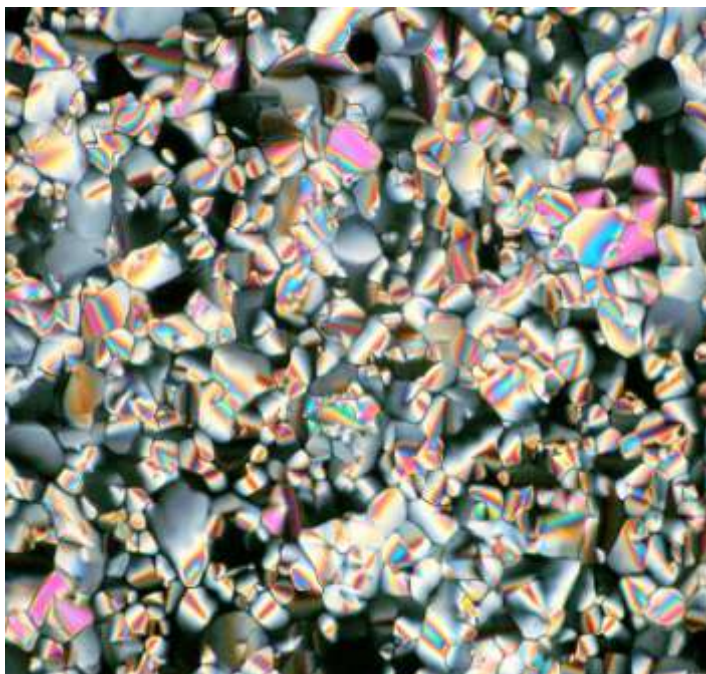


Figure 10. Optical photomicrograph of **29e** at 25 °C on cooling from the isotropic phase (Crossed Polarizers, Magnification X 200).

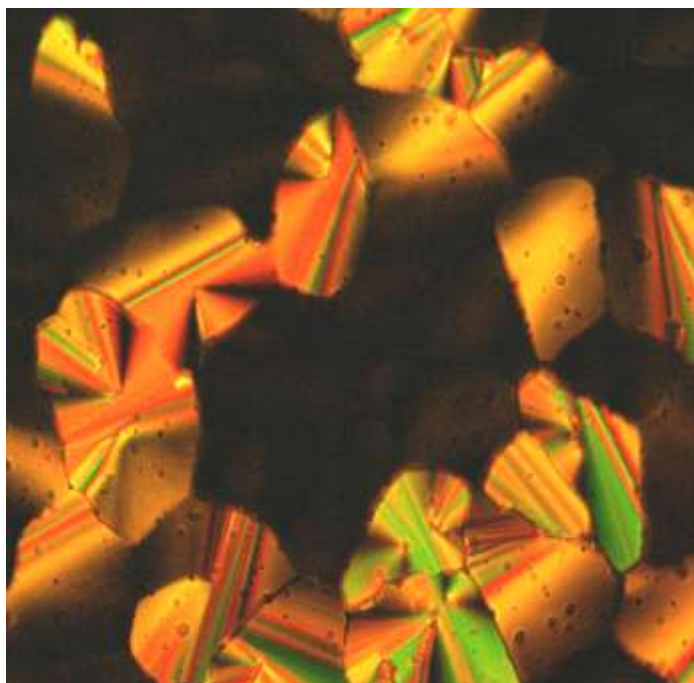


Figure 11. Optical photomicrograph of **30** at 25 °C on cooling from the isotropic phase (Crossed Polarizers, Magnification X 200).

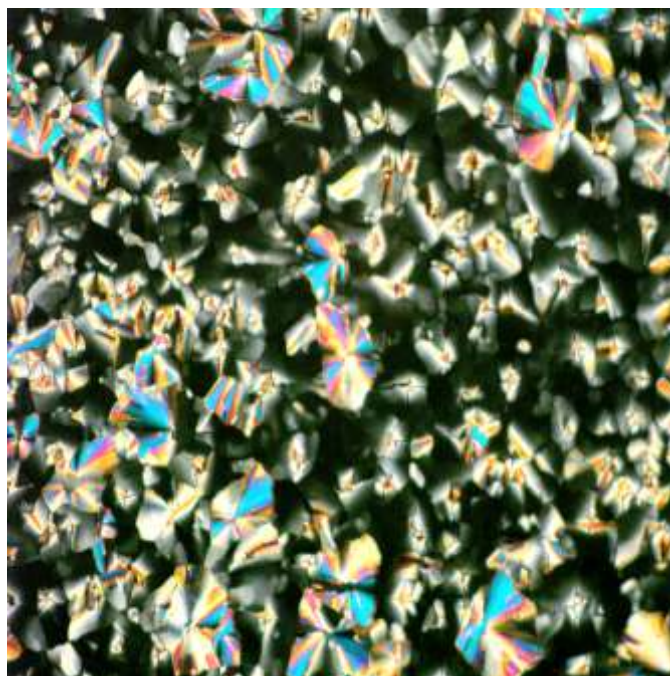


Figure 12. Optical photomicrograph of **31d** at 25 °C on cooling from the isotropic phase (Crossed Polarizers, Magnification X 200).

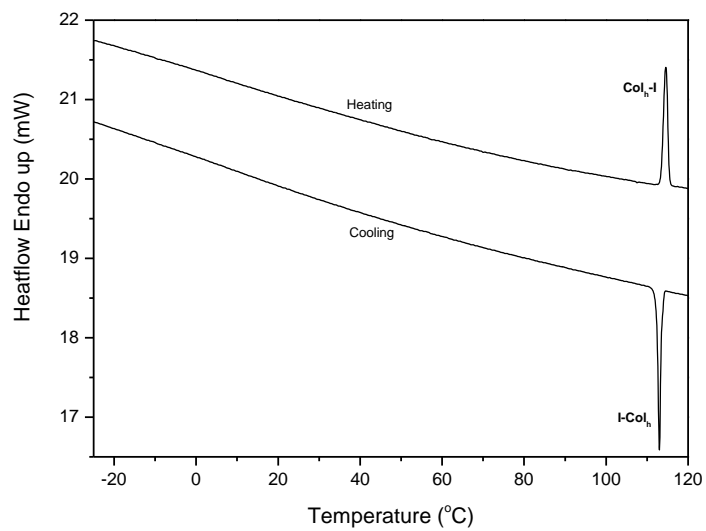


Figure 13. DSC thermogram of compound **30** on heating and cooling cycles (scan rate 5 °C min⁻¹).

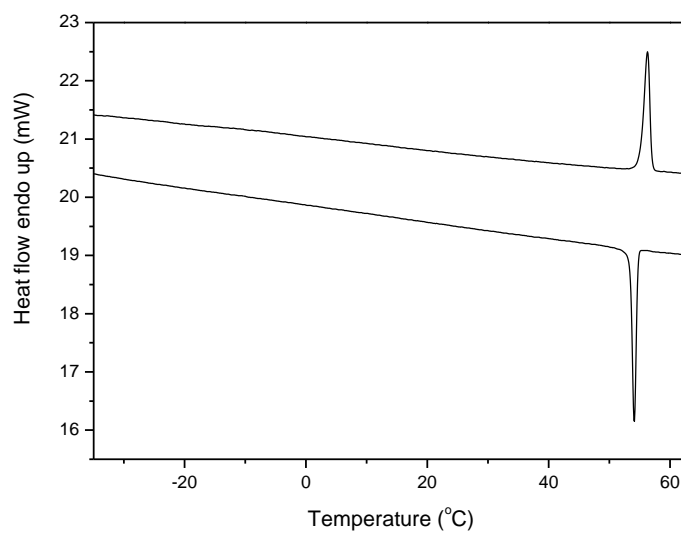


Figure 14. DSC thermogram of compound **29e** on heating and cooling cycles (scan rate 5 °C min⁻¹).

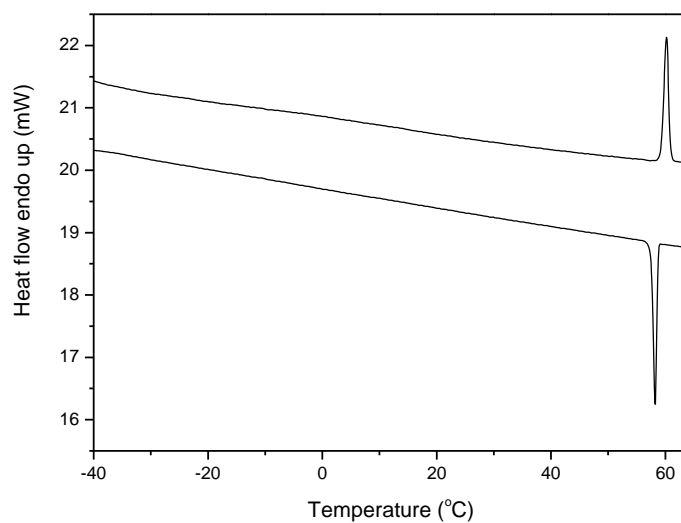


Figure 15. DSC thermogram of compound **31f** on heating and cooling cycles (scan rate 5 °C min⁻¹).

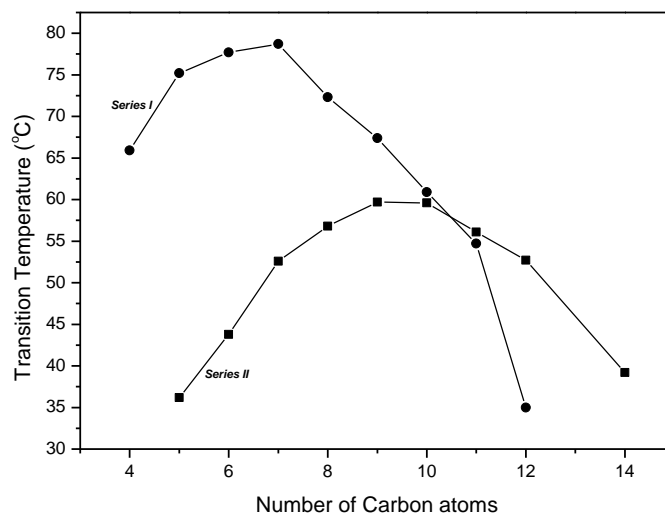


Figure 16. Variation of transition temperatures (CoI_n-I) with number of carbon atoms in the n-alkyl chains.

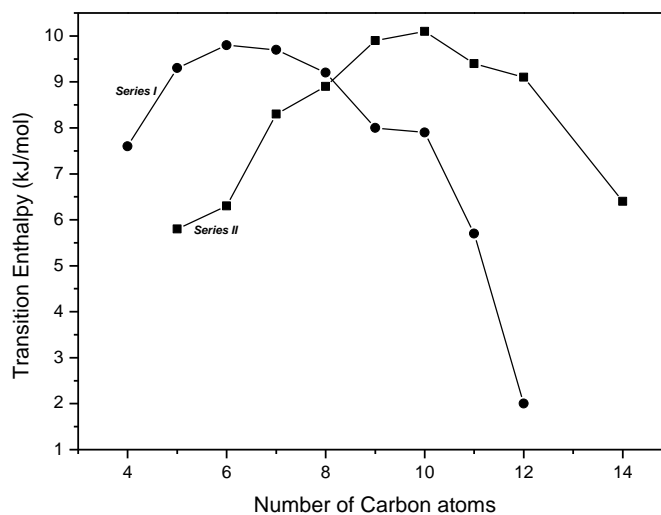
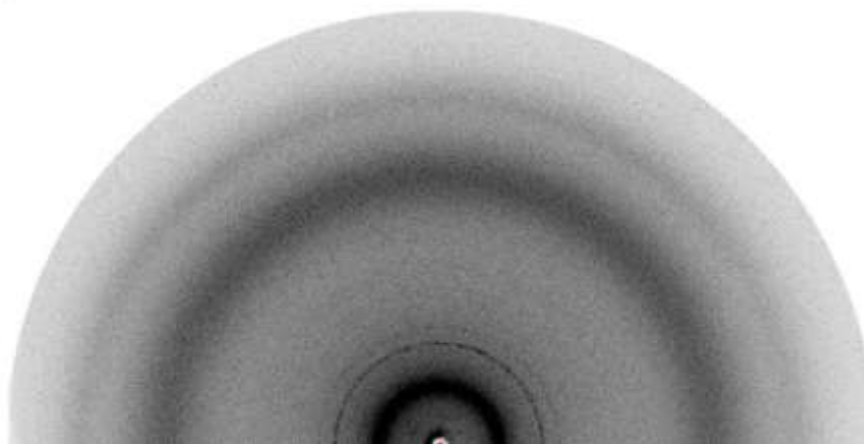
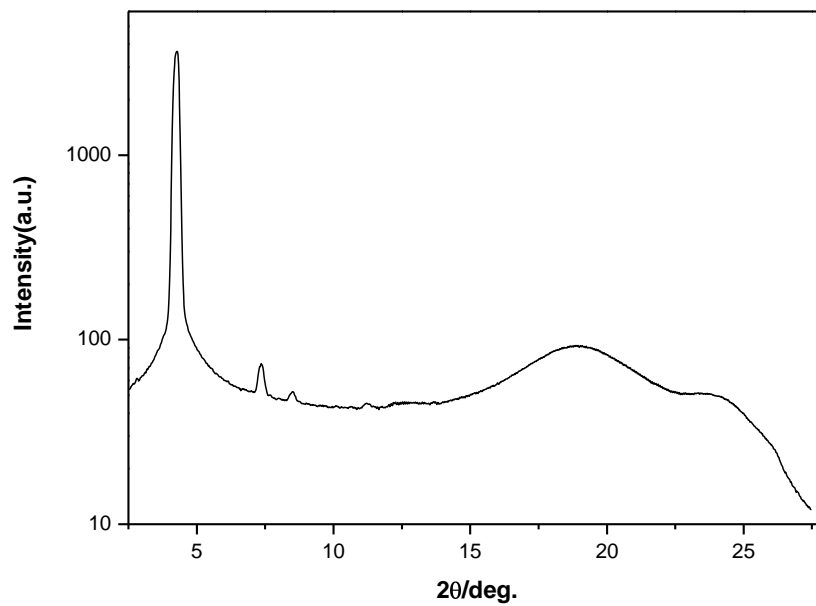


Figure 17. Variation of transition enthalpy ΔH (CoI_n-I) with number of carbon atoms in the n-alkyl chains.

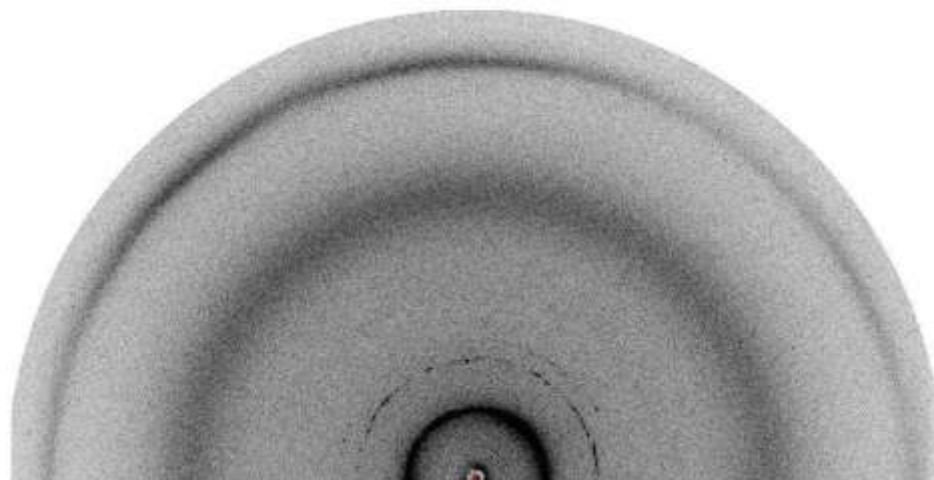


(a)

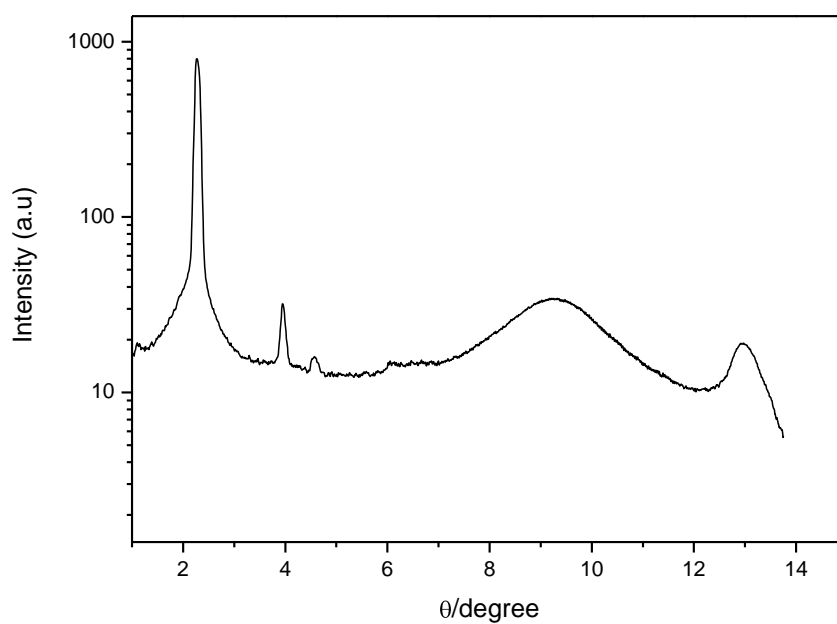


(b)

Figure 18. X-ray diffraction pattern (a) and its derived intensity vs θ graph (b) of the mesophase of compound **31d** recorded at 25 °C.



(a)

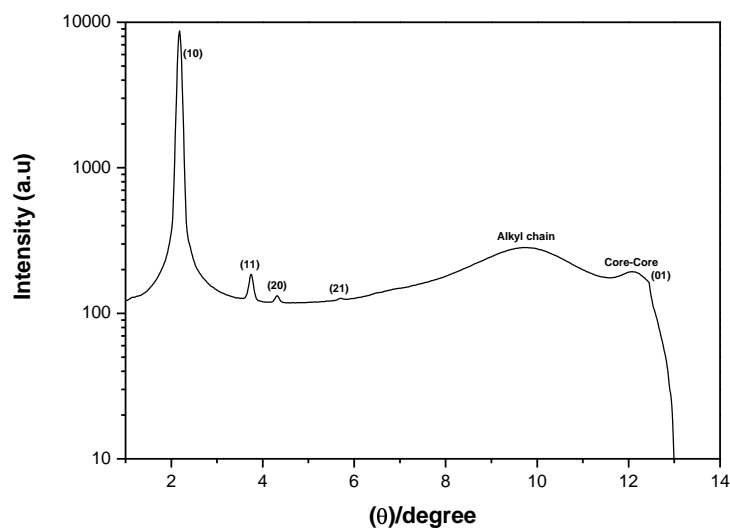


(b)

Figure 19. X-ray diffraction pattern (a) and its derived intensity vs θ graph (b) of the mesophase of compound **30** recorded at 25 °C.



(a)



(b)

Figure 20. X-ray diffraction pattern (a) and its derived intensity vs θ graph (b) of the mesophase of compound **29e** recorded at 25 °C.

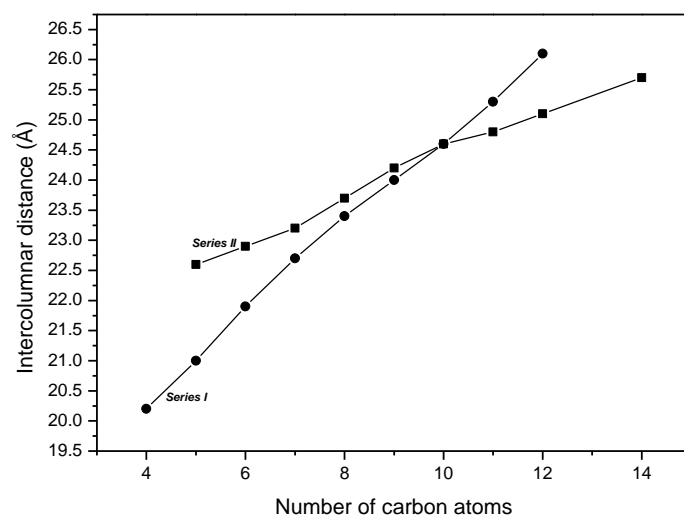


Figure 21. Variation of intercolumnar distances in both the series of compounds with number of carbon atoms in the n-alkyl chains.

CHAPTER 4

Synthesis and characterization of novel liquid crystalline oligomers

4.1 Part A: Molecular double cables: synthesis and mesomorphism

4.1.1 Introduction

The notable improvement in the performance of electronic devices based on organic semiconductors (organic π -conjugated soft materials) has attracted great interest in recent years [1]. Organic π -conjugated materials have successfully been tested for use in a number of electronic devices, such as field effect transistors, light emitting diodes and solar cells. The improved efficiency of organic devices has origins ranging from appropriate molecular design to well-defined structured layers essential for effective charge transport. Recently there have been tremendous efforts to achieve both p-type (hole conducting) and n-type (electron conducting) properties in organic semiconducting materials which are crucial for molecular electronics. One elegant approach for such materials is to covalently link electron donor and electron acceptor components at molecular level. These kinds of materials are expected to behave as intrinsic, non-composite p/n-type semiconductors. Such chemical tailoring could lead to the development of other molecular architectures and it is envisaged that the combination of covalent chemistry and molecular self-assembly will be crucial for the development of nano-engineered functional materials for electronic applications [1]. Among the diverse semiconductors, discotic liquid crystals (DLCs) play an important role in the design of

electronic devices [2]. Discotic liquid crystals are unique nanostructures with remarkable electronic and optoelectronic properties. Due to cofacial stacking of aromatic cores, disc-like molecules self assemble into one dimensional columnar wire and these columns in turn self organize themselves in various two-dimensional lattices. The transport along the columnar axis is much faster than between the columns. Due to their relatively high charge carrier mobilities, tendency to form highly ordered films of various thickness and self-healing of defects owing to their dynamic nature, discotic mesogens have been considered as attractive candidates for applications in organic electronic devices such as photovoltaic solar cells, light emitting diodes and field effect transistors [2].

Very recently a great deal of attention is being paid to liquid crystal oligomers [3]. The physical properties of liquid crystalline oligomers are significantly different from those of conventional low molar mass liquid crystals. Their purification and characterization are simple, owing to the restricted motion of the components liquid crystal oligomers provide and stabilize variety of fluid phases with fascinating functions and oligomeric approach provides a wide flexibility in molecular design towards multifunctional liquid crystals. However, compared to the number of calamitic oligomers, discotic oligomers are rare. In this context we are interested in the design and synthesis of novel functional discotic oligomeric materials and their mesophase behavior.

A careful literature survey reveals that while a number of discotic dimers, trimers and tetramers containing various molecular components and having different molecular topologies (linear, star shaped, etc.) have been prepared and studied [3], there is no report on monodisperse discotic liquid crystal pentamers. Higher oligomers like hexamers and heptamers are very few in number. Among the discotic liquid crystal oligomers, the star-

shaped heptamers are interesting materials. The first discotic liquid crystalline heptamers were reported by Ringsdorf's group [4]. These contain seven triphenylene units, one of the triphenylenes acts as the central core and the other six triphenylenes act as peripheral units **1**. These compounds exhibit columnar hexagonal phase by statistical arrangement of triphenylenes without any super column or super lattice formation in the mesophase. Interestingly these compounds undergo conformational changes at the air-water interface such that the peripheral triphenylene substituents sit perpendicular to (edge-on) and the central core sits parallel (face-on) to the interface [5]. This conformation of the molecules is preserved upon transfer to a solid substrate. Mullen *et al.* reported a star shaped discotic heptamer based on hexabenzocoronene (HBC) **2** [6]. This compound showed strong tendency to aggregate in solution and in bulk state. Physical gel formation was observed due to the presence of covalent intercolumnar interactions. Higher order was found in high-temperature columnar liquid crystalline phase due to the higher mobility of the molecules in comparison with the low-temperature solid. Holger *et al.* reported a discotic liquid crystalline heptamer based on electron rich and electron deficient triphenylene units **3** [7]. The central part of the molecule contains electron deficient hexaazatriphenylene surrounded by six normal triphenylene units. This compound shows a tendency to form spontaneous homeotropic alignment between two glass plates which is a requirement for such compounds to be employed in photovoltaic applications. Very recently Zelcer *et al.* have reported a discotic liquid crystalline heptamer of triphenylene containing siloxane spacers **4** [8]. Interestingly, this compound exhibits a super lattice formation where each heptamer shares one peripheral triphenylene with six adjacent

neighbors so that the distance between planes containing the cores is twice that of the regular hexagonal lattice.

R—C

R—C

Here, in this part of the chapter, we present the synthesis and characterization of the first examples of two monodisperse discotic liquid crystalline pentamers and two novel discotic liquid crystalline heptamers [9]. Our aim is many fold: (i) to realize monodisperse discotic liquid crystal pentamers; (ii) the molecular design is such that it contains the well studied electron rich triphenylene moiety [10] and electron deficient anthraquinone [11] as the hole [12] and electron transporting [13] components respectively which are analogous to fullerene tethered conjugated polymers, the so called double-cable polymers [14]. These molecular double-cables, owing to their incommensurate core sizes may stack one on top of the other in the columns to give columnar versions of double cable polymers, which could eventually provide side-by-side percolation pathways for electrons and holes in solar cells. One of the discotic heptamer contains triphenylene as the central core and as peripheral units as well connected via exclusively ether linkages, this compound can act as a coaxial molecular double cable for hole transport; (iii) Since star-shaped oligomers are known to undergo spontaneous homeotropic alignment, these star-shaped intrinsic p/n-type oligomers may self align homeotropically from isotropic melt between electrodes which is crucial for photovoltaic and other opto-electronic performances.

4.1.2 Results and Discussion

The synthetic route to the discotic pentamers **11** and **12** is shown in Scheme 1. hexapentyloxytriphenylene **6**, monohydroxypentakisipentyloxytriphenylene **7**, ω -bromosubstituted triphenylene **8**, and rufigallol **10** were prepared as reported [15, 16]. Rufigallol **10** was alkylated under mild etherification conditions with ω -bromo-substituted triphenylene **8** to furnish the pentamer **11** leaving the less reactive

intramolecularly hydrogen bonded hydroxyl groups at the 1-and 5-positions unreacted. The dihydroxy functionalized pentamer **11** was acetylated to its corresponding diacetate **12** with acetic anhydride and sulphuric acid under classical conditions. The chemical structures of the pentamers were confirmed by spectral techniques and elemental analysis. The notable spectral features of the pentamer **11** are as follows: in its proton NMR **11** shows a peak at δ 12.74 corresponding to two intramolecular hydrogen-bonded protons along with two aromatic-proton resonances at δ 7.8 and 7.3 corresponding to

Scheme 1. Synthesis of discotic liquid crystalline pentamers. Reagents and conditions: (i) FeCl_3 ; MeOH; (ii) Cat-B-Br; (iii) 1,12-Dibromododecane, MEK, Cs_2CO_3 ; (iv) H_2SO_4 , MW; (v) DMSO, NaOH, 90 °C, 20h, 10%; (vi) Ac_2O , H_2SO_4 .

triphenylene and anthraquinone in the ratio 12:1 (Figure 4) where as the diacetate **12** did not show any signal at δ 12.74 but instead demonstrated a singlet at δ 2.47 corresponding to the $-\text{COCH}_3$ protons (Figure 5).

The aromatic peak corresponding to anthraquinone protons shifted from δ 7.3 to 7.6 upon acetylation. Similarly pentamer **11** shows a signal at δ 186.3 in its ^{13}C NMR spectrum corresponding to intramolecular hydrogen-bonded quinone carbonyl groups (Figure 6). This signal was shifted to δ 180.1 in pentamer **12** (Figure 7), the acetyl carbonyl group appeared at δ 169.0. In addition, the FTIR spectrum of **12** shows the acetyl carbonyl absorption at 1763 cm^{-1} . The elemental analysis data are in very good agreement with the chemical structures of the star-shaped pentamers **11** and **12** suggesting the high purity of the materials. The synthesis of the heteroheptamer **13** containing anthraquinone as the central core and six triphenylenes as the periphery is shown in Scheme 2.

The heptamer **13** containing electron deficient anthraquinone core and electron rich triphenylene periphery was prepared from rufigallol **10** and ω -bromo-substituted triphenylene **8** in single step by irradiating the reaction mixture in microwave oven. It should be noted that microwave dielectric heating furnishes products within few minutes which is simple, efficient, rapid and economic. Classical reaction conditions to obtain the heptamer **13** always resulted in an inseparable mixture of less substituted byproducts. The identity and purity of the compound was established with the help of spectral and elemental analysis. The FT-IR spectrum of the heptamer does not exhibit the hydrogen bonded quinone carbonyl absorption but instead shows the hexasubstituted anthraquinone carbonyl absorption at 1666 cm^{-1} which demonstrates that the rufigallol is alkylated at all

Scheme 2. Synthesis of discotic liquid crystalline heptamer. Reagents and conditions: (i) FeCl₃; MeOH; (ii) Cat-B-Br, CH₂Cl₂; (iii) 1,12-Dibromododecane, MEK, Cs₂CO₃; (iv) H₂SO₄, MW; (v) Cs₂CO₃, NMP, MW, 10 min.

six phenolic positions. The ¹H NMR spectrum of **13** (Figure 8) shows two aromatic proton resonances at δ 7.8 and 7.59 ppm in the ratio of 18:1 corresponding to triphenylene and anthraquinone aromatic protons respectively in addition to methyl and methylene proton resonances expected from the molecular structure. ¹³C NMR spectrum of this heptamer exhibits only one quinone carbonyl resonance at δ 181.2 ppm in addition

to other aromatic and aliphatic carbon resonances, again confirming the hexasubstitution of the rufigallol (Figure 9). Moreover a poly dispersity index (PDI) of 1.03 determined by gel permeation chromatography (GPC) shows that the heptamer is free from less substituted byproducts. The above spectral features along with the elemental analysis data of compound **13** show the high purity of the heptamer. To compare the phase behavior of the above heptamer, another homoheptamer was prepared which contains the same number of peripheral triphenylene units with same number of methylene units in the spacers but the central electron deficient anthraquinone core is now replaced by electron rich triphenylene core itself. This compound can also act as a coaxial molecular double cable i.e. it contains two hole conducting paths separated from each other by insulating alkyl chains. The synthesis of this heptamer **17** is shown in Scheme 3.

Scheme 3. Synthesis of triphenylene based heptamer. Reagents and conditions: (i) 1,12-dibromododecane, K_2CO_3 , MEK; (ii) $FeCl_3$; MeOH; (iii) Cat-B-Br, CH_2Cl_2 ; (iv) Cs_2CO_3 , MEK, 72 hrs reflux, 55%.

The chemical structure of the compound **17** was established from its spectral and elemental analysis. The proton NMR spectrum of this compound (Figure10) does not

exhibit the $-\text{CH}_2\text{Br}$ proton resonance at δ 3.4 ppm as was displayed by the precursor **16** and the intensity of the Ar-OCH_2- proton resonance at δ 4.2 ppm increases as expected. The intensity ratios of the proton resonances are in very good agreement with its chemical structure. Its ^{13}C NMR spectrum (Figure 11) exhibits all the expected aromatic and aliphatic carbon resonances and does not show any carbon resonance corresponding to $-\text{CH}_2\text{Br}$. The elemental analysis data also shows the high purity and homogeneity of the heptamer **17**.

4.1.2.1 Mesophase behavior of the star-shaped oligomers

The mesophase behavior of the discotic pentamers and heptamers were studied by polarized light microscopy and differential scanning calorimetry. The transition temperatures were first observed by polarized light microscopy and then measured accurately by differential scanning calorimetry along with the associated transition enthalpies. All the compounds exhibited enantiotropic mesophases over wide range of temperatures. Under the polarizing optical microscope all the oligomers exhibit only one transition while heating and cooling, and this transition corresponds to the mesophase-isotropic transition. While cooling from the isotropic liquid all the oligomers display characteristic optical textures of discotic columnar mesophases as shown in Figure 12-15. When cooled slowly ($1\text{ }^\circ\text{C}/\text{min}$) from the isotropic liquid large homeotropic domains (columns perpendicular to the substrate) were obtained (Figure 14) for compound **13**. The fluidity of the mesophase decreases with decreasing temperature but there is no sign of crystallization and the optical textures remain unchanged at room temperature even after months.

DSC measurements of the pentamers and heptamers revealed only one first order transition for cooling and heating runs corresponding to the mesophase to isotropic transition as noticed by POM. Table 1 summarizes the transition temperatures and their associated enthalpy values. No actual glass transition could be detected in the range between -40 °C and the clearing points of the oligomers. Pentamer **11** showed the transition from columnar to isotropic at 143.6 °C on heating and while on cooling it exhibited an isotropic to columnar transition at 139 °C. There was no other detectable transition down to -40 °C as shown in Figure 16. Pentamer **12** upon heating showed a transition at 112.5 °C while on cooling the transition is at 106 °C. Similarly the heptamers **13** and **17** exhibit columnar to isotropic transitions at 123.8 and 136.8 °C on heating and on cooling isotropic to columnar transitions at 116.7 and 132.4 °C respectively (Figure 17 and 18). In subsequent heating and cooling cycles, the transitions were highly reproducible for all the compounds. On comparing the mesophase stability (temperature range) and mesophase order (transition enthalpy) of the oligomers it is noticed that the molecular symmetry and the number of alkyl chains present in the molecules play a significant role in addition to intramolecular hydrogen bonding in pentamers.

When comparing the transition temperatures of the two pentamers, it is very clear that the intramolecularly hydrogen bonded pentamer **11** possess higher clearing temperature than its corresponding diacetate derivative **12**, it could be because the hydrogen bonded anthraquinone core has bigger size than the non-hydrogen bonded anthraquinone. Between the pentamer **11** and its corresponding heptamer **13**, the pentamer possess higher clearing temperature probably owing to its hydrogen bonding and less number of alkyl chains as compared to the heptamer but the transition enthalpies

follow the reverse trend indicating efficient packing of the heptamer in the columnar phase owing to its higher symmetry. The heptamer **17** has both the clearing temperature and enthalpy higher than the heptamer **13**, suggesting the effect of molecular symmetry and homogeneity in these oligomers. The heptamer **17** possess C_3 symmetry whereas **13** possess C_2 symmetry and **17** is made up of identical cores (homogeneous) while **13** is made up of two different kinds of discotic cores (heterogeneous).

Table 1. Phase transition temperatures (peak, °C) and associated enthalpy changes (kJ/mol, in parentheses) of the novel star-shaped pentamers and heptamers.

Compound	Heating scan	Cooling scan
11	Col _h 143.6 (23.8) I	I 139.0 (22.4) Col _h
12	Col _h 112.5 (24.7) I	I 106.0 (25.1) Col _h
13	Col _h 123.8 (35.8) I	I 116.7 (35.8) Col _h
17	Col _h 136.8 (51.0) I	I 132.4 (51.1) Col _h

4.1.2.2 X-ray diffraction studies of the oligomers

The supramolecular organization of these oligomers in the mesophase was established by X-ray diffraction studied on unoriented samples. Qualitatively all the oligomers displayed similar diffraction patterns. Table 2 summarizes the *d*-spacings and lattice parameters of all the oligomers prepared. The lattice parameters of the oligomers are comparable to the monomer analog hexapentyloxy triphenylene **6**. Figure 19 shows the intensity versus θ plot derived from the diffraction pattern of compound **11** at room temperature.

Compounds **12**, **13** and **17** exhibited similar X-ray diffraction patterns (Figure 20 and 21). In the small angle region, three peaks were observed, one very strong and two weak peaks.

Table 2. Layer spacing and intercolumnar distances for the mesophase of the discotic oligomers deduced from X-ray measurements.

Compound	<i>d</i> -Spacing (Å)	Intercolumn distance (Å)	Interdisc distance (Å)
11	16.65	19.2	3.54
12	16.90	19.5	3.56
13	17.37	20.0	3.54
17	17.44	20.1	3.56

Taken in the ascending order of diffraction angle, the *d*-spacings of the first reflection (lowest angle and highest intensity) to the other two is in the ratio of 1: $1/\sqrt{3}$: $1/\sqrt{7}$. These values correspond to those expected from a two-dimensional hexagonal lattice. In the wide angle region there are two diffused peaks; a broad one at $\theta \sim 10^\circ$ and another narrow peak at higher angles. The broad peak with a *d*-spacing of $\sim 4.4\text{\AA}$ was due to the liquid like packing of the aliphatic chains. The relatively narrow peak, which is well separated from the broader one, corresponds to a spacing of 3.5\AA and is due to the core-to-core (intracolumnar) separation. All the features fit into the well known model for the Col_h phase in which the disc-like core of the molecules stack one on top of the other to form columns surrounded by alkyl chains and these columns in turn arrange

themselves in a two-dimensional hexagonal lattice. Unlike in monomeric discotic compounds, the columns formed by the oligomers are chemically linked. No small angle peak is exhibited by any of the oligomers corresponding either to ‘super column’ or ‘super lattice’ formation, which would have led to columnar double-cable formation, arising from the ideal top-on-top stacking of the star-shaped oligomer molecules. So, the triphenylene and anthraquinone subunits arrange themselves statistically to form the columnar hexagonal phase which is also entropically more favorable. Figure 1 shows the proposed model for the formation of hexagonal columnar phase by the discotic liquid crystal pentamers.

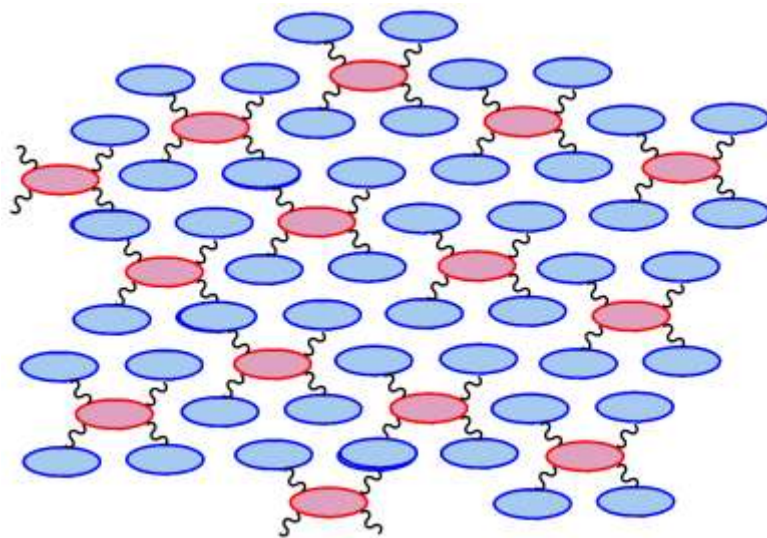


Figure 1. Proposed model for the hexagonal columnar phase exhibited by the star-shaped discotic pentamers.

In the model, the hexagonal unit cell is made up of five discotic units of the same pentamer and two discotic units from the adjacent pentamers and occasionally they share one discotic unit. However, this kind of arrangement is not strongly correlated to provide

any super lattice formation in the mesophase. The molecular dynamics in the mesophase is sufficient to offer a statistical arrangement. The heptamers possess the required number of discotic cores to build up the hexagonal lattice but they stack statistically probably because of entropic reasons thereby providing no super lattice in the mesophase. No indication of crystallization could be derived from the X-ray patterns of the oligomers, which is consistent with the experimental findings from polarizing optical microscopy and differential scanning calorimetry.

4.1.3 Conclusions

We have designed and synthesized the first examples of discotic liquid crystalline pentamers and two novel discotic liquid crystalline heptamers based on triphenylene and anthraquinone. The structural characterizations of the oligomers have been done by spectral and elemental analysis. The mesophase behavior of these star-shaped molecular double cables was studied by polarizing optical microscopy and differential scanning calorimetry. The columnar hexagonal mesophase structure of these discotic supermolecules was established from X-ray diffraction studies. The difunctional pentamers can be used as precursors for the synthesis of more novel pentamers, symmetrical and unsymmetrical star-shaped heptamers and mixed chain discotic liquid crystalline polymers containing both electron rich and electron deficient cores. These oligomers though do not form any super column but can be considered as a next step towards materials for organic photovoltaic.

4.2 Part B: Nanophase segregated mesophase morphology in self-organized disc-rod oligomesogens

One of the most active areas of research in liquid crystal science in recent years has been the search for the elusive biaxial nematic phase [17, 18], where the unique axes of the molecules arranged not only in a common direction (known as director) but also there is a correlation of the molecules in a direction perpendicular to the director (Figure 2). The hunt for this new liquid crystal phase began more than 30 years ago, when it was recognized that the molecules forming liquid crystals deviate from their presumed cylindrical shape [19]. In fact, the molecules are more lozenge-like, and it is because of this lowering of the molecular symmetry that two nematic phases should be possible. Indeed, the first claimed discovery of a biaxial nematic [20] was for a compound formed of spoon-like molecules, and similar claims soon followed for cross-shaped [21] and bone-shaped molecules [22]. Till now, there have been many claims [23, 24] for its discovery in low molar mass thermotropic liquid crystals, although experimental difficulties in unambiguously identifying the symmetry of these phases raise questions concerning these assignments. Recently, a biaxial N phase was obtained in bent core thermotropic mesogens [25].

Theoretical studies and mean field calculations [26], have shown that the biaxial nematic phase (N_b) is obtained by changing a shape biaxiality parameter (η) between a rod at one extreme ($\eta = 0$) and a disc ($\eta = 1$) at the other. The N_b phase exists over ranges such as $0.2 \leq \eta \leq 0.8$, but is most stable at $\eta = 0.4$. Such a structure is then properly intermediate between a rod and a disc, and this led to proposals that the N_b phase might be realized in rod/disc mixtures.

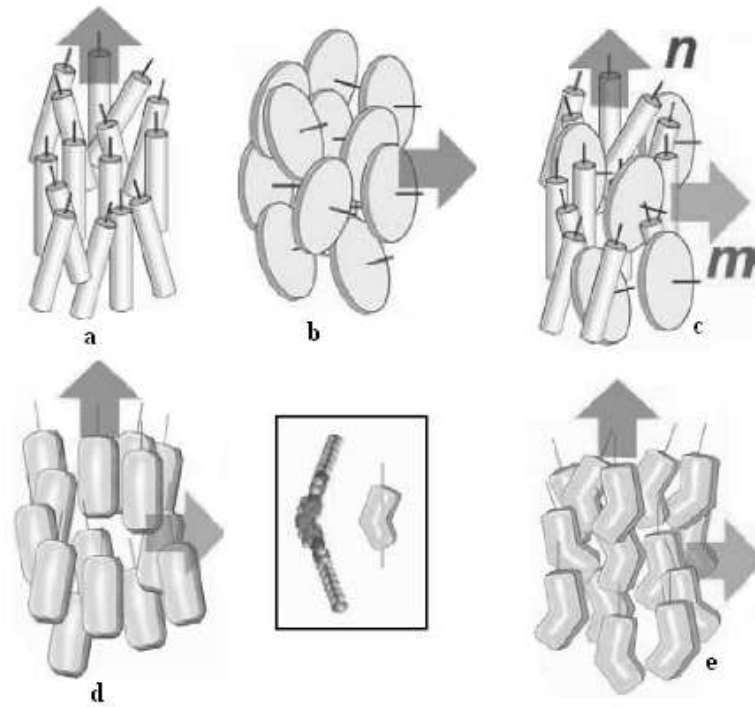


Figure 2. Schematic illustration of N phases with major n and minor m directors: (a) uniaxial N comprised of cylindrically symmetric mesogens (b) uniaxial discotic nematic (c) biaxial N phase by a mixture of rods and disks (d) biaxial nematic phase from anisotropic brick-like molecules and (e) biaxial N phase of bent-core mesogens.

In such a mixture the optimum packing arrangement has the long axes of the rods arranged perpendicularly to the short axes of the discs and hence, the system has two directors. This idea was investigated in theoretical approaches to the biaxial nematic phase formed from binary mixtures of rod- and disc-like molecules [27]. The situation with respect to physical mixtures is not so straightforward because a mixture of rods and discs should [28], and indeed does [29], separate into two uniaxial nematic phases, one rich in rods and the other rich in discs. However, theoretical work by Sharma *et al.* [30]

and by Vanakaras *et al.* [31] has shown that rod/disc mixtures can lead to N_b phases if the rod and disc are attracted more to one another than to each other.

One way to overcome this problem is to attach rod-like and disc-like units covalently via flexible alkyl spacers, so that they could not phase separate. The search for the thermotropic biaxial nematic phase prompted the synthesis of dimers consisting of one calamitic and discotic mesogenic units. The reported molecular systems are the interconnection between a rod and a disc and such dimers have recently been the subject of computer simulation study [32]. For example, Luckhurst *et al.* synthesized the first rod-disc dimers (**18**) by joining together the disc-shaped [pentakis(4-pentylphenylethynyl)] benzene and the rod shaped 4-cyanobiphenyl moieties through an ether linkage [33]. Some of these derivatives exhibited only monotropic phase behavior, probably due to the incompatibility of the discs and rods. It should be noted that the initial approaches to obtain biaxial nematic phases in disc-rod hybrid systems has been accomplished by attaching two nematogens (discotic nematogen and calamitic nematogen) to each other by various covalent linkages. They have either been attached to each other terminally or laterally. Bruce *et al.* [34] examined the molecular biaxiality which contains a pentayne disc joined to the lateral rod-like molecules (**19**). These kind of rod-disc oligomers have been considered as *shape-amphiphiles* since they are miscible with both rod- and disc-shaped liquid crystalline molecules. Mehl and coworkers [35] studied the miscibility of disc- and rod-shaped mesogens (**20**, **21**, **23**) in the N phase. Chiral nematic phase has also been obtained by adding a chiral chain to the linking unit of rods and disc **22** [36]. They also investigated multiple levels of order with N and several smectic phases in a material containing disc- and rod-like mesogenic units (**24**)

[37]. Multiple levels of order arise by combining nematogens and smectogens in the same molecule.

Recently, disc-shaped triphenylene moiety attached with three cyanobiphenyl units (**25**) has been reported [38] to form a thermodynamically stable layered phase. In these kind of systems both intra- and inter-molecular recognition of different incompatible parts leads to various novel mesophase morphologies.

The original molecular shape undergoes sufficient distortion in the mesophase leading to novel phase structures. By attaching six rod-like units radially to C_3 or C_2 symmetric central discotic cores, nematic, smectic and columnar phases have been reported.

Shimizu *et al.* reported both smectic and columnar phases in rod-disc compounds **26** [39] whereas Rahman *et al.* **27** [40], Imrie *et al.* and Jeong *et al.* **28** [41] reported nematic phase in rod-disc oligomers respectively.

Very recently Kumar *et al.*, **29** [42] Zhang *et al.* **30** [43] and Mehl *et al.* **31, 32** [44] reported both nematic and smectic phases in rod-disc hybrid oligomers.

Tricycloquinazoline (TCQ), a molecule of both biological and physical interest, is a useful core fragment for the remarkable family of discotic liquid crystals, mainly because of its extraordinary thermal and chemical stability as well as strong tendency to stack up and aggregate. The heterocyclic TCQ molecule as a central core for discotic liquid crystals is attractive for many other reasons; it possesses C_3 symmetry, its derivatives are colored and highly fluorescent, it sublimes without decomposition under atmospheric pressure at very high temperature, it tolerates strong oxidants and it is highly resistant to biological oxidation. This molecule exhibits intriguing physical

characteristics, such as low ionization potential, and interesting spectroscopic and electronic properties. The core is electron deficient in nature so that TCQ derivatives are suitable for doping with electron donors. The first organic one-dimensional n-conducting discotic liquid crystal based on TCQ has recently been reported [45].

The various liquid crystalline derivatives of TCQ include hexasubstituted thioethers **33** [46], ethers **34** [47] etc. Recently, room temperature electron deficient discotic liquid crystal **35** has been prepared from TQC by employing branched alkyl chains [48]. Very recently, layered liquid crystalline phases have been obtained from TCQ by ionic self-assembly technique [49].

In this part of the chapter, we present the design, synthesis and mesomorphism of a novel series of disc-rod oligomesogens in the search of bi(uni)axial nematic liquid crystals and to gain more insight into the structure-mesophase morphology relationship in these shape-amphiphilic oligomesogens, which seems to emerge as an independent subfield to bridge the gap between calamitic and discotic liquid crystals exhibiting both discotic and calamitic mesophases.

4.2.1 Results and discussion

The molecular design of the oligomesogens is such that six calamitic units (alkoxy cyanobiphenyls) are attached to a central tricycloquinazoline (TCQ) discotic core

radially, such type of molecular architectures are known to exhibit both calamitic and discotic mesophases. These are the first examples of radially attached rod-disc oligomers to exhibit nanophase-segregated mesophase morphology wherein rods and discs are segregated into separate sublayers to form smectic phase. Here it demonstrates the strong intermolecular interaction exhibited by the central discotic core which is reportedly evident to possess strong propensity to stack up and aggregate both in bulk state and solution and the intramolecular recognition among the calamitic units.

The synthesis of the novel disc-rod heptamers **41** is shown in Scheme 4. The ω -bromo alkoxy cyanobiphenyls (RBr) and the TCQ hexaacetate **40** are prepared following reported procedures [50, 51]. The chemical structures and purity of the prepared compounds were established by spectral and elemental analysis. The FT-IR spectra of the compounds do not exhibit any carbonyl absorption peak corresponding to acetyl group but instead shows the $-\text{CN}$ absorption peak suggesting the alkylation of all the acetyl groups in the product. Similarly the ^1H NMR spectra of the oligomers do not exhibit any proton signal corresponding to $-\text{COCH}_3$ protons but exhibit peaks corresponding to aromatic protons of cyanobiphenyl units (Figure 22). Characteristic aromatic proton signals from hexasubstituted TCQ core are observed at δ 7.71 and 6.9 ppm having equal intensity and corresponding to 3 protons. In addition, Ar-OCH_2 and $-\text{CH}_2-$ signals expected from the chemical structure are also observed having the required intensities. Similarly the ^{13}C NMR spectra of the compounds exhibit the expected carbon signals consistent with the chemical structure (Figure 23). The above spectral features and the elemental analysis data show the high purity of the compounds.

Scheme 4. Synthesis of novel disc-rod oligomesogens. *Reagents and conditions:* (i) HNO₃; (ii) Sn, AcOH; (iii) NH₄OAc, AcOH, sulfolane, reflux; (iv) 1. Pyridine, HCl, 230 °C; 2. Pyridine, Ac₂O; (v) RBr, KOH, DMSO, 40%.

4.2.1.1 Thermal phase behavior of the novel oligomesogens

The thermotropic mesophase behaviors of the compounds **41** have been studied by polarizing optical microscopy (POM) and differential scanning calorimetry (DSC). The phase transitions and their corresponding temperatures were first observed by POM and then accurately measured by DSC along with the associated transition enthalpies. Under polarizing microscope, while heating, the compounds which exhibit enantiotropic phase behavior, show solid to mesophase and mesophase to isotropic liquid transitions but the compounds in the mesophase do not display characteristic optical texture. But on cooling from the isotropic liquid, focal conic textures with homeotropic domains grow from the isotropic liquid at the isotropic-mesophase transition which is characteristic for smectic A

phase. A typical optical photo micrograph is shown in the Figure 24. The compound **41a** exhibits monotropic phase transition; on heating the compound passes from solid to isotropic liquid without any intervening mesophase but on cooling the compound displays focal conic textures followed by, surprisingly, a transition to an optically isotropic phase and then the compound crystallizes in the optically isotropic state (Figure 25). So this compound exhibits monotropic polymesomorphism. The higher homologues of the series tend to vitrify below the mesophase transition instead of crystallization while cooling.

Table 3. Phase transition temperatures ($^{\circ}\text{C}$, Peak temperature) and enthalpies (kJ/mol, in parentheses) of novel disc-rod hybrids. Cr = Crystal, SmA = smectic A, I = Isotropic, Cub = Cubic, X = glassy solid.

Compound	Heating scan	Cooling scan
41a	Cr 188.2 (105.6) I	I 173.4 (6.9) SmA 169.5 (12.4) Cub 156.4 (76.0) Cr
41b	Cr 131.0 (51.0) SmA 161.7 (17.3) I	I 159.8 (17.7) SmA 76.1 (20.2) Cr
41c	Cr 109.4 (32.0) SmA 155.6 (22.6) I	I 153.2 (22.5) SmA 63.9 (14.5) X
41d	Cr 93.5 (29.9) SmA 147.4 (23.7) I	I 144.8 (21.6) SmA

The phase transition temperatures and their associated enthalpy values collected from DSC measurements of the compounds **41** are listed in Table 3. As can be seen from the Table 3, the compound **41a** on heating passes to isotropic liquid at 188.2 $^{\circ}\text{C}$ and on cooling it exhibits two first order transitions before crystallization (Figure 26). The first transition at 173.4 $^{\circ}\text{C}$ corresponds to isotropic to smectic A phase transition, the second

one at 169.5 °C corresponds to smectic A to an optically isotropic phase transition as noticed by polarizing optical microscopy. On the basis of DSC and POM observations the second monotropic phase of the compound **41a** can be assigned as a cubic phase though its monotropic nature excludes the precise determination of the phase structure by X-ray diffraction method. This compound crystallizes in the cubic phase. Compound **41b** exhibits crystal to smectic A and smectic A to isotropic transitions on heating at 131 and 161.7 °C respectively (Figure 27). On cooling, isotropic to smectic A transition occurs at 159.8 °C whereas at 76.1 °C the compound crystallizes partially as observed in the optical microscope. Similarly the DSC thermogram of compound **41c** shows two first order transitions corresponding to crystal to smectic A and smectic A to isotropic transitions on heating, while on cooling this compound exhibits isotropic to smectic A transition at 153.2 °C and at 63.9 °C the compound undergoes a transition to a glassy solid state as was observed by X-ray diffraction studies. The compound **41d** displays similar behavior to that of compound **41c** during the DSC measurements except that while cooling no discernible transition could be obtained for smectic A to solid transition. Under polarizing microscope this compound seems to vitrify in the smectic phase. As can be noticed from the Table 3, the crystal to mesophase and the mesophase to isotropic transition temperatures decrease, as anticipated, with increase in the length of the methylene spacer connecting the discotic core to the calamitic peripheries. With increase in the spacer length, the compounds show a tendency to vitrify below the mesophase instead of crystallization. However, remarkable is the fact that the transition enthalpies of these compounds associated with the mesophase to isotropic transition are very high and are of the order of *ca.* 20 kJ/mol. Such high values of transition enthalpies suggest the

highly ordered organization of the mesogens in the mesophase [44]. Moreover the transition enthalpy values marginally increase with increase in the spacer length thereby suggesting the role of the flexible spacers towards efficient packing arrangement in the mesophase. The suppression of columnar phase and appearance of lamellar phase in these disc-rod hybrid compounds suggest that the central discotic core acts like a connecting unit to the calamitic peripheral units. The substitution of six calamitic units on the central discotic core has sufficiently distorted the gross molecular shape to exhibit calamitic mesophase. Probably because of strong recognition among the calamitic cyanobiphenyl units in the mesophase, the molecular shape is no more circular, it has been distorted to a non-circular shape by the uneven distribution of peripheral substituents around it. This type of molecular distortions is observed in cyanobiphenyl containing super molecules and dendrimers [52]. If we compare the discotic nematic behavior of recently reported molecules having identical molecular topology and containing same number of cyanobiphenyl units except the central triphenylene core to these novel oligomers [41], it seems that the bigger core size and high propensity of TCQ to stack and aggregate also plays a role in exhibiting lamellar phase than a fluid nematic phase by intermolecular recognition.

4.2.1.2 X-ray diffraction studies of the novel oligomers

The supramolecular organization of these disc-rod oligomers in the mesophase was studied by X-ray diffraction technique. X-ray diffraction experiments were carried out with samples taken in glass capillaries. The monotropic nature of the compound **41a** excludes its X-ray diffraction studies. All the other three compounds **41b-d** exhibit similar diffraction patterns in the mesophase. A typical X-ray diffraction pattern and its

derived one dimensional intensity versus θ graph are shown in Figure 28. They consist of two sharp peaks in the small angle region, whose spacings are in the ratio 1: 1/2, and a very diffuse peak at around 4.6 Å in the wide angle region. These features suggest that the mesophase is a smectic, consistent with their microscopy textures. The smectic periodicity (d) is found to be 42, 39 and 35 Å for **41d**, **41c** and **41b** respectively. In all cases the ratio of d to the length of the fully stretched molecule (l) is very close to 0.66. Interestingly, these patterns also contain a diffuse peak in the small angle region, whose spacing varies slightly with the spacer length, being 19, 17.5 and 16 Å for **41d**, **41c** and **41b** respectively. Similar diffuse peaks have been observed in the diffraction patterns of some mesogens containing both rod-like and disc-like moieties [37, 38, 44].

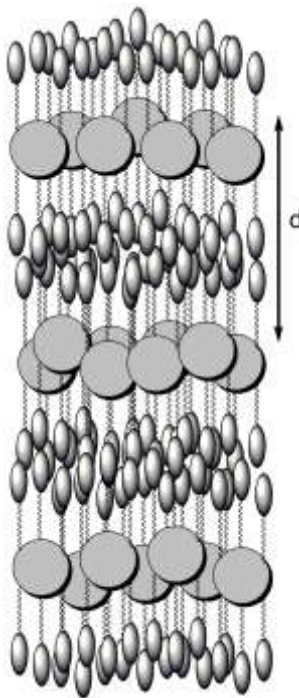


Figure 3. Proposed model for the structure of smectic phase exhibited by the novel disc-rod oligomesogens wherein the discs and rods nanophase segregate into alternating layers.

On the basis of the X-ray and microscopy data we can propose a structure for the mesophase of these compounds, which is schematically illustrated in Figure 3. In this smectic A structure the rods and discs microphase separate into alternating layers. This is made possible by the fact that the volume fraction of the disc is roughly half of that of the 6 rods in each molecule. The low d/l value of 0.66 is most probably a consequence of the conformational flexibility of the spacers, orientational disorder and partial interdigitation of the terminal-cyano groups of the rod-like segments known to occur in cyanobiphenyls [52]. We can not, nevertheless, rule out the possibility of a tilt in either/both layers. However, the observation of the microscopy textures characteristics of smectic A in all these compounds indicate that even if there is a tilt, it is not correlated across the layers. The diffuse peak in the wide angle region corresponds to the average separation of the rods and face-to-face separation of the discs, whereas the one in the small angle region arises from the side-to-side distance between the discs. As to be expected from the molecular structure, the latter increases slightly with the length of the spacer. The absence of a peak at around 3.8 Å indicates that the discs do not stack up to form long columns in the layers, but have only short-range positional correlations as in isotropic and nematic phases. From our diffraction data it is not possible to ascertain if the layers containing the discs form a two dimensional nematic or if their orientational order is also short-range. Even if the discs have long-range orientational order within each layer, the microscopy textures again suggest the lack of long-range correlations across the layers. The discotic layer will always be confined between two layers of calamitic mesogens and communication i.e. long range orientational order, between two adjacent layers of discotics seems unlikely.

4.2.2 Conclusions

A series of novel disc-rod oligomers have been designed, synthesized and their mesomorphism has been studied. These oligomers contain six calamitic alkoxy cyanobiphenyl units attached radially to a central tricycloquinazoline discotic core. These shape-amphiphilic oligomesogens exhibit nanophase segregated morphology in the smectic A phase wherein the calamitic and discotic units segregate into different sublayers. It is for the first time that this kind of hierarchical organization has been observed in oligomesogens having radial molecular topology and containing six rods. A cubic phase has also been observed for the first time in these kind of systems albeit monotropic in nature. The degree of order present in the mesophase of such systems is remarkably high. Owing to their shape-amphiphilicity it may be anticipated that calamitic and discotic mesogens with conventional mesophases may readily mix with these complex assemblies by simply inserting the liquid crystal into the appropriate layer. Study of such kind of disc-rod hybrid systems provides greater insight into the subtle intra- and intermolecular interactions involved in the self-assembling process of soft condensed matter.

4.3 Experimental

4.3.1 General information

General experimental conditions have been described in chapter 2.

4.3.2 Preparation of pentamers 11 and 12

Rufigallol **10** (60 mg, 0.2 mmol) was added to a round-bottomed flask containing ω -bromo-substituted triphenylene **8** (810 mg, 0.88 mmol) and sodium hydroxide (32 mg,

0.8 mmol) in DMSO (10 ml). The reaction was allowed to proceed at 90 °C with stirring under nitrogen for 20 hours. The reaction mixture was then extracted with chloroform, and after drying and solvent evaporation, product **11** was isolated and purified by repeated column chromatography (5% ethyl acetate in hexane) over silica gel. Finally, it was crystallized from chloroform by adding ethanol (Yield ~10%). Pentamer **11** was acetylated in acetic anhydride by adding catalytic amount of sulphuric acid and heating at 60 °C for 1 hour. Standard work-up furnished the diacetate **12** which was also precipitated from chloroform using ethanol.

Selected data for compound **11**: ^1H NMR (400 MHz, CDCl_3): δ 12.74 (s, 2H, -OH), 7.8 (s, 24H, Ar-H), 7.3 (s, 2H, Ar-H), 4.2 (t, 48H, $J = 6.4$ Hz, Ar-OCH₂-), 4.1 (m, 8H, Ar-OCH₂-), 1.2-1.9 (m, 200H, aliphatic CH₂), 0.9 (t, 60H, $J = 7.2$ Hz, CH₃); ^{13}C NMR (100 MHz, CDCl_3): δ 186.3, 157.9, 157.1, 149.0, 141.1, 128.8, 123.6, 111.7, 107.3, 104.6, 73.7, 69.7, 69.3, 30.3, 29.6, 29.2, 28.4, 26.2, 26.0, 22.6, 14.1; IR (KBr): ν_{max} 2924, 2852, 1618, 1558, 1508, 1456, 1377, 1338, 1313, 1261, 1168, 1137, 1041, 831, 721 cm^{-1} ; Elemental analysis: Calculated for $\text{C}_{234}\text{H}_{344}\text{O}_{32}$, C 76.6, H 9.45%; found C 76.1, H 9.5%; Polydispersity index (**PDI**) = 1.1.

12: ^1H NMR (400 MHz, CDCl_3): δ 7.8 (s, 24H, Ar-H), 7.6 (s, 2H, Ar-H), 4.1-4.2 (m, 56H, Ar-OCH₂-), 2.47 (s, 6H, -COCH₃), 1.2-1.9 (m, 200H, aliphatic CH₂), 0.9 (t, 60H, $J = 6.8$ Hz, CH₃); ^{13}C NMR (100 MHz, CDCl_3): δ 180.1, 169.0, 157.2, 149.0, 145.8, 143.9, 131.3, 123.6, 118.8, 108.7, 107.4, 74.0, 69.7, 69.4, 30.3, 29.6, 28.3, 26.2, 26.0, 23.0, 22.5, 20.9, 19.2, 14.1; IR (KBr): ν_{max} 2922, 2852, 1763, 1664, 1618, 1581, 1515, 1462, 1377, 1325, 1261, 1168, 1118, 1037, 831, 721 cm^{-1} ; Elemental analysis: Calculated for $\text{C}_{238}\text{H}_{348}\text{O}_{34}$, C 76.16, H 9.35%; found C 76.5, H 9.4%.

4.3.3 Preparation of heptamer 13

A mixture of rufigallol **10** (30 mg, 0.1 mmol), ω -bromo-substituted triphenylene **8** (2.77 gm, 3 mmol) and cesium carbonate (0.98 gm, 3 mmol) in NMP (2 ml) was thoroughly mixed in a glass vial and the mixture was loosely covered with a rubber septum and irradiated in a domestic microwave oven (LG, MS-192W) for 30 seconds and then the vial was taken out. After one minute the vial was again kept back and irradiated for another 30 seconds, this process was continued for 20 times and then the vial was cooled and ice water was added to it. The product was extracted with dichloromethane, after the solvent evaporation, the product was purified by repeated column chromatography (10% ethyl acetate in hexane) over silica gel. Finally, the product was precipitated from chloroform by adding excess methanol (Yield ~ 10%).

^1H NMR (400 MHz, CDCl_3) δ_{H} 7.8 (s, 36H, Ar-H from triphenylene), 7.59 (s, 2H, Ar-H from anthraquinone), 4.05-4.25 (m, 84H, Ar-OCH₂-), 1.3-1.9 (m, 300H, aliphatic CH₂), 0.96 (t, 90H, $J = 7\text{Hz}$, CH₃).

^{13}C NMR (100 MHz, CDCl_3) δ_{C} 181.2, 157.4, 153.9, 149.0, 147.0, 132.6, 123.6, 120.4, 107.5, 74.7, 74.1, 69.7, 69.1, 32.0, 31.4, 31.1, 30.9, 30.3, 29.7, 28.3, 27.3, 27.0, 26.7, 26.2, 26.0, 24.5, 23.4, 22.5, 14.0.

FT-IR ν_{max} ; 2924, 2852, 1666, 1618, 1574, 1518, 1462, 1439, 1377, 1317, 1263, 1169, 1134, 1041, 978, 827, 721 cm^{-1} .

Elemental analysis: Found: C, 77.07; H, 9.77 $\text{C}_{344}\text{H}_{512}\text{O}_{44}$ requires C, 77.20; H, 9.64%.

Polydispersity index (**PDI**) = 1.03

4.3.4 Preparation of heptamer 17

A mixture of compound **16** (90 mg, 0.05 mmol) and monohydroxy pentakispendyloxy triphenylene **7** (1.01 gm, 1.5 mmol) and cesium carbonate (0.98 gm, 3 mmol) in methyl ethyl ketone (20 ml) was refluxed for 72 hrs. The reaction mixture was cooled and filtered, after solvent evaporation the product was purified by column chromatography (10% ethyl acetate in hexane) over silica gel. Finally, the product was precipitated from dichloromethane by adding excess of ethanol (Yield, 55%).

¹H NMR (400 MHz, CDCl₃, Me₄Si) δ_{H} 7.8 (s, 42H, Ar-H), 4.22-4.19 (m, 84H, Ar-OCH₂-), 1.96-1.91 (m, 84H, aliphatic CH₂), 1.5-1.3 (m, 216H, aliphatic CH₂), 0.98-0.93 (m, 90H, -CH₃).

¹³C NMR (100 MHz, CDCl₃, Me₄Si) δ_{C} 148.8, 123.5, 107.2, 69.6, 29.7, 29.1, 28.3, 26.2, 22.5, 14.1.

FT-IR ν_{max} ; 2922, 2852, 1618, 1518, 1469, 1441, 1377, 1262, 1173, 1053, 979, 835, 721 cm⁻¹.

Elemental analysis: Found: C, 77.43; H, 9.30 C₃₄₈H₅₁₆O₄₂ requires C, 77.81; H, 9.68%.

4.3.5 Preparation of disc-rod oligomers 41

Powdered KOH (135 mg, 2.4 mmol) was mixed with DMSO (2 ml) at room temperature and stirred for 10 min. Hexaacetoxycyanobiphenyl **40** (66.8 mg, 0.1 mmol) followed by the appropriate ω -bromo alkoxybiphenyl (RBr, 2.4 mmol) was added and the reaction mixture was stirred at 55 °C for 24 h and then worked up by addition of ice-water and extracted with dichloromethane. The crude product was purified by column

chromatography (silica gel, hexane-ethyl acetate 1:1 followed by dichloromethane) and crystallized from acetone or precipitated from dichloromethane by adding ethyl acetate to afford pure yellow material in about 40% yield.

41a : ^1H NMR (400 MHz; CDCl_3 ; Me_4Si) δ_{H} 7.71 (s, 3H, Ar-H from TCQ), 7.65 (d, 12H, $J = 6.5$ Hz, Ar-H from biphenyl), 7.59 (d, 12H, $J = 6.5$ Hz, Ar-H from biphenyl), 7.49 (d, 12H, $J = 8.8$ Hz, Ar-H from biphenyl), 6.96 (d, 12H, $J = 8.9$ Hz, Ar-H from biphenyl), 6.90 (s, 3H, Ar-H from TCQ), 4.2-4.1 (m, 12H, Ar-OCH₂), 3.98-4.05 (m, 12H, Ar-OCH₂), 2.0-1.91 (m, 12H, CH₂), 1.89-1.82 (m, 12H, CH₂), 1.65-1.60 (m, 24H, CH₂). All other compounds give similar spectra except for more number of aliphatic methylene protons.

^{13}C NMR (100 MHz, CDCl_3 , Me_4Si) δ_{C} 159.7, 145.1, 132.6, 131.3, 128.3, 127.0, 119.1, 115.0, 110.1, 69.0, 67.9, 29.22, 28.9, 25.8.

FT-IR ν_{max} (KBr)/ cm^{-1} 2922, 2854, 2224, 1620, 1601, 1541, 1506, 1491, 1456, 1377, 1338, 1295, 1251, 1221, 1178, 1105, 822, 721, 667. All other compounds give similar spectra.

Elemental analysis : **41a**, Found: C, 77.64; H, 6.00; N, 7.01. $\text{C}_{135}\text{H}_{126}\text{N}_{10}\text{O}_{12}$ requires C, 77.94; H, 6.10; N, 6.73%. **41b**, Found: C, 78.20; H, 6.33; N, 5.81. $\text{C}_{147}\text{H}_{150}\text{N}_{10}\text{O}_{12}$ requires C, 78.51; H, 6.72; N, 6.23%. **41c**, Found, C, 79.30; H, 7.21; N, 5.50. $\text{C}_{159}\text{H}_{174}\text{N}_{10}\text{O}_{12}$ requires C, 79.01; H, 7.26; N, 5.79%. **41d**, Found: C, 78.90; H, 7.51; N, 5.80. $\text{C}_{171}\text{H}_{198}\text{N}_{10}\text{O}_{12}$ requires C, 79.44; H, 7.72; N, 5.42 %.

References

1. (a) M. Mas-Torrent and C. Rovira, *Chem. Soc. Rev.*, **37**, 827, (2008); (b) H. Alves, A. S. Molinari, H. Xie and A. F. Morpurgo, *Nat. Mater.*, **7**, 574, (2008); (c) L. Zang, Y. Che and J. S. Moore, *Acc. Chem. Res.*, **41**, 1596, (2008); (d) M. Cuccini, *Nature*, **5**, 605, (2006); (e) F. Chen and N. J. Tao, *Acc. Chem. Res.*, **42**, 429, (2009); (f) B. C. Thompson and J. M. J. Frechet, *Angew. Chem. Int. Ed.*, **47**, 58, (2008); (g) E. Menard, M. A. Meitl, Y. Sun, J. -U. Park, D. Jay-Lee, Y. -S. Nam, S. Jeon and J. A. Rogers, *Chem. Rev.*, **107**, 1117, (2007); (h) M. Berggren, D. Nilsson and N. D. Robinson, *Nat. Mater.*, **6**, 3, (2007); (i) N. Koch, *ChemPhysChem*, **8**, 1438, (2007); (j) Y. Sun, Y. Liu and D. Zhu, *J. Mater. Chem.*, **15**, 53, (2005); (k) H. E. Katz, *Chem. Mater.*, **16**, 4748, (2004); (l) S. R. Forrest, *Nature*, **428**, 911, (2004); (m) C. J Brabec, N. S. Sariciftci and J.C. Hummelen, *Adv. Funct. Mater.*, **11**, 15, (2001); (n) C. D. Dimitrakopoulos and P. R. L. Malenfant, *Adv. Mater.*, **14**, 99, (2002).
2. (a) S. Kumar, *Chem. Soc. Rev.*, **35**, 83, (2006); (b) F. Vera, J. L. Serrano and T. Sierra, *Chem. Soc. Rev.*, **38**, 781, (2009); (c) T. Kato, T. Yasuda, Y. Kamikawa and M. Yoshio, *Chem. Commun.*, 729, (2009); (d) S. Laschat, A. Baro, N. Steinke, F. Giesselmann, C. Hagele, G. Scalia, R. Judele, E. Kapatsina, S. Sauer, A. Schreivogel and M. Tosoni, *Angew. Chem. Int. Ed.*, **46**, 4832, (2007); (e) S. Sergeyev, W. Pisula and Y. H. Geerts, *Chem. Soc. Rev.*, **36**, 1902, (2007); (f) J. Wu, W. Pisula and K. Müllen, *Chem. Rev.*, **107**, 718, (2007).
3. (a) S. Kumar, *Liq. Cryst.*, **32**, 1089, (2005); (b) C. T. Imrie and P. A. Henderson, *Chem. Soc. Rev.*, **36**, 2096, (2007); (c) C. T. Imrie and P. A. Henderson, *Curr.*

- Opin. Colloid Interface Sci.*, **7**, 298, (2002); (d) C. T. Imrie, *Struct. Bonding*, **95**, 149, (1999); (e) C. T. Imrie and G. R. Luckhurst, In *Handbook of Liquid Crystals*; D. Demus, J. Goodby, G. W. Gray, H.-W. Spiess, V. Vill, Eds.; Wiley-VCH: Weinheim, Vol. 2B, Chapter X, p.801, (1998).
4. T. Plesnivý, H. Ringsdorf, P. Schumacher, U. Nutz and S. Diele, *Liq. Cryst.*, **18**, 185, (1995).
 5. N. C. Maliszewskyj, P. A. Heiney, J. Y. Josefowicz, T. Plesnivý, H. Ringsdorf and P. Schumacher, *Langmuir*, **11**, 1666, (1995).
 6. L. Zhi, J. Wu and K. Mullen, *Org. Lett.*, **7**, 5761, (2005).
 7. S. H. Eichhorn, N. Fox, and B. Bornais, *Mater. Res. Soc. Symp. Proc.*, **836**, L 4.6.1, (2005).
 8. A. Zelcer, B. Donnio, C. Bourgogne, F. D. Cukiernik, and D. Guillon, *Chem. Mater.*, **19**, 1992, (2007).
 9. H. K. Bisoyi and S. Kumar, *Tetrahedron Lett.*, **49**, 3628, (2008).
 10. S. Kumar, *Liq. Cryst.*, **31**, 1037, (2004).
 11. S. Kumar, *Phase Transitions*, **81**, 113, (2008).
 12. D. Adam, P. Schuhmacher, J. Simmerer, L. Haussling, K. Siemensmeyer, K. H. Etzbach, H. Ringsdorf, and D. Haarer, *Nature*, **371**, 141, (1994).
 13. S. Chandrasekhar, V. S. K. Balaguruswamy, *Proc. Royal Soc. Lond. A*, **458**, 1783, (2002).
 14. A. Cravino, and N. S. Sariciftci, *J. Mater. Chem.*, **12**, 1931, (2002).

15. (a) S. Kumar, J. J. Naidu and S. K. Varshney, *Liq. Cryst.*, **30**, 319, (2003); (b) S. Kumar and M. Manickam, *Chem. Commun.*, 1615, (1997); (c) S. Kumar and M. Manickam, *Synthesis*, 1119, (1998).
16. (a) H. K. Bisoyi and S. Kumar, *Tetrahedron Lett.*, **48**, 4399, (2007); (b) K. S. Raja, S. Ramakrishnan and V. A. Raghunathan, *Chem. Mater.*, **9**, 1630, (1997).
17. G. R. Luckhurst, *Thin Solid Films*, **393**, 40, (2001).
18. D. W. Bruce, *Chem. Rec.*, **4**, 10, (2004).
19. M. J. Freiser, *Phys. Rev. Lett.*, **24**, 1041, (1970).
20. J. Malthete, H. T. Nguyen, A. M. Levelut, *J. Chem. Soc. Chem. Commun.*, 1548, (1986).
21. S. Chandrasekhar, B. R. Ratna, B. K. Sadashiva, N. V. Raja, *Mol. Cryst. Liq. Cryst.*, **165**, 123, (1998).
22. K. Praefck, B. Kohne, D. Singer, D. Demus, P. Pelzel, D. Diele, *Liq. Cryst.*, **7**, 589, (1990).
23. G. R. Luckhurst, *Nature*, **430**, 413, (2004).
24. G. R. Luckhurst, *Angew. Chem. Int. Ed.*, **44**, 2834, (2005).
25. B. R. Acharya, A. Primak, S. Kumar, *Phys. Rev. Lett.*, **92**, 145506, (2004).
26. (a) J. P. Straley, *Phys. Rev. A*, **10**, 1881, (1974) ; (b) N. Boccara, R. Mejdani, L. De Seze, *J. Phys.*, **38**, 149, (1977).
27. R. Alben, *J. Chem Phys.*, **59**, 4299, (1973).
28. P. Palffy-Muhoray, J. R. de Bruyn, D. A. Dummur, *J. Chem Phys.*, **82**, 5294, (1985).

29. (a) R. Pratibha, N. V. Madhusudana, *Mol. Cryst. Liq. Cryst.*, **1**, 111, (1985); (b) R. Hashim, G. R. Luckhurst, F. Prata, S. Romana, *Liq. Cryst.*, **15**, 283, (1993).
30. S. R. Sharma, P. Palffy-Muhoray, B. Bergersen, D. A. Dunmur, *Phys. Rev. A*, **32**, 3752, (1985).
31. A. G. Vanakaras, S. J. McGrother, G. Jackson, D. J. Photinos, *Mol. Cryst. Liq. Cryst.*, **323**, 199, (1998).
32. M. A. Bates, G. R. Luckhurst, *Phys. Chem. Chem. Phys.*, **7**, 2821, (2005).
33. I. D. Fletcher, G. R. Luckhurst, *Liq. Cryst.*, **18**, 175 (1995).
34. (a) J. J. Hunt, R. W. Date, B. A. Timimi, G. R. Luckhurst, D. W. Bruce, *J. Am. Chem. Soc.*, **123**, 10115, (2001); (b) R. W. Date, D. W. Bruce, *J. Am. Chem. Soc.*, **125**, 9012, (2003).
35. (a) D. Apreutesei, G. Mehl, *Mol. Cryst. Liq. Cryst.*, **449**, 107, (2006); (b) D. Apreutesei, G. H. Mehl, *Chem Commun.*, 609, (2006); (c) P. H. J. Kouwer, G. H. Mehl, *J. Am. Chem. Soc.*, **125**, 11172, (2003).
36. P. H. J. Kouwer, C. J. Welch, G. Mcrobbie, B. J. Dodds, L. Priest and G. H. Mehl, *J. Mater. Chem.*, **14**, 1798, (2004).
37. P. H. J. Kouwer, G. H. Mehl, *Angew. Chem. Int. Ed.*, **115**, 6197, (2003).
38. P. H. J. Kouwer, J. Pourzand, G. H. Mehl, *Chem. Commun.*, 66, (2004).
39. Y. Shimizu, A. Kurobe, H. Monobe, N. Terasawa, K. Kiyohara, K. Uchida, *Chem Commun.*, 1676, (2003).
40. M. L. Rahman, C. Tschierske, M. Yusoff, S. Silong, *Tetrahedron Lett.*, **46**, 2303, (2005).

41. C. T. Imrie, Z. Lu, S. J. Picken, Z. Yildirim, *Chem. Commun.*, 1245, (2007); (b) K. Jeong, A. J. Jing, B. Monsdorf, M. J. Graham, F. W. Harris and S. Z. D. Cheng, *J. Phys. Chem. B*, **111**, 767, (2007).
42. S. K. Pal, S. Kumar and J. Seth, *Liq. Cryst.*, **35**, 521, (2008).
43. C. Zhang, Z. He, J. Wang, Y. Wang and S. Ye, *J. Mol. Liq.*, **138**, 93, (2008).
44. P. H. J. Kouwer and G. H. Mehl, *J. Mater. Chem.*, **19**, 1564, (2009).
45. N. Boden, R. C. Borner, R. J. Bushby and J. Clements, *J. Am. Chem. Soc.*, **116**, 10807, (1994).
46. E. Keinan, S. Kumar, S. P. Singh, R. Garlando, and E. J. Wachtel, *Liq. Cryst.*, **11**, 157, (1993).
47. S. Kumar, E. J. Wachtel and E. Keinan, *J. Org. Chem.*, **58**, 3821, (1993).
48. S. Kumar, D. S. S. Rao, and S. K. Prasad, *J. Mater. Chem.*, **9**, 2751, (1999).
49. J. Kadam, C. F. J. Faul and U. Scherf, *Chem, Mater*, **16**, 3867, (2004).
50. V. Percec, M. Lee and H. Jonsson, *J. Polym. Sci. Part A, Polym. Chem.*, **29**, 327, (1991).
51. S. Kumar, *Mol. Cryst. Liq. Cryst.*, **289**, 247, (1996).
52. (a) J. W. Goodby, G. H. Mehl, I. M. Sage, R. P. Tuffin, G. Mackenzie, R. Auzely-Velty, T. Benvegnu and D. Plusquellec, *Chem. Commun.*, 2057, (1998); (b) I. M. Sage and J. W. Goodby, *J. Mater. Chem.*, **15**, 26, (2005); (c) C. Tschierske, *J. Mater. Chem.*, **11**, 2647, (2001); (d) R. Deschenaux, B. Donnio and D. Guillon, *New J. Chem.*, **31**, 1064, (2007).

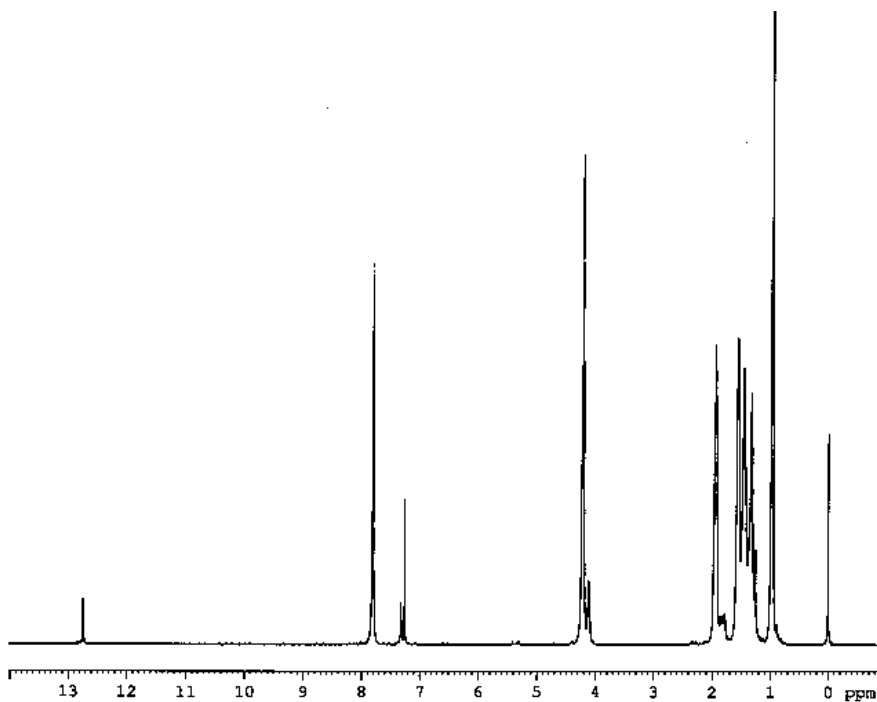


Figure 4. ¹H NMR spectrum of the pentamer **11**.

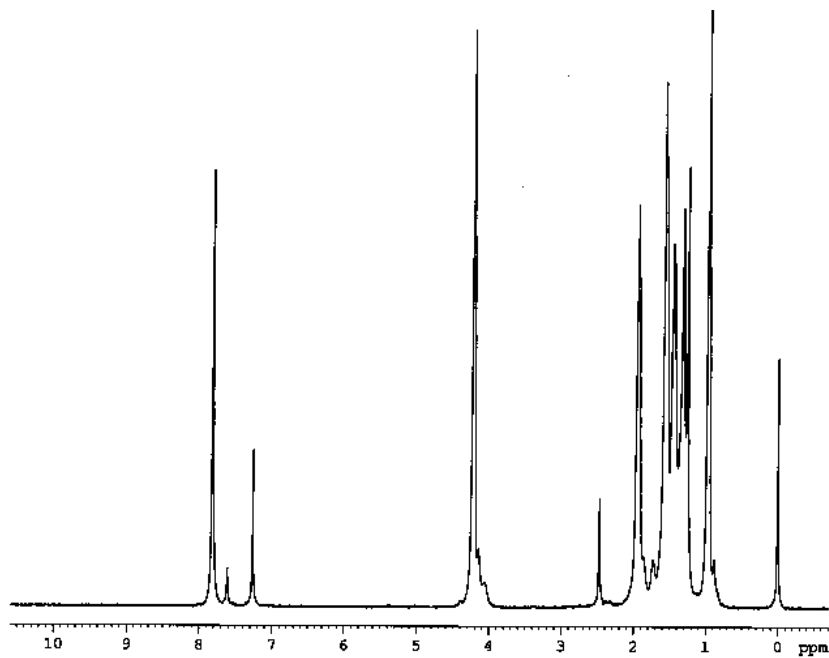


Figure 5. ¹H NMR spectrum of the diacetate pentamer **12**.

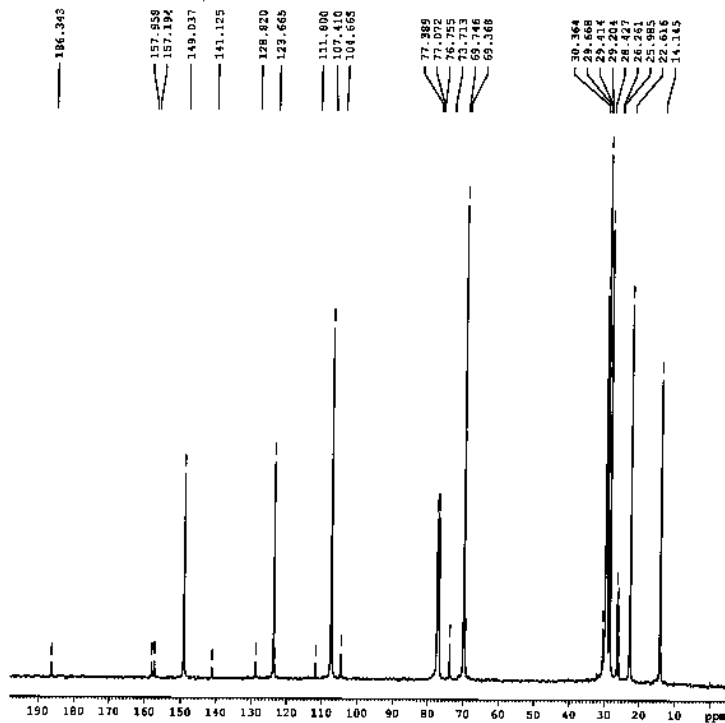


Figure 6. ^{13}C NMR spectrum of the pentamer **11**.

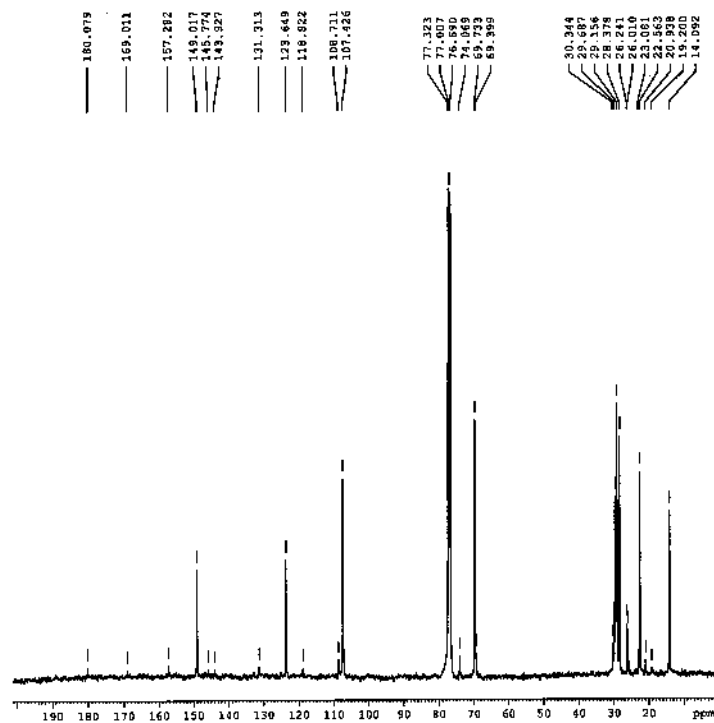


Figure 7. ^{13}C NMR spectrum of the diacetate pentamer **12**.

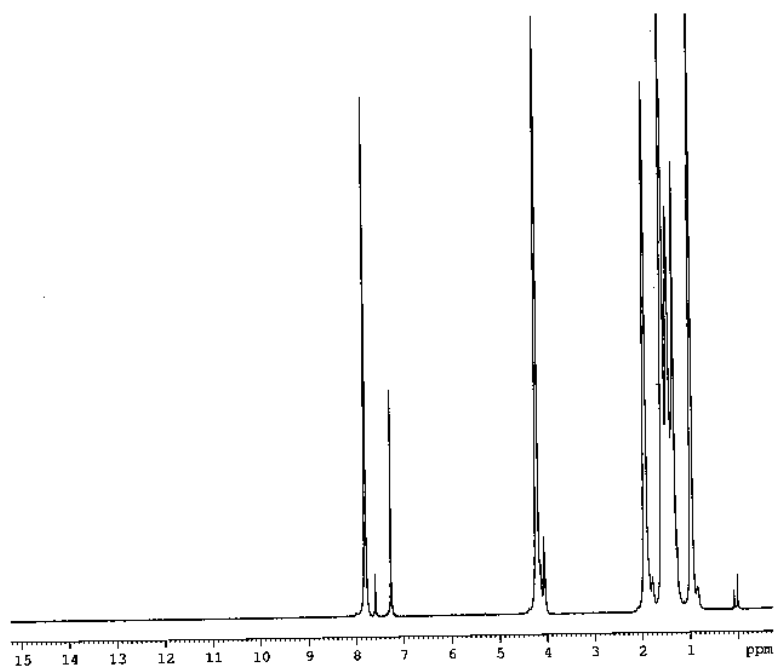


Figure 8. ^1H NMR spectrum of the discotic heptamer **13**.

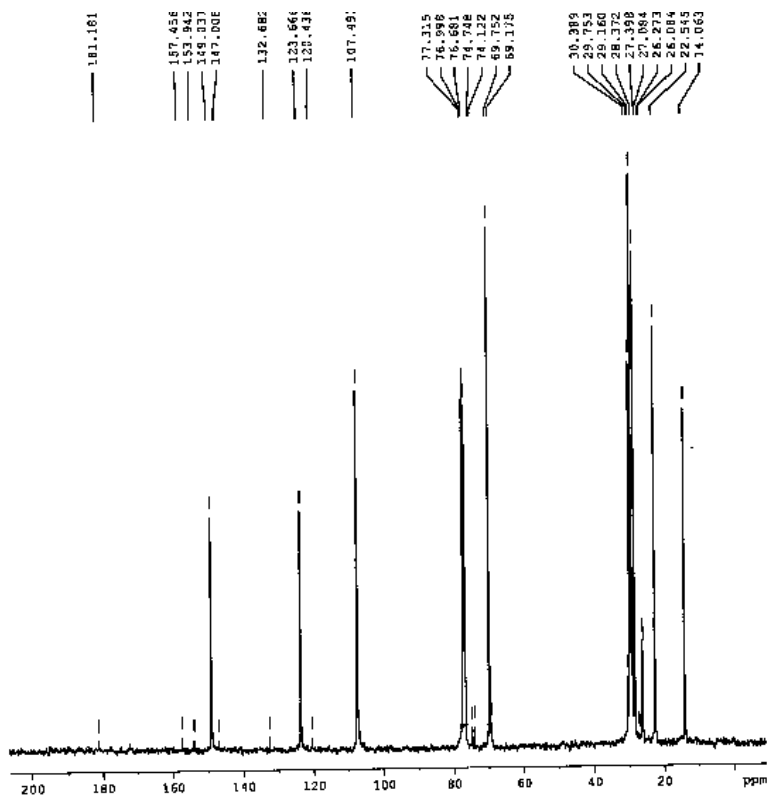


Figure 9. ^{13}C NMR spectrum of the discotic heptamer **13**.

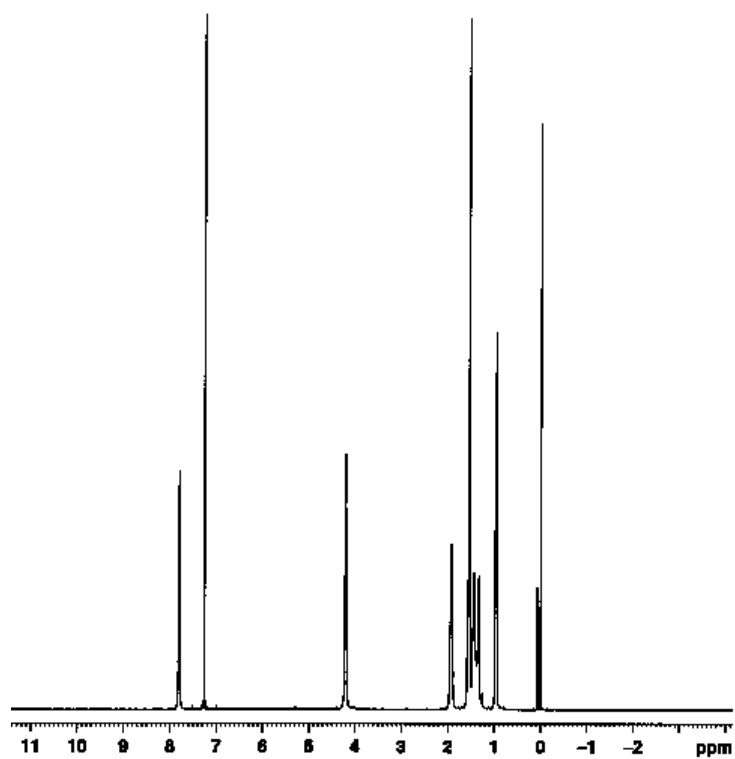


Figure 10. ^1H NMR spectrum of the triphenylene based heptamer **17**.

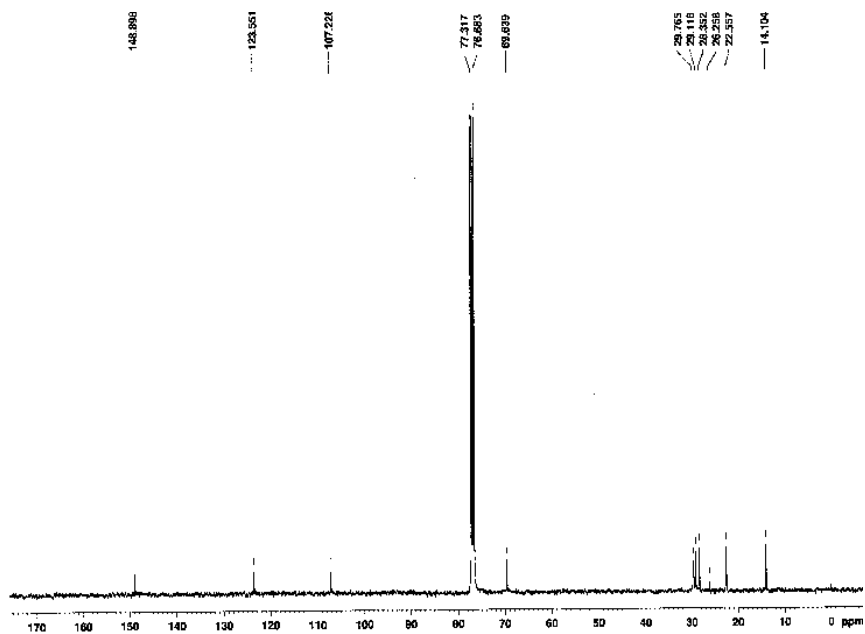


Figure 11. ^{13}C NMR spectrum of the triphenylene based heptamer **17**.

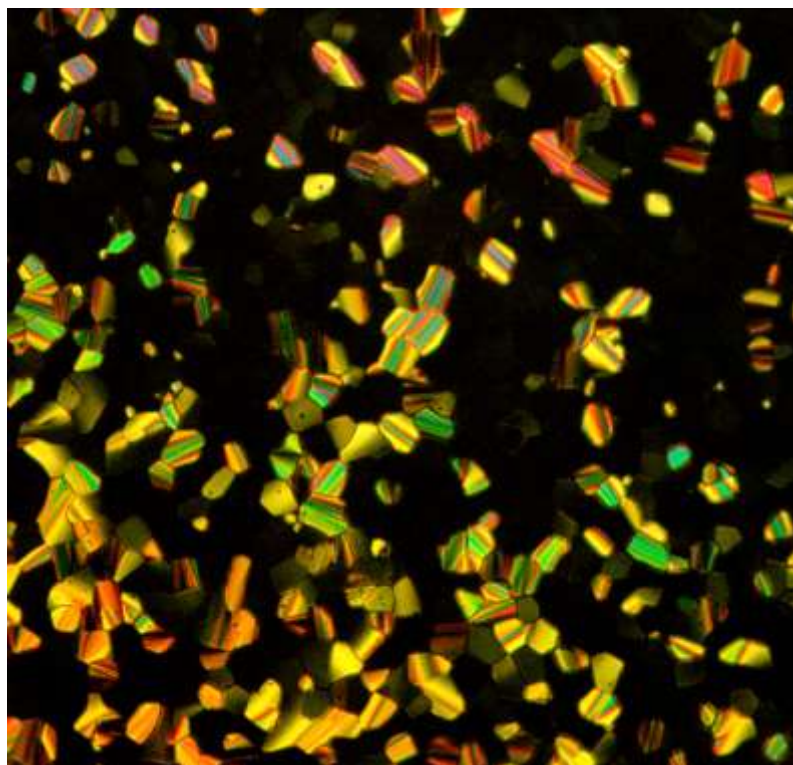


Figure 12. Optical photomicrograph of Compound **11** at 25 °C on cooling from the isotropic liquid (crossed polarizers, magnification X 200).

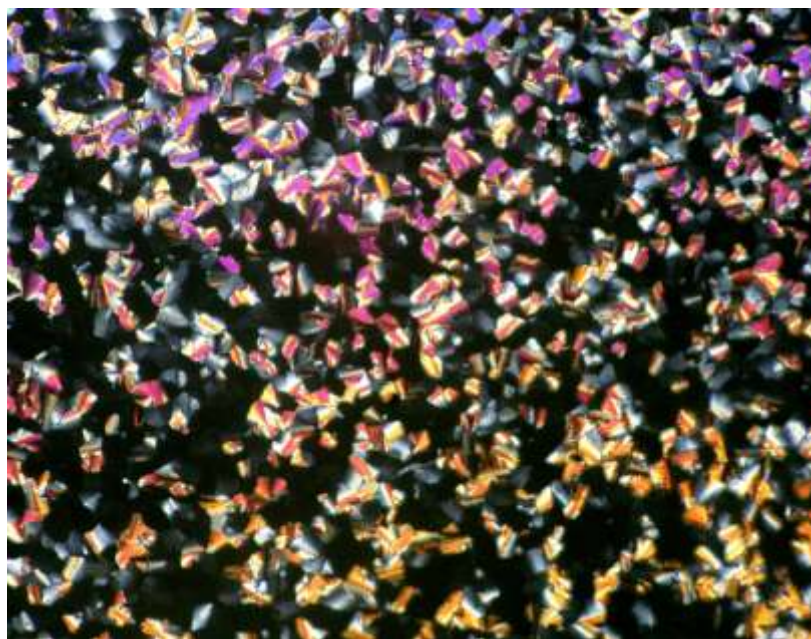


Figure 13. Optical photomicrograph of compound **12** at 25 °C on cooling from the isotropic liquid (crossed polarizers, magnification X 200).

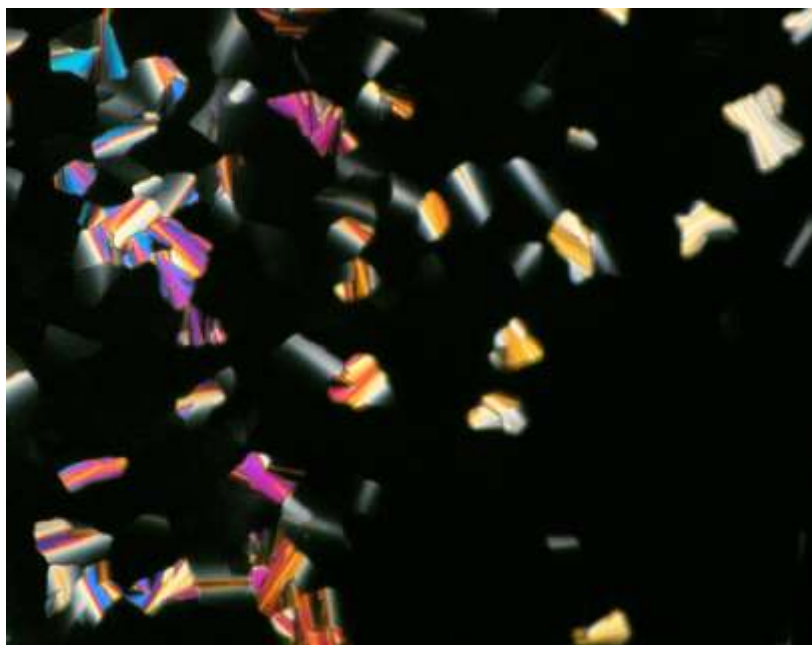


Figure 14. Optical photomicrograph of compound **13** at 25 °C on cooling from the isotropic liquid (crossed polarizers, magnification X 200).

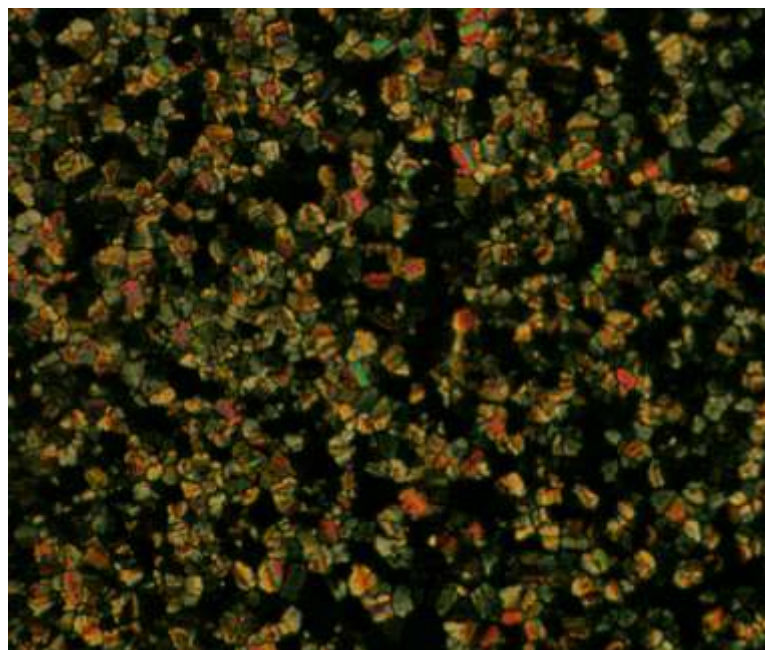


Figure 15. Optical photomicrograph of compound **17** at 25 °C on cooling from the isotropic liquid (crossed polarizers, magnification X 200).

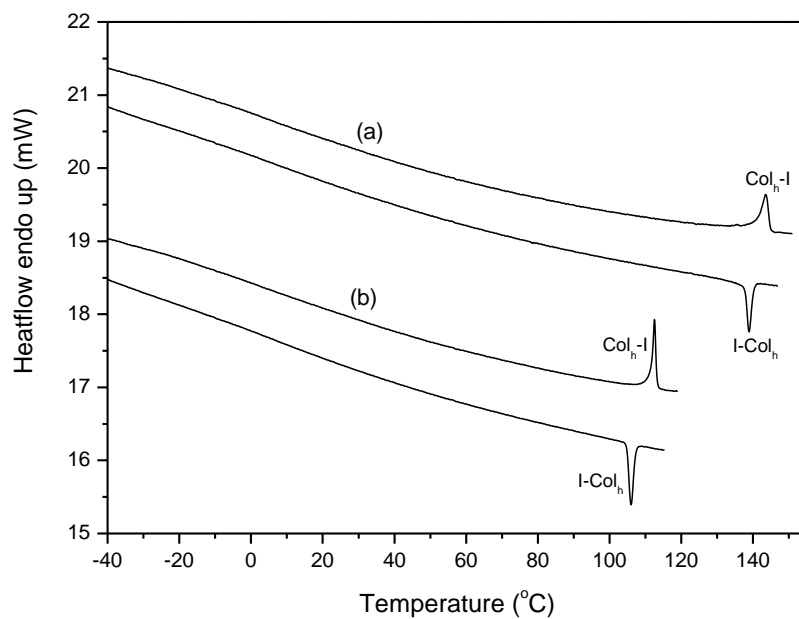


Figure 16. DSC thermograms for **11** (a) and **12** (b) on heating and cooling (scan rate of 5 °C/min.).

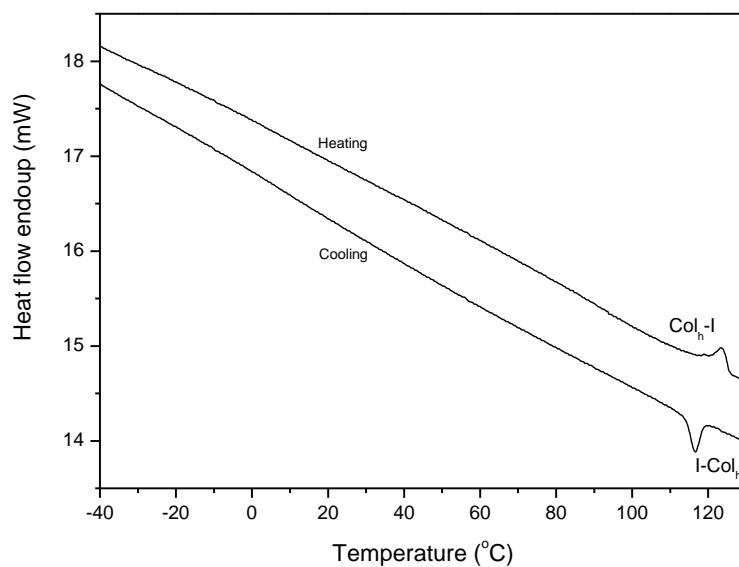


Figure 17. DSC thermogram of compound **13** on heating and cooling (scan rate of 5 °C/min.).

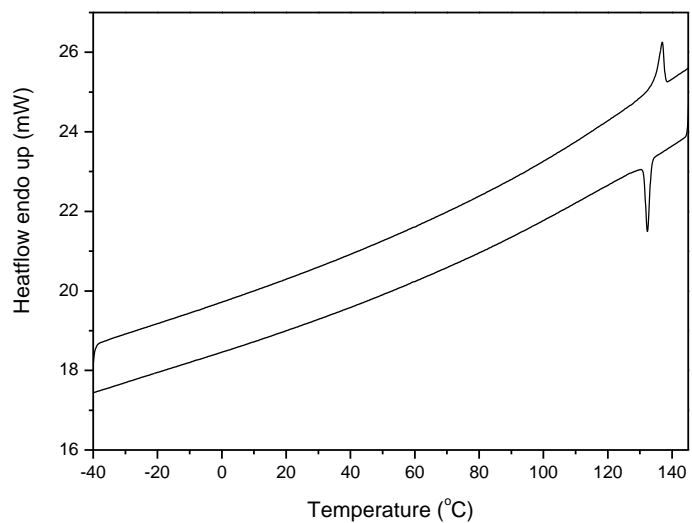


Figure 18. DSC thermogram of compound **17** on heating and cooling (scan rate of 5 °C/min.).

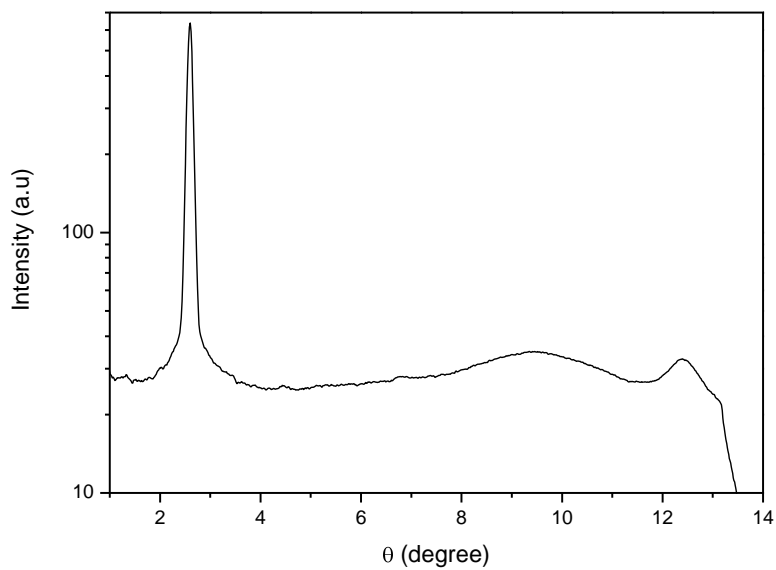
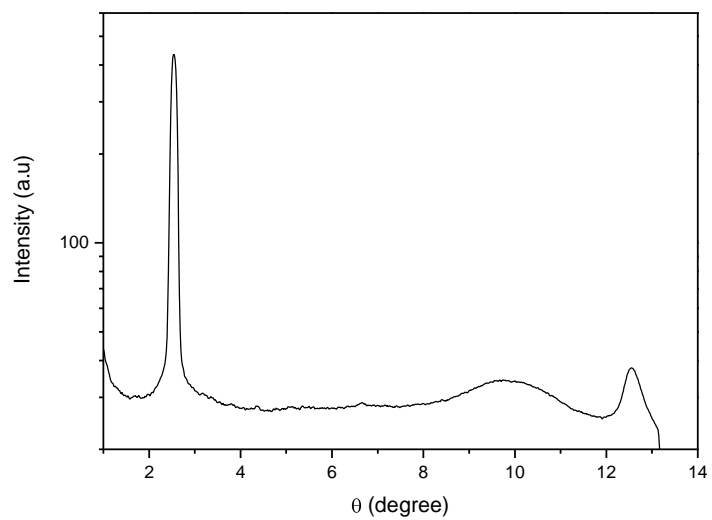


Figure 19. The one-dimensional intensity vs θ profile derived from the X-ray diffraction pattern of **11** at 25 °C.



(a)

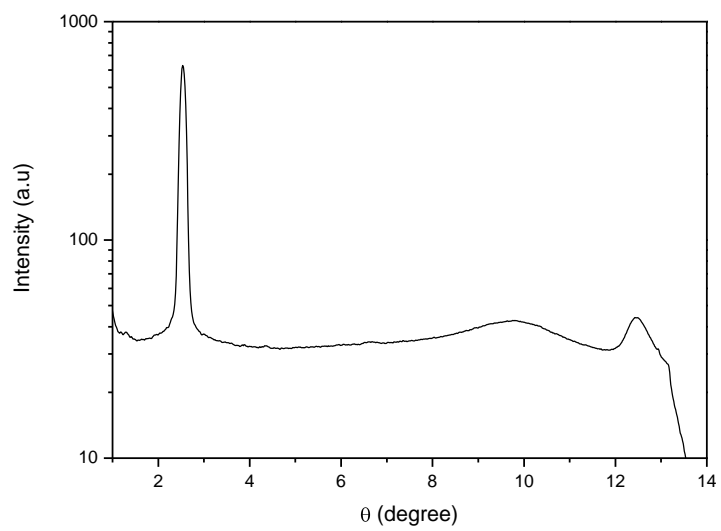


(b)

Figure 20. The one-dimensional intensity vs θ profile (b) derived from the X-ray diffraction pattern (a) of **13** at 25 °C.



(a)



(b)

Figure 21. The one-dimensional intensity vs θ profile (b) derived from the X-ray diffraction pattern (a) of compound **17** at 25 °C.

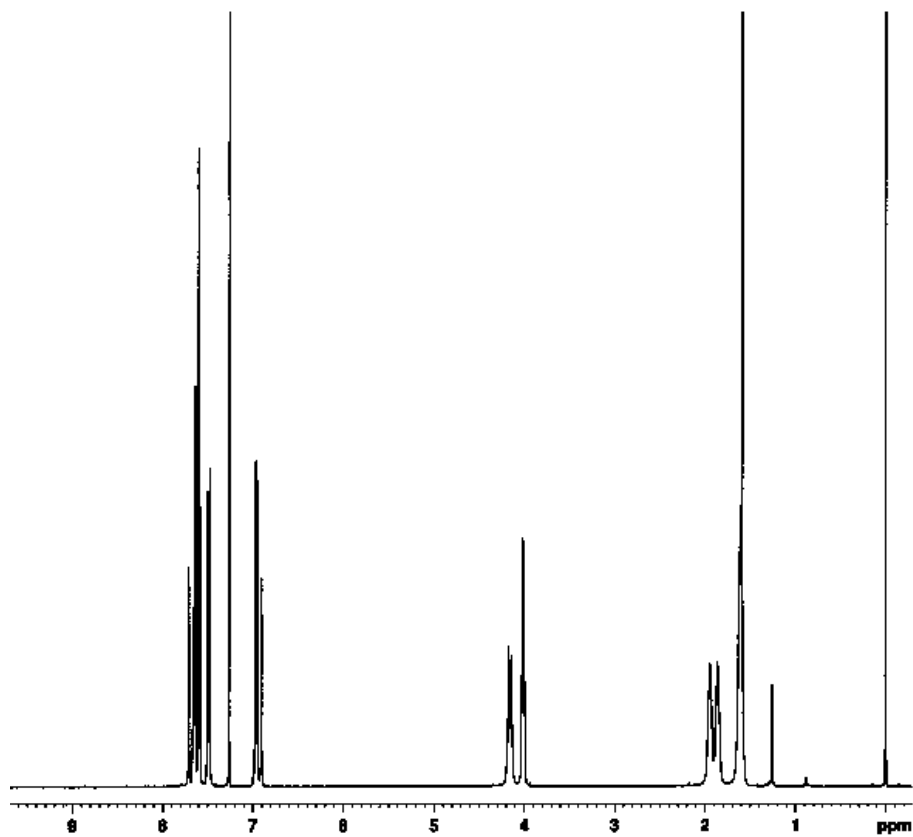


Figure 22. ^1H NMR spectrum of the disc-rod oligomesogen **41a**.

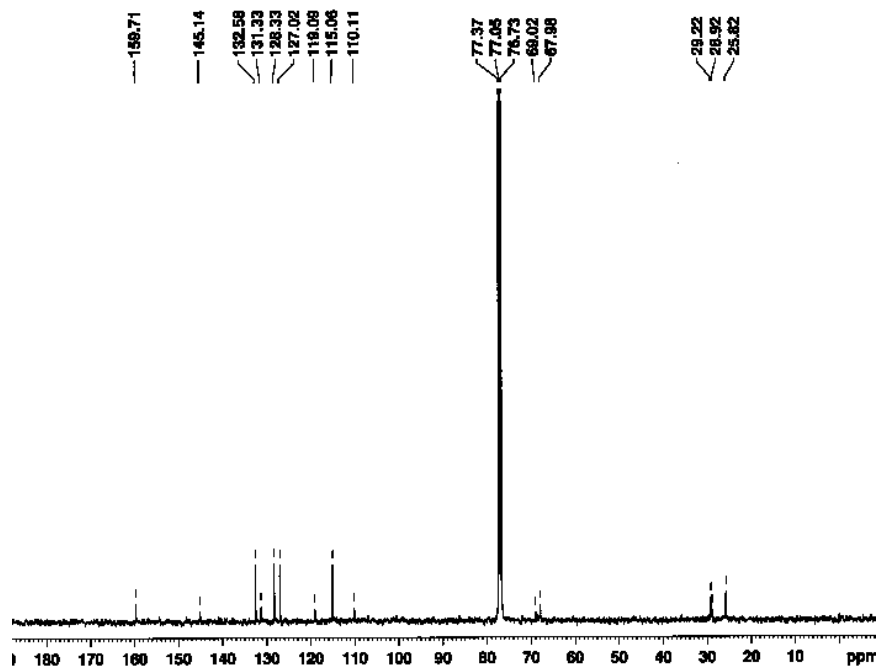


Figure 23. ^{13}C NMR spectrum of the disc-rod oligomesogen **41a**.

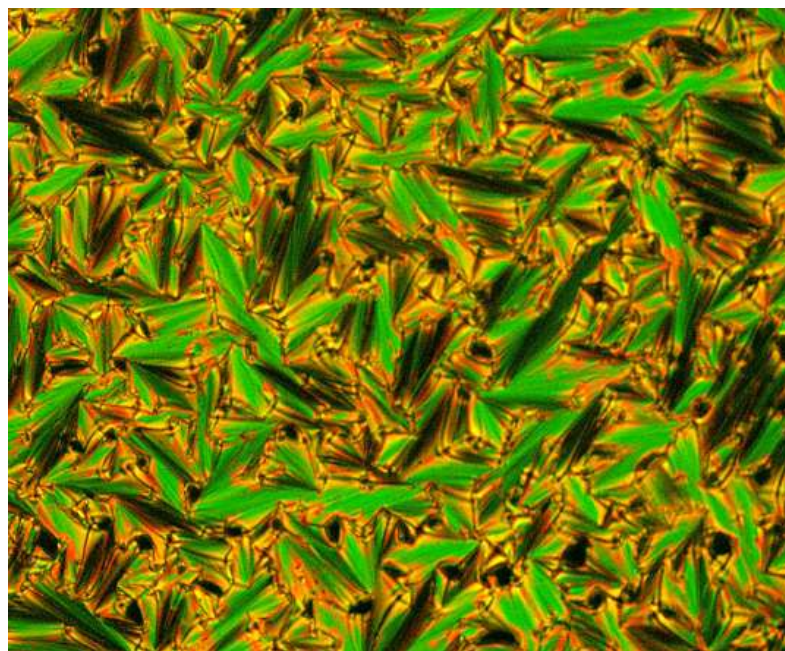


Figure 24. Optical photomicrograph of compound **41c** at 145 °C on cooling from the isotropic liquid (crossed polarizers, magnification X 200).

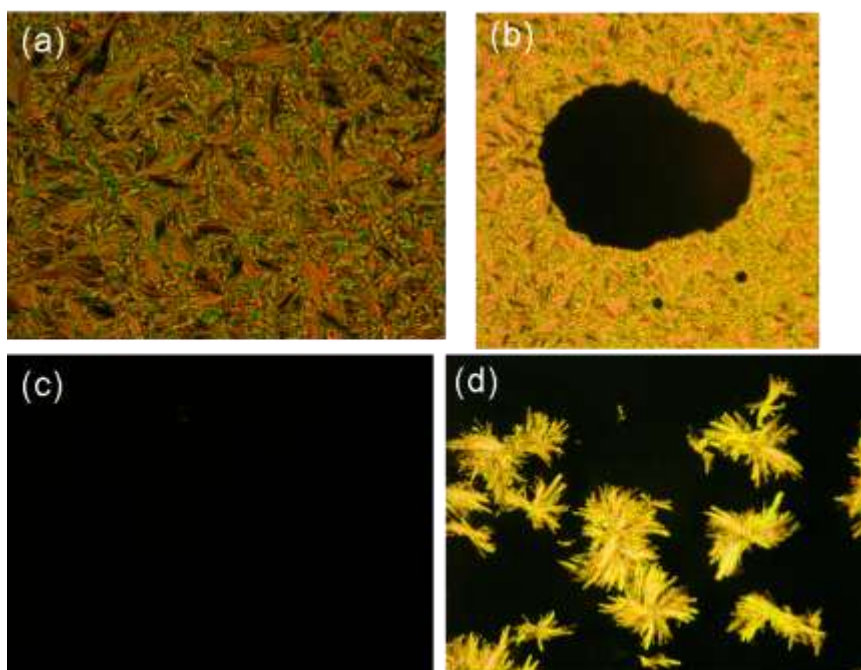


Figure 25. Optical photomicrographs of compound **41a** in the smectic A phase (a) and cubic phase (c). (b) and (d) are showing transitions to cubic and crystalline phase respectively. Crossed polarizers (magnification X 200).

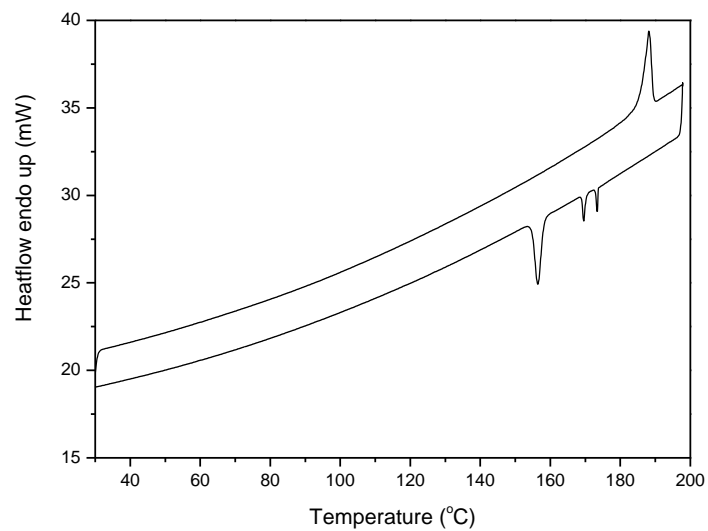


Figure 26. DSC thermogram of compound **41a** on heating and cooling (scan rate of 5 °C/min.).

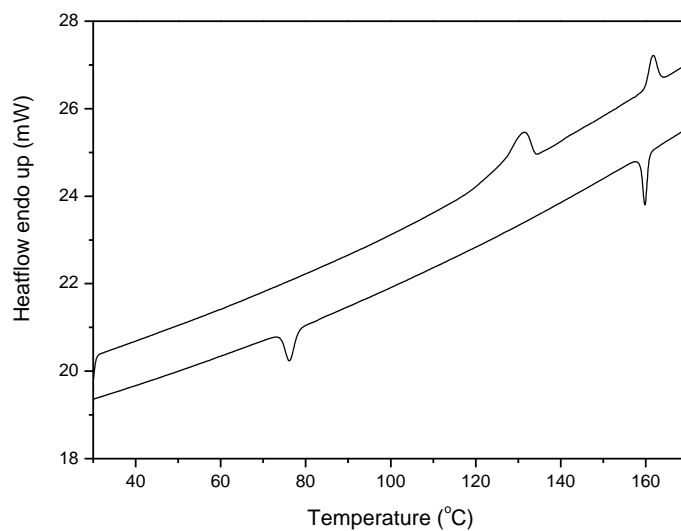
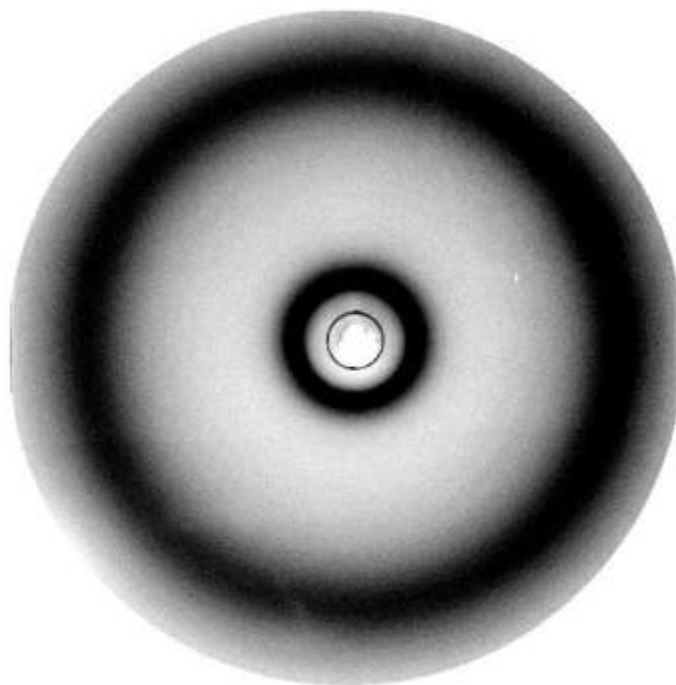
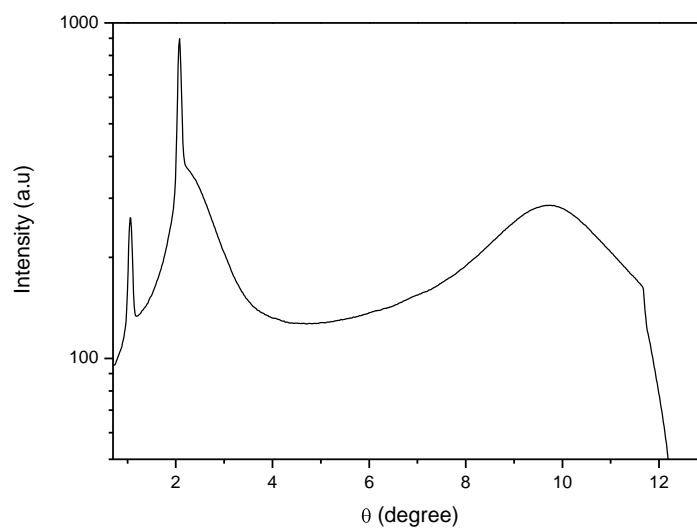


Figure 27. DSC thermogram of compound **41b** on heating and cooling (scan rate of 5 °C/min.).



(a)



(b)

Figure 28. The one-dimensional intensity vs θ profile (b) derived from the X-ray diffraction pattern (a) of compound **41d** in the mesophase.

CHAPTER 5

Functionalized Carbon nanotubes in the supramolecular order of discotic liquid crystals

5.1 Introduction

The serendipitous discovery of carbon nanotubes (CNTs) by Iijima in 1991 has generated tremendous activity in most areas of science and technology as a result of their unprecedented physical and chemical properties [1]. CNTs, the fourth allotrope of carbon, after diamond, graphite and fullerene, are one dimensional, well ordered all-carbon hollow cylinders of graphite with a high aspect ratio.

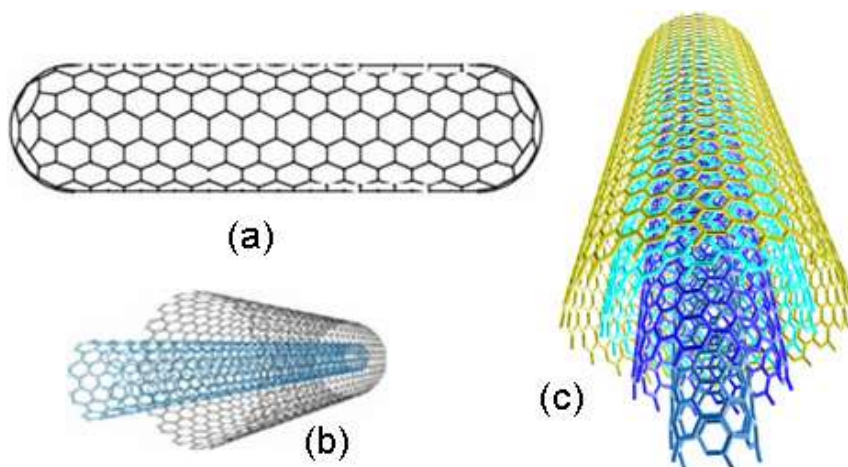


Figure 1. Carbon nanotubes (a) single walled, (b) double walled and (c) multiwalled.

Generally CNTs are classified in two categories based on their structure and dimensions: single-walled carbon nanotubes (SWNT), which consist of one layer of cylindrical

graphene and have diameters from 0.4-2.0 nm and lengths in the range 20-1000 nm; and multi-walled carbon nanotubes (MWNT), which contain several concentric graphene sheets and greater dimensions with diameters in the range of 1.4-100 nm and lengths from 1 to a few microns (Figure 1). Recent progress in synthesis has allowed the production of tubes with exactly two concentric carbon sheets, and hence the introduction of the concept of double-walled carbon nanotubes (DWNT) [2]. SWNTs can be either metallic or semiconducting depending on the sheet direction about which the graphite sheet is rolled to form a nanotube cylinder. CNTs can be prepared by several methods, such as, chemical vapour deposition (CVD), carbon arc-discharge methods, high pressure carbon monoxide (HiPCO) method and laser ablation. These preparation methods yield random mixtures of tubes of various diameters, chirality, length distributions and different electronic properties [3]. All SWNTs and MWNTs are synthesized using catalysts, hence metal nanoparticles are likely to be present along with unwanted carbon particles such as graphite, amorphous carbon and non-tubular fullerenes. Carbon nanotubes are chemically extremely inert and practically insoluble. Strong van der Waals interactions between adjacent nanotubes promote clustering into crystalline ropes which in turn aggregate into strongly entangled and unorganized networks or bundles. Different protocols for post-growth CNT fractionation according to chirality and diameter have recently been described [4]. Different methods to separate semiconductive CNTs from conductive CNTs have been developed and exploited in their applications [5]. Synthetic strategies to chemically modify the side wall or tube-end by molecular or biomolecular components have been reported to obtain purified and soluble carbon nanotubes [6]. Other common techniques used to functionalize CNT are noncovalent exohedral with

polymers and surfactants and endohedral functionalization with fullerenes, etc [7]. The combination of superlative mechanical, thermal and electronic properties displayed by SWNTs and MWNTs make them ideal for a wide range of applications, such as, conductive and high-strength composites, catalyst supports in heterogeneous catalysis, energy-storage and energy-conversion devices, field emitters, transistors, sensors, gas storage media, tips for scanning probe microscopy and molecular wires. A large number of biomedical applications of CNTs have also been envisaged and demonstrated [8]. The synthesis, characterization, physical properties and applications of CNTs have been extensively covered in several reviews [9]. Despite the extraordinary promise of CNTs, their realistic application as one-dimensional conductors or semiconductors has been restricted because of difficulties in aligning them in the desired direction. Well-arrayed CNTs are highly desirable for the preparation of a variety of nanodevices, particularly where one dimensional charge migration is important. Recent studies have proved that the alignment of CNTs plays a critical role in the properties of nanotube based materials [10]. There have been several attempts to develop well-aligned CNTs during growth by the chemical vapor deposition (CVD) process [11]. One of the earliest reported methods of aligning MWNTs is based on cutting thin slices (50-200 nm) of a CNT-polymer composite [12]. Various other methods to align CNTs have been proposed by applying magnetic and electric field, shear flow or mechanical techniques. However, processing materials with well-controlled CNT alignment still remains a challenge.

There has been growing interest in the field of dispersion of CNTs in both thermotropic and lyotropic liquid crystalline (LC) phases besides mesophase behavior of CNTs themselves and preparation of CNTs from discotic liquid crystals [13]. One of the

most important applications of optoelectronic devices based on liquid crystals is liquid crystal display (LCD). To optimize the performance of an LCD, it usually requires prior knowledge of physical parameters of the LC mixture, such as the elastic constants of deformation, dielectric and optical anisotropies, conductivity and rotational viscosity. Mixing CNTs into thermotropic LC hosts has become one of the attempted approaches to modify the physical properties of LCs along with CNT alignment in LC matrix. LCs have the long range orientational order rendering them to be anisotropic phases. If CNTs can be well dispersed in LC matrix, they will in general align with their long axes along the LC director (Figure 2) to minimize distortions of the LC director field and thus the free energy. Dispersion of CNTs in LCs can provide us a cheap, simple, versatile and effective means of controlling nanotube orientation on macroscopic scale with no restrictions on nanotube type.

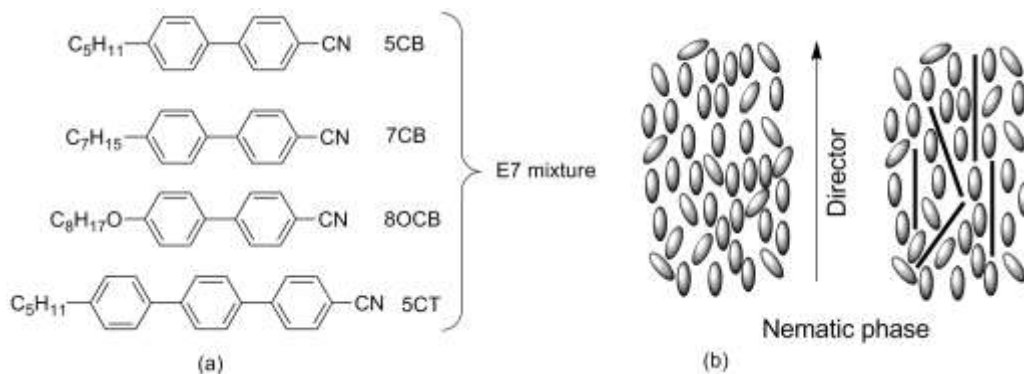


Figure 2. Commercial E7 mixture (a) and alignment of carbon nanotubes in nematic phase (b).

The advantages of thermotropic LCs in this context are twofold. One, using existing alignment techniques, well developed for display industry, the ground state of the LC and

hence of the dispersed CNTs can easily be determined on macroscopic scale. Second, the easy and speed of changing the director field by means of electric or magnetic fields can lead to switches based on reorientation of CNTs. The most commonly used thermotropic LCs for dispersing CNTs are E7 and 5CB which are shown in Figure 2. To our knowledge, the first report on doping of carbon nanotubes in liquid crystals is by Lee and Chiu in the year 2001 after one decade of CNTs discovery, who observed self-diffraction by gratings in nematic liquid crystals doped with multiwalled carbon nanotubes [14]. In the same year 2001, on the basis of continuum-based density functional theory, Somoza *et al.* proposed that CNTs should form a columnar phase or lyotropic liquid crystalline phase in the presence and absence of van der Waals interactions [15]. Subsequently, Lee *et al.* have observed efficient coherent light amplification with very high gains [16], discovered the scenario pertaining to the surface-sustained permanent gratings [17] and strong beam coupling effects [18] in nematic liquid crystal and carbon nanotube mixtures. However, the work of Lynch and Patrick in 2002 caught the attention when they achieved high degree of CNT alignment along the nematic director field by taking the advantage of self-assembly properties of nematic liquid crystals and then removing the LC by vacuum suction leaving the CNTs alignment intact [19]. Khoo *et al.* have observed an extremely large electro-optically induced photorefractive effect in nematic liquid crystals doped with SWNTs and explained the basic mechanisms and conditions necessary for such nonlinearities [20]. It has been shown that doping with nanotubes can effectively reduce the DC driving voltage and improve the switching behavior of a twisted nematic-LC cell [21]. Voltage-dependent transmittance and capacitance under AC and DC electric field showed that the residual DC, which is related to an image

sticking problem in liquid crystal displays, was greatly reduced due to the ion trapping by CNTs following strong charge transfer from the adjacent LC molecules [22]. Similarly under applied AC voltage the electro-optical properties of CNT doped TN-LCD cells are rectified by reducing the driving voltage and rise time [23]. Huang *et al.* have studied the electro-optical characteristics of twisted nematic (TN) mode and chiral homeotropic liquid crystal mode cells filled with +ve and -ve dielectric anisotropy liquid crystals doped with CNTs [24]. The improved electro-optical characteristics of the cells were attributed to the viscosity of the LC mixture. Comparison of SWNT and MWNT doped twisted nematic cells shows that MWNTs are superior additives to SWNTs which is attributed to metallic character of MWNTs [25]. Local deformation of liquid crystal director induced by translational motion of carbon nanotubes under in-plane field was studied in a CNT-doped nematic LC cell [26]. The CNTs were well aligned with the LC director, when a critical AC field was applied, the CNTs began translational motion between the electrodes as a result of electrophoretic motion thereby causing deformation of local director field. Minute addition of carbon nanotubes suppress the undesired field screening effect and increases the charge mobilities in the presence of a strong field which is attributed to the parallel alignment of both the long axis of carbon nanotubes and the nematic director along the electric field [28]. The influence of CNTs on the elastic constant was studied and it was found that CNTs increase the effective elastic constant of the LC-CNT dispersions [28]. Rotational viscosity is the most practical physical parameter for designing a fast response LC device. It has been shown that rotational viscosity of the LC is decreased by doping the CNT additive [29]. The effect of CNTs on the electro-optical characteristic of the IPS (in-plane switching) mode is studied which

shows that the effective retardation value of the CNTs-doped LC cell was reduced and its operation voltage was increased slightly compared with that in the pure LC cell [30]. Dierking *et al.* have studied the alignment and reorientation of doped carbon nanotubes in LC cells under both electric and magnetic fields along with the change in the conductivity of the LC cell upon reorientation of the CNTs with the liquid crystal director field [31]. Recently, they have also studied the reorientation dynamics of CNTs in liquid crystal medium [32]. Very interestingly, Cervini *et al.* have aligned MWNTs by a template assisted method using a homeotropically aligned liquid crystalline monomer that was subsequently polymerized to a rigid polymeric material which led to retention of the orientation of both the mesogens and more importantly the nanotubes [33]. This should be a promising route towards achieving composite materials with novel functionality or enhanced electrical, mechanical and/or thermal properties due to the presence of aligned CNTs at sufficient concentration. Da Cruz *et al.* have dispersed SWNTs in nematic LC, the materials were studied by X-ray scattering and observed unusual responses to magnetic fields [34]. Preparation of nanotube gel was reported by Islam *et al.* [35]. Nematic elastomers with aligned carbon nanotubes exhibiting reversible infrared and electromechanical actuation [36], and superelongation of carbon nanotube aggregates in liquid crystal medium [37] is also reported. The effect of carbon nanotubes on phase transitions of nematic liquid crystals and antiferroelectric chiral smectic liquid crystals are also reported [38]. In contrast to alignment of CNTs with liquid crystals, the alignment of liquid crystals has been achieved by CNTs as well [39]. Scalia *et al.* have studied the interaction between CNTs and liquid crystal molecules by Raman spectroscopy [40]. To understand the alignment of CNTs in LC medium and the dynamic

response of CNTs under an external field, theoretical studies have been carried out to reveal the interaction between CNTs and LC by using density functional calculations. The study shows that there is a considerable charge transfer from LC molecule to the CNT which induces a permanent dipole moment on the CNT and this plays an important role for electro-optical responses of CNTs in the LC cells [41].

There are less examples of inclusion of carbon nanotubes into lyotropic liquid crystals. However, as lyotropic LCs are water based and common in biological and living systems, it could be very interesting to use CNT-lyotropic LC mixtures for biotechnological applications. Unfortunately, recent toxicological studies of CNTs indicate that CNTs could be as harmful as asbestos and, therefore, extensive studies are required before their *in vivo* medical application.

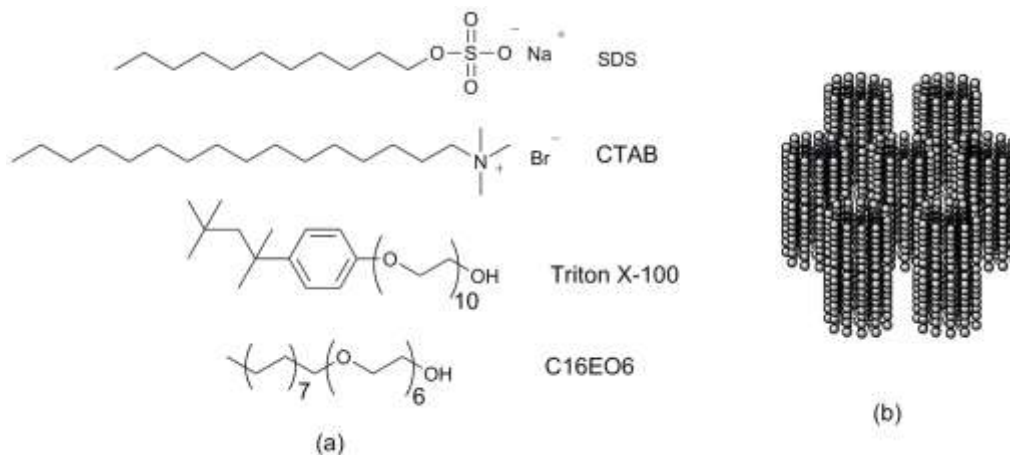


Figure 3. Common surfactants used for the dispersion of carbon nanotubes (a) and the columnar hexagonal phase formed by these surfactants in aqueous medium (b).

In contrast to thermotropic LC-CNT composites, the lyotropic LC-CNT composites can be prepared in two different ways. One can start by preparing an isotropic

low-surfactant-concentration suspension of CNTs and then that can be made liquid crystalline by adding more quantity of surfactant (Figure 3) or it can be added to an already prepared lyotropic liquid crystal sample. The insertion of CNTs into lyotropic liquid crystalline phases was first investigated in 2006 by Weiss *et al.* [42]. They observed that both the d -spacing and viscosity of the hexagonal columnar phase increased with increase of carbon nanotube concentration. Subsequently, Lagerwall *et al.* have aligned carbon nanotubes in the lyotropic nematic liquid crystals formed by both rod shaped and disc shaped micelles (Figure 4) [43]. Raman measurements indicated that the nanotubes are aligned along the LC director and allowed the determination of the order parameter.

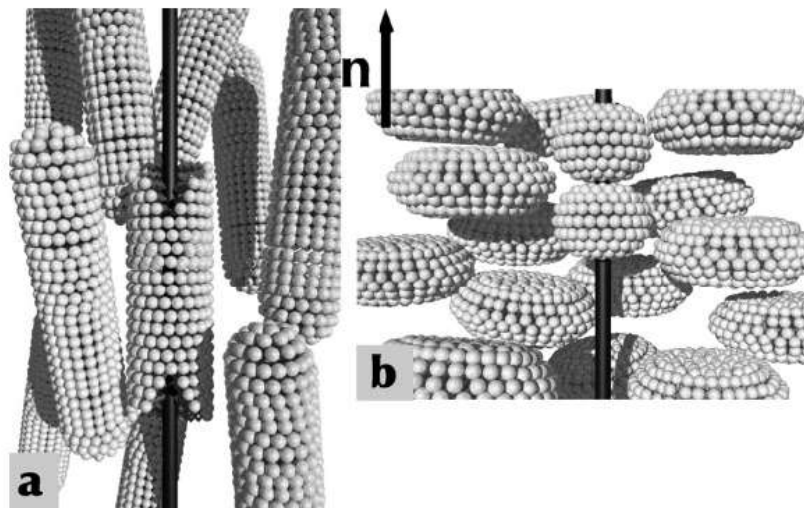


Figure 4. Alignment of carbon nanotubes by lyotropic nematic liquid crystals formed by cylindrical (a) and disc-shaped (b) micelles.

Jiang *et al.* have dispersed carbon nanotubes in a lyotropic liquid crystal formed in room-temperature ionic liquids [44]. As observed earlier, here also it was observed that the d -

spacing as well as the viscosity of the medium was increased with increase in nanotube concentration. Recently, it was observed that CNTs incorporate into ordered lyotropic liquid crystalline phase while preserving the native d -spacing [45]. Very recently, Lagerwall *et al.* have combined cat- and anionic surfactants to form a liquid crystalline colloidal suspension of carbon nanotubes, which by virtue of the spontaneously formed hexagonal columnar LC structure, are uniaxially aligned over macroscopic areas [46]. The nanotube concentration is so high that thin and highly aligned filaments can be drawn and deposited in selected directions on arbitrary surfaces, after which the LC template can be rinsed away to yield an unprecedented degree of control in the practical realization of carbon nanotube based devices and materials.

Carbon nanotubes can be viewed as highly anisometric rigid rod-like particles. Like other anisotropic and one dimensional molecules, CNTs can form lyotropic liquid crystalline phase. This research field has been developed by the groups of Windle, Poulin and Smalley. The basis for this phenomenon is the classical Onsager argument for liquid crystal phase formation in concentrated suspensions of rigid rods; if the aspect ratio of the rods and their concentration are both large enough the free energy of the system is reduced by forming a nematic phase [47]. Several experimental contributions have been reported, all of them describing different ways of making liquid crystalline phases of carbon nanotubes in solution. These systems form nematic phases via acid functionalization, acid protonation, gradual evaporation or absorption of amphiphilic molecules. The first report describing the nematic liquid crystalline phase behavior of MWNTs was in 2003 by Song *et al.* [48]. Later this group studied in detail the isotropic-nematic transitions in dispersions of MWNTs [49]. They have also exploited the

mesophase behavior of CNTs to separate short nanotubes from longer nanotubes which have strong tendency to form liquid crystalline phases [50]. Recently they have reported the size-dependence and elasticity of liquid crystalline multiwalled carbon nanotubes [51]. Lyotropic liquid crystalline phases of SWNT have been achieved by protonating the side walls of CNTs in strong acids [52]. The protonation of SWNTs sidewalls eliminates van der Waals interactions and promotes the dispersion process, at higher concentrations SWNTs form nematic phases. Another approach to obtain liquid crystalline phase from unmodified SWNT is reported by Badaire *et al.* [53]. They have dispersed CNTs by non-covalent wrapping of denatured DNA to CNTs which exhibits nematic phase but retains the intrinsic properties of CNTs. The liquid crystalline behavior of CNT solutions has been exploited to fabricate highly oriented carbon nanotube arrays for thin film transistors [54]. Liquid crystal behavior of SWNTs dispersed in biological hyaluronic acid solutions has been stabilized and studied [55]. Recently pyrene functionalized poly methyl methacrylate (PMMA) has been used for non-covalent functionalization of MWNTs which at high concentration self organize into ordered domains and hence exhibit liquid crystalline phase in PMMA as well as in PEG 400 matrices [56]. This offers the potential to align nanotubes at high volume fractions. While nematic phases have been experimentally reported, no evidence of smectic phases of carbon nanotubes has ever been shown. The observation of a smectic phase of rods necessitates a polydispersity as narrow as possible; the actual polydispersity of carbon nanotubes does not allow the formation of lamellar phases.

Preparation of carbon nanotubes typically requires high temperature or high pressure. It is well known that in these cases the reactions are chemically complicated

and difficult to control and one serious problem is the separation of the catalysts from the nanotube product as typically most of the catalyst particles are encapsulated into the nanotubes. Moreover, the orientation of the graphene layers in the nanotubes is important from their application point of view. To form ordered graphite nanostructures without metal catalysts and with desired graphene layer orientations, one possible approach is carbonization within a discotic columnar mesophase. From this point of view, the columnar super structures of discotic liquid crystals are worth precursors as the molecules possess a nano graphene subunit as the aromatic core and these molecules stack one on top the other to build up columns which in turn organize themselves in different two dimensional lattices. Upon carbonization under a controlled heating process the preorganized ordered columnar superstructures can be converted into nanotubes. Mullen *et al.* have produced nanotubes from thermotropic discotic liquid crystals [57], whereas Crawford *et al.* [58] have produced nanotubes from both thermotropic and lyotropic discotic liquid crystals. Pyrolysis of well-defined discotic molecules in the bulk state produced novel carbon nano and microstructures. The temperatures are much lower than the normally used graphitization temperatures (2000-3000 °C). Recently a template method has been used to fabricate uniform carbon nanotubes by pyrolysis of graphitic molecule hexabenzocoronene (HBC) in porous alumina membranes. Graphene molecules aligned along the channels and kept the order under slow heating procedures, after the template removal uniform carbon nanotubes with ordered graphene orientations were obtained in quantitative yield. Interestingly, the orientation of the graphene layers is perpendicular to the tube axis due to the preorganization of the disc-like molecules in the template. This is different from the case of normal carbon nanotubes, in which the

graphene layers are parallel to the tube axis. Discotic molecules can also be converted into 1D carbon nanotube with well-controlled graphene layers orientation under template directed solid state pyrolysis process. Hill *et al.* have reported a unique approach to self-assembled graphitic nanotubes from an amphiphilic hexabenzocoronene (Figure 5) [59]. In sharp contrast to the above nanotubes, their nanotubes consists of graphitic wall formed from numerous molecular graphene sheets stacked parallel to the long axis of the tube. The proposed structure of the nanotube consists of helically rolled-up bilayer tapes composed of π -stacked HBC units, where the inner and outer HBC layers are connected by interdigitation of the hydrophobic alkyl chains while the hydrophilic ethylene oxide chains are located on both sides of the tubular wall. The π -stacked HBC units provide a charge carrier transport pathway. Suitable chemical modification of the amphiphilic HBCs results in the formation of nanotubes with various interesting physical properties.

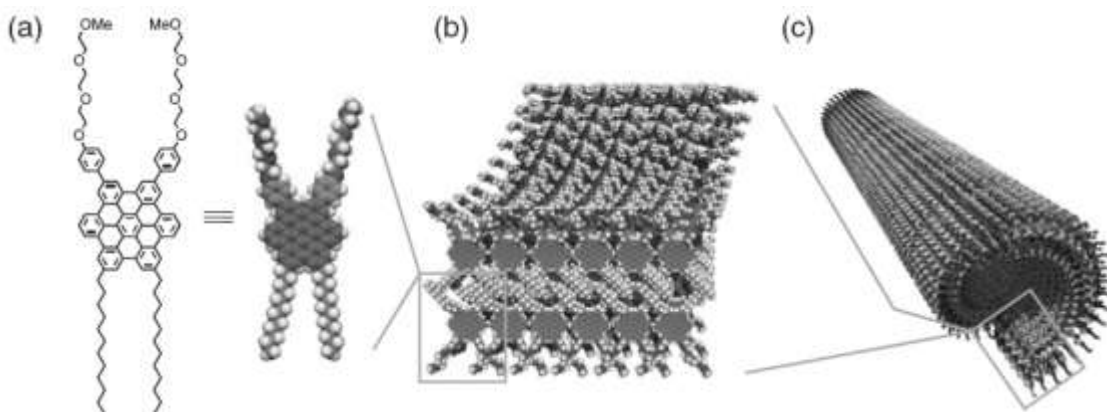


Figure 5. Schematic structures of (a) HBC amphiphile, (b) self assembled bilayer tape and (c) graphitic nanotube.

Another interesting thing about these nanotubes is the formation of discotic columnar mesophase upon heating these graphitic nanotubes. Properties of liquid crystalline materials confined to restricted geometries are important from their potential applications point of view in electro-optics but imaging the molecular ordering in nanoscale confinements is very difficult. Recently Crawford *et al.* have obtained images of liquid crystalline ordering by covalently capturing discotic liquid crystals filled in multiwalled carbon nanotubes followed by carbonization. This shows face-on anchoring of the molecules due to strong π - π interaction at the interface [60].

The insertion (dispersion) of CNTs in the supramolecular order of discotic liquid crystalline monomers and polymers may lead to novel materials with interesting properties useful for device applications. The ordered columnar phases, in contrast to isotropic and nematic phases, can offer wider opportunity for processing material with oriented nanotubes, a critical factor considering the strongly anisotropic properties of CNTs. Moreover, there are a lot of similarities between CNTs and discotic liquid crystals; first, both CNTs and DLCs are anisotropic materials. Second, both the materials possess self-assembling properties and often form hexagonal aggregates. Third and more important is the one dimensional (1D) conductivity properties of both CNTs and DLCs. Conductivity along the columnar axis of DLCs is several orders of magnitude greater than perpendicular to it [61], so also in CNTs, the conductivity along the CNT axis is much more higher than across the axis. Therefore, both the materials can be considered as “molecular wires”. With this in mind, we have initiated a research program to disperse functionalized CNTs into the columnar matrix of liquid crystalline discotic monomers and polymers [62].

5.2 Results and discussion

At the beginning, we attempted to disperse acid-purified SWNTs into the columnar matrix of hexabutyloxy triphenylene (H4TP) in minute quantities but we observed that the purified CNTs form aggregates in the columnar phase which can be clearly seen under polarizing optical microscope (Figure 7). It should be noticed that H4TP is a crystalline solid material at room temperature and forms a highly ordered plastic columnar phase at high temperature [63]. Unlike the thermotropic calamitic nematic phase described above it fails to disperse purified CNTs adequately. Then we turned towards chemical functionalization of carbon nanotubes to make them compatible with the discotic liquid crystal matrix and to see if these functionalized nanotubes exhibit any mesomorphism themselves. The acid-purified and carboxylic acid-functionalized carbon nanotubes were chemically functionalized at the ends and sidewalls by a hydroxyl functionalized H4TP derivative (Scheme 1). SWNTs **5** were purchased from Carboxlex Inc., (USA)-AP grade and purified as reported [64]. The resultant carboxylic acid groups-terminated SWNTs were converted into acid chloride groups (SWNT-COCl, **6**) by treatment with thionyl chloride (Scheme 1). The hydroxyl-terminated triphenylene **4** was prepared by the etherification of monohydroxy-pentabutyloxytriphenylene **3** with 1-bromohexanol under classical reaction conditions and fully characterized from its spectral and elemental analysis. Discotic-functionalized SWNTs **7** were prepared by mixing SWNT-COCl **6** with hydroxyl-terminated triphenylene **4** and heating at 80 °C for 48 hr under anhydrous reaction conditions. The product was purified by column chromatography over silica gel. These functionalized SWNTs (f-SWNTs) were highly soluble in common organic solvents like, dichloromethane, chloroform, THF, etc. The

formation of discotic-functionalized SWNTs was confirmed by IR, ^1H NMR, ^{13}C NMR and TGA studies. The FT-IR spectrum of discotic-functionalized SWNTs displays clearly the ester carbonyl stretching at 1737 cm^{-1} (Figure 8).

Scheme 1. Functionalization of carbon nanotubes with triphenylene based discotic liquid crystalline compound.

The ^1H NMR signals are compatible with the successful covalent attachment of the triphenylene units to the SWNT. The $-\text{OCH}_2$ signal for hydroxyl-terminated triphenylene **4** shifts from 3.6 ppm (Figure 9) to 4.1 ppm which is expected for an ester functionality (Figure 10). The ^{13}C NMR also supports the functionalization of SWNTs.

The signal at δ 62.9, corresponding to the carbon connected to -OH group (Figure 11), shifts to δ 68.9 for the carbon connected to -COO- group (Figure 12). However, no carbonyl carbon signal was detected. This could be because of the very long relaxation times of the nanotube carbons [65]. The thermo gravimetric analysis displays two partially overlapping peaks in the region 200-400 °C (approximately 60% weight reduction) which may be attributed to the loss of triphenylene units. The high temperature (450-650 °C) weight loss of about 40% is likely due to the loss of SWNTs. However, the triphenylene-capped SWNTs **7** were found to be non-liquid crystalline. The waxy-solid melts at about 40 °C to the isotropic phase.

Scanning tunneling microscopy (STM) imaging of the discotic functionalized carbon nanotubes has been carried out in constant current mode on highly oriented pyrolytic graphite (HOPG) surface using +100 mV sample bias voltage and 1 nA tunneling current to get the size of the individual carbon nanotubes. The image is shown in Figure 13. Small and large aggregates of functionalized carbon nanotubes are seen in the Figure 13. The average lengths of the aggregates vary from 70 to 100 nm.

Liquid crystalline composites of functionalized SWNTs (f-SWNTs) and triphenylene-based discotic liquid crystal namely hexabutyloxytriphenylene (H4TP) were prepared by sonicating the two components in dichloromethane followed by removal of solvent and drying in vacuum. Three compositions (by weight) of f-SWNTs: H4TP (**7a**: 2% f-SWNTs; **7b**: 5% f-SWNTs and **7c**: 10% f-SWNTs) were prepared and analyzed by differential scanning calorimetry and polarizing optical microscopy. All the f-SWNTs-H4TP composites **7a**, **7b** and **7c** were found to be liquid crystalline in nature. They show classical textures of columnar mesophase upon cooling from the isotropic phase (Figure

14). Data obtained from the heating and cooling cycles of DSC are collected in Table 1. The DSC traces obtained on heating and cooling runs for pure H4TP and composite **7c** are shown in Figure 15. The insertion of CNTs decreases the mesophase-isotropic transition temperatures significantly but the crystals to mesophase transitions do not change much. This is logical as the insertion of CNTs is expected to reduce the ordering of the cores. Similar effects have been observed on the insertion of gold nanoparticles into a discotic liquid crystalline matrix [66].

Table 1. Phase transition temperatures ($^{\circ}\text{C}$, peak) and transition enthalpies (J/g in parentheses) of SWNT-DLC composites on heating and cooling cycles. Cr = crystal, Cr* = partially crystallized, Col_p = columnar plastic phase, Col_h = hexagonal columnar mesophase, I = isotropic.

Composite	Heating	Cooling
H4TP	Cr 89 (37) Col _p 146 (31) I	I 144.1 (31) Col _p 79.6 (3.6) Cr*
7a	Cr 89 (37) Col _h 143 (23) I	I 140.6 (22.8) Col _h 78.8 (3.8) Cr*
7b	Cr 90 (35.4) Col _h 142 (19) I	I 138.5 (18.9) Col _h 78.8 (3.7) Cr*
7c	Cr 89.6 (30.6) Col _h 135 (11) I	I 134.1 (11.5) Col _h 78.5 (3.4) Cr*

The X-ray diffraction patterns were recorded for composite **7c** and for pure H4TP under same conditions at 125 $^{\circ}\text{C}$. X-ray data for H4TP were in agreement with the reported data [67]. The one-dimensional intensity vs. 2θ profile for the composite **7c** is

shown in Figure 16. The overall features observed are consistent with the structure of the Col_h phase. It should be noted that pure H4TP forms a more ordered Col_p phase [67] which is characterized by three-dimensional crystal-like order in a hexagonal lattice, while the discs within the columns are able to rotate about the columnar axis.

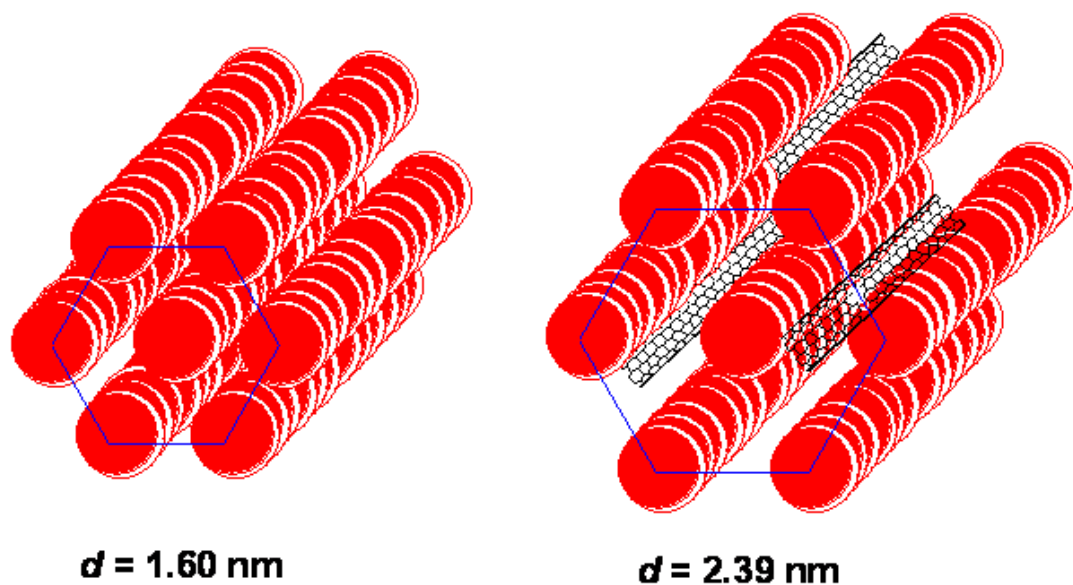


Figure 6. Schematic representation of the insertion of SWNTs in the supramolecular order of a columnar mesophase. The significant shift of about 0.8 nm in the reflection toward larger d spacing demonstrates insertion of SWNTs in the hexagonal columnar phase.

The insertion of SWNT allows the positional freedom of discs and thus, all the composites display classical Col_h phase. A significant shift of 0.8 nm in the reflection toward larger d spacing for the composite **7c** was observed. While pure H4TP exhibits reflections with d spacing corresponding to 1.61 nm, it was 2.39 nm in the case of composite **7c**. This clearly indicates the insertion of SWNT in the supramolecular order

of the columnar phase. A schematic representation of the insertion of SWNTs in the columnar mesophase is shown in Figure 6.

The DC conductivity studies of the H4TP and H4TP: f-CNTs nanocomposites were carried out in ITO coated glass sandwich cells (10mm x 5 mm) with a inter electrode separation of 50 μm . Current measurements were carried out using a Keithley pico ammeter (Model 480) along with a constant voltage source and a temperature controller. The Figure 17 shows the DC conductivity values measured at different temperatures for pure H4TP (inset) and the mixture of 2%, 5% and 10% of f-CNTs and H4TP nanocomposites while cooling from isotropic temperature. There is a significant increase in DC conductivity by two orders of magnitude upon doping with 10 % f-CNTs. The measured conductivity values also increase with increasing temperature. Changes in the slopes of the conductivity–temperature plots are observed for all the compositions. For example for the 10% f-CNT doped sample the conductivity begins to increase around 80 $^{\circ}\text{C}$, indicative of phase transition from crystalline to columnar mesophase. The changes in conductivity during phase transition is also indicative of more mobile charge carriers in the mesophase, which can be explained by less lateral interactions between H4TP and triphenylene functionalized CNTs.

The increase in electrical conductivity of the nanocomposites arises due to the highly delocalized π electron density of triphenylene. Since the SWNTs are intercalated in hexagonal columnar phase along the director, the triphenylene molecules covalently bonded to CNTs and the TP molecules of the matrix together constitute a conduction pathway for the electron flow. The single wall carbon nanotubes can serve as the electron acceptor component in donor-acceptor system with the electron rich triphenylene

molecules acting as donors. We therefore infer that these f-CNTs, which are intercalated in the TP matrix, provide the necessary conducting path for the electron hopping resulting in the enhanced conductivity of the composite.

In conclusion, spectral analysis shows the successful functionalization of carbon nanotubes with discotic liquid crystalline molecules and scanning tunneling microscopy (STM) imaging shows the presence of carbon nanotubes in a reasonable length scale after functionalization with discotics. POM, DSC and X-ray results of the composites indicate intercalation of SWNTs into the matrix of discotic liquid crystals. The insertion of SWNTs causes a minor shift in the transition temperatures. The additional order of Col_p phase is destroyed to give normal Col_h phase. The significant shift of 0.8 nm in the reflection toward larger d spacing is attributed to the integration of SWNTs in the hexagonal columnar phase along the director. These nanocomposite materials having extended delocalized π -electron systems, possess very high electrical conductivity i.e. two orders of magnitude more than the pure discotic compound. These SWNTs-discotic liquid crystal hybrid systems may be important for many device applications such as photoconductors, light emitting diodes, photovoltaic solar cells, sensors, thin film transistors, as the dispersed SWNTs can be aligned in the desired direction using well-established liquid crystal alignment technologies [61].

5.3 Carbon nanotubes in triphenylene and rufigallol-based room temperature monomeric and polymeric discotic liquid crystals.

We have also studied the dispersion of commercial octadecylamine (ODA) functionalized CNTs in the columnar phases of triphenylene and rufigallol based discotic monomers and

polymers which may lead to novel materials with interesting properties useful for device applications. Both triphenylene and rufigallol derivatives are earlier known discotic liquid crystals which form columnar mesophases [68, 63]. The effect of nanotubes on phase behavior of electron-rich triphenylene derivatives and electron-deficient anthraquinone derivatives has been investigated.

5.4 Results and discussion

To investigate the effect of carbon nanotubes on the mesophase behavior of electron deficient rufigallol derivatives we have prepared novel room temperature liquid crystalline rufigallol derivatives. The synthesis of electron deficient novel room-temperature liquid crystalline monomer **10** and polymer **11** is outlined in Scheme 2.

Scheme 2. Synthesis of room-temperature liquid crystalline anthraquinone monomer and polymer. Reaction conditions and reagents; (i) H₂SO₄, MW; (ii) 3,7-dimethyloctylbromide, NaOH, DMSO, 90 °C, 35%; (iii) 1,12-dibromododecane, Cs₂CO₃, *o*-dichlorobenzene, 90 °C, 60%.

Commercially available gallic acid **8** was converted to rufigallol **9** as reported [68]. Rufigallol **9** was alkylated with 3, 7- dimethyloctylbromide under mild etherification conditions to afford the tetraalkoxy rufigallol **10**. Surprisingly the branched chain substituted tetraalkoxy compound **10** exhibits liquid crystalline behavior at room

temperature contrary to its straight chain analogous which do not show any liquid crystalline property, this could be because the branched chains fill the necessary space around the core to induce mesomorphism [68]. Thermal behavior of the compound was investigated by polarizing optical microscopy (POM) and differential scanning calorimetry (DSC). This compound shows columnar hexagonal to isotropic transition at 115.7 °C while heating and isotropic to columnar hexagonal transition at 114.1 °C while cooling, no other transitions are observed while heating and cooling (scan rate 5 °C/min.) in between -30°C and the isotropic temperature in the DSC thermogram which supports the POM observation. Texture of columnar phase observed under POM for this compound **10** at room temperature is shown in Figure 18a. Columnar hexagonal mesophase structure of this compound was established by X-ray diffraction studies. The intensity vs θ graph derived from the diffraction pattern of the compound at room temperature is shown in Figure 19a. In the low angle region three sharp peaks, one strong and two weak, are seen whose d -spacings are in the ratio of 1: $1/\sqrt{3}$: $1/\sqrt{4}$. Identifying the first peak with the Miller index 100, the ratios confirm to the expected values from a two dimensional hexagonal lattice. In the wide angle region two diffused reflections are seen. The broad one centered at about 4.5Å corresponds to the liquid like order of the aliphatic chains. The relatively sharper one seen at about 3.4 Å and well separated from the broad one is due to the stacking of the molecular cores one on top of another. All the above mentioned features are characteristics of the Col_h phase. Three compositions (by weight) of this compound were made by adding the dichloromethane solution of ODA functionalized carbon nanotubes. Three compositions (**10a**: 0.5%; **10b**: 1%; **10c**: 2%) were prepared and analyzed by DSC, POM and X-ray diffraction. All the composites

10a-c were also found to be room temperature liquid crystalline like the pure host compound **10**. These composites, under POM, exhibit classical textures of columnar mesophase upon cooling from the isotropic phase as shown in Figure 18b. Data obtained from the heating and cooling cycles of DSC with a scan rate of 5 °C per minute for these composites are collected in Table 2. The insertion of CNTs decreases the mesophase-isotropic phase transition temperature. With increase in the percentage of the CNTs the mesophase-isotropic transition temperature decreases (Table 2). This is logical as the insertion of CNTs is expected to reduce the ordering of the cores. The X-ray diffraction pattern of the composite **10c** at room temperature shows similar features as that of compound **10** confirming to hexagonal columnar mesophase of the composites as shown in Figure 19b. Since these composites **10a-c** contain very little amount of functionalized carbon nanotubes we do not observe any significant increase in the intercolumnar distance of the pure compound **10** in these composites. The columnar mesophase structure is not destroyed by the inclusion of functionalized carbon nanotubes only the columnar to isotropic transition temperature decreases with increase in the amount of carbon nanotubes. When we tried to insert more than 2% CNTs in the columnar liquid crystal, those composites still exhibit liquid crystalline property but under polarizing microscope we could observe small aggregates of CNTs which means the CNTs are not homogeneously dispersed in the liquid crystal matrix of the composites when CNTs percentage is more.

The dihydroxy functionalized molecule **10** was polymerized to a main chain electron deficient liquid crystalline polyether **11** as shown in the Scheme 2 to study the phase behavior of its nanocomposites with carbon nanotubes. The mesophase behavior of

this polymer was characterized by polarizing optical microscopy and differential scanning calorimetry. This polymer which could be deformed at room temperature shows, under microscope, only one transition on heating. When cooled from the isotropic state it does not exhibit any characteristic texture but a sandy birefringence texture as shown in the Figure 20a appears slowly from the isotropic liquid. The DSC thermogram of the compound shows only one transition at 56.3 °C while heating corresponding to columnar to isotropic transition but on cooling it does not show any discernible transition. The mesophase structure of the polymer was established to be a rectangular columnar phase with lattice parameters $a = 42.02 \text{ \AA}$ and $b = 19.80 \text{ \AA}$. The intensity vs θ graph derived from the X-ray diffraction pattern of the polymer at room temperature shows five reflections in the small angle region as shown in the Figure 21a with two strong reflections at lower angles. Two strong peaks in the small angle region is characteristic of a rectangular columnar phase and the observed other three weak peaks in the small angle region can be indexed for a rectangular lattice. So upon polymerization the columnar hexagonal structure of the monomer **10** is transformed to a more ordered columnar rectangular phase as has been observed for main chain polyethers of rufigallol [68]. As in the case of monomer, we have prepared three different compositions (**11a**: 0.5%; **11b**: 1% and **11c**: 2%) of the polymer by adding functionalized carbon nanotube solution to the polymer followed by sonication and solvent removal. The mesophase behaviors of all these three compositions were characterized by POM, DSC and X-ray diffraction studies. They also exhibit the sandy texture under polarizing microscope when cooled from the isotropic state as shown in the Figure 20b. Data obtained from the heating cycle of DSC for these composites are collected in Table 2. As expected the isotropic transition

temperature of the composites decreases with increase in the CNT quantity. But the mesophase structure of these composites remains rectangular as confirmed by X-ray diffraction of the composites as shown in Figure 21b.

To investigate the effect of carbon nanotubes on the mesophase behavior of electron rich triphenylene derivatives we have synthesized novel room temperature liquid crystalline triphenylene derivatives. The synthesis of novel room-temperature liquid crystalline triphenylene monomer **16** and polymer **17** is outlined in Scheme 3.

Scheme 3. Synthesis of room-temperature liquid crystalline triphenylene monomer and polymer. Reaction conditions and reagents; (i) $C_5H_{11}Br$, K_2CO_3 , MEK; (ii) $FeCl_3$, CH_2Cl_2 and CH_3OH ; (iii) Cat-B-Br, CH_2Cl_2 ; (iv) 3, 7-dimethyloctylbromide, Cs_2CO_3 , MEK, 62%; (v) 1,12-dibromododecane, Cs_2CO_3 , NMP, 110 °C, 54%.

The dihydroxy intermediate **15** has been prepared and isolated as reported [69]. Upon replacement of two pentyloxy chains by 3, 7-dimethyloctyloxy branched chains the compound **16** exhibits liquid crystalline property at room temperature. This could be due

to the unsymmetrical substitution of alkoxy chains on the core and stereoheterogeneity introduced by the branched alkoxy chains. Under polarized optical microscope the compound **16** exhibits classical broken fan texture of hexagonal columnar phase when cooled from the isotropic phase as shown in Figure 22a. This compound shows columnar hexagonal to isotropic transition at 69 °C on heating and isotropic to columnar hexagonal transition at 67 °C while cooling, no other transitions are observed while heating and cooling in between -30°C and the isotropic temperature in the DSC thermogram as shown in Figure 23. The mesophase structure of the compound was established with the help of X-ray diffractometry. In the small angle region there are two reflections, one strong and one weak. The ratio of the *d*-spacings of these two peaks is 1: $1/\sqrt{3}$, which corresponds to a two dimensional hexagonal lattice. In the wide angle region two reflections are observed one very broad and another relatively sharp peak. The broad peak centered at about 4.7 Å is due to the liquid like order of the alkyl chains surrounding the aromatic cores; the other peak centered at about 3.6 Å is due to the stacking of the aromatic cores one on the top of another which constitute the columns. All these features are characteristic of the columnar hexagonal phase. Three different mixtures of functionalized carbon nanotubes were made with this room temperature liquid crystalline triphenylene derivative. All these compositions (**16a**: 0.2%; **16b**: 1% and **16c**: 2%) were analyzed with POM, DSC and X-ray diffraction. Under polarizing optical microscopy these composites develop classical broken fan textures of columnar hexagonal phase as

Table 2. Phase transition temperatures (peak °C) and associated enthalpies (J/gm, in parentheses) of novel liquid crystalline compounds and their composites with functionalized carbon nanotubes (scan rate 5 °C/min.). Col_h = hexagonal columnar, Col_r = columnar rectangular, I = isotropic, * = from polarized optical microscopy (POM).

Sample	Heating Scan	Cooling Scan
10	Col _h 115.7 (6.4) I	I 114.1 (6.3) Col _h
10a	Col _h 113.0 (6.0) I	I 110.7 (6.0) Col _h
10b	Col _h 112.0 (6.0) I	I 109.8 (5.9) Col _h
10c	Col _h 109.5 (5.5) I	I 107.6 (5.6) Col _h
11	Col _r 56.3 (3.3) I	-
11a	Col _r 47.7 (1.9) I	-
11b	Col _r 43.3 (2.0) I	-
11c	Col _r 39.2 (1.0) I	-
16	Col _h 69.0 (6.0) I	I 67.0 (6.0) Col _h
16a	Col _h 67.2 (5.1) I	I 65.6 (5.1) Col _h
16b	Col _h 64.4 (3.8) I	I 61.8 (3.7) Col _h
16c	Col _h 63.8 (3.6) I	I 61.7 (3.6) Col _h
17	Col _h 89 I*	-
17a	Col _h 83 I*	-
17b	Col _h 80 I*	-

shown in the Figure 22b just like the pure host compound **16**. As with those of anthraquinone derivative composites the columnar to isotropic phase transition temperature decreases with increasing the nanotube quantity and the transitions are broadened. Data collected during the heating and cooling cycles of DSC of the pure compound and the composites are collected in Table 2. X-ray diffraction patterns of the composites show similar features to that of the pure compound confirming to columnar hexagonal phase of the composites as shown in Figure 24a. In the X-ray diffraction patterns of these composites also we do not observe any significant change in the intercolumnar distance as compared to the pure compound **16**. So the inclusion of CNTs to the columnar matrix destabilizes the phase to small extent but retains the mesophase structure intact. In order to see the effect of CNTs on triphenylene based main chain polymers we have synthesized the polymer **17** as shown in Scheme 3 from the dihydroxy precursor **15**. The liquid crystalline phase behavior of this polymer was studied by POM, DSC and X-ray diffraction. This highly viscous compound does not show any peak during heating and cooling in the DSC thermogram, but it exhibits a birefringence texture like the above mentioned anthraquinone polymer under polarizing microscope when cooled from isotropic state as shown in Figure 25a. When heated from room temperature this polymer passes slowly to isotropic state at 89 °C and upon cooling the birefringence texture appears slowly under polarizing microscope. In order to confirm the mesophase structure we have carried out the X-ray diffraction study of the polymer. Only one strong reflection is observed in the small angle region of the X-ray diffraction pattern, though it is difficult to assign the mesophase structure with only one peak in the small angle region nevertheless given the general mesophase structure of triphenylene based discotic

monomers and polymers [63] we consider this to be a columnar hexagonal phase. Moreover, miscibility of the mesophase of the polymer **17** with the mesophase of compound **16** confirms the columnar hexagonal structure. Two different nanocomposites (**17a**: 0.5%; **17b**: 1%) of the polymer with functionalized carbon nanotubes were prepared and their liquid crystalline properties were studied by POM and X-ray. Like the pure polymer, these composites do not give any peak in their DSC thermograms so the transition temperatures were determined only by POM. The mesophase to isotropic transition temperatures as observed under polarizing optical microscope of these composites are listed in Table 2. Here also the mesophase to isotropic transition temperature decreases and broadens as the amount of carbon nanotubes increases in the matrix. The sandy texture exhibited by the composites when cooled from isotropic state is shown in the Figure 25b. In all textures some change in the colour was seen upon doping CNTs. This could be because of the disturbed alignment of molecules by the CNTs. X-ray diffraction pattern of the composites show similar features to that of the pure polymer as shown in Figure 24b which again shows that the mesophase is not destroyed by the inclusion of carbon nanotubes though large quantity of carbon nanotubes could not be dispersed homogeneously in the matrix.

5.5 Conclusions

We have synthesized two novel monomeric and two novel polymeric discotic liquid crystals and studied the effect of inclusion of carbon nanotubes on their mesophase behavior. The insertion of carbon nanotubes in small amounts does not affect the mesophase structure of the pure compounds but bring down the isotropic transition

temperatures. With increase in the amount of carbon nanotubes, the isotropic transition temperature decreases in all the composites. We have previously shown that in discotic liquid crystal- carbon nanotube composites, SWNTs align in the hexagonal columnar phase along the director. These room temperature liquid crystalline nanocomposites with broad mesophase ranges and different electronic properties may be important for many device applications, such as photoconductors, light-emitting diodes, photovoltaic solar cells, sensors and thin-film transistors etc.

5.6 Experimental

5.6.1 General information

General information has been described in chapter 2.

5.6.2 Preparation of hydroxyl functionalized triphenylene 4

The monohydroxy functionalized triphenylene **3** was prepared following the published methods [69]. To a solution of **3** (0.605 g, 1 mmol) in methyl ethyl ketone (MEK) (20 ml) was added cesium carbonate (0.652 g, 2 mmol) and 6-bromo-1- hexanol (0.362 g, 2 mmol) and the reaction mixture was refluxed for 24 hrs. After cooling, the reaction mixture was filtered, solvent evaporated and the product was purified by column chromatography (silica gel, hexane ethyl acetate 10:1). Yield 70 %. ¹H NMR (400 MHz, CDCl₃): δ = 7.84 (s, 6H), 4.24 (t, *J* = 6.5 Hz, 12H), 3.69 (m, 2H), 2.1-0.8 (m, 44H aliphatic protons). ¹³C NMR (100MHz, CDCl₃): δ = 149.1, 123.7, 107.6, 70.8, 69.7, 62.9, 32.7, 31.5, 29.7, 29.4, 26.0, 25.6, 19.3, 13.9. Elemental analysis: calculated for C₄₄H₆₄O₇, C 74.96, H 9.15%; found C 74.66, H 9.09%.

5.6.3 Functionalization of CNTs

As prepared (AP-grade) single walled carbon nanotubes (200 mg) were refluxed in 2.6 M nitric acid (75 ml) at 125 °C for 48 hrs and then the brown colored solution was transferred to centrifuge tubes and centrifuged after decanting the acid solution, deionised water was added and centrifuged several times till neutral. Then the single walled carbon nanotubes were vacuum dried to obtain dry purified nanotubes. The Purified single walled carbon nanotubes (10 mg) were refluxed in thionyl chloride (20 ml) for 15 hours and then the excess of thionyl chloride was removed under reduced pressure. Then 500 mg of hydroxyl functionalized triphenylene **4** was added to it and the mixture was heated at 80 °C under anhydrous conditions for 48 hrs. The mixture was cooled and dissolved in dichloromethane and passed through a silica column (hexane ethyl acetate 20:1) to isolate the product **7**. IR: ν_{\max} 2957, 2928, 2853, 1737, 1616, 1514, 1468, 1435, 1387, 1263, 1172, 1070, 1034, 964, 835 cm^{-1} . ^1H NMR (400 MHz, CDCl_3): δ = 7.85 (s, 6H, Ar-H), 4.3-4.05 (m, 14H, OCH_2 and COOCH_2), 2.1-0.8 (m, 44H, aliphatic protons). ^{13}C NMR (100MHz, CDCl_3): δ = 149.1, 145.9, 145.4, 123.7, 107.6, 106.8, 104.5, 70.9, 69.7, 68.9, 37.1, 31.9, 30.3, 29.7, 26.1, 22.7, 19.4, 14.0.

5.6.4 Preparation of liquid crystalline nanocomposites **7c**

4 mg of compound **7** was dissolved in 5 ml of dichloromethane and to this solution, was added 36 mg of H4TP. The solution was sonicated for about 5 min and then the solvent was removed followed by drying the mixture in vacuum. The other composites **7a** and **7b** were prepared in the same procedure and analyzed.

5.6.5 Synthesis of 1,5-dihydroxy-2,3,6,7-tetrakis(3,7-dimethyloctyloxy)-9,10-anthraquinone, **10**

To a solution of Rufigallol **9** (1.52 g, 5 mmol), 3,7-dimethyl octylbromide (4.86 g, 22 mmol) in DMSO (10 mL) was added NaOH (0.8 g, 20 mmol) and the mixture was stirred for about 20 hours at 90°C. After cooling the reaction mixture, water was added and the aqueous solution was extracted with chloroform. After solvent evaporation the product was precipitated from chloroform into methanol thrice to obtain the pure product **10** (1.51 g, Yield 35%). ¹H NMR: δ_H 12.76 (s, 2H, Ar-OH), 7.4 (s, 2H, Ar-H), 4.23-4.13 (m, 8H, ArOCH₂), 1.9-1.1 (m, 40H, aliphatic CH₂ and -CH), 0.98 (d, 6H, *J* = 6.3 Hz, -CH-CH₃), 0.95 (d, 6H, *J* = 6.6 Hz, CH₃), 0.88 (d, 12H, *J* = 4.5 Hz, CH₃), 0.85 (d, 12H, *J* = 4.5 Hz, CH₃); ¹³C NMR: δ_C 186.4, 158.1, 157.3, 141.2, 128.9, 111.8, 104.8, 72.1, 67.8, 39.3, 37.3, 36.1, 31.1, 29.8, 29.7, 28.8, 28.0, 24.7, 22.6, 19.6; FT-IR: (ν_{max}) 2922, 2854, 1616, 1569, 1506, 1456, 1427, 1365, 1315, 1280, 1226, 1138, 1095, 1045, 950, 864, 802, 723 cm⁻¹. Elemental analysis. Found: C, 75.0; H, 10.71. C₅₄H₈₈O₈ requires C, 74.96; H, 10.25%.

5.6.6 Polymerization of 1,5-dihydroxy-2,3,6,7-tetrakis(3,7-dimethyloctyloxy)-9,10-anthraquinone

A solution of tetraalkoxy anthraquinone **10** (0.865 g, 1 mmol), 1,12-dibromododecane (0.328 g, 1 mmol) and cesium carbonate (1.3 g, 4 mmol) in *o*-dichlorobenzene (5 mL) was stirred at 90 °C under argon for 10 days. The reaction mixture was then cooled and 20 mL of chloroform was added to it. The organic layer was separated and washed with water and dried. The solvent was removed under reduced pressure to yield the crude

polymer **11**. It was further purified by repeated precipitation from chloroform into methanol. Yield 60%. ^1H NMR: δ_{H} 7.6 (s, 2H, Ar-H), 4.03-4.18 (m, 12H, ArOCH₂), 1.1-2.0 (m, 60H, aliphatic -CH₂ and -CH), 0.8-1.0 (m, 36H, -CH₃); ^{13}C NMR: δ_{C} 181.2, 157.4, 153.9, 147.0, 132.6, 120.4, 107.0, 74.7, 72.4, 67.5, 45.2, 39.2, 37.3, 36.1, 32.8, 30.4, 29.7, 27.9, 27.3, 27.1, 26.1, 24.7, 22.7, 22.6, 19.6; FT-IR:(ν_{max}) 2924, 2854, 1666, 1572, 1462, 1377, 1319, 1282, 1132, 1094, 771, 721. Mol. Wt. ~ 13691; PDI = 1.44.

5.6.7 Synthesis of 2,6-Bis(3,7-dimethyloctyloxy)-3,7,10,11-tetrakis(pentyloxy)-triphenylene, 16

To a solution of 2,6-dihydroxy triphenylene **15** (0.605g, 1 mmol) in MEK (10 mL), 3,7-dimethyloctylbromide (0.885g, 4 mmol) and cesium carbonate (1.3g, 4 mmol) was added and the reaction mixture was refluxed overnight. After cooling, the reaction mixture was filtered and solvent evaporated and the product was purified by column chromatography followed by precipitation from dichloromethane into ethanol. Yield 62%. ^1H NMR: δ_{H} 7.8 (s, 6H, ArH), 4.2-4.3 (m, 12H, ArOCH₂), 1.15-2.0 (m, 44H, aliphatic CH₂ and CH), 1.03 (d, 6H, $J = 6$ Hz, CH₃), 0.98 (t, 12H, $J = 6$ Hz, CH₃), 0.87 (d, 12H, $J = 5.6$ Hz, CH₃); ^{13}C NMR: δ_{C} 149.0, 123.6, 107.4, 69.7, 68.0, 39.2, 37.4, 36.4, 30.0, 29.1, 28.3, 27.9, 24.7, 22.5, 19.7, 14.0; FT-IR: (ν_{max}) 2922, 2854, 1616, 1514, 1464, 1435, 1379, 1263, 1171, 1053, 976, 870, 837, 771, 729. Elemental Analysis; Found: C, 78.69; H, 11.05, C₅₈H₉₂O₆ requires C, 78.68; H, 10.47%.

5.6.8 Polymerization of 2,6-dihydroxy-3,7,10,11-tetrakis(pentyloxy)-triphenylene

A solution of 2,6-dihydroxy triphenylene **15** (0.423 g, 0.7 mmol), 1,12-dibromododecane (0.23 g, 0.7 mmol) and cesium carbonate (0.326 g, 1 mmol) in NMP (2 mL) was submerged into a preheated oil bath at 110 °C and stirred for 1 hour and cooled. Water was added and resulting solid repeatedly washed with water and ethanol. Reprecipitation from dichloromethane with ethanol afforded the polymer **17** (295 mg). ¹H NMR: δ_H 7.8 (s, 6H, Ar-H), 4.2 (t, 12H, *J* = 6 Hz, ArOCH₂), 1.94 (m, 12H, OCH₂CH₂) 1.3-1.6 (m, 32H, Aliphatic CH₂), 0.98 (t, 12H, *J* = 6.8 Hz, -CH₃); ¹³C NMR: δ_C 149.0, 123.6, 107.4, 69.7, 69.1, 32.8, 29.7, 29.5, 29.1, 28.3, 26.2, 22.5, 14.0; FT-IR: (ν_{max}) 2924, 2852, 1620, 1504, 1456, 1377, 1261, 1169, 1040, 977, 810, 770, 721 cm⁻¹; Mol. Wt. ~ 13515; PDI = 1.92.

5.6.9 Preparation of liquid crystalline nanocomposites with ODA functionalized carbon nanotubes

Novel nanocomposites (by weight) of monomeric and polymeric liquid crystalline compounds were prepared as follows; the commercial octadecylamine (ODA) functionalized SWNTs (25 mg) were dissolved in dichloromethane (10 mL) and the insoluble portion was filtered using PTFE membrane (0.45μ). The soluble portion was dried under vacuum to know the exact amount of soluble SWNTs. It was found to be 10 mg. The soluble SWNTs were re-dissolved in 20 mL of dichloromethane. Calculated amount of this solution was added to the liquid crystal monomers (**10** and **16**) and main chain polymers (**11** and **17**). The solution was sonicated for a few minutes followed by

removal of solvent and drying under vacuum to make different functionalized SWNT-DLC composites.

References

1. (a) S. Iijima, *Nature*, **354**, 56, (1991); (b) S. Iijima and T. Ichihashi, *Nature*, **363**, 603, (1993).
2. J. L. Hutchison, N. A. Kiselev, E. P. Krinichnaya, A.V. Krestenin, R.O. Loutfy, A. P. Morawsky, V. E. Muradyan, E. D. Obraztsova, J. Sloans, S.V. Terekhov and D. N. Zakharov, *Carbon*, **39**, 761, (2001).
3. (a) Special Issue on Carbon Nanotubes, *Acc. Chem. Res.*, **35**, 997, (2002); (b) *Carbon Nanotubes: Synthesis, Structure, Properties and Applications*, ed. M. Dresselhaus, G. Dresselhaus and Ph. Avouris, Springer-Verlag, Berlin, (2001).
4. (a) M. Arnold, A. Green, J. Hulvat, S. Stupp and M. Hersam, *Nat. Nanotechnol.*, **1**, 60, (2006); (b) M. Zheng, A. Jagota, M. S. Strano, A. P. Stanos, P. Barone, S. G. Chou, B. A. Dinner, M. S. Dresselhaus, R. S. McLean, G. B. Onoa, G. G. Samsonidze, E. D. Semke, M. Usrey, and D. J. Walls, *Science*, **302**, 1545, (2003).
5. R. M. Tromp, A. Afzali, M. Freitag, D. B. Mitzi and Z. Chen, *Nano Lett.*, **8**, 469, (2008).
6. E. Katz and I. Willner, *ChemPhysChem*, **5**, 1084, (2004).
7. (a) X. Peng and S. S. Wong, *Adv. Mater.*, **21**, 625, (2009); (b) D. Tasis, N. Tagmatarchis, A. Bianco and M. Prato, *Chem. Rev.*, **106**, 1105, (2006).

8. (a) Y. Lin, S. Taylor, H. Li, K. A. S. Fernando, L. Qu, W. Wang, L. Gu, B. Zhou and Y. -P. Sun, *J. Mater Chem.*, **14**, 527, (2004); (b) L. Lacerda, A. Bianco, M. Prato and K. Kostarelos, *J. Mater. Chem.*, **18**, 17, (2008).
9. (a) A. Hirsch, *Angew. Chem. Int. Ed.*, **41**, 1853, (2002); (b) P. M. Ajayan, *Chem. Rev.*, **99**, 1787, (1999); (c) R. H. Baughman, A. A. Zakhidov and W. A. deHeer, *Science*, **297**, 787, (2002); (d) T. -J. Park, S. Banerjee, T. Hemraj-Benny and S. S. Wong, *J. Mater. Chem.*, **16**, 141, (2006); (e) J. Wang, *Electroanalysis*, **17**, 7, (2005); (f) S. Banerjee, M. G. C. Kahn and S. S. Wong, *Chem. Eur. J.*, **9**, 1898, (2003).
10. X. -L. Xie, Y. -W. Mai, X. -P. Zhou, *Material Science and Engineering: Reports*, **49**, 89, (2005).
11. (a) W. Z. Li, S. S. Xie, L. X. Qian, B. H. Chang, B. S. Zou, W. Y. Zhou, R. A. Zhao and G. Wang, *Science*, **274**, 1701, (1996); (b) Z. F. Ren, Z. P. Huang, J. W. Xu, J. H. Wang, P. Bush, M. P. Siegal and P. N. Provencio, *Science*, **282**, 1105, (1998).
12. P. M. Ajayan, O. Stephan, C. Colliex and D. Trauth, *Science*, **265**, 1212, (1994).
13. (a) C. Zakri, *Liq. Cryst. Today*, **16**, 1, (2007); (b) C. Zakri and P. Poulin, *J. Mater Chem.*, **16**, 4095, (2006); (c) J. P. F. Lagerwall and G. Scalia, *J. Mater. Chem.*, **18**, 2890, (2008); (d) S. Zhang and S. Kumar, *Small*, **4**, 1270, (2008).
14. W. Lee and C. -S. Chiu, *Optics Letters*, **26**, 521, (2001).
15. A. M. Somoza, C. Sagui and C. Roland, *Phys. Rev. B*, **63**, 081403(R), (2001).
16. W. Lee, and S. -L. Yeh, *Appl. Phys. Lett.*, **79**, 4488, (2001).

17. (a) W. Lee, H. -Y. Chen, and S. -L. Yeh, *Optics Express*, **10**, 482, (2002); (b) W. Lee, and H. -C. Chen, *J. Phys. D: Appl. Phys.*, **35**, 2260, (2002).
18. W. Lee, S. -L. Yeh, C. -C. Chang, and C. -C. Lee, *Optics Express*, **9**, 791, (2001).
19. M. D. Lynch and D. L. Patrick, *Nano. Lett.*, **2**, 1197, (2002).
20. I. C. Khoo, J. Ding, Y. Zhang, K. Chen and A. Diaz. *Appl. Phys. Lett.*, **82**, 3587, (2003).
21. W. Lee, C. -Y. Wang and Y. -C. Shih, *Appl. Phys. Lett.*, **85**, 513, (2004).
22. I. -S. Baik, S. Y. Jeon, S. H. Lee, K. A. Park, S. H. Jeong, K. H. An and Y. H. Lee, *Appl. Phys. Lett.*, **87**, 263110, (2005).
23. W. Lee and Y. -C. Shih, *J. Soc. Info. Dis.*, **13**, 743, (2005).
24. C. -Y. Huang, C. -Y. Hu, H. -C. Pan, and K. -Y. Lo, *Jpn. J. Appl. Phys.*, **44**, 8077, (2005).
25. H. -Y. Chen and W. Lee, *Optical Review*, **12**, 223, (2005).
26. I. -S. Baik, S. Y. Jeon, S. J. Jeong, S. H. Lee, K. H. An, S. H. Jeong, and Y. H. Lee, *J. Appl. Phys.*, **100**, 074306, (2006).
27. H. -Y. Chen and W. Lee. *Appl. Phys. Lett.*, **88**, 222105, (2006).
28. (a) R. Dhar, A. S. Pandey, M. B. Pandey, S. Kumar and R. Dabrowski, *Appl. Phys. Express*, **1**, 121501, (2008); (b) C. -Y. Huang, H. -C. Pan and C. -T. Hsieh, *Jpn. J. Appl. Phys.*, **45**, 6392, (2006).
29. H. -Y. Chen, W. Lee and N. A. Clark, *Appl. Phys. Lett.*, **90**, 033510, (2007).
30. S. Y. Jeon, S. H. Shin, S. J. Jeong, S. H. Lee, S. H. Jeong, Y. H. Lee, H. C. Choi and K. J. Kim, *Appl. Phys. Lett.*, **90**, 121901, (2007).

31. (a) I. Dierking, G. Scalia, P. Morales and D. LeClere, *Adv. Mater.*, **16**, 865, (2004); (b) I. Dierking and S. E. San, *Appl. Phys. Lett.*, **87**, 233507, (2005); (c) I. Dierking, G. Scalia and P. Morales, *J. Appl. Phys.*, **97**, 044309, (2005).
32. I. Dierking, K. Casson and R. Hampson, *Jpn. J. Appl. Phys.*, **47**, 6390, (2008).
33. R. Cervini, G. P. Simon, M. Ginic-Markovic, J. G. Matisons, C. Huynh and S. Hawkins, *Nanotechnology*, **19**, 175602, (2008).
34. C. Da Cruz, P. Launois and M. Veber, *J. Nanosci. Nanotech.*, **4**, 86, (2004).
35. M. F. Islam, A. M. Alsayed, Z. Dogic, J. Zhang, T. C. Lubensky and A. G. Yodh, *Phys. Rev. Lett.*, **92**, 088303, (2004).
36. (a) S. Courty, J. Mine, A. R. Tajbakhsh and M. Terentjev, *Euro. Phys. Lett.*, **64**, 654, (2003); (b) L. Yang, K. Setyowati, A. Li, S. Gong and J. Chen, *Adv. Mater.*, **20**, 2271, (2008).
37. S. J. Jeong, K. A. Park, S. K. Jeong, H. J. Jeong, K. H. An, C. W. Nah, D. Pribat, S. H. Lee and Y. H. Lee, *Nano. Lett.*, **7**, 2178, (2007).
38. (a) H. Duran, B. Gazdecki, A. Yamashita and T. Kyu, *Liq. Cryst.*, **32**, 815, (2005); (b) J. P. F. Lagerwall, R. Dabrowski and G. Scalia, *J. Non-Cryst. Solids*, **353**, 4411, (2007); (c) M. Kimura, N. Miki, N. Adachi, Y. Tatewaki, K. Ohta and H. Shirai, *J. Mater. Chem.*, **19**, 1086, (2009).
39. (a) R. A. Mrozek, B. -S. Kim, V. C. Holmberg and T. A. Taton, *Nano. Lett.*, **3**, 1665, (2003); (b) J. M. Russel, S. Oh, I. LaRue, O. Zhou and E. T. Samulski, *Thin Solid Films*, **509**, 53, (2006).
40. G. Scalia, J. P. F. Lagerwall, M. Haluska, U. Dettlaff-Weglikowska, F. Giesselmann and S. Roth, *Phys. Stat. Sol. B*, **243**, 3238, (2006).

41. (a) K. A. Park, S. M. Lee, S. H. Lee and Y. H. Lee, *J. Phys. Chem. C*, **111**, 1620, (2007); (b) P. van der Scoot, V. Popa-Nita and S. Kralj, *J. Phys. Chem. B*, **112**, 4512, (2008).
42. V. Weiss, R. Thiruvengadathan and O. Regev, *Langmuir*, **22**, 854, (2006).
43. (a) J. Lagerwall, G. Scalia, M. Haluska, U. Dettlaff-Weglikowska, S. Roth and F. Giesselmann, *Adv. Mater.*, **19**, 359, (2007); (b) J. P. F. Lagerwall, G. Scalia, M. Haluska, U. Dettlaff-Weglikowska, F. Giesselmann and S. Roth, *Phys. Stat. Sol. B*, **243**, 3046, (2006).
44. W. Jiang, B. Yu, W. Liu and J. Hao, *Langmuir*, **23**, 8549, (2007).
45. E. Navit-Roth, R. Yerushalmi-Rozen and O. Regev, *Small*, **4**, 1459, (2008).
46. G. Scalia, C. von Buhler, C. Hagele, S. Roth, F. Giesselmann and J. P. F. Lagerwall, *Soft Matter*, **4**, 570, (2008).
47. I. Onsager, *Ann. Ny. Acad. Sci.*, **51**, 627, (1949).
48. W. Song, I. A. Kinloch and A. H. Windle, *Science*, **302**, 1363, (2003).
49. W. Song and A. H. Windle, *Macromolecules*, **38**, 6181, (2005).
50. S. Zhang, I. A. Kinloch and A. H. Windle, *Nano. Lett.*, **6**, 568, (2006).
51. W. Song and A. H. Windle, *Adv. Mater.*, **20**, 3149, (2008).
52. (a) S. Ramesh, L. M. Ericson, V. A. Davis, R. K. Saini, C. Kittrell, M. Pasquali, W. E. Billups, W. W. Adams, R. H. Hauge and R. E. Smalley, *J. Phys. Chem. B*, **108**, 8794, (2004); (b) V. A. Davis, L. M. Ericson, A. N. G. Parra-Vasquez, H. Fan, Y. Wang, V. Prieto, J. A. Longoria, S. Ramesh, R. K. Saini, C. Kittrell, W. E. Billups, W. W. Adams, R. H. Hauge, R. E. Smalley and M. Pasquali, *Macromolecules*, **37**, 154, (2004); (c) P. K. Rai, R. A. Pinnick, A. N. G. Parra-

- Vasquez, V. A. Davis, H. K. Schmidt, R. H. Hauge, R. E. Smalley and M. Pasquali, *J. Am. Chem. Soc.*, **128**, 591, (2006).
53. (a) S. Badaire, C. Zakri, M. Maugey, A. Derre, J. N. Barisci, G. Wallace and P. Poulin, *Adv. Mater.*, **17**, 1673, (2005); (b) C. Zamora-Ladezma, C. Blanc, M. Maugey, C. Zakri, P. Poulin and E. Anglaret, *Nano. Lett.*, **8**, 4103, (2008).
54. (a) H. Ko and V. V. Tsukruk, *Nano. Lett.*, **6**, 1443, (2006); (b) R. Duggal, F. Hussain and M. Pasquali, *Adv. Mater.*, **18**, 29, (2006).
55. S. E. Moulton, M. Maugey, P. Poulin and G. G. Wallace, *J. Am. Chem. Soc.*, **129**, 9452, (2007).
56. S. Meuer, L. Braun, and R. Zentel, *Chem. Commun.*, 3166, (2008).
57. (a) L. Zhi, J. Wu, J. Li, U. Kolb and K. Mullen, *Angew. Chem. Int. Ed.*, **44**, 2120, (2005); (b) J. Wu, B. E. Hamaoui, J. Li, L. Zhi, U. Kolb and K. Mullen, *Small*, **1**, 210, (2005); (c) L. Gherghe, C. Kubel, G. Lieser, H. -J. Rader and K. Mullen, *J. Am. Chem. Soc.*, **124**, 13130, (2002).
58. (a) C. Chan, G. Crawford, Y. Gao, R. Hurt, K. Jian, H. Li, B. Sheldon, M. Sousa and N. Yang, *Carbon*, **43**, 2431, (2005); (b) M. E. Sousa, S. G. Cloutier, K. Q. Jian, B. S. Weissman, R. H. Hurt and G. P. Crawford, *Appl. Phys. Lett.*, **87**, 173115, (2005); (c) M. E. Sousa, C. Chan, K. Jian, Y. Gao, R. H. Hurt, G. P. Crawford and N. Yang, *Mol. Cryst. Liq. Cryst.*, **435**, 107/[767], (2005).
59. J. P. Hill, W. Jin, A. Kosaka, T. Fukushima, H. Ichihara, T. Shimomura, K. Ito, T. Hashizume, N. Ishii and T. Aida, *Science*, **304**, 1481, (2004).
60. K. Jian, R. H. Hurt, B. W. Sheldon and G. P. Crawford, *Appl. Phys. Lett.*, **88**, 163110, (2006).

61. (a) S. Kumar, *Chem. Soc. Rev.*, **35**, 83, (2006); (b) S. Laschat, A. Baro, N. Steinke, F. Giesselmann, C. Hagele, G. Scalia, R. Judele, E. Kapatsina, S. Sauer, A. Schreivogel and M. Tosoni, *Angew. Chem. Int. Ed.*, **46**, 4832, (2007); (c) S. Sergeyeve, W. Pisula and Y. H. Geerts, *Chem. Soc. Rev.*, **36**, 1902, (2007); (d) J. Wu, W. Pisula and K. Mullen, *Chem. Rev.*, **107**, 718, (2007); (e) Y. Shimizu, K. Oikawa, K. Nakayama and D. Guillon, *J. Mater. Chem.*, **17**, 4223, (2007); (f) N. Boden, R. J. Bushby, J. Clements and B. Movaghar, *J. Mater. Chem.*, **9**, 2081, (1999); (g) R. J. Bushby and O. R. Lozman, *Curr. Opin. Solid State Mater. Sci.*, **6**, 569, (2002); (h) R. J. Bushby and O. R. Lozman, *Curr. Opin. Colloid Interface Sci.*, **7**, 343, (2002); (i) H. Takezoe, K. Kishikawa and E. Gorecka, *J. Mater. Chem.*, **16**, 2412, (2006); (j) K. Ohta, K. Hatsusaka, M. Sugibayashi, M. Ariyoshi, K. Ban, F. Maeda, R. Naito, K. Nishizawa, A. M. van de Craats and J. M. Warman, *Mol. Cryst. Liq. Cryst.*, **397**, 25, (2003); (k) A. N. Cammidge and R. J. Bushby, In *Handbook of Liquid Crystals*; ed. D. Demus, J. Goodby, G. W. Gray, H.-W. Spiess, and V. Vill, Wiley-VCH: Weinheim, Vol. **2B**, Chapter VII, p.693, (1998).
62. (a) S. Kumar and H. K. Bisoyi, *Angew. Chem. Int. Ed.*, **46**, 1501, (2007); (b) H. K. Bisoyi and S. Kumar, *J. Mater. Chem.*, **18**, 3032, (2008).
63. (a) S. Kumar, *Liq. Cryst.*, **31**, 1037, (2004); (b) S. Kumar, *Liq. Cryst.*, **32**, 1089, (2005).
64. J. Liu, A. G. Rinzler, H. Dai, J. H. Hafner, R. K. Bradley, P. J. Boul, A. Lu, T. Iverson, K. Shelimov, C. B. Huffman, F. Rodriguez-Macias, Y. -S. Shon, T. R. Lee, D. T. Colbert, R. E. Smalley, *Science*, **280**, 1252, (1998).

65. X. -P. Tang, A. Kleinhammes, H. Shimoda, L. Fleming, K. Y. Bennoune, S. Sinha, C. Bower, O. Zhou, Y. Wu, *Science*, **288**, 492, (2000).
66. S. Kumar and V. Lakshminarayanan, *Chem. Commun.*, 1600, (2004).
67. J. Simmerer, B. Glusen, W. Paulus, A. Ker, P. Schuhmacher, D. Adam, K. -H. Etzbach, K. Siemensmeyer, J. H. Wendorff, H. Ringsdorf, D. Haarer, *Adv. Mater.*, **8**, 815, (1996).
68. S. Kumar, *Phase Transitions*, **81**, 113, (2008).
69. (a) S. Kumar and M. Manickam, *Synthesis*, 1119, (1998); (b) S. Kumar and M. Manickam, *Chem. Commun.*, 1615, (1997); (c) S. Kumar and S. K. Varshney, *Synthesis*, 305, (2001).

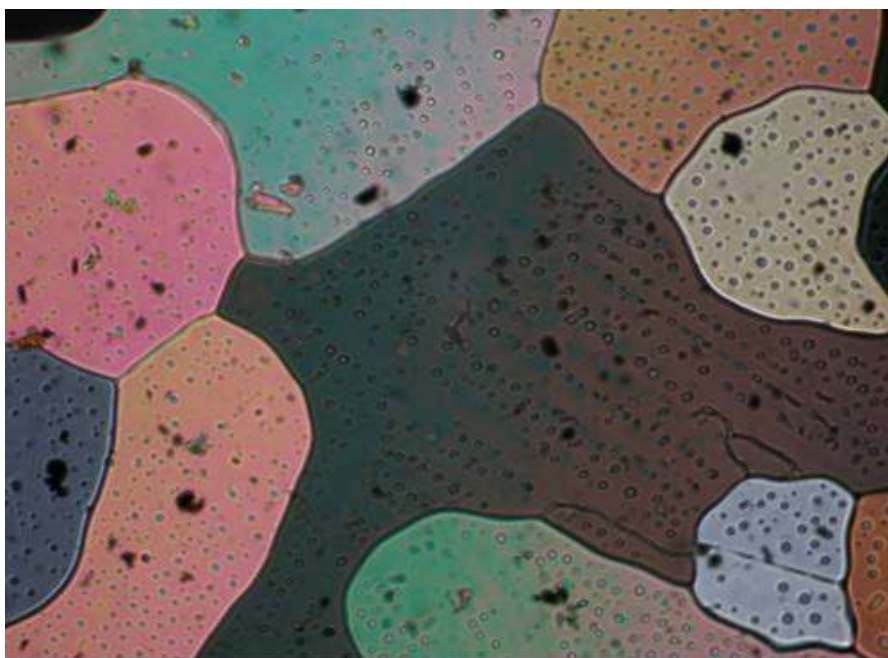


Figure 7. POM image of H4TP dispersed with purified carbon nanotubes (crossed polarizer, 200 X magnifications), the nanotube aggregates can be clearly seen in the photomicrograph suggesting inhomogeneous dispersion of carbon nanotubes.

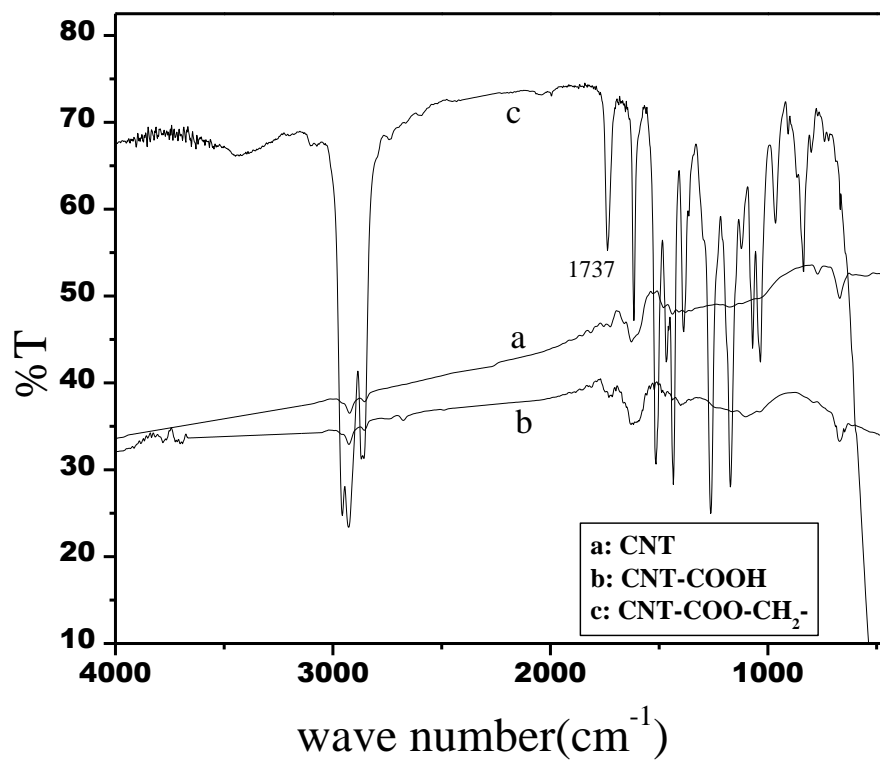


Figure 8. FT-IR spectra of unfunctionalized (a), carboxyl-functionalized (b) and triphenylene-functionalized SWNTs (c). The ester stretching absorption peak (1737 cm⁻¹) can be clearly noticed in the triphenylene functionalized SWNTs (c).

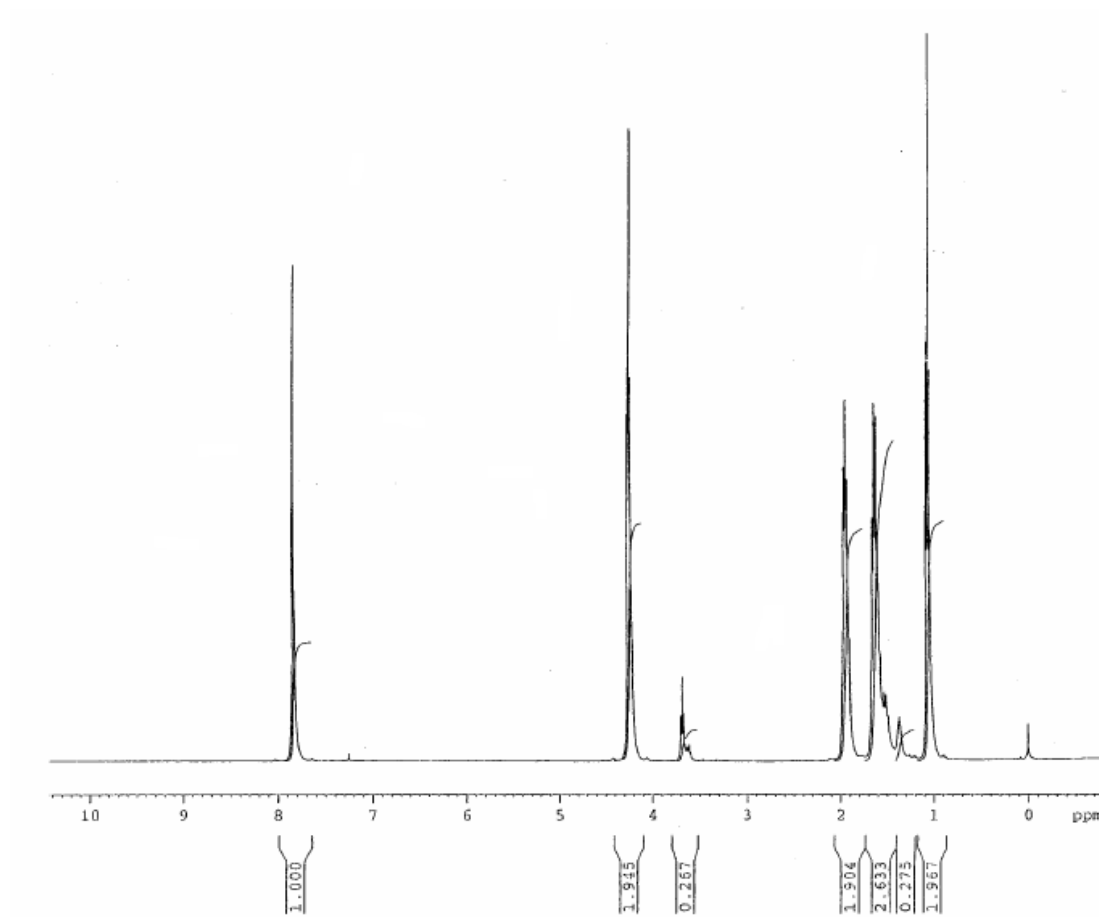


Figure 9. ^1H NMR spectrum of hydroxyl functionalized triphenylene derivative **4**.

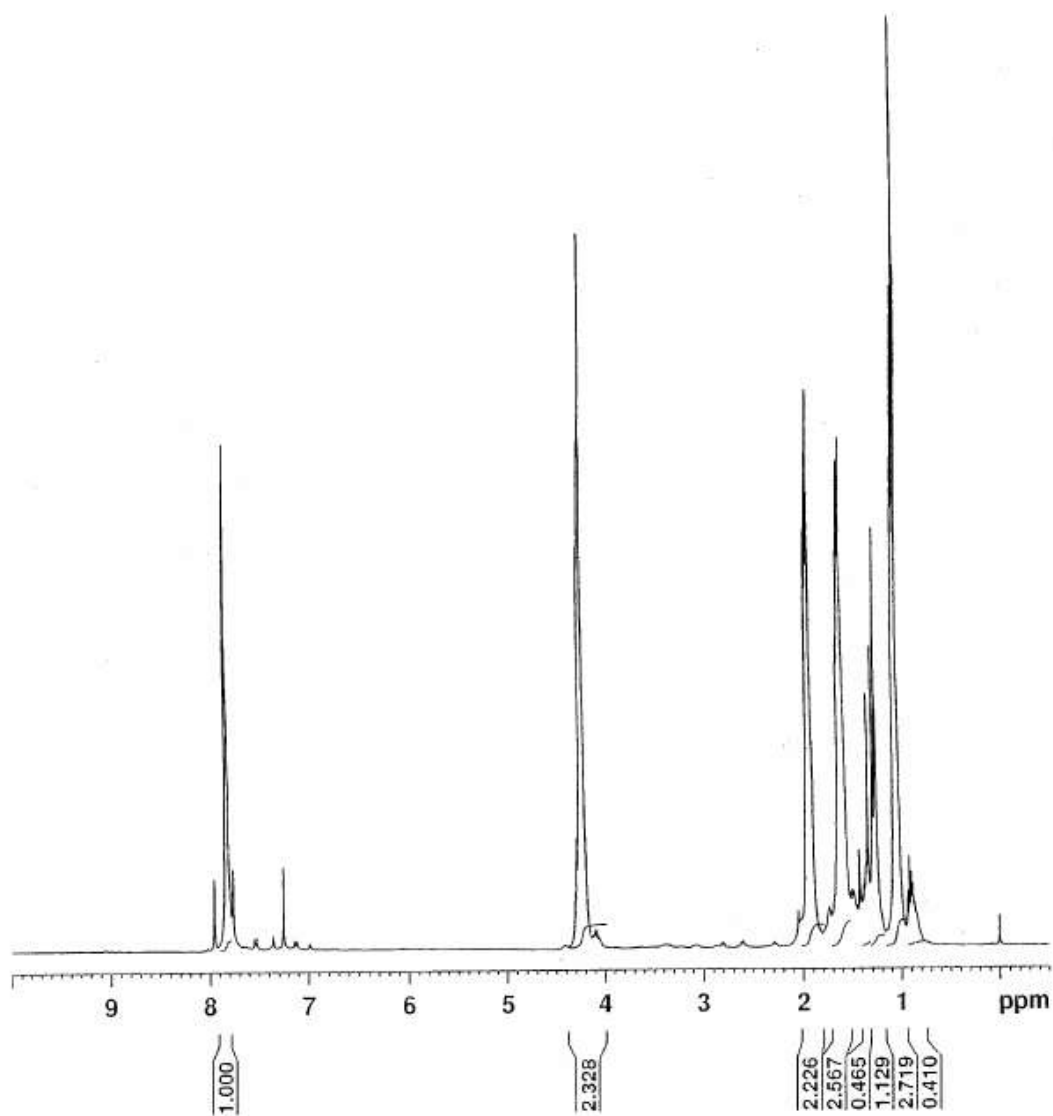


Figure 10. ^1H NMR spectrum of discotic functionalized carbon nanotubes **7**.

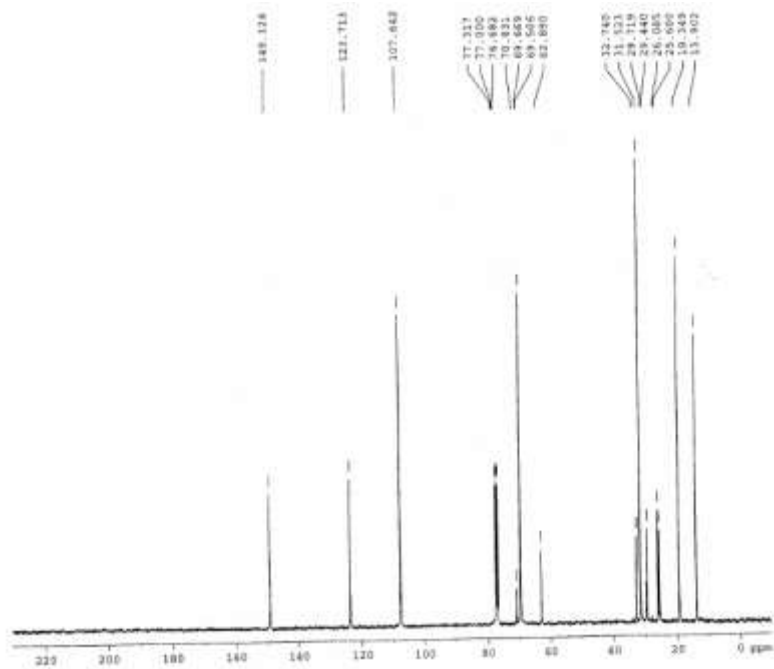


Figure 11. ^{13}C NMR spectrum of hydroxyl functionalized triphenylene compound **4**.

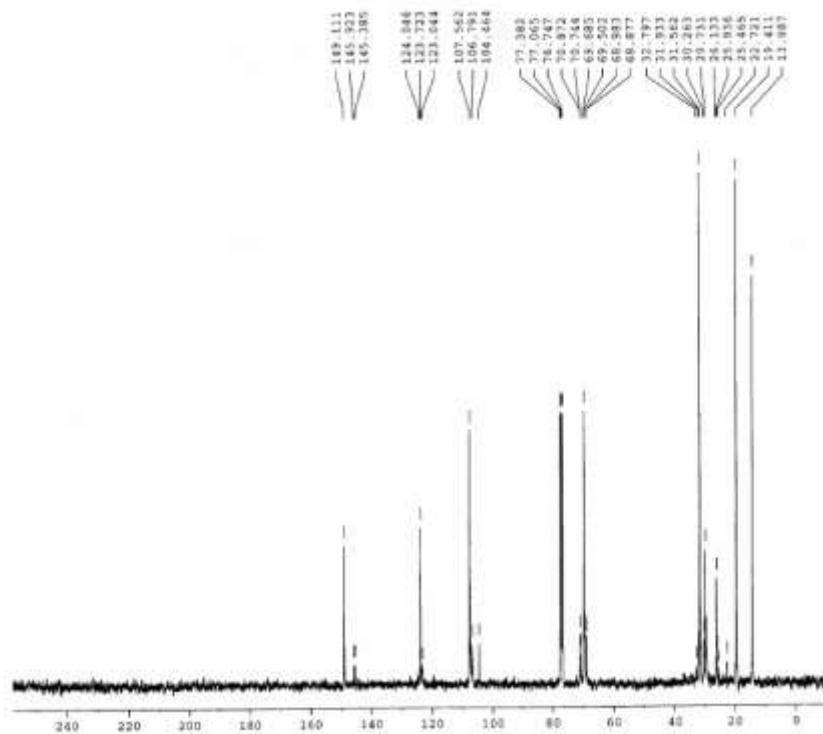


Figure 12. ^{13}C NMR spectrum of discotic functionalized carbon nanotubes **7**.

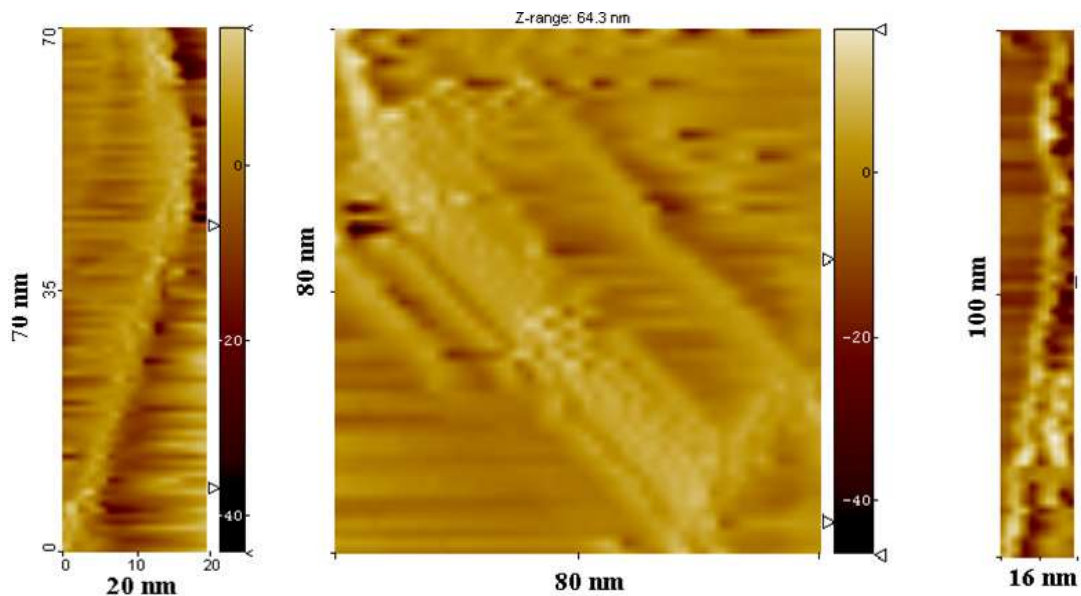


Figure 13. Scanning tunneling microscope (STM) images (constant current image) of functionalized carbon nanotubes on highly oriented pyrolytic graphite (HOPG) surface.

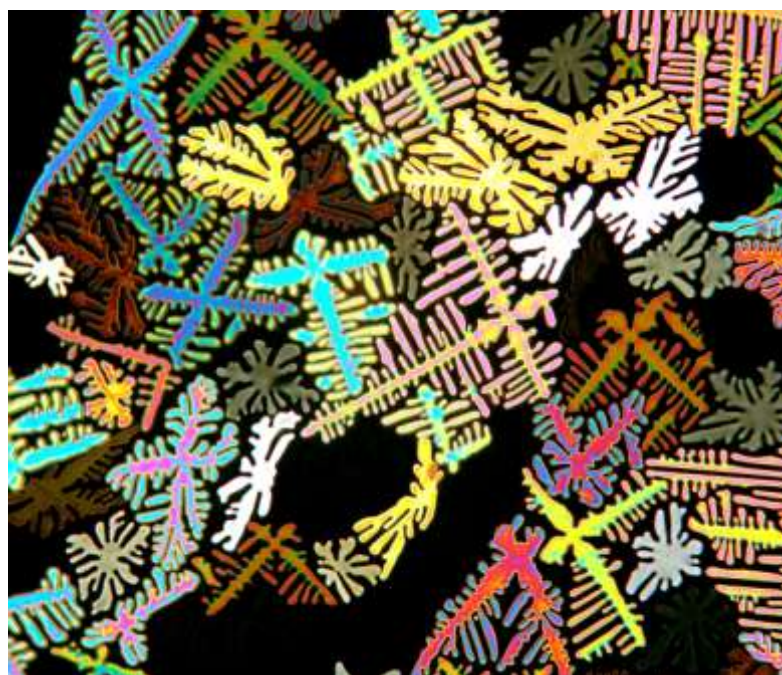


Figure 14. POM image of the columnar phase of **7c** at 130 °C on cooling from the isotropic phase (crossed polarizers; 500 X magnification).

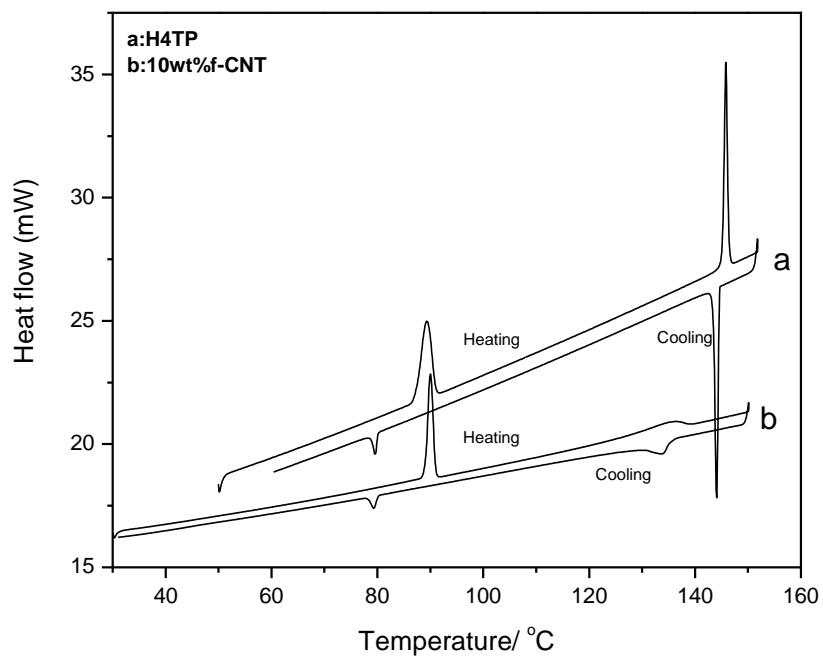


Figure 15. DSC traces of compound H4TP (a) and composite **7c** (b) on heating and cooling (scan rate $5\text{ }^{\circ}\text{C min}^{-1}$).

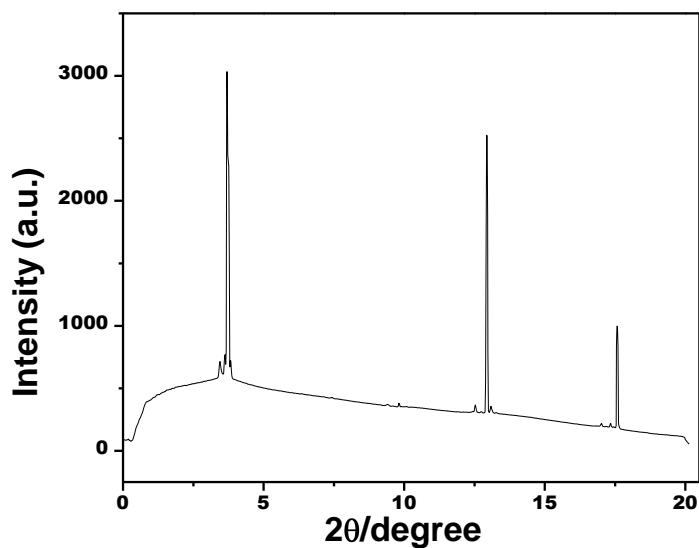


Figure 16. One dimensional intensity vs 2θ profile derived from X-ray diffraction pattern for composite **7c** at $125\text{ }^{\circ}\text{C}$.

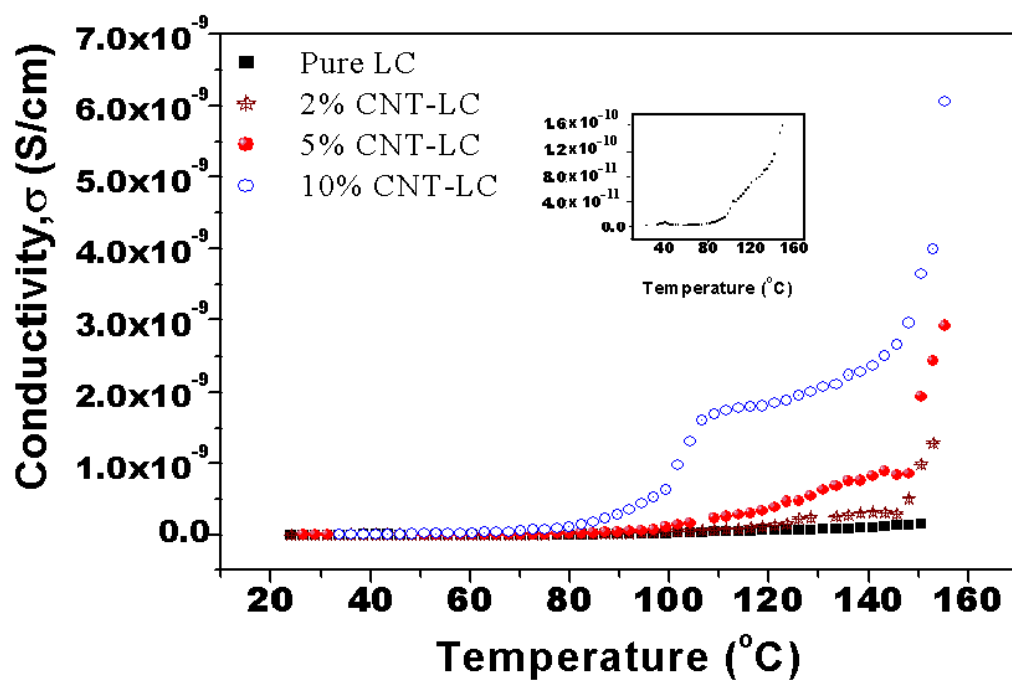


Figure 17. The figure shows the DC conductivity values measured at different temperatures for pure H4TP (inset) and the mixture of 2% ,5% and 10% of f-CNTs and H4TP nanocomposites while cooling from isotropic phase.

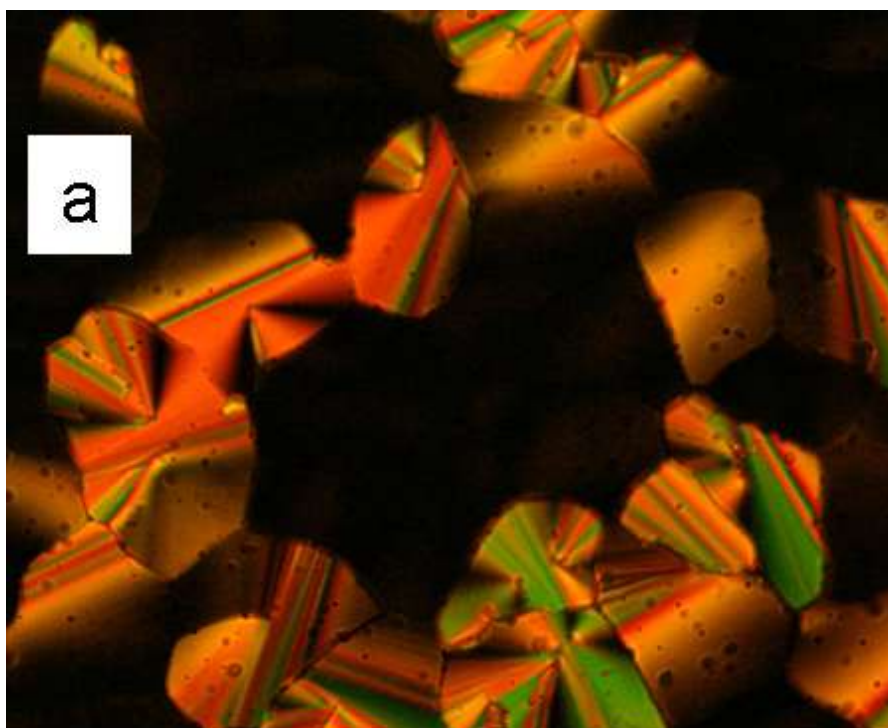


Figure 18. Optical photomicrograph of (a) **10** and (b) composite **10b** at 25 °C on cooling from the isotropic liquid (crossed polarizers, magnification X 200).

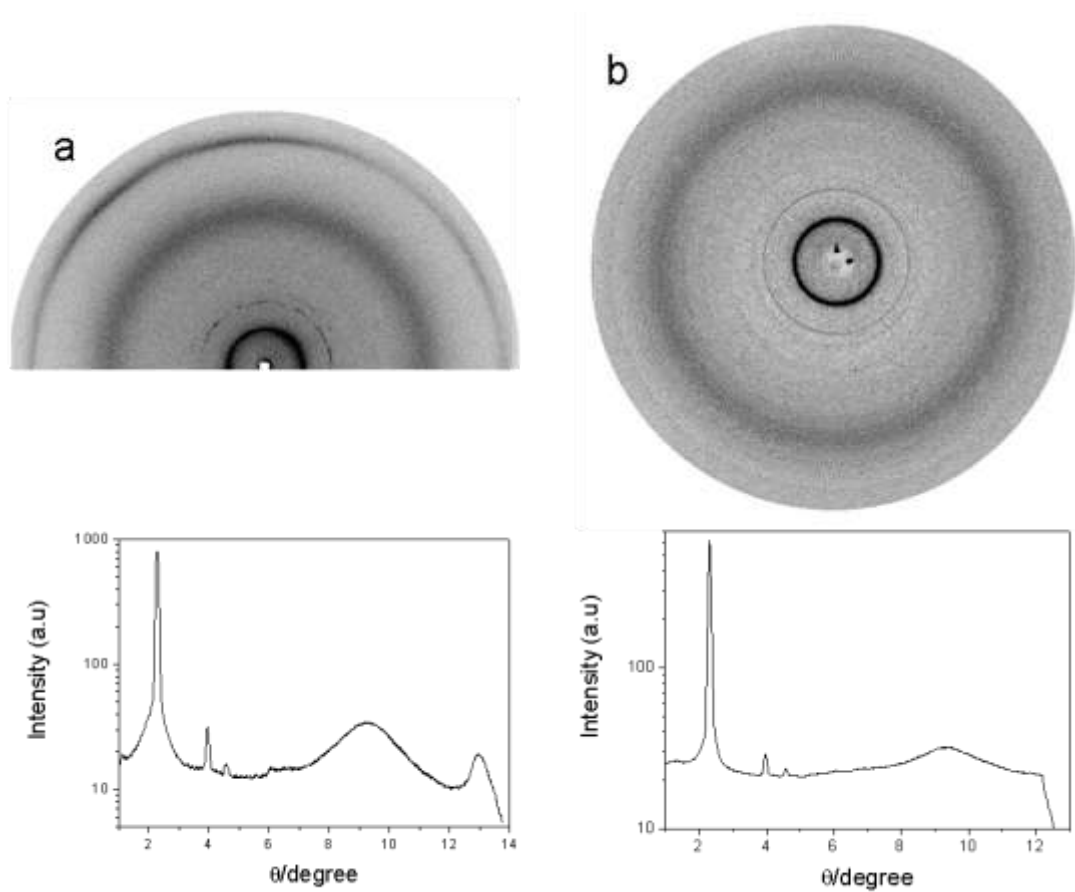


Figure 19. X-Ray diffraction patterns and the derived one-dimensional intensity vs. θ profiles for (a) compound **10** and (b) for the composite **10b** at 25 °C.

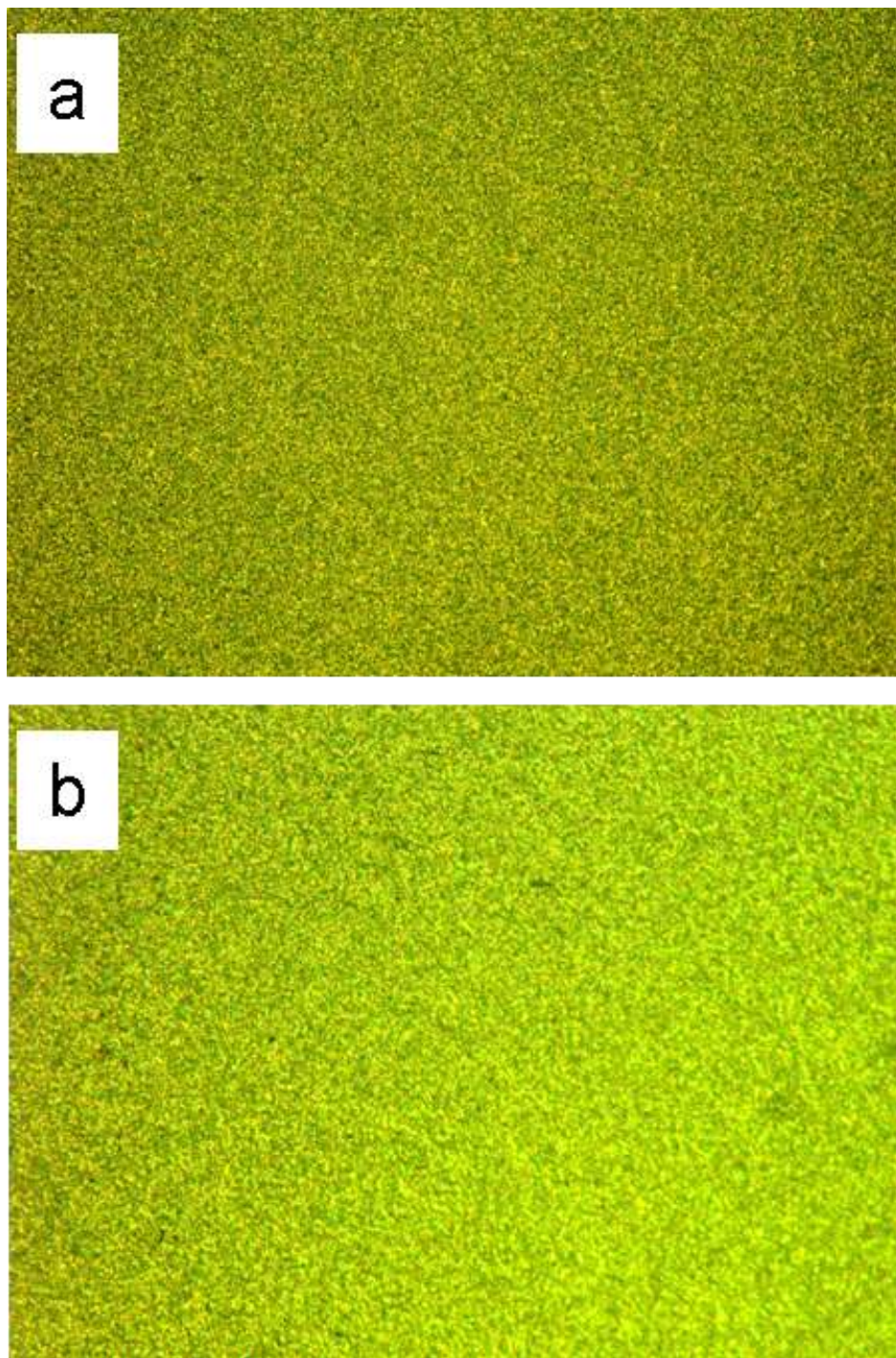


Figure 20. Optical photomicrographs of (a) polymer **11** and (b) its composite **11b** at 25 °C on cooling from the isotropic liquid (crossed polarizers, magnification X 200).

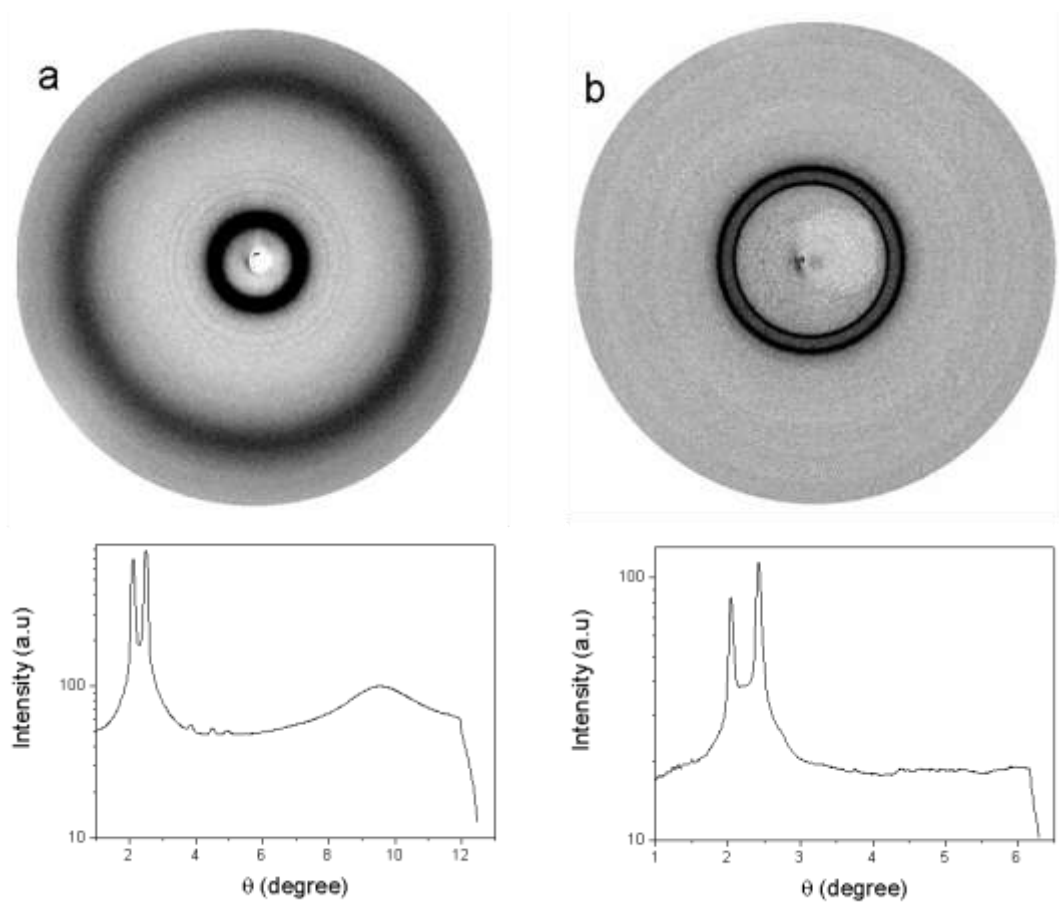


Figure 21. X-Ray diffraction patterns and the derived one-dimensional intensity vs. θ profiles for (a) polymer **11** and (b) for the composite **11c** at 25 °C.

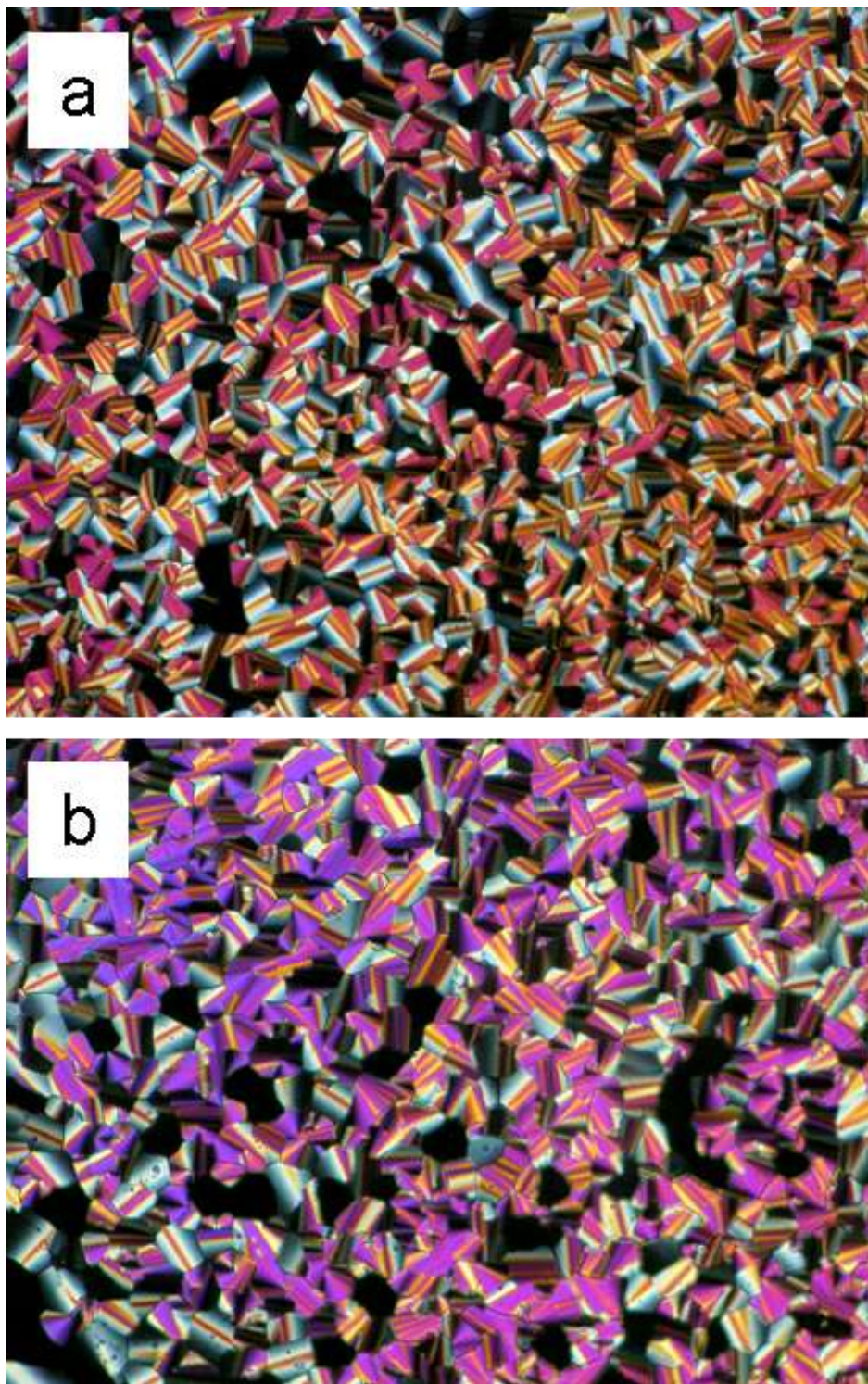


Figure 22. Optical photomicrographs of (a) compound **16** and (b) its composite **16c** at 25 °C on cooling from the isotropic liquid (crossed polarizers, magnification X 200).

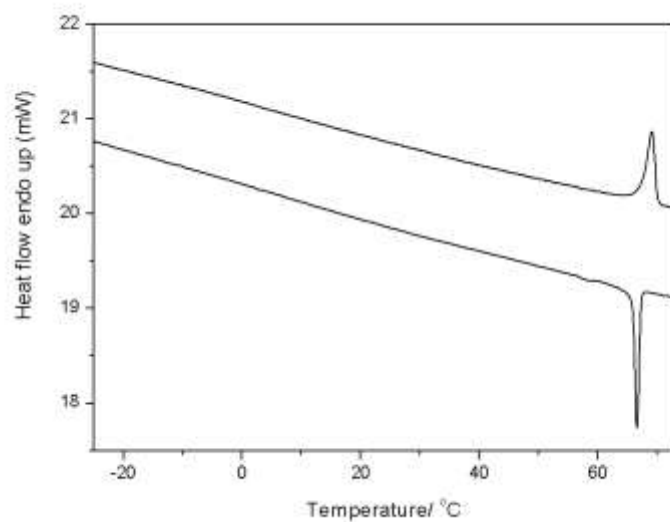


Figure 23. DSC thermogram for compound **16** on heating and cooling (scan rate of 5 °C/min.).

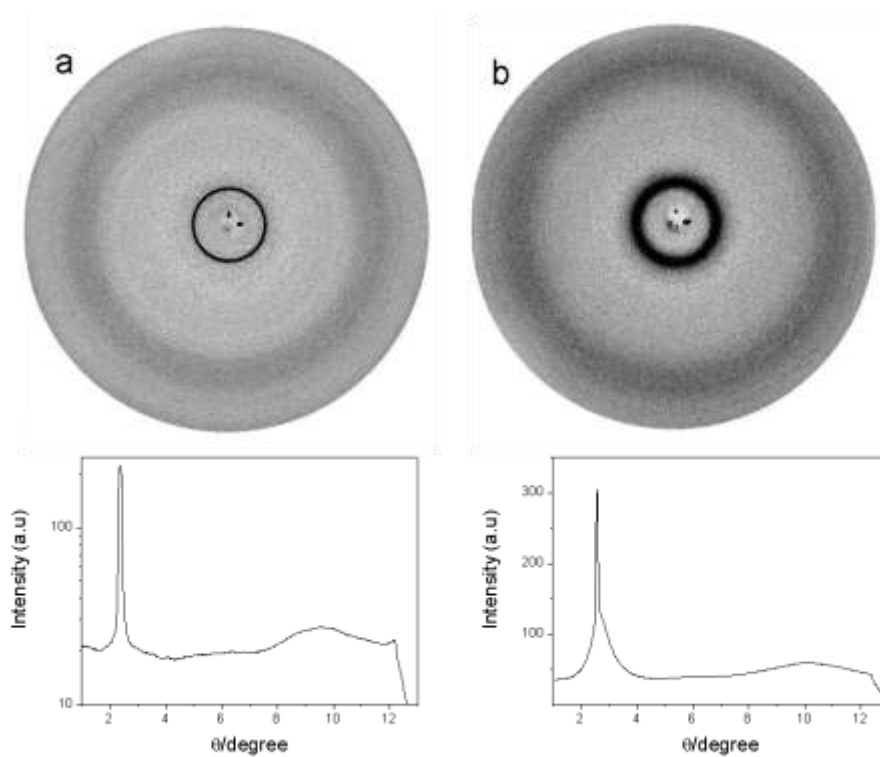


Figure 24. X-Ray diffraction patterns and the derived one-dimensional intensity vs. θ profiles for (a) composite **16c** and (b) for the composite **17a** at 25 °C.

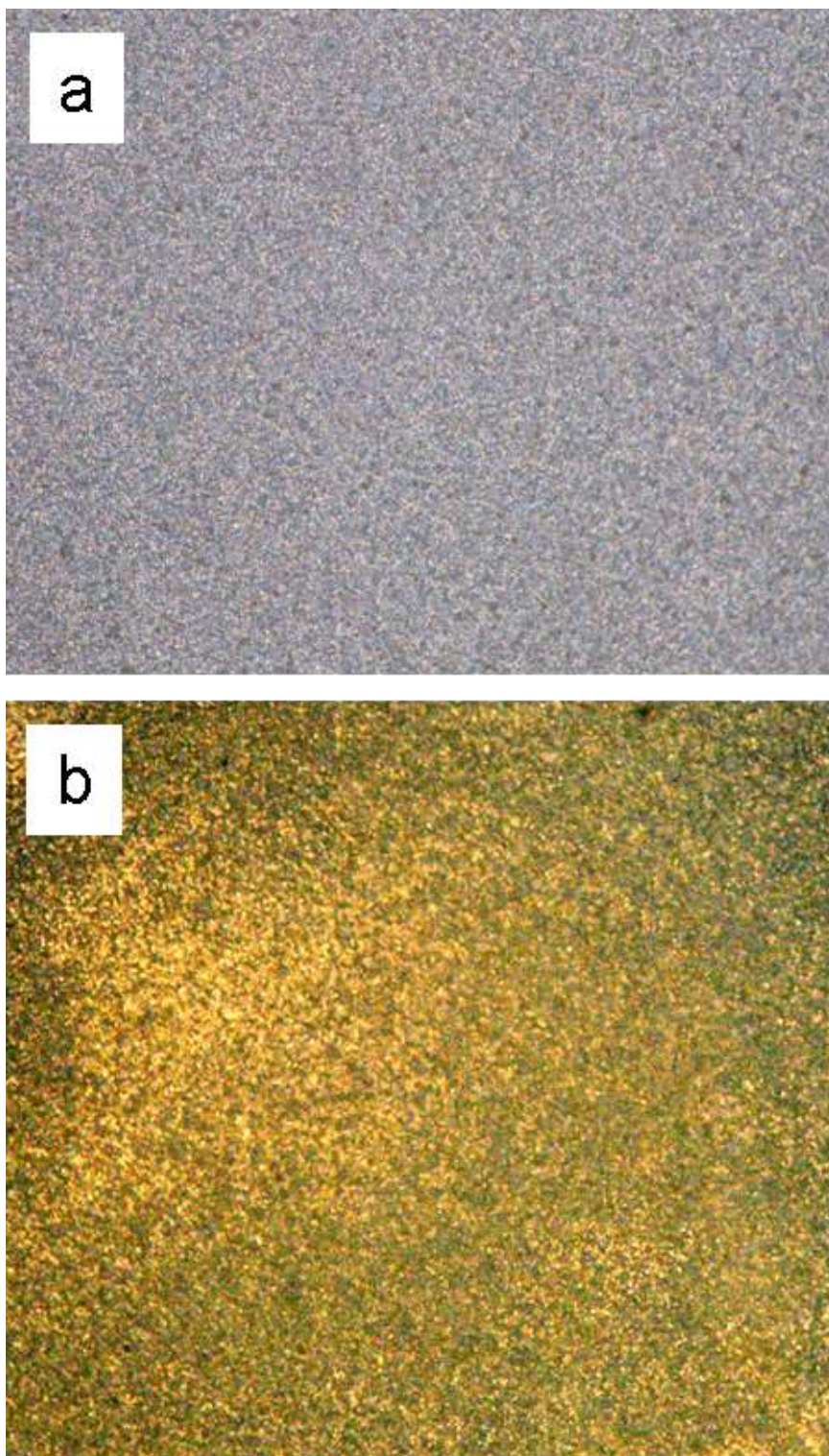


Figure 25. Optical photomicrographs of (a) polymer **17** and (b) its composite **17a** at 25 °C on cooling from the isotropic liquid (Crossed polarizers, magnification X 200).

CHAPTER 6

Summary

In this chapter, we summarize some of the important results and conclusions derived from this thesis work, which deals with ‘*synthesis and characterization of novel mesogenic materials*’. We briefly discuss the diverse possibilities and scope for future work based on the results obtained from our experimental work. Broadly, the research work that has been reported in this thesis can be classified as follows:

Chapter 1 is an introductory chapter and mainly deals with the physical properties of discotic liquid crystals, making them ideal candidates for various optical and electronic devices such as optical compensation films, photocopiers, laser printers, photovoltaic cells, light emitting diodes, field effect transistors, and holographic data storage. Beginning with an over view of liquid crystals, this chapter mainly focuses the major classes of columnar mesophases formed by discotic liquid crystals, their efficient and elegant synthetic procedures, photo and electrical conductivity, macroscopic alignment of columnar phases, relevant mesomorphic and physical properties and finally, some applications and perspectives in material science, nanoscience and molecular electronics.

Though the introduction to liquid crystals is little bit voluminous, nevertheless, while reflecting the authors’ familiarity and awareness about many facets of the research field it is hoped to provoke the readers to appreciate that pursuing a degree in this young, fascinating and fast developing research field is worthwhile given the potential of the materials as organic semiconductors in contemporary research.

Chapter 2 describes green chemistry approach to the synthesis of liquid crystalline materials. Here, we have adopted two main themes of green chemistry; one is the use of microwave dielectric heating, and the other one is to use ionic liquids both as solvent and reagent in the reaction medium. The first part of the chapter deals with the synthesis of commercially important alkoxy cyanobiphenyls and their dimers using microwave dielectric heating in excellent yields within one minute. The reaction conditions were initially optimized by preparing one member of the respective series and then the reproducibility and versatility was demonstrated by preparing other members of both the series.

The second part of the chapter deals with microwave assisted synthesis of monohydroxy functionalized triphenylenes by using ionic reagents. Subsequently, these monohydroxy functionalized triphenylenes were converted to novel unsymmetrical hexaalkoxy triphenylenes by using branched alkyl chains. The chemical structure of all the compounds have been characterized by spectral and elemental analysis. The mesophase behavior of the compounds was studied by polarizing optical microscopy, differential scanning calorimetry and X-ray diffraction studies. All the compounds exhibit enantiotropic columnar hexagonal phase with a broad range of temperature and at lower temperatures. Some of the compounds exhibit spontaneous alignment tendency in the mesophase as noticed by X-ray diffraction studies. The inter columnar distance, as anticipated, increases with increase in the number of carbon atoms in the alkyl chains.

Chapter 3 describes microwave assisted facile synthesis of rufigallol and its novel room-temperature liquid crystalline derivatives. Initially rufigallol was synthesized by microwave heating in very good yield within about one minute. Subsequently, this

rufigallol was converted to novel room temperature liquid crystalline derivatives by using branched alkyl chains with help of microwave heating. The chemical structures of these compounds were characterized by spectral techniques and elemental analysis. The mesophase behavior of all the compounds was studied by POM and DSC. The mesophase structure of the compounds was established by XRD. Most of the compounds exhibit room temperature mesophase over a broad range of temperature with a single mesophase structure. These room-temperature liquid crystalline electron-deficient discotic liquid crystals may find various device applications. One of the tetraalkoxy derivatives containing only four branched alkyl chains exhibit remarkable mesophase stability, which can be used as a potential precursor to prepare various unsymmetrical hexasubstituted derivatives, main chain polymers and metallomesogens etc.

Chapter 4 deals with novel liquid crystalline oligomers containing both electron-rich and electron-deficient discotic cores and novel disc-rod oligomers. The initial part of the chapter deals with first examples of discotic liquid crystalline pentamers and novel discotic star shaped heptamers. All these discotic super molecules exhibit columnar phase over a very broad range of temperature. The supramolecular organization of these super molecules has been established by X-ray diffraction studies. Though these compounds do not form any super column or super lattice, they can be considered as next step towards materials for organic photovoltaic. The difunctional pentamers can be used to prepare various novel pentamers, unsymmetrical heptamers and mixed chain polymers containing both electron rich and deficient discotic cores.

The later part of the chapter deals with novel disc-rod oligomers having tricycloquinazoline as the central core and six alkoxy cyanobiphenyls as the periphery.

These shape-amphiphilic heptamers exhibit nanophase-segregated mesophase morphology in the smectic A phase wherein discs and rods are segregated into alternating sublayers. It is for the first time that this kind of hierarchical organization has been observed in disc-rod hybrid systems having radial molecular topology and containing six rods. For the first time, a cubic phase has also been observed in one of the compounds albeit monotropic in nature. Study of such type of systems provide greater insight into the various subtle intra- and intermolecular interactions involved in the self-assembling process of soft condensed matter.

Chapter 5 focuses on functionalized carbon nanotubes in the supramolecular order of discotic liquid crystals. First part of the chapter deals with discotic-functionalized carbon nanotubes, their characterization by spectral and imaging techniques. Liquid crystalline nanocomposites have been prepared by dispersing these discotic-decorated carbon nanotubes in hexabutyloxytriphenylene and the phase behavior of the composites have been studied by POM, DSC and XRD. It has been observed that the functionalized carbon nanotubes align along the columnar axis. So carbon nanotubes can be aligned in the desired direction by using the well established liquid crystal alignment techniques.

The last part of this chapter addresses the effect of dispersion of functionalized carbon nanotubes on the phase behavior of room-temperature discotic liquid crystalline monomers and novel discotic main chain polymers. By preparing various composites, it has been observed that with increase in the carbon nanotube concentration the phase transition temperatures of the monomers and polymers are lowered but the mesophase structure is not affected. These room-temperature liquid crystalline nanocomposites with broad mesophase ranges and different electronic properties may be important for many

device applications such as photoconductors, light-emitting diodes, photovoltaic solar cells, gas sensors and thin film transistors etc.

As final conclusions, it may be stated that the thesis deals with the synthesis and characterization of mesogenic materials varying from archetypal alkoxybiphenyls and their dimers to contemporary nanomaterials and materials for organic electronics, using traditional as well as modern synthetic methods and green chemical processes. The thesis work spans across monomeric to polymeric discotic liquid crystals via monodisperse oligomers, pure liquid crystalline compounds and composites, liquid crystals with conventional and unconventional mesophase structures and room-temperature discotic liquid crystals with broad mesophase range and single mesophase structure with different electronic (electron rich or p-type and electron deficient or n-type) properties.

Some of the findings of this thesis have been published/communicated in the following international journals.

1. Microwave-assisted facile synthesis of liquid-crystalline alkoxybiphenyls and their dimers.

Hari Krishna Bisoyi and Sandeep Kumar, *Phase Transitions*, **2006**, 79, 285-292.

2. Aligned carbon nanotubes in the supramolecular order of discotic liquid crystals. Sandeep Kumar and Hari Krishna Bisoyi, *Angew. Chem. Int. Ed.*, **2007**, 46, 1501-1503.

3. Synthesis of monohydroxy-functionalized triphenylene discotics: green chemistry approach.

- Santanu Kumar Pal, Hari Krishna Bisoyi and Sandeep Kumar, *Tetrahedron*, **2007**, 63, 6874-6878.
4. Microwave-assisted synthesis of rufigallol and its novel room temperature liquid crystalline derivatives.
Hari Krishna Bisoyi and Sandeep Kumar, *Tetrahedron Letters*, **2007**, 48, 4399-4402.
 5. Microwave-assisted facile synthesis of liquid crystalline non-symmetrical hexaalkoxytriphenylenes containing a branched chain and their characterization.
Hari Krishna Bisoyi and Sandeep Kumar, *J. Phys. Org. Chem.*, **2008**, 21, 47-52.
 6. Green chemistry approach to the synthesis of liquid crystalline materials.
Sandeep Kumar, Hari Krishna Bisoyi and Santanu Kumar Pal, *Mol. Cryst. Liq. Cryst.*, **2008**, 480, 287-294.
 7. First example of monodisperse discotic liquid crystal pentamers: synthesis and mesomorphism.
Hari Krishna Bisoyi and Sandeep Kumar, *Tetrahedron Letters*, **2008**, 49, 3628-3631.
 8. Carbon nanotubes in triphenylene and rufigallol-based room temperature monomeric and polymeric discotic liquid crystals.
Hari Krishna Bisoyi and Sandeep Kumar, *J. Mater. Chem.*, **2008**, 18, 3032-3039.
 9. Room-temperature electron-deficient discotic liquid crystals: facile synthesis and mesophase characterization.
Hari Krishna Bisoyi and Sandeep Kumar, *New J. Chem.*, **2008**, 32, 1974-1980.
 10. Carbon nanotubes in discotic liquid crystals.

Hari Krishna Bisoyi and Sandeep Kumar, *J. Ind. Inst. Sci.*, **2009**, 89.

11. A nanophase segregated mesophase morphology in self-organized novel disc-rod oligomesogens. Hari Krishna Bisoyi, V. A. Raghunathan and Sandeep Kumar, *Chem. Commun.*, **2009**, 7003-705.
12. Discotic nematic liquid crystals: science and technology. Hari Krishna Bisoyi and Sandeep Kumar, *Chem. Soc. Rev.*, **2010**, 39, 264-285.
13. Molecular double cables: synthesis and mesomorphism. Hari Krishna Bisoyi and Sandeep Kumar, Manuscript under preparation.

SYNOPSIS

Synthesis and Characterization of Novel Mesogenic Materials

INTRODUCTION

Liquid crystals (LCs) are unique functional soft materials which combine both *order* and *mobility* on molecular, supramolecular and macroscopic levels [1]. Liquid crystals are accepted as the fourth state of matter after solid, liquid and gas. Liquid crystals form a state of matter intermediate between the crystalline solid and the isotropic liquid state. For this reason, they are referred to as intermediate phases or *mesophases*. This is a true thermodynamic stable state of matter. The constituents of the mesophase are called *mesogens*. The mesogens can be organic (forming thermotropic and lyotropic phases), inorganic (metal oxides forming lyotropic phases) [2] or organometallic (metallomesogens) [3] etc. LCs are important in material science as well as in the life science. Important applications of thermotropic LCs are electrooptic displays, temperature sensors and selective reflecting pigments. Lyotropic systems are incorporated in cleaning process, and are important in cosmetic industries. They are used as templates for the preparation of mesoporous materials and serve as model systems for biomembranes. LCs are important in living matter. Most important are the biological membranes, DNA can form lyotropic mesophases etc. Anisotropic fluid states of rigid polymers are used for processing of high strength fibers like Kevlar. LCs can potentially

be used as new functional materials for electron, ion, molecular transporting, sensory, catalytic, optical and bio-active materials. LCs are extremely diverse since they range from DNA to high strength synthetic polymers like Kevlar (used for bullet-proof vests, protective clothing, high performance composites for aircraft and automotive industries) and from small organic molecules like alkyl and alkoxyphenyls used in liquid crystal displays (LCDs) to self-assembling amphiphilic soap molecules. Recently their biomedical applications such as in controlled drug delivery, protein binding, phospholipid labeling, and in microbe detection have been demonstrated. Apart from material science and bio-science, LCs are now playing significant role in nanoscience and nanotechnology such as synthesis of nanomaterials using LCs as template, the design of LC nanomaterials, alignment and self assembly of nanomaterials using LC phases and so on. Owing to their dynamic nature, photochemically, thermally or mechanically induced structure changes of liquid crystals can be used for the construction of stimuli-responsive materials. Although LCs have diverse applications such as temperature sensing, solvents in chemical reactions, in chromatography, in spectroscopy, in holography, etc., they are primarily known for their extensive exploitation in electrooptical display devices such as watches, calculators, telephones, personal organizers, laptop computers, flat panel television etc.

The fundamental requirement for any substance to exhibit a liquid crystalline phase is the geometric shape anisotropy of the constituents, interaction anisotropy and microsegregation of the incompatible molecular parts. In the liquid crystalline phase the *molecules diffuse* throughout the sample while maintaining some *positional and orientational order* albeit short-ranged. The ability of the molecules to move among the

various lattice sites imparts fluidity to these structures, but since all directions within the phase are not identical, they are anisotropic rather than isotropic fluids. So liquid crystals combine the anisotropic properties of solids and fluidity of liquids. Among all types of liquid crystals, discotic (disc-shaped) liquid crystalline materials are of fundamental importance not only as models for the study of energy and charge migration in self-organized systems but also as functional materials for device applications such as one-dimensional conductors, photoconductors, photovoltaic solar cells, light emitting diodes, gas sensors, thin film transistors etc [4]. The negative birefringence films formed by polymerized nematic discotic liquid crystals have been commercialized as compensation foils to enlarge the viewing angle of commonly used twisted nematic liquid crystal displays [5].

This thesis deals with the synthesis and characterization of novel mesogenic materials varying from archetypal alkoxycyanobiphenyls and their dimers to contemporary nanomaterials (carbon nanotubes) and materials for organic electronics, using traditional as well as modern synthetic methods and green chemical processes (microwave heating and ionic liquids). The thesis work spans across monomeric to polymeric discotic liquid crystals via monodisperse oligomers, pure liquid crystalline compounds and composites, discotic liquid crystals with conventional and unconventional mesophase structures and room-temperature discotic liquid crystals with broad mesophase range and single mesophase structure with different electronic (electron rich or p-type and electron deficient or n-type) properties. All the synthesized materials have been characterized by nuclear magnetic resonance spectroscopy (NMR), ultraviolet spectroscopy (UV), infrared spectroscopy (IR), elemental analysis, gel permeation

chromatography (GPC), thermo gravimetric analysis (TGA), polarizing optical microscopy (POM), differential scanning calorimetry (DSC), X-ray diffractometry (XRD), scanning tunneling microscopy (STM) and conductivity studies etc.

Herein, this thesis describes new approaches to functional liquid crystals and shows how the molecular engineering of liquid crystals leads to the formation of a variety of new self-organized soft and nano functional materials. In what follows, we have briefly described some of the significant results and conclusions derived from our experimental work.

CHAPTER 1

This is an introductory chapter to liquid crystals in general like their classification and important significance in material science, life science, nanoscience and their dominance in electrooptical display devices. However, the chapter focuses in greater detail on the physical properties of discotic liquid crystals, making them ideal candidates for various optical and electronic devices such as optical compensation films, photocopiers, laser printers, photovoltaic cells, light emitting diodes, field effect transistors, gas sensors and holographic data storage [4]. Beginning with an over view of thermotropic liquid crystals and their brief history, this chapter mainly focuses the major classes of columnar mesophases formed by discotic liquid crystals, their efficient and elegant synthetic procedures, photo and electrical conductivity, macroscopic alignment of columnar phases, relevant mesomorphic and physical properties and finally, some applications and perspectives in material science, nanoscience and molecular electronics.

CHAPTER 2

This chapter describes green chemistry approach to the synthesis of liquid crystalline materials. Here, we have adopted two main themes of green chemistry; one is the use of microwave dielectric heating, and the other one is to use ionic liquids both as solvent and reagent in the reaction medium [6]. The first part of the chapter deals with the synthesis of commercially important alkoxy cyanobiphenyls and their dimers using microwave dielectric heating in excellent yields within one minute (Scheme 1). The reaction conditions were initially optimized by preparing one member of the respective series and then the reproducibility and versatility was demonstrated by preparing other members of both the series. While the phase transition temperatures of the alkoxy cyanobiphenyls are identical to the literature values, the phase transition temperatures of all the dimers are slightly higher than the reported values and thus demonstrate the cleanness of the protocol. This facile and clean protocol can be employed for the synthesis of many other liquid crystalline materials.

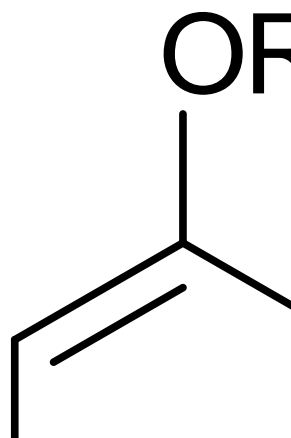
Scheme 1

Monohydroxy-functionalized triphenylenes are valuable precursor molecules for the preparation of variety of discotic dimers, oligomers, polymers, networks, dendrimers and unsymmetrical derivatives [7]. However, because of synthetic problems the full potential of these materials have not yet been fully explored. A few methods have been

developed for the synthesis of monohydroxy-functionalized triphenylenes, but most of these involve expensive and/or hazardous reagents. So we were looking for an alternative less expensive and less hazardous method to prepare mono-functionalized triphenylene. The second part of the chapter deals with microwave assisted synthesis of monohydroxy functionalized triphenylenes by using ionic reagents (Scheme 2).

Scheme 2

Subsequently, these monohydroxy functionalized triphenylenes were converted to novel unsymmetrical hexaalkoxy triphenylenes by using branched alkyl chains (Scheme 3). The chemical structure of all the compounds have been characterized by spectral and elemental analysis. The mesophase behavior of the compounds was studied by polarizing optical microscopy, differential scanning calorimetry and X-ray diffraction studies. All the compounds exhibit enantiotropic columnar hexagonal phase with a broad range of temperature. Some of the compounds exhibit spontaneous alignment tendency in the mesophase as noticed by X-ray diffraction studies.



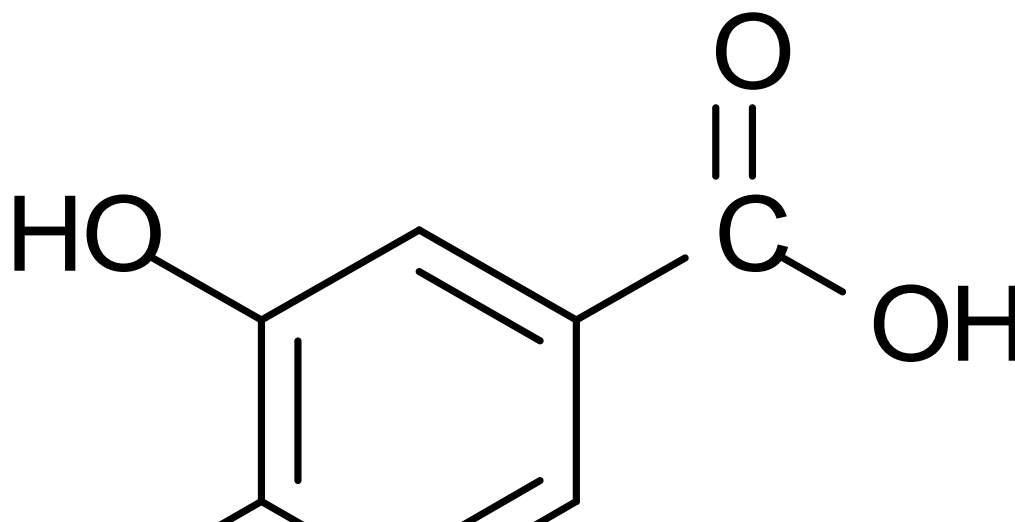
Scheme 3

The manipulation of the molecular architecture provides the opportunity to obtain homeotropically aligned films of self-assembled materials with low clearing temperature and wide mesophase range which is essential for the implementation of these kind of materials in electronic devices like light emitting diodes, photovoltaic solar cells etc.

CHAPTER 3

Rufigallol is a molecule of both biological and materials science interest [8]. However, there are no new efficient methods to prepare rufigallol. Chapter 3 describes microwave assisted facile synthesis of rufigallol and its novel room-temperature liquid crystalline derivatives. Discotic liquid crystals can function as p-type or n-type organic semiconductors. The most widely synthesized and studied discotic liquid crystals are electron rich π -conjugated materials and are better hole carriers (p-type semiconductors) [9]. Few examples of electron deficient (n-type) discotic liquid crystals are reported in the literature which are very less as compared to p-type discotic liquid crystals [10]. Thus novel n-type liquid crystalline materials are required as electron transporting layers for

organic light emitting diodes and organic photovoltaic solar cells. Moreover, efforts have been made to prepare room-temperature electron-rich discotic liquid crystals [9] but room-temperature electron-deficient discotic liquid crystals are rare. Therefore, it is of great practical interest to prepare rufigallol-based room-temperature electron deficient discotic liquid crystals. Initially rufigallol was synthesized by microwave heating in very good yield within about one minute (Scheme 4). Subsequently, this rufigallol was converted to novel room temperature liquid crystalline derivatives by using branched alkyl chains with help of microwave heating.



Scheme 4 Synthesis of rufigallol and its novel liquid crystalline derivatives. *Reagents and conditions:* (i) H₂SO₄, MW, 90 sec., 84%; (ii) RBr, DMSO, NaOH; (iii) R'Br, Cs₂CO₃, NMP, MW, 3 min.; (iv) R'Br, NaOH, DMSO; (v) RBr, Cs₂CO₃, NMP, MW, 3-4 min.

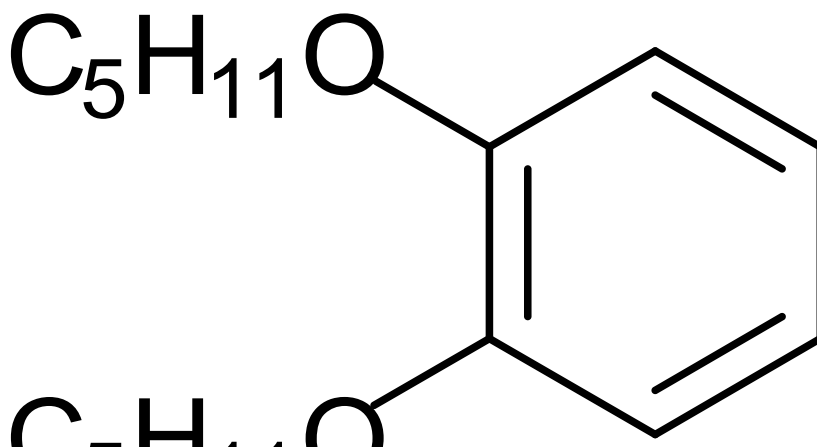
The chemical structures of these compounds were characterized by spectral techniques and elemental analysis. The mesophase behavior of all the compounds was studied by POM and DSC. The mesophase structure of the compounds was established

by XRD. Most of the compounds exhibit room temperature mesophase over a broad range of temperature with a single mesophase structure. These room-temperature liquid crystalline electron-deficient discotic liquid crystals may find various device applications. One of the tetraalkoxy derivatives containing only four branched alkyl chains exhibit remarkable mesophase stability, which can be used as a potential precursor to prepare various unsymmetrical hexasubstituted derivatives, main chain polymers and metallomesogens etc.

CHAPTER 4

Liquid crystal oligomers are interesting materials since the physical properties of these materials are significantly different from those of conventional low molar mass liquid crystals. Their purification and characterization are simple as compared to high molar mass polymers. Owing to the restricted motion of the components liquid crystal oligomers provide and stabilize variety of fluid phases with fascinating functions and oligomeric approach provides a wide flexibility in molecular design towards multifunctional liquid crystals. However, compared to the number of calamitic oligomers, discotic oligomers are rare and discotic liquid crystal pentamers are not reported [11]. Chapter 4 deals with novel liquid crystalline oligomers containing both electron-rich and electron-deficient discotic cores and novel disc-rod oligomers. The initial part of the chapter deals with first examples of discotic liquid crystalline pentamers (Scheme 5) and novel discotic star shaped heptamers (Scheme 6 and 7). These compounds can be considered as molecular double cables since they possess two charge transporting paths in the same molecule. All these discotic super molecules exhibit columnar phase over a

very broad range of temperature. The supramolecular organization of these super molecules has been established by X-ray diffraction studies.



Scheme 5 Synthesis of discotic liquid crystalline pentamers. Reagents and conditions: (i) FeCl_3 ; MeOH; (ii) Cat-B-Br; (iii) 1,12-Dibromododecane, MEK, Cs_2CO_3 ; (iv) H_2SO_4 , MW; (v) DMSO, NaOH, 90 °C, 20h, 10%; (vi) Ac_2O , H_2SO_4 .

Though these compounds do not form any super column or super lattice, they can be considered as next step towards materials for organic photovoltaic. The difunctional pentamers can be used to prepare various novel pentamers, unsymmetrical heptamers and mixed chain polymers containing both electron rich and deficient discotic cores.



Scheme 6 Synthesis of discotic liquid crystalline heptamer. Reagents and conditions: (i) H_2SO_4 , MW; (ii) Cs_2CO_3 , NMP, MW, 10 min.

Scheme 7 Synthesis of triphenylene based heptamer. Reagents and conditions: (i) 1,12-dibromododecane, K_2CO_3 , MEK; (ii) FeCl_3 ; MeOH; (iii) Cat-B-Br, CH_2Cl_2 ; (iv) Cs_2CO_3 , MEK, 72 hrs reflux, 55%.

The later part of the chapter deals with novel disc-rod oligomers having tricycloquinazoline as the central core and six alkoxyphenyls as the periphery (Scheme 8).



Scheme 8 Synthesis of novel disc-rod oligomesogens. *Reagents and conditions:* (i) HNO_3 ; (ii) Sn, AcOH; (iii) NH_4OAc , AcOH, sulfolane, reflux; (iv) 1. Pyridine, HCl, 230 °C; 2. Pyridine, Ac_2O ; (v) RBr, KOH, DMSO, 40%.

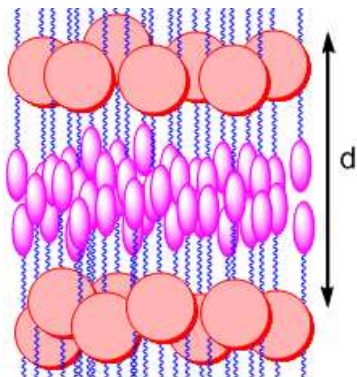


Figure 1. Nanophase-segregated structure in the smectic A mesophase of the disc-rod oligomers wherein discs and rods segregate into alternating sublayers.

These shape-amphiphilic heptamers exhibit nanophase-segregated mesophase morphology in the smectic A phase wherein discs and rods are segregated into alternating sublayers (Figure 1). It is for the first time that this kind of hierarchical organization has been observed in disc-rod hybrid systems having radial molecular topology and containing six rods. It is envisaged that calamitic and discotic liquid crystals can readily mix with these assemblies by simply inserting the liquid crystal into the appropriate layer without altering the symmetry of the phase. For the first time, a cubic phase has also been observed in one of the compounds albeit monotropic in nature. Study of such type of systems provide greater insight into the various subtle intra- and intermolecular interactions involved in the self-assembling process of soft condensed matter.

CHAPTER 5

Carbon nanotubes (CNTs), the fourth allotrope of carbon, after diamond, graphite and fullerene, are one dimensional, well ordered all-carbon hollow cylinders of graphite with very high aspect ratio. The combination of superlative mechanical, thermal and electronic properties displayed by carbon nanotubes make them ideal for a wide range of applications, such as, conductive and high-strength composites, energy storage and energy-conversion devices, field emitters, transistors, actuators, sensors, gas storage media, tips for scanning probe microscopy, molecular wires etc [12]. Despite the extraordinary promise of carbon nanotubes, their realistic application as one-dimensional conductors or semiconductors has been restricted because of difficulties in aligning them in the desired direction. There have been several attempts to align carbon nanotubes where one dimensional charge migration is important. However, processing materials with well-controlled carbon nanotube alignment still remains a challenge.

The insertion (dispersion) of carbon nanotubes in the supramolecular order of discotic liquid crystalline monomers and polymers may lead to novel materials with interesting properties useful for device applications. The ordered columnar phases, in contrast to isotropic and nematic phases, can offer wider opportunity for processing material with oriented nanotubes, a critical factor considering the strongly anisotropic properties of carbon nanotubes [13]. Moreover, there are a lot of striking similarities between carbon nanotubes and discotic liquid crystals; first, both CNTs and discotic liquid crystals (DLCs) are anisotropic materials. Second, both the materials possess self-assembling properties and often form hexagonal aggregates. Third and more important is the one dimensional (1D) conductivity properties of both CNTs and DLCs. Conductivity along the columnar axis of DLCs is several orders of magnitude greater than perpendicular to it, so also in CNTs, the conductivity along the CNT axis is much more higher than across the axis. Therefore, both the materials can be considered as “molecular wires”. With this in mind, we have initiated a research program to disperse functionalized CNTs into the columnar matrix of liquid crystalline discotic monomers and polymers.

Chapter 5 focuses on functionalized carbon nanotubes in the supramolecular order of discotic liquid crystals. First part of the chapter deals with discotic-functionalized carbon nanotubes (Scheme 9), their characterization by spectral and imaging techniques. Liquid crystalline nanocomposites have been prepared by dispersing these discotic-decorated carbon nanotubes in hexabutyloxytriphenylene and the phase behavior of the composites have been studied by POM, DSC and XRD. It has been observed that the functionalized carbon nanotubes align along the columnar axis (Figure 2).

Scheme 9

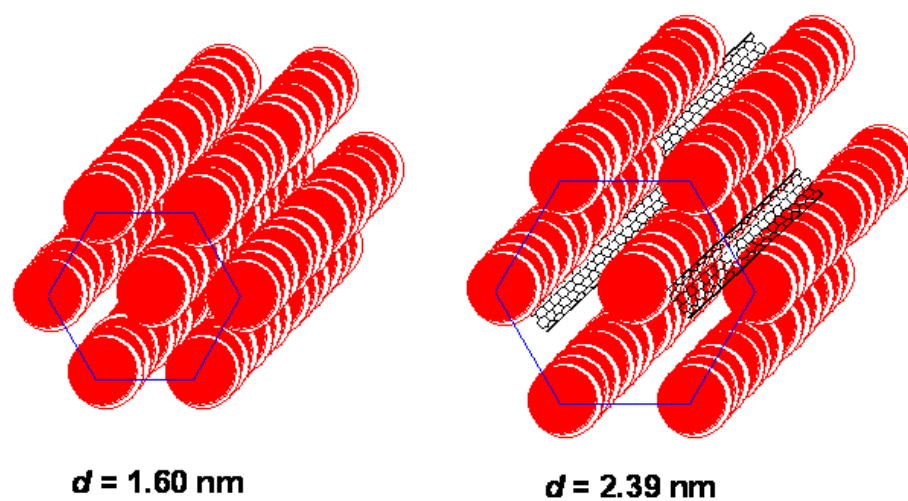


Figure 2. Schematic representation of the insertion of SWNTs in the supramolecular order of a columnar mesophase.

So carbon nanotubes can be aligned in the desired direction by using the well established liquid crystal alignment techniques.

The last part of this chapter addresses the effect of dispersion of functionalized carbon nanotubes on the phase behavior of room-temperature discotic liquid crystalline monomers and novel discotic main chain polymers (Scheme 10). By preparing various composites, it has been observed that with increase in the carbon nanotube concentration the phase transition temperatures of the monomers and polymers are lowered but the mesophase structure is not affected. These room-temperature liquid crystalline nanocomposites with broad mesophase ranges and different electronic properties may be important for many device applications such as photoconductors, light-emitting diodes, photovoltaic solar cells, gas sensors and thin film transistors etc.



Scheme 10 Synthesis of room-temperature liquid crystalline triphenylene monomer and polymer. Reaction conditions and reagents; (i) $C_5H_{11}Br$, K_2CO_3 , MEK; (ii) $FeCl_3$, CH_2Cl_2 and CH_3OH ; (iii) Cat-B-Br, CH_2Cl_2 ; (iv) 3, 7-dimethyloctylbromide, Cs_2CO_3 , MEK, 62%; (v) 1,12-dibromododecane, Cs_2CO_3 , NMP, 110 °C, 54%.

CHAPTER 6

The thesis is concluded with a chapter, which summarizes some the important results and conclusions derived from this thesis work, which deals with ‘*synthesis and characterization of novel mesogenic materials*’. We briefly discuss the diverse possibilities and scope for future work based on the results obtained from our experimental work.

Some of the findings of this thesis have been published/communicated in the following international journals.

1. Microwave-assisted facile synthesis of liquid-crystalline alkoxybiphenyls and their dimers.

Hari Krishna Bisoyi and Sandeep Kumar, *Phase Transitions*, **2006**, 79, 285-292.

2. Aligned carbon nanotubes in the supramolecular order of discotic liquid crystals.

Sandeep Kumar and Hari Krishna Bisoyi, *Angew. Chem. Int. Ed.*, **2007**, 46, 1501-1503.

3. Synthesis of monohydroxy-functionalized triphenylene discotics: green chemistry approach.

Santanu Kumar Pal, Hari Krishna Bisoyi and Sandeep Kumar, *Tetrahedron*, **2007**, 63, 6874-6878.

4. Microwave-assisted synthesis of rufigallol and its novel room temperature liquid crystalline derivatives.

Hari Krishna Bisoyi and Sandeep Kumar, *Tetrahedron Letters*, **2007**, 48, 4399-4402.

5. Microwave-assisted facile synthesis of liquid crystalline non-symmetrical hexaalkoxytriphenylenes containing a branched chain and their characterization. Hari Krishna Bisoyi and Sandeep Kumar, *J. Phys. Org. Chem.*, **2008**, 21, 47-52.
6. Green chemistry approach to the synthesis of liquid crystalline materials. Sandeep Kumar, Hari Krishna Bisoyi and Santanu Kumar Pal, *Mol. Cryst. Liq. Cryst.*, **2008**, 480, 287-294.
7. First example of monodisperse discotic liquid crystal pentamers: synthesis and mesomorphism. Hari Krishna Bisoyi and Sandeep Kumar, *Tetrahedron Letters*, **2008**, 49, 3628-3631.
8. Carbon nanotubes in triphenylene and rufigallol-based room temperature monomeric and polymeric discotic liquid crystals. Hari Krishna Bisoyi and Sandeep Kumar, *J. Mater. Chem.*, **2008**, 18, 3032-3039.
9. Room-temperature electron-deficient discotic liquid crystals: facile synthesis and mesophase characterization. Hari Krishna Bisoyi and Sandeep Kumar, *New J. Chem.*, **2008**, 32, 1974-1980.
10. Carbon nanotubes in discotic liquid crystals. Hari Krishna Bisoyi and Sandeep Kumar, *J. Ind. Inst. Sci.*, **2009**, 89.
11. Nanophase segregated mesophase morphology in self-organized novel disc-rod oligomesogens. Hari Krishna Bisoyi, V. A. Raghunathan and Sandeep Kumar, Communicated.
12. Molecular double cables: synthesis and mesomorphism. Hari Krishna Bisoyi and Sandeep Kumar, Manuscript under preparation.

References

1. (a) *Handbook of Liquid Crystals*, eds. D. Demus, J. Goodby, G. W. Gray, H. W. Spiess, V. Vill, Wiley-VCH, Weinheim, Vol **I-III**, (1998); (b) B. Bahadur (ed.), *Liquid Crystals-Application and Uses*, Vol **I-III**, World Scientific, Singapore (1990); (c) S. Chandrasekhar, *Liquid Crystals*, 2nd ed., Cambridge University Press, Cambridge (1992); (d) P. J. Collings and M. Hird, *Introduction to Liquid Crystals-Chemistry and Physics*, Taylor & Francis Ltd., London (1997); (e) P. G. de Gennes and J. Prost, *The Physics of Liquid Crystals*, 2nd ed. Oxford University press, New York, (1993).
2. A. S. Sonin, *J. Mater. Chem.*, **8**, 2557, (1998).
3. J. L. Serrano, *Metallomesogens-Synthesis, Properties and Application*, VCH Weinheim, (1996).
4. (a) S. Kumar, *Chem. Soc. Rev.*, **35**, 83, (2006); (b) T. Kato, T. Yasuda, Y. Kamikawa and M. Yoshio, *Chem. Commun.*, 729, (2009); (c) S. Laschat, A. Baro, N. Steinke, F. Giesselmann, C. Hagele, G. Scalia, R. Judele, E. Kapatsina, S. Sauer, A. Schreivogel, M. Tosoni, *Angew. Chem. Int. Ed.*, **46**, 4832, (2007); (d) S. Sergeyev, W. Pisula, Y. H. Geerts, *Chem. Soc. Rev.*, **36**, 1902, (2007); (e) J. Wu, W. Pisula, K. Mullen, *Chem. Rev.*, **107**, 718, (2007).
5. K. Kawata, *Chem. Rec.*, **2**, 59, (2002);
6. (a) C. O. Kappe, *Chem. Soc. Rev.*, **37**, 1127, (2008); (b) *Ionic Liquids in Synthesis*, P. Wasserscheid and T. Welton (eds), Wiley-VCH, Weinheim, (2002).
7. (a) S. Kumar and M. Manickam, *Synthesis*, 1119, (1998); (b) S. Kumar and M. Manickam, *Chem. Commun.*, 1615, (1997).

8. S. Kumar, *Phase Transitions*, **81**, 113, (2008).
9. S. Kumar and S. K. Varshney, *Angew. Chem. Int. Ed.*, **39**, 3140, (2000).
10. S. Kumar, D. S. Shankar Rao, S. K. Prasad, *J. Mater. Chem.*, **9**, 2751, (1999).
11. (a) S. Kumar, *Liq. Cryst.*, **32**, 1089, (2005); (b) S. Kumar, *Liq. Cryst.*, **31**, 1037, (2004).
12. (a) Special Issue on Carbon Nanotubes, *Acc. Chem. Res.*, **35**, 997, (2002); (b) *Carbon Nanotubes: Synthesis, Structure, Properties and Applications*, ed. M. Dresselhaus, G. Dresselhaus and Ph. Avouris, Springer-Verlag, Berlin, (2001).
13. C. Zakri, *Liq. Cryst. Today*, **16**, 1, (2007).

Signature of the Research Fellow

Signature of the Research Guide

Hari Krishna Bisoyi

Prof. Sandeep Kumar